AREVA

Realistic Large Break LOCA Methodology for Pressurized Water Reactors

Topical Report

September 2013

AREVA Inc.

Nature of Changes

Item	Section(s) or Page(s)	Description and Justification
1	All	Changes incorporated into Revision 3 are too extensive to itemize. Therefore, this version is considered to be an entire rewrite.
2	Pages 1-6, 2-13, 8.1-10, 8.2-776 and 8.5-55	Correction of reference dates or revision numbers.
3	Page 3-25	Changes made based on the SE comment process.
4	Page 7-155	Typographical errors were corrected and the equation numbering reference was corrected.
5	Table 8.2-13	Markups in Table 8.2-13 were added.
6	Figure 8.2-298	Figure 8.2-298 is obsolete and should have been replaced. The figure included in previous transmittals of the topical report is based on the old EMF-2102 Rev. 0 figure and it shows the out-of-date component numbering in the nodalization scheme – the nodalization itself is unchanged and correct. Figure 8.2-298 in EMF-2103P-A Rev. 3 has been replaced with the correct one from EMF-2102 Rev. 1.
7	Page 8.4-11	Changes were made based on the SE comment process.
8	Figure 8.4-2	Markups to the captions were added.
9	Figure 8.4-3	Markups to the captions were added.
10	Figure 8.4-4	Markups to the captions were added.
11	Figure 8.4-18	Markups to the captions were added.
12	Page 8.5-36	Changes were made based on the SE comment process.
13	Figure 8.5-5	The caption of Figure 8.5-5 was updated with the correct reference number.
14	Section 8.6	Reference numbering was formatted consistent with the rest of the document.
15	Page 9-22	An additional clarification inserted related to the SE comment process.
16	Page A-71	Changes were made based on the SE comment process.
17	Page A-129	Appendix A page A-129 section A.2.3.6.4, the equation was corrected to include the entire term in the exponent.
18	Table A-7	Table A-7 has been updated to correct a typographical error in the cell indicating the mean for the natural logarithm of metal-water reaction constant. Also in Table A-7 a correction to the standard deviation of the Tmin distribution was made.
19	Table B-17	Caption was formatted consistent with the captions within the section.

AREVA Inc.

EMF-2103NP
Revision 3

Realistic Large Break LOCA Methodology for Pressurized Water Reactors
Topical Report

Page ii

Contents

AREVA Inc.

EMF-2103NP
Revision 3

Realistic Large Break LOCA Methodology for Pressurized Water Reactors
Topical Report

Page viii

List of Tables

AREVA, Inc.

Realistic Large Break LOCA Methodology for Pressurized Water Reactors
Topical Report

EMF-2103NP
Revision 3

Page xi

AREVA Inc.

EMF-2103NP
Revision 3

Realistic Large Break LOCA Methodology for Pressurized Water Reactors
Topical Report

Page xiv

AREVA Inc.

EMF-2103NP
Revision 3

Realistic Large Break LOCA Methodology for Pressurized Water Reactors
Topical Report

Page xv

List of Figures

AREVA Inc.

EMF-2103NP
Revision 3

Realistic Large Break LOCA Methodology for Pressurized Water Reactors
Topical Report

Page xvii

AREVA Inc.

EMF-2103NP
Revision 3

Realistic Large Break LOCA Methodology for Pressurized Water Reactors
Topical Report

Page xviii

AREVA Inc.

EMF-2103NP
Revision 3

Realistic Large Break LOCA Methodology for Pressurized Water Reactors
Topical Report

Page xxii

AREVA Inc.

EMF-2103NP
Revision 3

Realistic Large Break LOCA Methodology for Pressurized Water Reactors
Topical Report

Page xxiv

AREVA Inc.

EMF-2103NP
Revision 3

Realistic Large Break LOCA Methodology for Pressurized Water Reactors
Topical Report

Page xxvi

AREVA Inc.

EMF-2103NP
Revision 3

Realistic Large Break LOCA Methodology for Pressurized Water Reactors
Topical Report

Page xxxv

AREVA Inc.

EMF-2103NP
Revision 3

Realistic Large Break LOCA Methodology for Pressurized Water Reactors
Topical Report
Page xxxvii

AREVA Inc.   EMF-2103NP
Revision 3
Realistic Large Break LOCA Methodology for Pressurized Water Reactors
Topical Report   Page xxxviii

AREVA Inc.

Realistic Large Break LOCA Methodology for Pressurized Water Reactors
Topical Report

EMF-2103NP
Revision 3

Page xliii

AREVA Inc.

EMF-2103NP
Revision 3

Realistic Large Break LOCA Methodology for Pressurized Water Reactors
Topical Report

Page Iv

AREVA Inc.

Realistic Large Break LOCA Methodology for Pressurized Water Reactors
Topical Report

EMF-2103NP
Revision 3
Page lvi

Nomenclature

Acronym	Definition
ACC	accumulator
ANP	advanced nuclear products
ANS	American Nuclear Society
ASME	American Society of Mechanical Engineers
BIASI	Biasi CHF multiplier
BLCL	broken loop cold leg
BLHL	broken loop hot leg
BOCR	beginning of core recovery
BST	blowdown suppression tank
BWR	boiling water reactor
CCFL	countercurrent flow limitation
CCTF	Cylindrical Core Test Facility
CE	Combustion Engineering
CFR	Code of Federal Regulations
CHF	critical heat flux
CLPD	cold leg pump discharge
CONMAS	interfacial condensation heat transfer coefficient multiplier
CONMSG	interfacial condensation heat transfer coefficient multiplier, vapor
CSAU	Code Scaling, Applicability, and Uncertainty
CWO	core-wide oxidation
DEG	double-ended guillotine
DFFBHTC	dispersed flow film boiling heat transfer coefficient
DIW	deionized water tank
DMS	document management system
DNB	departure from nucleate boiling
ECC	emergency core cooling
ECCS	emergency core cooling system
EDR	Experimental Data Report
EHL	end of heated length
EMDAP	evaluation model development and assessment process
EPRI	Electric Power Research Institute
F-R	Forslund-Rohsenow
FCTF	Fuel Cooling Test Facility

Acronym	Definition
FIJ	Interphase friction multiplier
FILMBL	film boiling
FIMIST	post-CHF mist flow regime
FLECHT	Full Length Emergency Cooling Heat Transfer
FSRR	fuel swelling, rupture, and relocation
HA	hot assembly
HEM	homogeneous equilibrium model
HHSI	high head safety injection
HPC	high probability of compliance
HPI	high pressure injection
HPSI	high pressure safety injection
HTP	high thermal performance
IET	Integral Effects Test
ILCL	intact loop cold leg
ILHL	intact loop hot leg
INEEL	Idaho National Environmental Engineering Laboratory (formerly INEL)
INEL	Idaho National Engineering Laboratory
ISP	International Standard Problem
JAERI	Japan Atomic Energy Research Institute
KWU	Kraftwerk Union (SPC), now AREVA GmbH
LANL	Los Alamos National Laboratory
LBLOCA	large break loss-of-coolant accident
LHGR	linear heat generation rate
LHSI	low head safety injection
LOCA	loss-of-coolant accident
LOCE	loss-of-coolant experiment
LOFT	Loss of Fluid Test
LOOP	Loss of Offsite Power
LPCI	low pressure coolant injection
LPSI	low pressure safety injection
MCT	maximum clad temperature
MLHGR	maximum linear heat generation rate
MLO	maximum local oxidation
MSIV	main steam isolation valve
MTC	moderator temperature coefficient
NAI	Numerical Applications, Inc.

Acronym	Definition
NPP	nuclear power plant
NRC	United States Nuclear Regulatory Commission
ORNL	Oak Ridge National Laboratory
PCT	peak cladding temperature
PDTF	Product Development Test Facility
PFM	pipe flow meter
PIE	post-irradiation examination
PIRT	Phenomena Identification and Ranking Table
PLC	programmable logic controllers
PMF	probability mass function
PWR	pressurized water reactor
QA	Quality Assurance
QLR	Quick Look Report
RABS	reflood assisted bypass system
RABV	reflood assisted bypass valve
RCP	reactor coolant pump
RCS	reactor coolant system
RHR	residual heat removal
RLBLOCA	realistic large break loss-of-coolant accident
RWST	refueling water storage tank
SBLOCA	small break loss-of-coolant accident
SCTF	Slab Core Test Facility
SDR	Software Development Record
SEASET	System Effects and Separate Effects Tests
SET	Separate Effects Test
SG	steam generator
SI	Safety Injection
SIT	Safety Injection Tank
SMART	SMall Array Reflood Test
SPC	Siemens Power Corporation
SQAP	Software Quality Assurance Program
SRP	Standard Review Plan
SRR	swelling, rupture, and relocation
THTF	Thermal-Hydraulic Test Facility
TMDPJUN	time-dependent junction
TMDPVOL	time-dependent volume

Acronym	Definition
TMINK	maximum temperature for transition boiling
UCSP	upper core support plate
UPTF	Upper Plenum Test Facility
UTL	upper tolerance limit(s)
UTP	upper tie plate

ABSTRACT

AREVA NP had developed and licensed a large-break loss-of-coolant accident (LOCA) methodology for Westinghouse 3- and 4-loop designs and Combustion Engineering 2x4 designs (April 2003). The licensed methodology uses a statistical sampling approach for the propagation of uncertainty and non-parametric statistical evaluation of the results following the Wilks method. In this method, uncertainty contributors are ranged individually to determine the expected peak cladding temperature (PCT), Maximum Local Oxidation (MLO) and total Core-Wide Oxidation (CWO) response.

In this report, an alternative uncertainty methodology is developed resolving the multi-variate evaluation. This methodology replaces the Revision 0 Wilks technique. In this technique, the results for PCT, MLO, and CWO provide simultaneous coverage for the specific criteria. The new technique resolves the NRC staff's previous concerns with AREVA's statistical approach. Several model upgrades have been included in the current version of the Evaluation Model and details of the changes are presented herein. The method is called the AREVA PWR Realistic LBLOCA (RLBLOCA) Revision 3.

This report documents a road map to the methodology, patterned after the Code Scaling, Applicability, and Uncertainty (CSAU) methodology. The thermal-hydraulic computational tool used in AREVA's RLBLOCA Revision 3 is S-RELAP5. The models and correlations used in the code are also documented here. The sections describing the models and correlations are taken from the approved topical report with minimal revisions. Application to a Westinghouse and AREVA 3-loop and 4-loop plant designs along with a Combustion Engineering 2x4 plant design are given as a demonstration of RLBLOCA Revision 3, following the technical bases of the methodology changes.

1.0   INTRODUCTION

This report describes the AREVA NP Inc. (AREVA) methodology developed for the realistic evaluation of a large break loss-of-coolant accident (LBLOCA) for pressurized water reactors (PWRs) with recirculation (U-tube) steam generators. Specifically, Westinghouse 3- and 4-loop designs; Combustion Engineering (CE) 2x4 designs; and AREVA 3- and 4-loop designs, all with fuel assembly lengths of 14 feet or less and emergency core cooling system (ECCS) injection to the cold legs, are covered.

The methodology was originally developed by AREVA in the early 2000s and approved by the NRC as EMF 2103(P)(A), Revision 0 in April 2003 (Reference 1-1). The current work, Revision 3, provides additional technical evaluations (clad swelling, rupture, and fuel relocation), not included in Revision 2 (Reference 1-2), those in Supplement 1 and others (Reference 1-3), and modifies the documentation to follow the recommendations of Regulatory Guide 1.203 (Reference 1-4), Evaluation Model Development and Assessment Process (EMDAP). The structure of Revision 0 and Revision 2 followed the steps identified in NUREG/CR-5249, "Quantifying Reactor Safety Margins" (Reference 1-5) which describes the uncertainty evaluation methodology called Code Scaling, Applicability, and Uncertainty (CSAU) and its application to a LBLOCA. The documentation and supporting material was previously provided in four separate documents: EMF-2103, Revision 2 – the topical report itself, the corresponding Supplement 1 to Revision 2, EMF-2100 – the S-RELAP5 models and correlations code manual (Reference 1-6), and, EMF-2102 – the code verification and validation document (Reference 1-7). As mentioned above, to provide a comprehensive description of the evaluation model, the material has been reorganized into the structure outlined in the EMDAP, presented in the Regulatory Guide 1.203 (Reference 1-4), and is provided in a unitary report. The present document, Revision 3, represents this version of the RLBLOCA methodology.

1.1   *Roadmap*

Table 1-1 below summarizes the modifications and improvements applied to the AREVA EMF-2103(P)(A) Revision 0 and subsequent RLBLOCA methodology packages. Further details on these upgrades are presented in Section 2.3.

Table 1-1   Summary of Improvements from Revision 0 Methodology

Technical Upgrade	Description & Implementation Phase	Upgrade Status
Wong-Hochreiter Correlation	The Forslund-Rohsenow correlation is no longer used in the core heat transfer to determine the fuel cladding temperature. For the dispersed flow film boiling regime in the core, Wong-Hochreiter with enhancements replaces the use of Sleicher-Rouse. Implemented in Revisions 2 and 3	See Note 1.
Rod-to-Rod Radiation	The Rod-to-Rod Radiation upgrade more accurately predicts reflood heat transfer. Provision for separate radiation enclosures for each burned rod is provided. Implemented in Revisions 2 and 3	See Note 1.
Cold Leg Condensation Model	More accurate modeling of the cold leg condensation during the pumped ECC injection phase resulting in near saturated fluid conditions at the downcomer entrance which conservatively increases the potential for downcomer boiling. Implemented in Transition Package and Revision 3	See Note 2.
Statistical Evaluation	Upgraded with the application of a multivariate evaluation. Implemented in Revision 3	See Note 1.
Fuel Performance Code	The fuel initial conditions code COPERNIC replaces RODEX3A, providing a better prediction of burnup dependent fuel pellet thermal conductivity. Implemented in Revision 2	See Note 1.
Second Cycle Fuel	Direct calculation of second cycle fuel performance is accomplished through this upgrade, expanding the range of evaluations and ensuring that fuel experiencing the second burn will be evaluated and, if limiting, recognized as limiting. Implemented in Transition Program, Supplement 1	See Note 2.

Technical Upgrade	Description & Implementation Phase	Upgrade Status
Break Modeling	Break modeling approach was altered from EMF-2103, Rev. 0 to follow the Regulatory Guide 1.157 guidance. The split versus double-ended break type is no longer related to break area. Implemented in Transition Program	See Note 2.
Interfacial Drag Package	The S-RELAP5 code has been significantly upgraded with modified interfacial drag package. Implemented in Revision 2	See Note 1.
Reported Local Cladding Oxidation	Interior oxidation of the cladding accounted for compliance with the maximum local oxidation criteria. Implemented in Supplement 1	See Note 1.
Decay Heat Simulation	The treatment of decay heat, which in EMF-2103, Rev. 0 had been sampled according to the standard deviation presented in the 1979 ANS standard, has been replaced by a fixed, non-sampled, application of the 1979 ANS standard. Implemented in Supplement 1	See Note 2.
Fuel Swelling, Rupture and Relocation	The fuel swelling, rupture and relocation model, based on a statistical approach, has been added to improve the evaluation of fuel rod rupture during LOCA through mechanistic behavior and it includes a sub-channel cooling model. Implemented in Revision 3	See Note 1.
Clarification of Single Failure	The treatment of single failure within the EM is upgraded to clarify the approach. Implemented in Revision 3	See Note 2.
Correction to the Steam Absorptivity	A correction to the steam absorptivity was made and a conservative limit was set on the pressure in computing the vapor absorption coefficient. Implemented in Revision 3	See Note 1.
Core Nodalization	The core nodalization has been slightly changed to align the node boundaries with the bottom of the grid spacers, rather than the grid centerline. Implemented in Revision 3	See Note 1.

AREVA Inc.

Realistic Large Break LOCA Methodology for Pressurized Water Reactors
Topical Report

EMF-2103NP
Revision 3

Page 1-5

Technical Upgrade	Description & Implementation Phase	Upgrade Status
Grid Spacer Droplet Breakup Heat Transfer Enhancement	A model to increase the heat transfer downstream of a grid spacer due to droplet breakup was added. Implemented in Revision 3	See Note 1.
Interphase Heat Transfer	The interphase heat transfer for mist flow has been improved to obtain better agreement with separate effects reflood test data. Implemented in Revision 3	See Note 1.
SG Tube Inlet Interfacial Drag	Modification of the steam generator tube inlet drag as a result of an error correction to the level tracking model. Implemented in Revision 3	See Note 1.
Sampling of Core Power	The core power is treated deterministically using the nominal power plus uncertainty. Implemented in Revision 2	See Note 2.
Treatment of GDC-35	The GDC-35 requirement of off-site power is satisfied by [ ] Implemented in Revision 3	See Note 1.

Notes:

1. This EM element of EMF-2103, Rev. 3 has not yet been reviewed and approved by the NRC.

2. This EM element of EMF-2103, Rev. 3 has been reviewed and approved by the NRC in several LARs, most recently in the following reference:
Letter from T. Orf, NRC to M. Nazar, Florida Power and Light Company, "St. Lucie Plant, Unit 1 – Issuance of Amendment Regarding Extended Power Uprate (TAC No. ME5091)," July 9, 2012 (ADAMS Accession No. ML 12181A019).

1.2   *References*

1-1   EMF-2103(P)(A) Revision 0, "Realistic Large Break LOCA Methodology," Framatome ANP Richland, Inc., April 2003.

1-2   EMF-2103(P) Revision 2, "Realistic Large Break LOCA Methodology,"
       AREVA NP, Inc., November 2010.

1-3   EMF-2103(P) Revision 2, Supplement 1, "Realistic Large Break LOCA
       Methodology," AREVA NP, Inc., December 2011.

1-4   Regulatory Guide 1.203, "Transient and Accident Analysis Methods,"
       U.S. NRC, December 2008.

1-5   NUREG/CR-5249, "Quantifying Reactor Safety Margins, Application of
       Code Scaling, Applicability, and Uncertainty Evaluation Methodology to
       a Large Break, Loss-of-Coolant Accident," U.S. NRC, December 1989.

1-6   EMF-2100(P) Revision 16, "S-RELAP5 Models and Correlations Code
       Manual," AREVA NP, Inc., December 2011.

1-7   EMF-2102(P) Revision 1, "S-RELAP5 Code Verification and Validation,"
       AREVA NP, Inc., November 2010.

AREVA Inc.

Realistic Large Break LOCA Methodology for Pressurized Water Reactors
Topical Report

EMF-2103NP
Revision 3

Page 2-1

2.0   SUMMARY

This section provides an overview of the methodology and its development. Revision 3 is a comprehensive improvement to the original RLBLOCA methodology documented in EMF-2103(P)(A) Revision 0 (Reference 2-1). A large body of the work that supported Revision 0 still remains applicable to Revision 3 and implicitly to Revision 2 (Reference 2-10). Thus, although the documentation provided herein is complete and self-sufficient, much of the content is the same as was provided in Revision 0 and Revision 2.

The development of the Revision 0 and Revision 2 of the RLBLOCA methodology followed the Regulatory Guide 1.157 (Reference 2-2) and the CSAU methodology (Reference 2-3). In December 2005, the NRC published the Regulatory Guide 1.203 (Reference 2-4) which describes an acceptable Evaluation Model Development Process and Assessment (EMDAP) to guide the development and assessment of the EMs that may be used to analyze transient and accident behavior within the design basis of a nuclear power plant. Regulatory Guide 1.203 supports the CSAU methodology (Reference 2-3) as an application of the EMDAP principles in the quantification of uncertainties for a best-estimate LBLOCA evaluation methodology. Additionally, the Standard Review Plan (Reference 2-5) points to Regulatory Guide 1.157 as one of the frames providing guidance and requirements for the EMs that may be used to demonstrate compliance with the acceptance criteria for ECCS performance.

This report provides a description of the AREVA PWR realistic LBLOCA (RLBLOCA) methodology and demonstrates its application to representative nuclear power plants. The methodology development followed the CSAU methodology and the documentation is provided, to the extent possible, in a format consistent with the steps outlined in the Regulatory Guide 1.203 EMDAP.

AREVA Inc.

EMF-2103NP
Revision 3

Realistic Large Break LOCA Methodology for Pressurized Water Reactors
Topical Report

Page 2-2

The AREVA RLBLOCA EM adheres to the six basic principles of EM development and assessment outlined in Regulatory Guide 1.203:

1. Determine requirements for the evaluation model.

2. Develop an assessment base consistent with the determined requirements.

3. Develop the evaluation model.

4. Assess the adequacy of the evaluation model.

5. Follow an appropriate quality assurance protocol during the EMDAP.

6. Provide comprehensive, accurate, up-to-date documentation.

2.1   *Evaluation Model Approach Overview*

The AREVA Realistic Large Break LOCA evaluation model is based on the forward propagation of input uncertainty through Monte-Carlo simulations with random sampled inputs and the application of nonparametric statistics to characterize and evaluate potential large break LOCA results for the population of possible large break LOCAs. In this endeavor, the LOCA predictions of S-RELAP5 and the support codes, as impacted by the uncertainties of key parameters, are accepted as representing large break LOCA results from accidents within the population. This acceptance is based on a wide range of the validation and benchmarking analyses covering the range of potential application of the methodology. The code package is then executed repeatedly with correlation and input variation sampled randomly according to the probability of their occurrence to establish a set of possible large break LOCA results from within the population. This set of cases comprises a sampling of the population and can be evaluated by order statistics approaches to characterize the population and determine the probability distribution of LOCA results. [

]

This population is determined through the establishment of the scenario for large break LOCAs and is basically all LOCAs from breaks in high pressure pipes with total discharge areas between 0.1 and 2 times the cross-sectional area of the largest cold leg pipe in the system. The specific steps in the evaluation of a plant are:

1. Establish a base S-RELAP5 model, including the containment model for the plant (described in Section 9.1),

2. Based on a random selection, execute as many LOCA cases, each an event from the population of LOCAs, as required to produce 95 percent confidence that 95 percent of the population meets the criteria of 10CFR50.46.

A. Determine sampled parameters randomly and run S-RELAP5 to steady state (described in Section 9.2).

B. Initiate the break and execute S-RELAP5 through to the completion of the resultant transient (described in Section 9.3).

C. Extract the calculated values for each of the three parameters limited by 10CFR50.46 (peak cladding temperature, maximum cladding oxidation, and maximum hydrogen generation), [

] and determine if the results corresponding to the 95/95 bound meets the 10CFR50.46 limits (described in Section 9.4).

2.2   *Report Organization*

This report is structured in 10 Sections covering the 20 steps outlined in Regulatory Guide 1.203, EMDAP, and overlapping the 14 steps defined in CSAU. A brief description of the report structure is provided below.

Section 1.0 Introduction

The introduction provides a short history of the RLBLOCA methodology from Revision 0 to the present report.

Section 2.0 Summary and Conclusions

The summary presents conclusions as to how this evaluation meets NRC requirements for licensing analysis use to verify that plant systems meet the regulations, an overview of the realistic methodology, the organization of the report, and a listing of the changes to the EM incorporated into Revision 3.

Section 3.0 Regulatory Requirements

This section describes the regulatory requirements for the RLBLOCA EM and specifically how they are satisfied.

Section 4.0 Scenario Identification

This section describes the first two steps of the EMDAP, namely Element 1, Step 1 (E1.S1) Specify Analysis Purpose, Transient Class, and Power Plant Class and E1.S2 Specify Figures of Merit. The corresponding steps from the CSAU methodology are Step 1 Scenario Specification (Reference 2-10, Section 2.1) and Step 2 Nuclear Power Plant Selection (Reference 2-10, Section 2.2).

Section 5.0 Evaluation Model Requirements

This section presents the Evaluation Model requirements and summarizes them in the Phenomena Identification and Ranking Table (PIRT), which provides the basis for determining code applicability (does the code properly model the important phenomena); establishing the assessment matrix (identifying test data that contain the appropriate phenomena during each accident phase), and identifying phenomenological parameters to be ranged and quantified for evaluating uncertainties. Section 5.0 corresponds to Element 1, Steps 3 and 4 (E1.S3 and E1.S4) of EMDAP and CSAU Step 3, and it incorporates Section 2.3 of Reference 2-10.

Section 6.0 Assessment Data Base Description

This section provides the objectives for the assessment base, identifies the existing data being used for EM development, presents an assessment matrix which lists the test facilities, the actual tests analyzed from each test facility, and the associated phenomena being examined. This section covers applicable steps from Element 2 of EMDAP and corresponds to CSAU Step 7 (Section 3.1 of Reference 2-10).

Section 7.0 Evaluation Model Computer Codes Description

This section describes in detail the S-RELAP5 code, including the COPERNIC and ICECON modules used in the evaluation model. It provides detailed descriptions of the models and correlations implemented in S-RELAP5 and relevant to the RLBLOCA EM. This section addresses Steps 10 through 13 of the Element 3 and Steps 13, 15, 16, and 17 of Element 4 of EMDAP. It also covers Steps 4, 5, and 6 of the CSAU methodology. The content provided in this section originates mainly from the relevant segments of EMF-2100 S-RELAP5 Models and Correlations Code Manual (Reference 2-6), as well as Sections 3.4, 3.5, 3.6 of Reference 2-10, and the relevant portions from the ICECON theory and user's manual (References 2-7 and 2-8). New content has been added to describe the revised model for Fuel Swelling, Rupture and Relocation (FSRR).

Section 8.0 Assessment Results

This section presents the results of the assessment process intended to demonstrate the code capabilities for simulation of important phenomena primarily associated with large-scale PWR systems LBLOCA. The material previously presented in Reference 2-10, Sections 3.3 and 3.4 has been greatly expanded by including all the relevant material from EMF-2102 S-RELAP5 Code Verification and Validation (Reference 2-9). Section 8.0 addresses the remaining steps from Element 4 of EMDAP as well as Steps 9 and 10 of the CSAU.

Section 9.0 Evaluation Model Implementation

This section describes the implementation of the Evaluation Model, including the nodalization definition and the sensitivity and uncertainty analysis, covering Step 9 and 11 through 14 of the CSAU. The relevant sections from Supplement 1 of Revision 2 (Reference 2-11) have also been incorporated into this section.

Section 10.0 Quality Assurance

This section outlines the Quality Assurance (QA) requirements fulfilled in preparing the package.

Appendices

Appendix A presents in an abridged format the model input development guidelines and the analysis guidelines as currently implemented in the internal AREVA calculation process for performing RLBLOCA licensing analyses

Appendix B describes sample licensing analyses performed with the RLBLOCA EM for three base models of NPPs, each representative of a specific class.

Appendix C addresses SER restrictions on Revision 0, which are no longer applicable to Revision 3.

Appendix D presents system analysis time step sensitivity study to demonstrate the adequacy of S-RELAP5 numerics.

2.3   *Technical Upgrades from Revision 0 of the Methodology*

Although the Revision 3 documentation is complete and self-contained, the methodology builds on and incorporates much of the Revision 0 approach. The following list contains the additions or changes from Revision 0 and identifies their previous documentation. This includes items of the "Transition Program," additions included in Revision 2, those added in Supplement 1 to Revision 2, and additions originally provided here in Revision 3.

1. Wong-Hochreiter Correlation – Revisions 2 and 3

   The Forslund-Rohsenow (F-R) correlation is no longer used in the core heat transfer that determines the fuel cladding temperature. The F-R correlation is still used for the passive metal heat structure heat transfer. For the dispersed flow film boiling regime in the core, Wong-Hochreiter with enhancements replaces the use of Sleicher-Rouse. This alteration was adopted as a model improvement. The modified approach to flow film boiling in the core is presented in Section 7.6.7.2 and is assessed in Sections 8.2.1, 8.2.4, 8.4.1 and 8.4.4. A temperature correction was added to the Wong-Hochreiter heat transfer correlation and is also presented in Section 7.6.7.2, while its impact is qualitatively assessed in Section 8.1.5.

2. Rod-to-Rod Radiation – Revisions 2 and 3

   A rod-to-rod radiation model has been incorporated into the methodology and the reflood heat transfer benchmarking has been redone. This upgrade was incorporated to more accurately assess reflood heat transfer by recognizing the individual components of the process. The alteration is presented in Section 7.6.8.2 and assessed in Sections 8.2.5, 8.5.2.4 and 8.6.2.1. The model was subsequently revised in Revision 3 to implement separate radiation enclosures for each burned rod, rather than one enclosure for all burned rods. The model change is presented in Appendix A and its impact qualitatively assessed in Section 8.1.5.

3. Cold Leg Condensation Model – Transition Package and Revision 3

   A cold leg condensation model, specific to both the accumulator and the pumped injection period of the accident, has been incorporated. The revised model predicts more accurately the cold leg condensation during the pumped ECC injection phase resulting in near saturated fluid conditions at the downcomer entrance, thus conservatively increasing the potential for downcomer boiling. This alteration is presented in Sections 8.2.9, 8.2.10, and 8.5.1.14.

4. Statistical Evaluation – Revision 2

   The statistical evaluation has been upgraded to provide a multivariate evaluation.
   This alteration is presented in Section 9.4.

5. COPERNIC Fuel Performance Code – Revision 2

   This change has been applied in response to NRC concerns over thermal
   conductivity degradation. The COPERNIC fuel performance code has replaced
   RODEX3A as the source of fuel initial conditions. COPERNIC is NRC approved for
   application to M5 cladding.

6. Second Cycle Fuel – Transition Program, Supplement 1

   The methodology has been upgraded such that a direct calculation of second cycle
   fuel performance is accomplished. This expands the range of evaluations and
   ensures that fuel experiencing its second burn will be evaluated and, if limiting,
   recognized as limiting. This alteration is presented in Appendix A.

7. Break Modeling – Transition Program

   The break modeling was altered from EMF-2103, Revision 0 to concur with the
   approach outlined in Regulatory Guide 1.157. The split versus double-ended break
   type is no longer related to break area. This alteration is presented in Section
   8.5.2.6.

8. Interfacial Drag Package – Revision 2

   The interfacial drag package has been modified with improved logic for transition
   between flow regimes to cover a wider range of experimental data. This serves to
   update the state-of–the-art of S-RELAP5. The details of this alteration are
   presented in Section 7.5.2.

AREVA Inc.

EMF-2103NP
Revision 3

Realistic Large Break LOCA Methodology for Pressurized Water Reactors
Topical Report

Page 2-10

9. Reported Local Cladding Oxidation – Supplement 1

The accounting of the operational (pre-transient) and interior oxidation of the cladding for compliance with the maximum local oxidation criteria of 10 CFR 50.46 is presented in Section 7.9.3.5 and Appendix A, sub-section A.2.3.10.

10. Decay Heat Simulation – Supplement 1

The decay heat calculation, which in EMF-2103, Revision 0 had been sampled according to the standard deviation presented in the 1979 ANS standard, has been replaced by a fixed, non-sampled, application of the 1979 standard which bounds possible decay heat values for Uranium Oxide fuel. The change, previously presented in Supplement to Revision 2, provides assurance that the transient power of the fuel rod is not undervalued. The fixed, non-sampled application of the 1979 standard bounds the best estimate method. The details of this change are presented in Section 8.5.1.17.

11. Fuel Swelling Rupture and Relocation (FSRR) Modeling – Revision 3

A model for FSRR based on a statistical approach for geometry and the evaluation of cooling for a fuel rod isolated from other ruptures has been added. This model improves the evaluation of fuel rod rupture during LOCA through a mechanistic approach and it includes a sub-channel cooling model. The details of this change are presented in Section 7.9.3.3.

12. Clarification of Single Failure – Supplement 1

The documentation of the treatment of single failure within the evaluation model is upgraded to clarify the approach. The revised documentation is provided in Appendix A, sub-section A.2.4.1.1.

13. Correction to the Steam Absorptivity – Revision 3

A correction to the steam absorptivity was made. In computing the vapor absorption coefficient, the pressure is conservatively truncated at **[   ]** psi. This alteration is presented in Section 7.6.8.1 and its impact qualitatively assessed in Section 8.1.5.

14. Core Nodalization – Revision 3

The core nodalization has been slightly changed to align the node boundaries with the bottom of the grid spacers, rather than the grid centerline. The change in the core nodalization effectively changes the hydrodynamic volume boundaries such that they are aligned with the bottom of the grid spacers, in support of the implementation of the grid droplet shattering model (item #15 below). This alteration is presented in Section 9.0 and Appendix A and its impact qualitatively assessed in Section 8.1.5.

15. Grid Spacer Droplet Breakup Heat Transfer Enhancement – Revision 3

A model to increase the heat transfer downstream of a grid spacer due to droplet breakup was added. The implementation of a model to increase the heat transfer downstream of a grid spacer is expected to have an impact during reflood above the mid-plane of the core. This alteration is presented in Section 7.5.4.10.1 and its impact verified in Sections 8.2.3 and 8.4.1.

16. Interphase Heat Transfer – Revision 3

The interphase heat transfer for mist flow was modified to raise steam and cladding temperatures and to obtain better agreement with test data from separate effects reflood tests. The details of this change are presented in Section 7.5.4.

17. Steam Generator Tube Inlet Interfacial Drag – Revision 3

An error correction to the level tracking model required modification of the steam generator tube inlet drag. The model change is presented in Appendix A and its impact is qualitatively assessed in Section 8.1.5.

AREVA Inc.

EMF-2103NP
Revision 3

Realistic Large Break LOCA Methodology for Pressurized Water Reactors
Topical Report

Page 2-12

18. Sampling of Core Power – Revision 2

The methodology has been changed such that core power is treated deterministically using the nominal power plus uncertainty. The model change is presented in Section 3.1.3.2.2.

19. Treatment of GDC-35 – Revision 3

GDC-35 states that the plant shall be able to mitigate design basis accidents with or without offsite power available. The methodology satisfies this requirement by determining the most severe condition between these two configurations by

[

] The change is discussed in Section A.2.4.2.

2.4 *References*

2-1   EMF-2103(P)(A) Revision 0, "Realistic Large Break LOCA Methodology," Framatome ANP Richland, Inc., April 2003.

2-2   Regulatory Guide 1.157, "Best-Estimate Calculations of Emergency Core Cooling System Performance," U.S. NRC, May 1989.

2-3   NUREG/CR-5249, "Quantifying Reactor Safety Margins, Application of Code Scaling, Applicability, and Uncertainty Evaluation Methodology to a Large Break, Loss-of-Coolant Accident," U.S. NRC, December 1989.

2-4   Regulatory Guide 1.203, "Transient and Accident Analysis Methods," U.S. NRC, December 2008.

2-5   NUREG-0800, "Standard Review Plan, Section 15.6.5 Loss-Of-Coolant Accidents Resulting from Spectrum of Postulated Piping Breaks within the Reactor Coolant Pressure Boundary," Revision 3, U.S. NRC, March 2007.

2-6   EMF-2100(P) Revision 16, "S-RELAP5 Models and Correlations Code Manual," AREVA NP, Inc., December 2011.

2-7   EMF-CC-039(P) Revision 4, "ICECON: A Computer Program Used to
        Calculate Containment Back Pressure for LOCA Analysis (Including Ice
        Condenser Plants)," December 2007.

2-8   EMF-CC-039(P) Supplement 1 Revision 5, "ICECON Code User's
        Manual: A Computer Program Used to Calculate Containment Back
        Pressure for LOCA Analysis (Including Ice Condenser Plants)," July
        2007.

2-9   EMF-2102(P) Revision 1, "S-RELAP5 Code Verification and Validation,"
        AREVA NP, Inc., November 2010.

2-10   EMF-2103(P) Revision 2, Realistic Large Break LOCA Methodology,
        AREVA NP, Inc., November 2010.

2-11   EMF-2103(P) Revision 2, Supplement 1, "Realistic Large Break LOCA
        Methodology," AREVA NP, Inc., December 2011.

3.0   REGULATORY REQUIREMENTS

10 CFR 50.46, "Acceptance Criteria for Emergency Core Cooling Systems for Light-Water Nuclear Power Reactors," paragraph (a)(1)(i) requires that light-water nuclear reactors fueled with uranium oxide pellets within cylindrical Zircaloy or ZIRLO cladding must be provided with an emergency core cooling system (ECCS) that must be designed so that its calculated cooling performance following postulated loss-of-coolant accidents (LOCA) conforms to the criteria set forth in paragraph 50.46(b). Paragraph (a)(1)(i) of 10 CFR 50.46 briefly outlines the requirements for an acceptable evaluation model, and requires demonstration that the calculated ECCS cooling performance criteria, set forth in paragraph (b) of 10 CFR 50.46, be met with a high degree of probability. The ECCS cooling performance criteria outlined in 10 CFR 50.46(b) is as follows:

1. Peak cladding temperature. The calculated maximum fuel element cladding temperature shall not exceed 2200 °F.

2. Maximum cladding oxidation. The calculated total oxidation of the cladding shall nowhere exceed 0.17 times the total cladding thickness before oxidation. As used in this subparagraph total oxidation means the total thickness of cladding metal that would be locally converted to oxide if all the oxygen absorbed by and reacted with the cladding locally were converted to stoichiometric zirconium dioxide. If cladding rupture is calculated to occur, the inside surfaces of the cladding shall be included in the oxidation, beginning at the calculated time of rupture. Cladding thickness before oxidation means the radial distance from inside to outside the cladding, after any calculated rupture or swelling has occurred but before significant oxidation. Where the calculated conditions of transient pressure and temperature lead to a prediction of cladding swelling, with or without cladding rupture, the unoxidized cladding thickness shall be defined as the cladding cross-sectional area, taken at a horizontal plane at the elevation of the rupture, if it occurs, or at the elevation of the highest cladding temperature if no rupture is calculated to occur, divided by the average circumference at that elevation. For ruptured cladding, the circumference does not include the rupture opening.

3. Maximum hydrogen generation. The calculated total amount of hydrogen generated from the chemical reaction of the cladding with water or steam shall not exceed 0.01 times the hypothetical amount that would be generated if all of the metal in the cladding cylinders surrounding the fuel, excluding the cladding surrounding the plenum volume, were to react.

4. Coolable geometry. Calculated changes in core geometry shall be such that the core remains amenable to cooling.

5. Long-term cooling. After any calculated successful initial operation of the ECCS, the calculated core temperature shall be maintained at an acceptably low value and decay heat shall be removed for the extended period of time required by the long-lived radioactivity remaining in the core.

Criteria 1, 2, and 3 are addressed by the RLBLOCA methodology. The remaining two criteria, coolable geometry and long-term cooling, are treated separately during plant specific evaluations.

The methodology complies with the revised LOCA ECCS rule as issued by the NRC in 1989 (Reference 3-1). This rule allows the use of realistic LOCA evaluation models in place of the prescribed conservative evaluation models specified by 10 CFR 50 Appendix K, provided that it can be established with a high probability that the criteria of 10 CFR 50.46(b) are met.

The basis for the revised rule is a large body of research performed after the 1973 LOCA ECCS rule was implemented, which shows the prescribed Appendix K analysis methods are unnecessarily conservative. A compendium of ECCS research (Reference 3-2) was issued by the NRC in 1988 and references the relevant thermal-hydraulic research upon which the realistic LOCA rule was based.

The realistic evaluation model rule does not prescribe the analytical methods or uncertainty techniques to be used. However, Regulatory Guide 1.157 (Reference 3-3) was issued to provide guidance for realistic LOCA analyses. The NRC also independently developed and demonstrated the code scaling, applicability and uncertainty (CSAU) methodology (Reference 3-4) for quantifying uncertainties in realistic codes. The 95th percentile of the probability distribution is accepted (Reference 3-3) as providing the level of conservatism required by the 10 CFR 50.46.

AREVA Inc.

EMF-2103NP
Revision 3

Realistic Large Break LOCA Methodology for Pressurized Water Reactors
Topical Report

Page 3-4

3.1   *NUREG-0800, NRC Standard Review Plan (SRP) Compliance*

Section 15.6.5, Revision 3 of the NRC's SRP covers "Loss-of-Coolant-Accidents resulting from spectrum of postulated piping breaks within the reactor coolant pressure boundary." Specific SRP acceptance criteria acceptable to meet the relevant requirements of the NRC's regulations identified above are as follows for the review described in this SRP section. The SRP is not a substitute for the NRC's regulations, and compliance with it is not required. However, an applicant is required to identify differences between the design features, analytical techniques, and procedural measures proposed for its facility and the SRP acceptance criteria and evaluate how the proposed alternatives to the SRP acceptance criteria provide acceptable methods of compliance with the NRC regulations. Specific criteria necessary to meet the relevant requirements of the regulations identified above and necessary to meet the TMI Action Plan requirements are as follows:

1. An evaluation of ECCS performance has been performed by the applicant in accordance with an evaluation model that satisfies the requirements of 10 CFR 50.46. Regulatory Guide 1.157 and Section I of Appendix K to 10 CFR Part 50 provide guidance on acceptable evaluation models. For the full spectrum of reactor coolant pipe breaks, and taking into consideration requirements for reactor coolant pump operation during a small break loss-of-coolant accident, the results of the evaluation must show that the specific requirements of the acceptance criteria for ECCS are satisfied as given below. This also includes analyses of a spectrum of large break and small break LOCAs to ensure boric acid precipitation is precluded for all break sizes and locations.

The analyses should be performed in accordance with 10 CFR 50.46, including methods referred to in 10 CFR 50.46(a)(1) or (2). The analyses must demonstrate sufficient redundancy in components and features, and suitable interconnections, leak detection, isolation, and containment capabilities such that the safety functions could be accomplished assuming a single failure in conjunction with the availability of onsite power (assuming offsite electric power is not available, with onsite electric power available; or assuming onsite electric power is not available with offsite electric power available). Additionally the LOCA methodology used and the LOCA analyses should be shown to apply to the individual plant by satisfying 10 CFR 50.46(c)(2), and the analysis results should meet the performance criteria in 10 CFR 50.46(b).

A. The calculated maximum fuel element cladding temperature does not exceed 1200 °C (2200 °F).

B. The calculated total local oxidation of the cladding does not exceed 17 percent of the total cladding thickness before oxidation. Total local oxidation includes pre-accident oxidation as well as oxidation that occurs during the course of the accident.

C. The calculated total amount of hydrogen generated from the chemical reaction of the cladding with water or steam does not exceed 1 percent of the hypothetical amount that would be generated if all of the metal in the cladding cylinders surrounding the fuel, excluding the cladding surrounding the plenum volume, were to react.

D. Calculated changes in core geometry are such that the core remains amenable to cooling.

E. After any calculated successful initial operation of the ECCS, the calculated core temperature is maintained at an acceptably low value and decay heat is removed for the extended period of time required by the long-lived radioactivity.

AREVA Inc.

Realistic Large Break LOCA Methodology for Pressurized Water Reactors
Topical Report

EMF-2103NP
Revision 3

Page 3-6

AREVA's Compliance Statement: Sections 3.1.1 through Section 3.1.4 describes how AREVA's RLBLOCA methodology is in compliance with number one above. This topical report does not address numbers 1.D and 1.E; however, if the results of the LOCA evaluation meet the first three criteria of 10 CFR 50.46, items D and E should inherently be met.

2. The radiological consequences of the most severe LOCA are within the guidelines of and 10 CFR 100 or 10 CFR 50.67. For applications under 10 CFR Part 52, reviewers should use SRP Section 15.0.3, "Radiological Consequences of Design Basis Accidents - for ESP, DC and COL Applications."

AREVA's Compliance Statement: AREVA performs radiological consequences analysis of design basis accidents to demonstrate compliance with the dose limits specified in either 10 CFR 100 (for those operating power plants that make use of the classical methodology, through implementation of Regulatory Guides 1.3, 1.4 or 1.195) or 10CFR 50.67 (for those operating plants that have adopted the Alternative Source Term (AST) methodology, through implementation of Reg. Guide 1.183).

3. The TMI Action Plan requirements for II.E.2.3, II.K.2.8, II.K.3.5, II.K.3.25, II.K.3.30, II.K.3.31, and II.K.3.40 have been met.

AREVA's Compliance Statement: The TMI Action Plan requirements discussed in number three above are for a Small Break LOCA accident (SBLOCA), this topical report covers the LBLOCA accident.

The following sections describe the regulatory positions from RG 1.157 and how the RLBLOCA methodology follows the guidance provided.

AREVA Inc.

Realistic Large Break LOCA Methodology for Pressurized Water Reactors
Topical Report

EMF-2103NP
Revision 3

Page 3-7

3.1.1 Regulatory Position 1, "Best-Estimate Calculations

Regulatory Position 1 of RG 1.157 summarizes the regulatory movement from Appendix K-type calculations to a "best-estimate" or realistic analysis, reflecting the increased understanding of safety analysis obtained since the substantial conservatisms imposed during the early application of regulatory oversight. General attributes expected in a best-estimate calculation are described in this position. Specifically, any calculational procedure determined to be a best-estimate code in the context of RG 1.157 or for use under Paragraph 50.46(a)(1) should be compared with applicable experimental data to ensure that the calculation of important phenomena is realistic. NUREG/CR-5429 and RG 1.203 provide guidance for developing a best-estimate code, identifying important phenomena, and comparing the code to applicable experimental data.

AREVA NP has developed S-RELAP5, a RELAP5-based thermal-hydraulic system code, for performing realistic analyses of a large break loss-of-coolant accident (LBLOCA) in pressurized water reactors (PWRs) in compliance with the revised LOCA Emergency Core Cooling System (ECCS) rule (Reference 3-1). RELAP5 is a light water reactor (LWR) transient analysis code developed at the Idaho National Engineering Laboratory (INEL) for the U. S. Nuclear Regulatory Commission (NRC) as part of the NRC's best-estimate transient code development program.

Comparisons of S-RELAP5 calculations with data obtained from separate-effects and integral-effects tests have been used to determine the overall uncertainty and biases of the calculation, as recommended in Regulatory Position 1. The integral test simulations were also used to verify that important phenomena (such as emergency core cooling (ECC) bypass or entrainment/de-entrainment in the upper plenum) are adequately predicted. Following the guidance of NUREG/CR-5429 and RG 1.203, a peer reviewed Phenomena Identification and Ranking Table (PIRT) was used to identify the important phenomena (Section 5.2). Therefore, EMF-2103 meets the guidance of regulatory Position 1 of RG 1.157 by following the guidance of NUREG/CR-5429 and RG 1.203 in developing a best-estimate code, identifying important phenomena and comparing the code to experimental data that is applicable to the expected use of the model.

3.1.2   Regulatory Position 2, "Considerations for Thermal-Hydraulic Best-Estimate Codes"

Regulatory Position 2 describes the special considerations for thermal-hydraulic best-estimate codes. Some features that are acceptable for use in best-estimate codes are described with the caveat that models that address these features may be used only under the basic condition that a specific model is acceptable if it has been compared with applicable experimental data and shown to provide reasonable predictions. This document shows that the code to be applied in this methodology meets these considerations; and, therefore, can be used as a "best-estimate code."

3.1.2.1   Basic Structure of the S-RELAP5 Code

The thermal-hydraulic code used by AREVA NP for best-estimate LBLOCA analyses is an improved version of RELAP5 originally developed and assessed by the NRC and its contractors as part of the NRC's best-estimate transient code development program. S-RELAP5 is described in detail in Section 7.1.2.

The hydrodynamics modeling includes many generic component models and some special process models, all of which are described in detail in Section 7.0.

3.1.3   Regulatory Position 3, "Best-Estimate Code Features"

Specific examples of features that are considered acceptable best-estimate models are given in Regulatory Positions 3. Each of the features is discussed below.

3.1.3.1   Initial and Boundary Conditions and Equipment Availability

To identify the initial and boundary conditions and equipment available during the event, the event to be evaluated must be identified and well defined. NUREG/CR-5249 provides the CSAU process for defining the event scenario.

According to the CSAU process, the first step in the construction of a realistic evaluation model is the identification and description of the event to be evaluated. This is termed the event scenario. For the modeling described herein, the event is that of a LOCA. A reasonable and useful definition is provided by the Standard Review Plan (Reference 3-5).

> Loss-of-coolant accidents (LOCA) are postulated accidents that would result from the loss of reactor coolant, at a rate in excess of the capability of the normal reactor coolant makeup system, from piping breaks in the reactor coolant pressure boundary. The piping breaks are postulated to occur at various locations and include a spectrum of break sizes, up to a maximum pipe break equivalent in size to the double-ended rupture of the largest pipe in the reactor coolant pressure boundary.

A large break LOCA initiates with an instantaneous rupture of a reactor coolant system (RCS) pipe, resulting in the rapid loss-of-coolant from the RCS. It is the coolant loss and its replacement with emergency coolant that is the subject assessment of LBLOCA evaluation models. Two top level considerations apply to the model presented here:

1. The rupture or break occurs in the RCS piping. Although it is possible to envision ruptures in components, those events are considered beyond the design basis and not subjects for this evaluation model.

2. This evaluation model applies only to the larger possible breaks, break areas greater than 0.1 times the cross-sectional area of the largest flow area pipe within the RCS. Smaller breaks are evaluated with a separate evaluation model.

The rate of coolant loss is governed, in part, by the break area, which ranges from 0.1 times the largest pipe area to twice the area of the pipe within which the rupture occurred. For plants covered by this evaluation model, the break can occur in three locations:

1. The hot leg pipe between the reactor vessel and the steam generator (hot leg break).

2. The cold leg between the steam generator and the reactor coolant pump (pump suction break).

3. The cold leg between the reactor coolant pump and the reactor vessel (pump discharge break).

A LBLOCA evaluation must consider breaks at all of these locations. However, as shown in Section 4.0, the pump discharge break is the greatest challenge to the emergency equipment and results in the most severe consequences for the reactor core. Although a great deal of the modeling herein is applicable to any of the break locations; it is specific only for pump discharge breaks.

The initial conditions, boundary conditions, and equipment availability during the event are discussed in general in Section 4.1.1. The guidance for Regulatory Position 3.1 has been met by a well-defined event and appropriate initial, boundary conditions and available equipment for the event.

3.1.3.2   Sources of Heat during a Loss-of-Coolant Accident

Regulatory Guide 1.157 requires that the following sources of heat be accounted for:

*   Initial Stored Energy of the Fuel.

*   Fission Heat.

- Decay of Actinides.

- Fission Product Decay Heat.

- Metal-Water Reaction.

- Heat Transfer from Reactor Internals.

- Primary to Secondary Heat Transfer.

3.1.3.2.1   Initial Stored Energy of the Fuel

The initial stored energy in the fuel is based on calculations performed with AREVA's
COPERNIC (Reference 3-6) computer code, which is a detailed fuel rod code whose
models have been developed from, and benchmarked against, appropriate in-pile and
out-of-pile experiments. This code has been reviewed and approved by the NRC for
application to the current methodology.

The physical models of the COPERNIC code contain a number of model parameters
that are not accessible to measurement. These parameters can be indirectly
determined by calibration against experimental data. An experimental database has
been built that includes data and experimental results for a large number of fuel rods
irradiated in test and commercial reactors.

The behavior of these rods is calculated with the code and the results are compared to
the experimental data. Since the thermal and mechanical models are strongly coupled
by a series of feedback loops, code calibration is a long process that requires numerical
methods and multiple iterations.

The phase following the calibration is the validation: a comparison of the results from
the calibrated code to the experimental results. The main parameters used to perform
calibration and validation are the following:

- Fuel centerline temperature.

- Fission gas release.

AREVA Inc.

EMF-2103NP
Revision 3

Realistic Large Break LOCA Methodology for Pressurized Water Reactors
Topical Report

Page 3-12

- Helium balance.

- Pellet densification and swelling.

- Cladding diameter change due to creepdown.

- Cladding geometry change due to pellet-cladding mechanical interaction (PCMI).

- Cladding axial growth.

- Cladding waterside corrosion.

The goal is for the code to provide a best-estimate response (i.e., little or no bias on the average and no significant trend of local biases throughout the applicability range).

The COPERNIC calibration/validation database spans more than several thousand fuel rods irradiated in test and commercial reactors. For each rod, data is available to characterize the fuel rod and the irradiation history, as well as results of measurements recorded in real time and/or post-irradiation examination (PIE) results.

3.1.3.2.2 Fission Heat

[

]

AREVA Inc.

Realistic Large Break LOCA Methodology for Pressurized Water Reactors
Topical Report

EMF-2103NP
Revision 3

Page 3-13

3.1.3.2.3   *Decay of Actinides*

[

]

3.1.3.2.4   *Fission Product Decay Heat*

[

]

AREVA Inc.

Realistic Large Break LOCA Methodology for Pressurized Water Reactors
Topical Report

EMF-2103NP
Revision 3

Page 3-14

[

]

AREVA Inc.

EMF-2103NP
Revision 3

Realistic Large Break LOCA Methodology for Pressurized Water Reactors
Topical Report

Page 3-15

Model Evaluation Procedure for Fission Product Decay Heat

[

]

[

]

3.1.3.2.5   Metal-Water Reaction Rate

Energy released through the transient oxidation of cladding is calculated using the Cathcart-Pawel correlation for oxide layer growth, as described in Section 7.9.3.5. The sum of the pre-transient and transient oxidation is compared to the total cladding maximum oxidation limit.

3.1.3.2.6   Heat Transfer from Reactor Internals

The heat release from the reactor vessel walls affects the ECC bypass during the early refill phase of a LBLOCA when the primary system is depressurizing. During the reflood phase, the heat release from the downcomer walls affects downcomer boiling. The results from UPTF Tests 6 and 7 demonstrated that S-RELAP5 will over-predict ECC bypass; however, the downcomer wall temperature was much lower than would be expected in an actual operating plant. Therefore, the hot wall effects can only be partially evaluated using these tests. The hot wall effect can be separated out since it is expected that there is a direct relationship with the degree of nucleate boiling in the downcomer and ECC bypass. To maximize the hot wall effect, heat transfer in the downcomer can be locked into nucleate boiling during the refill phase by raising the CHF point to a high value. In the AREVA NP methodology, the hot wall effect during the refill phase [

]

During the reflood phase, the downcomer vessel wall heat release is conduction limited and depends on the mesh spacing used in the S-RELAP5 input model. The mesh spacing used to model the downcomer vessel was verified by using a simple benchmark having a closed form solution. The results show that S-RELAP5 will adequately calculate the heat release from the downcomer vessel wall during the reflood phase of a LBLOCA in a PWR.

3.1.3.2.7   Primary-to-Secondary Heat Transfer

The analysis of steam generator heat transfer is essentially identical to the traditional approach used by other large thermal-hydraulic codes. Steam generator models for Westinghouse and CE PWRs include inlet plenums, exit plenums and U-tubes on the primary side and downcomer, boiler region, swirl vanes, separator, and steam dome on the secondary side. The inlet and exit plenums are modeled with a component used to describe a single volume and its junctions with the steam generator U-tubes and RCS piping. The U-tubes are modeled with eight (excluding the tube sheet) equal-length volumes (four with +90° orientation and four with -90° orientation). On the secondary side, the downcomer is represented by a seven volume component and the boiler region is modeled with a component with four volumes matching the volume elevation on the primary side. Above the boiler region, the swirl vanes and separator volumes are each modeled with a specialized component, and the steam dome region is modeled with a single volume.

The dominant phenomena of importance are the steady-state heat balance and steam binding during reflood. Heat balance is ensured by the use of control systems controlling feed water and steam flow depending on steam generator inventory. Benchmark simulations of the CCTF tests (Section 8.2.13) showed S-RELAP5 conservatively estimates the steam binding effect in the steam generator tubes.

3.1.3.2.8   Thermal Parameters for Swelling and Rupture of the Cladding and Fuel Rods

There is a potential for an increase in cladding heat load due to possible clad ballooning and rupture followed by fuel relocation.   [

]

A statistical model of the swelling and rupture of fuel rod cladding with a consequent relocation of fuel material was developed. The model utilizes system and core conditions determined during the RLBLOCA uncertainty analysis. This model statistically evaluates the geometric considerations of swelling, rupture, and fuel relocation in a fuel rod.   [

] The model will be evaluated by the Nuclear Regulatory Commission staff for applicability within the methodology described herein.

3.1.3.2.9   Other Core Thermal Parameters

Additional parameters (e.g., thermal properties of materials, behavior of control systems) are treated in a best-estimate fashion with a significant history of experimental evidence to support them.

3.1.3.3   Blowdown Phenomena

3.1.3.3.1   *Break Characteristics and Flow*

Break flow is a function of break area and critical flow uncertainty.   [

]

The S-RELAP5 HEM critical flow model applied in this methodology was assessed by comparison to full-scale critical flow tests at the Marviken facility, (Section 8.2.7).

[

]

This methodology is considered to be in compliance with Regulatory Position 3.1.

3.1.3.3.2   ECC Bypass

"The best-estimate code should contain a calculation of the amount of injected cooling water that bypasses the vessel during the blowdown phase of the loss-of-coolant accident."

[

]

The dominant downcomer LBLOCA phenomena (e.g., condensation, hot wall effects, multi-dimensional flow, CCFL, entrainment) affect the refill period. These phenomena primarily influence the duration of ECCS bypass. The hot wall effect is conservatively treated by forcing nucleate boiling for any portion of the downcomer in contact with water. The S-RELAP5 code prediction of the ECC bypass during the refill phase of a LOCA was demonstrated to be conservative through the assessment of UPTF Tests 6 and 7 (Section 8.2.9.3). In addition, a CCFL correlation developed by MPR Associates has been used in the sample plant cases (Appendix B) to demonstrate that S-RELAP5 conservatively calculates the bottom of core recovery (or beginning of core reflood) time. The MPR correlation is described in Section 8.6.2.2.7. Acceptable downcomer entrainment during the reflood phase was demonstrated for the CCTF benchmarks discussed in Section 8.2.13.

Based on these results, it is concluded that S-RELAP5 will appropriately calculate the ECC bypass, the core recovery time, and will calculate realistic downcomer entrainment during the reflood phase of a LBLOCA in PWRs where the ECCS delivery to the reactor vessel is not limited to locations adjacent to the broken cold leg.

AREVA Inc.

EMF-2103NP
Revision 3

Realistic Large Break LOCA Methodology for Pressurized Water Reactors
Topical Report

Page 3-21

3.1.3.3.3 Noding Near the Break and ECCS Injection Point

Regulatory Guide 1.157 states: "Sufficient sensitivity studies should be performed on the noding and other important parameters to ensure that the calculations provide realistic results."

The AREVA NP break model is either a double-ended guillotine with discharge from both cold leg volumes or a split with discharge from both cold leg volumes. The difference between the guillotine and the split is that the flow path between the two cold leg volumes at the break plane is preserved for a split break and closed for a guillotine break.

Generally, using small volume sizes is disadvantageous when S-RELAP5 attempts to simulate highly nonlinear phenomena (e.g., phenomena created by rapidly changing water properties). In this situation, parameters exploited by the closure relationships (e.g., water properties used to predict choked flow) may vary widely from one case to another. The cold leg volumes selected, being somewhat large, tend to reduce variability.

3.1.3.3.4 Frictional Pressure Drop

The wall friction model consists of two main parts:

1. Computing the overall two-phase wall-friction pressure drop.

2. Apportioning the total wall friction into liquid and vapor components.

Section 7.5.5 describes the development of this model. In general, the two-phase friction multiplier approach, with the two-phase multiplier calculated from the Heat Transfer and Fluid Flow Service (HTFS) modified Baroczy correlation, is used to obtain the total wall-friction pressure drop, which is independent of flow regimes. The phasic friction factor model, from which Chisholm developed a theoretical basis for the Lockhart-Martinelli friction correlation, is used to develop the phasic partition factors, which depend on flow regimes.

AREVA Inc.

EMF-2103NP
Revision 3

Realistic Large Break LOCA Methodology for Pressurized Water Reactors
Topical Report

Page 3-22

The Ferrell-McGee test section was modeled by S-RELAP5 using the specified flow rate for the inflow boundary conditions, the test pressure for the outlet boundary condition, and the specified pipe dimensions where the area change included form losses. The calculated two-phase pressure drop from the Ferrell-McGee simulation was within 10 percent of the measured data and, therefore, is in agreement with the data. This agreement demonstrates that the two-phase wall friction is acceptable, especially at low pressures, and that using the single-phase loss coefficient for abrupt area changes under two-phase conditions is also acceptable. Therefore, S-RELAP5 is expected to accurately model the two-phase frictional pressure drop and the two-phase pressure drop form loss modeling in the RLBLOCA Revision 3 plant model during a LBLOCA analysis.

3.1.3.3.5 Momentum Equation

Regulatory Guide 1.157 requires that the following effects be taken into account in the two-phase conservation of momentum equation:

- Temporal change in momentum.

- Momentum convection.

- Area change momentum flux.

- Momentum change due to compressibility.

- Pressure loss resulting from wall friction.

- Pressure loss resulting from area change.

- Gravitational acceleration.

These effects are each treated in a manner consistent with that utilized by state-of-the-art USNRC research codes, and are assessed to the individually verified and assessed against the significant base of benchmarks and experimental evidence (Section 8.0).

3.1.3.3.6   Critical Heat Flux

Regulatory Guide 1.157 states:

> "Best estimate models developed from appropriate steady-state or transient
> experimental data should be used in calculating critical heat flux (CHF)
> during loss-of-coolant accidents. The codes in which these models are used
> should contain suitable checks to ensure that the range of conditions over
> which these correlations are used are within those intended."

Critical heat flux (CHF) determines the boundary between nucleate boiling and
transition boiling. In general, correlations are used to compute critical heat flux. The
CHF correlation used by the S RELAP5 is from RELAP5/MOD2 and is composed of the
Biasi correlation for high flow rate, and the modified Zuber correlation for low flow rate,
as documented in Section 7.6.4.1.

The Bennett Heated Tube Tests were conducted by the UKAEA Research Group to
measure the dry-out (or critical heat flux (CHF)) location and the surface temperature
profiles in the region beyond the dry-out point. Calculations for Test Case 5-358 and
Test Case 5-379 were performed, and are documented in Section 8.2.2. The main
purpose of the assessment is to validate the applicability of the Biasi CHF correlation.
Post-CHF heat transfer is also examined. The assessment applies to both LBLOCA and
SBLOCA.

3.1.3.3.7   Post-CHF Blowdown Heat Transfer

With regards to post-CHF blowdown heat transfer, RG 1.157 states:

> "Models of heat transfer from the fuel to the surrounding fluid in the post-
> CHF regimes of transition and film boiling should be best estimate models
> based on comparison to applicable steady-state or transient data. Any
> model should be evaluated to demonstrate that it provides acceptable
> results over applicable ranges. Best-estimate models will be considered

AREVA Inc.

Realistic Large Break LOCA Methodology for Pressurized Water Reactors
Topical Report

EMF-2103NP
Revision 3

Page 3-24

acceptable provided their technical basis is demonstrated with appropriate data and analysis."

The post-CHF heat transfer model includes provisions for thermal radiation between structures (rod-to-rod). This adds to the current model, which already includes thermal radiation from structures to the fluid (rod-to-droplets and rod-to-steam). The rod-to-rod radiation model is only applied to the hot rod because its power level is elevated compared to its surroundings. Applying rod-to-rod radiation exclusively to the hot rod logically leads to the development of separate heat transfer uncertainties for the hot rod and the rest of the core.

The core wide heat transfer uncertainty was developed from code comparisons using the FLECHT-SEASET reflood test data as discussed in Section 8.4.1. These comparisons were used to derive the heat transfer multipliers that are applied to film boiling (FILMBL) heat transfer and dispersed flow film boiling heat transfer (DFFBHTC).

[

]

Assessment of this configuration is performed by using the same FLECHT-SEASET reflood tests that were used to determine the heat transfer multipliers FILMBL and DFFBHTC, as discussed in Section 8.4.1.

---

[1] [

]

AREVA Inc.

EMF-2103NP
Revision 3

Realistic Large Break LOCA Methodology for Pressurized Water Reactors
Topical Report

Page 3-25

[

]

3.1.3.3.8   Pump Modeling

The S-RELAP5 PUMP component model has been modified to apply two-phase pump performance degradation data as described in Section 7.8.1.3. The EPRI pump data is more appropriate for use in PWR pump analysis than is the Semiscale pump data traditionally used for this purpose. The basic approach to pump modeling is to superimpose a quasi-static model for pump performance on the RELAP5 volume-junction flow path representation. The pump is a volume-oriented component, and the head developed by the pump is apportioned equally between the suction and discharge junctions that connect the pump volume to the system. The pump model is interfaced with the two-fluid hydrodynamic model by assuming the head developed by the pump is similar to a body force. Therefore, the head term appears in the mixture (sum) momentum equation; but, like the gravity body force, it does not appear in the difference momentum equation used in RELAP5. Numerical treatment of the head term is described in Section 7.8.1.4.

AREVA Inc.

EMF-2103NP
Revision 3

Realistic Large Break LOCA Methodology for Pressurized Water Reactors
Topical Report

Page 3-26

3.1.3.3.9   Core Flow Distribution During Blowdown

The core region extends from the bottom of the active core to the top of the upper core support plate.   [

]

The most important contributor to nodalization sensitivity is expected to be core nodalization because it directly affects the liquid distribution in the core. The key phenomena of importance influenced by nodalization are the heat transfer modes, entrainment/de-entrainment, multi-dimensional flow, stored energy, oxidation, core power distribution, and decay heat. Since the heat transfer modes, entrainment/de-entrainment, hot region power and stored energy are treated statistically, adequate representation of multi-dimensional flow phenomenon is of prime relevance for nodalization. The node lengths are the smallest defined for the S-RELAP5 plant model; hence, they will define the Courant limit.

[

]

3.1.3.4 Post-Blowdown Phenomena

3.1.3.4.1 Containment Pressure

To provide a more accurate break pressure boundary condition for S-RELAP5 best estimate LOCA analysis, a detailed containment model has been interfaced to S-RELAP5. This containment model is derived from the AREVA NP licensing code ICECON (Reference 3-8). ICECON is capable of simulating pressure-temperature transients in both dry containments and ice condenser containments. The S-RELAP5/ICECON code interface allows ICECON to be run concurrently with S-RELAP5, providing a calculation of containment pressure that is consistent with the break mass flow rate and specific enthalpy currently being generated by S-RELAP5. With the concurrent execution of S-RELAP5 and ICECON, an accurate break pressure boundary condition is always available in S-RELAP5, and the need for manual exchange of data between the two codes is eliminated.

Because the ICECON model provides only containment pressure and temperature for S-RELAP5, a simple model is adequate. For a dry containment, the ICECON model is a single volume representing the containment space within the inner steel liner. This simple model is also used for annular or sub-atmospheric containments. For an ice condenser containment, the model has four volumes:

1. The lower compartment containing the reactor primary coolant system; the upper compartment containing the refueling channel.

2. The refueling equipment and polar cranes.

3. The ice chest containing borated ice for condensing steam discharged to the containment.

4. The dead-end volume containing the auxiliary pipe tunnel, the fan accumulator compartments and the instrument room.

The dominant parameter of interest related to the containment model is containment pressure. The goal of the modeling is to provide a reasonable prediction that remains responsive to the industry held perception that lower containment pressures increase steam binding and restrict the reflooding process by imposing higher steam specific volumes. Three modeling concepts ensure this:

1. The heat structure modeling is in line with the recommendations of NUREG-0800 Branch Technical Position 6.2 (Reference 3-5). This ensures that the interior heat absorbing structures are modeled with recognition of the probable best-estimate characterization.

2. The containment condensing heat transfer is a practical bound of benchmark data for ten experiments. Although the benchmarks were conducted using GOTHIC (Reference 3-9, Figure 5-42, Page 5-48), the result was the establishment of a benchmark data set for the condensing heat transfer coefficient to the Uchida correlation. [

                                                                                ]

3. The containment volume is treated statistically by ranging from its best-estimate value to the maximum possible free volume within the containment exterior walls. The free volume is a major determinant in establishing the containment pressure. This volume cannot be larger than the volume within the outer containment walls. Because the volume within the outer walls is easy to compute, the use of this volume as an upper bound to the free volume ensures that a reasonable-to-conservative volume is applied.

The combination of these three factors provides assurance that the containment pressure applied in the RLBLOCA calculation is conservative but not so much so as to seriously bias the results.

3.1.3.4.2 Calculation of Post-Blowdown Thermal Hydraulics for Pressurized Water Reactors

The refill and reflood phases of the transient are calculated on a best-estimate basis, taking into consideration the thermal and hydraulic characteristics of the core, the ECCS performance, and important reactor systems. The distribution of water and steam in the reactor vessel is calculated directly from the S-RELAP5 conservation equations, and appropriate constitutive relations.

For the S-RELAP5/ICECON code interface, break flow junction variables (e.g., velocities, specific enthalpies, densities, void fractions) are transferred each time step from S-RELAP5 to ICECON. These variables are then used in ICECON to generate a new containment pressure which is transferred back to S-RELAP5 and used to alter the pressure in the time-dependent volume or volumes which represent the containment in the S-RELAP5 model. At each time step, S-RELAP5 performs the necessary data transfers between the two codes and calls for execution of the external code. After execution of the external code, control is returned to S-RELAP5, which continues execution.

A series of sensitivity studies was performed using S-RELAP5 with the ICECON interface to demonstrate the equivalence of the Tagami-Uchida and Uchida best estimate condensation heat transfer formulations. These studies were performed using best estimate S-RELAP5 and ICECON input models for a three-loop PWR with dry containment. The simulated transient was a double-ended large break LOCA with the break located in a reactor coolant pump discharge pipe. [

]

3.1.3.5 Steam Interaction with Emergency Core Cooling Water in Pressurized Water Reactors

A cold leg condensation model was developed using several Westinghouse/EPRI 1/3-scaled Tests, UPTF Test 8 (Phase A, Run 111 and Phase B, Run 112) and Test 25, to calculate a proper cold leg condensation rate during the accumulator and pumped injection period. The condensation model consists of biases (multipliers) on the liquid and vapor side heat transfer coefficients that determine the condensation due to steam–water mixing. The condensation model is described in detail in Section 8.4.2. With the model described, S-RELAP5 is found to calculate acceptable cold leg condensation for the selected UPTF and EPRI tests.

3.1.3.6 Post Blowdown Heat Transfer for Pressurized Water Reactors

During refilling of the reactor vessel and ultimate reflooding of the core, the heat transfer calculations should be based on a best-estimate calculation of the fluid flow through the core, accounting for unique emergency core cooling systems. The calculations should also include the effects of any flow blockage calculated to occur as a result of cladding swelling or rupture. Heat transfer calculations that account for two-phase conditions in the core during refilling of the reactor vessel should be justified through comparisons with experimental data. Best-estimate models will be considered acceptable provided their technical basis is demonstrated through comparison with appropriate data and analyses.

When heat flux from the fuel rods and any other metal masses exceeds the CHF, the heat transfer is calculated using correlations specific to the heat transfer regimes. The single-phase vapor, transition boiling and film boiling regimes constitute the post-CHF heat transfer regimes. For each of these regimes, the effects of radiation heat transfer also are considered. The calculation of the appropriate heat transfer correlations is shown in Section 7.6.7. In conclusion, the model for single-phase vapor heat transfer used in S-RELAP5 can be applied to a full-scale PWR LBLOCA.

3.1.3.7 Other Features of Best Estimate Codes

Other features required of a best estimate code are that it contain models in sufficient detail to predict important phenomena, and that it be validated against experimental data.

3.1.3.7.1 Completeness

Verification that the S-RELAP5 code contains models in sufficient detail to predict phenomena that are important to demonstrate compliance with the acceptance criteria specified in paragraph 50.46(b) of 10 CFR Part 50 (e.g., peak cladding temperature) is an essential part of code development and is documented in software development records required by quality assurance procedures. Since S-RELAP5 was originally developed from an existing code not under AREVA NP control, a supplemental code verification was performed and documented for the original submittal (Revision 0) of the realistic LOCA methodology (Reference 3-10). All code modifications made since the completion of this verification have been made within the AREVA Software Quality Assurance Program (SQAP) in compliance with 10 CFR 50 Appendix B. The SQAP ensures that all code development satisfies software quality expectations of CSAU, including source code control and maintenance of User/Functional/Theoretical descriptions of all related codes.

3.1.3.7.2 Data Comparisons

Validation of the S-RELAP5 Code is documented in Section 8.0. The separate effects tests (SET) included in the verification and validation were from the following facilities:

- Oak Ridge National Laboratory (ORNL) Thermal Hydraulic Test Facility (THTF).

- Bennett Tube Tests.

- Full-Length Emergency Cooling Heat Transfer System Effects and Separate Effects Tests (FLECHT SEASET).

  - Steam Cooling.

  - Test 31504 for assessment of heat transfer.

- Product Development Test Facility (PDTF) SMall Array Reflood (SMART) Tests.

- Marviken Tests.

- GE Level Swell Test 1004-3.

- Upper Plenum Test Facility (UPTF) Tests.

    - Tests 6 and 7.

    - Test 8.

    - Tests 10 Run 080 and 12 Run 014.

    - Tests 10B and 29B.

    - Test 11 (used to determine CCFL coefficients only).

- Westinghouse/Electric Power Research Institute (W/EPRI) One-Third Scale Tests.

- FRIGG-2 Tests.

- Slab Core Test Facility (SCTF) Tests.

- Cylindrical Core Test Facility (CCTF) Tests.

- Multi-dimensional Flow Tests.

- Achilles International Standard Problem (ISP) #25.

- Ferrell-McGee.

- Moby Dick.

The integral effects tests (IET) chosen for this validation are:

- The Loss-of-Fluid Test (LOFT) tests.

- The Semiscale tests.

3.1.4 Regulatory Position 4, "Estimation of Overall Calculational Uncertainty"

The objective of this section is to describe how plant compliance to the criteria of
10 CFR 50.46 with high probability is demonstrated. For the AREVA NP RLBLOCA
evaluation model, high probability was defined as having 95 percent confidence that
95 percent of LBLOCAs will meet the acceptance criteria of 10 CFR 50.46. This is
accomplished by applying non-parametric statistical techniques to the calculation results
of the evaluation. The key premise is that the RLBLOCA evaluation tool, S-RELAP5
and the attendant codes, is accurate in representing the possible LBLOCAs and the
frequency with which specific LBLOCA results will occur. Therefore, S-RELAP5
contains the domain of all possible LBLOCA results within the scenario. Extracting
information about this domain is done by random sampling (running individual LOCA
calculations referred to as cases or events) with random values for the initial conditions
and the parameter values, including those that alter the simulation of important
phenomena and deducing from those samples the content of the domain. To
accomplish this entails two requirements:

The calculation evaluation tool, S-RELAP5 and COPERNIC, must be established as
sufficiently accurate or conservatively biased such that any calculation provides a result
that is accurate or conservative for the sampled choices.

A method of evaluating the results sampled from the domain be established to provide
accurate probability and confidence.

Section 3.1.4.1 presents the establishment and evaluation of the first requirement, and
Section 3.1.4.2 presents the second.

3.1.4.1 Determination of the Effect of Reactor Input Parameters and State

The uncertainties associated with the prediction of LOCA results can be categorized
into three groups:

1. Fixed design factors (e.g., system geometry) that do not change, but that can still
    only be rendered in approximation,

AREVA Inc.

EMF-2103NP
Revision 3

Realistic Large Break LOCA Methodology for Pressurized Water Reactors
Topical Report

Page 3-34

2. Operational processes (e.g., core power peaking), which do not change during the transient, but vary across the spectrum of conditions at which a LOCA may occur.

3. Phenomena, which evolve during the transient (e.g., core heat transfer coefficients), and may take on differing normalized performance across the spectrum of LOCAs within the domain.

The treatment of fixed design factors and operational processes are discussed in Section 3.1.4.1.1 and Section 3.1.4.1.2, respectively. The treatment and development of uncertainty distributions for phenomena is presented in Sections 8.4 and 8.5.

3.1.4.1.1   *Fixed Design Factors*

Uncertainties associated with fixed design parameters are addressed by maintaining adherence to nodalization guidelines and identifying phenomenological uncertainties from code assessment studies applying those guidelines. Within the development of the methodology the guidelines for fixed structure or condition are applied, contingent on experimental restrictions, to a wide variety of experiments and benchmark evaluations, Section 8.0. The benchmarks serve to develop the uncertainties of correlations or phenomena modeling and to establish the ability of the modeling guidelines to produce fixed design models capable of allowing replication of the LOCA physical phenomena.

3.1.4.1.2   *Operational Process*

In contrast to phenomenological or fixed design factors, process parameters characterize the state of operation of the plant and are, to various degrees, controllable by plant operators so that realistic variations can be expected. The importance of these parameters must be established and, for those of significance, the ability of the model to predict appropriate results must be validated and an appropriate uncertainty distribution established.

From an operational standpoint, the NPP operating state is a function of the time in cycle (burnup and power distribution) and the actual conditions present in the various NPP components. Treating these process parameters statistically accounts for higher order behavior by including all possible combinations in the domain of possible LOCAs.

As part of the AREVA RLBLOCA methodology development, a review was performed to identify the NPP parameters that are to be addressed in the performance of a LBLOCA analysis. The identified parameters are provided in Table 7-3. The basis for inclusion in this list comes from three sources: PIRT, plant-specific technical specifications, and utility requests.

To treat a parameter statistically, the parameter uncertainty must be quantified in terms of biases and distributions. Quantifying this uncertainty with plant data is the best approach. At most plants, histories of parameters values (e.g., RCS flow rate, core inlet temperature, pressurizer condition, accumulator parameters, containment temperature) are maintained and useable for quantifying RLBLOCA analysis uncertainties. Operational uncertainty is defined as the true fluctuation of a parameter during normal operation. Setting the uncertainty distribution for a process parameter requires addressing the impact of measurement uncertainty for the parameter.

The choice of distribution may be influenced by how a utility manages a given process parameter. For example, using a uniform distribution may properly reflect the control provided for a parameter if that control is random within a range. A uniform distribution is also considered a conservative approach in that equal likelihood is given for values at the limits of the distribution where the strongest influence is expected. However, if the there is an expectation that the true distribution is substantially non-uniform, the actual distribution can be used.

Treatment of Time in Cycle

The time in cycle establishes the fuel rod properties and the lower bound for the global power peaking factor Fq. Power history calculations are performed using the methodology described in Section 9.3.1.3. Typically, fuel rod data for 20 to 40 burnup steps are explicitly written from a cycle power history calculation. The methodology examines potential limiting fuel conditions during both the first and second cycle of fuel rod operation. Fuel rod data are, therefore, provided for the first and second cycle of fuel rod operation. Third cycle fuel is sufficiently depleted that it cannot rise to the possibility of being the limiting fuel within the core and is not evaluated by the methodology.

Once the fuel rod histories for the fuel rod sub-code are found as described above, the axial and radial power shapes for the S-RELAP5 core model are selected as by the method described in Section 9.3.1.4.

Treatment of General Design Criterion-35

GDC-35 states that the plant shall be able to mitigate design basis accidents with or without off site power available. The methodology does this by [

] Further details are provided in Appendix A.

3.1.4.2 Performance of NPP Sensitivity Calculations and Determination of Combined Bias and Uncertainty

The evaluation uses a Monte Carlo procedure for propagation of uncertainty, in which a probabilistically based inputs sampling procedure is used in conjunction with a series of code runs to develop a mapping from analysis inputs to analysis results. To do this, the calculation of several individual LOCA possibilities must be conducted. Each of these possibilities must have the performance of key parameters or conditions determined randomly. This is accomplished by assigning an individual PDF to each of the parameters to be varied or sampled by the methodology. The PDFs are then seeded, using standard techniques, with independent random numbers to specify the performance of each parameter for a given case. After the accumulation of the results for several possible LOCAs, the group of results is evaluated to determine the probability of compliance to LOCA criteria.

3.1.4.2.1 Statistical Approach

[

]

3.1.4.2.2 *Application of Methodology*

The AREVA NP RLBLOCA methodology is a statistics-based methodology; therefore, the application does not involve the evaluation of different deterministic calculations. Instead, a minimum set of LOCA calculations, as detailed in Section 9.0, are performed with the values of key parameters randomly varied over identified uncertainty ranges. The methodology has the advantage of being able to treat a large number of parameters by randomly varying each parameter in each single calculation. This random selection process is repeated to define a large number of RLBLOCA calculations, all of which are then run.

All criteria are shown to be met simultaneously with at least 95 percent probability and 95 percent confidence by comparing the peak cladding temperature, local oxidation and core-wide oxidation values to their related criteria.

3.2 *References*

3-1 "Emergency Core Cooling Systems; Revisions to Acceptance Criteria," Federal Register, Vol. 53, No. 180, September 16, 1988, 10 CFR Part 50.

3-2 NUREG-1230, "Compendium of ECCS Research for Realistic LOCA Analysis," December 1988.

3-3 Regulatory Guide 1.157, "Best-Estimate Calculations of Emergency Core Cooling System Performance," U.S. NRC, May 1989.

3-4 NUREG/CR-5249, "Quantifying Reactor Safety Margins, Application of Code Scaling, Applicability, and Uncertainty Evaluation Methodology to a Large Break, Loss-of-Coolant Accident," U.S. NRC, December 1989.

3-5 NUREG-0800, U.S. Nuclear Regulatory Commission Standard Review Plan.

3-6 BAW-10231P-A, Revision 1, COPERNIC Fuel Rod Design Computer Code, Framatome ANP, January 2004.

AREVA Inc.

Realistic Large Break LOCA Methodology for Pressurized Water Reactors
Topical Report

EMF-2103NP
Revision 3

Page 3-39

3-7   ANSI/ANS-5.1-1979, American National Standard for Decay Heat
       Power in Light Water Reactors, approved August 29, 1979.

3-8   EMF-CC-39(P), Revision 3, ICECON: A Computer Program Used to
       Calculate Containment Back Pressure for LOCA Analysis (Including Ice
       Condenser Plants), Siemens Power Corporation, July 2004.

3-9   NAI 8907-09, Revision 10, Version 7.2b(QA), *GOTHIC Containment
       Analysis Package Qualification Report*, EPRI, Palo Alto, California,
       March 2009.

3-10   EMF-2102(P) Revision 0. S-RELAP5: Code Verification and Validation,
       AREVA NP Inc., August 2001.

3-11   Best-Estimate Calculations of Emergency Core Cooling System
       Performance, Regulatory Guide 1.157, May 1989.

4.0   SCENARIO IDENTIFICATION

4.1   *Analysis Purpose, Transient Class, and Power Plant Class*

The event scenario to be evaluated is that of a Loss-of-Coolant Accident (LOCA). The purpose of the analysis is to show compliance with 10 CFR 50.46(b)(1), (b)(2), and (b)(3) acceptance criteria, as previously discussed in Section 3.0. Section 4.1.1 addresses the scenario specification, Section 4.1.2 identifies the class of nuclear power plants covered in by the presented methodology, and Section 4.2 identifies the figures of merit.

4.1.1   Scenario Specification

The NRC Standard Review Plan (Reference 4-1) provides the definition of a LOCA event as:

> Loss-of-coolant accidents (LOCA) are postulated accidents that would result from the loss of reactor coolant, at a rate in excess of the capability of the normal reactor coolant makeup system, from piping breaks in the reactor coolant pressure boundary. The piping breaks are postulated to occur at various locations and include a spectrum of break sizes, up to a maximum pipe break equivalent in size to the double-ended rupture of the largest pipe in the reactor coolant pressure boundary.

A large break LOCA initiates with an instantaneous rupture of a reactor coolant system (RCS) pipe, resulting in the rapid loss-of-coolant from the RCS. It is the coolant loss and its replacement with emergency coolant that is the subject assessment of LBLOCA evaluation models. Two top level considerations apply to the model presented here:

1. The rupture or break occurs in the RCS piping. Although it is possible to envision ruptures in components, those events are considered beyond the design basis and not subjects for this evaluation model.

2. This evaluation model applies only to the larger possible breaks, break areas greater than 0.1 times the cross-sectional area of the largest flow area pipe within the RCS. Smaller breaks are evaluated with a separate evaluation model.

The rate of coolant loss is governed, in part, by the break area, which ranges from 0.1 times the area of the largest pipe area to twice the area of the pipe within which the rupture occurred. For plants covered by this evaluation model (Section 4.1.2), the break is postulated to occur in one of three locations:

1. The hot leg pipe between the reactor vessel and the steam generator (hot leg break).

2. The cold leg between the steam generator and the reactor coolant pump (pump suction break).

3. The cold leg between the reactor coolant pump and the reactor vessel (pump discharge break).

A LBLOCA evaluation must consider breaks at all three of these locations. However, as will be shown in the following text, the pump discharge break is the greatest challenge to the emergency equipment and results in the most severe consequences for the reactor core. Although a great deal of the modeling for the evaluation model is applicable to any of the break locations; it is specific only for pump discharge breaks.

To support the pump discharge as the most limiting break location, it is useful to describe a simplified LBLOCA scenario:

The postulated break occurs and substantial RCS coolant is expelled to the containment. The emergency systems are activated and inject replacement coolant into the cold legs between the reactor coolant pump and the reactor vessel. This coolant transfers to the reactor vessel and subsequently to the core to provide core cooling.

AREVA Inc.

Realistic Large Break LOCA Methodology for Pressurized Water Reactors
Topical Report

EMF-2103NP
Revision 3

Page 4-3

If the break occurs in the pump discharge piping, up to one-third, depending on the plant being evaluated, of the emergency coolant can flow directly out the break into the containment bypassing the reactor vessel, thus not providing core cooling. Because of the design of the RCS loop where the emergency coolant is injected into the cold legs, this direct emergency coolant loss cannot occur for a hot leg break; essentially all of the emergency coolant must pass through the reactor vessel, providing core cooling in the process. Thus, a hot leg break, with its high flooding rate, refills the core with water sooner than either pump discharge or pump suction breaks and, therefore, is much less severe.

The relation of a pump suction break to a pump discharge break is similar to that with a hot leg break in that there is no immediate loss of emergency coolant through the break. Although it is possible to lose emergency coolant through the break by entrainment, the efficiency of that process is less than that for a pump discharge break. The emergency coolant must backflow through the reactor coolant pump to the suction side of the pump before discharging through the break. The resistance of the backflow from the reactor vessel, through the reactor coolant pump to the break, is higher for a pump suction break than the resistance from the core outlet through the hot leg pipe connecting to the break, thus making emergency coolant delivery to the core easier for pump suction breaks. Therefore, because a pump discharge break more easily discharges all coolant, particularly liquid coolant, to the containment and is most likely to discharge the emergency coolant to the break, it can be identified as the worst break location. Accordingly, the hot leg break and pump suction break can be eliminated from specific consideration within this methodology.

The following details the progression of the scenario. An LBLOCA event is typically described in three phases:

1. Blowdown. For realistic evaluations, the blowdown phase is defined as the time period from initiation of the break until flow from the accumulators or safety injection tanks (SITs) begins to discharge. This definition is different than the traditional definition of blowdown, which extends the blowdown period until the RCS pressure approaches containment pressure. The blowdown phase typically lasts between 12 and 25 seconds, depending on the break size.

2. Refill. The refill phase lasts from the end of blowdown until a fluid mixture, supported by ECCS water, penetrates the bottom of the active core region.

3. Reflood. The reflood phase lasts from the end of refill until the core is quenched.

Following the initiation of the break, the blowdown phase is characterized by a sudden depressurization from operating pressure down to the saturation pressure of the hot leg fluid. For larger cold leg breaks, an immediate flow reversal and stagnation occurs in the core due to flow out the break, which causes the fuel rods to pass through critical heat flux (CHF), usually within 1 second following the break. Following this initial rapid depressurization, the RCS depressurizes at a more gradual rate. Reactor trip and emergency injection signals occur when either the low pressure setpoint or the containment high-pressure setpoint are reached. However, for LBLOCA, reactor trip and scram are essentially inconsequential, as reactor shutdown is accomplished by moderator feedback. During blowdown, core cooling is supported by the natural evolution of the RCS flow pattern as driven by the break flow.

When the system pressure falls below the accumulator (or SIT) pressure, flow from the accumulator is injected into the cold legs ending the blowdown period and initiating the refill period. Once the system pressure falls below the respective shutoff heads of the high head safety injection (HHSI) pumps and the low head safety injection (LHSI) pumps, and the system startup time delays are met, Safety Injection System flows begin injecting into the RCS. While some of the ECCS flow bypasses the core and goes directly out of the break, the downcomer and lower plenum gradually refill until the mixture in the lower head and lower plenum regions reaches the bottom of the active core and the reflood period begins. Core cooling is supported by the natural evolution of the RCS flow pattern as driven by the break flow and condensation on the emergency coolant being injected. Towards the end of the refill period, heat transfer from the fuel rods is relative low, steam cooling and rod-to-rod radiation being the primary mechanisms.

Once the lower plenum is refilled to the bottom of the fuel rod heated length, refill ends and the reflood phase begins. Substantial ECCS fluid was retained in the downcomer during refill. This provides the driving head to move coolant into the core. As the mixture level moves up the core, steam is generated and liquid is entrained, providing cooling in the upper core regions. As the two-phase mixture expands into the upper plenum, some liquid may de-entrain and flow downward back into the cooler core regions. The remaining entrained liquid passes into the steam generators where it vaporizes, adding to the steam that must be discharged through the break and out of the system. The difficulty of venting steam is, in general, referred to as steam binding. It acts to impede core reflood rates. With the initiation of reflood, a quench front starts to progress up the core. With the advancement of the quench front, the cooling in the upper regions of the core increases, eventually arresting the rise in fuel rod surface temperatures. Later the core is quenched and a pool cooling process is established that can maintain the cladding temperature near saturation, so long as the ECCS provides makeup for the boiling.

AREVA Inc.

EMF-2103NP
Revision 3

Realistic Large Break LOCA Methodology for Pressurized Water Reactors

Topical Report

Page 4-6

The RLBLOCA methodology must analyze the probable and possible consequences of the scenario (a LBLOCA at the pump discharge) and determine that the plant will meet the 10 CFR 50.46 criteria, as discussed in Section 3.0, with high probability.

4.1.2   Nuclear Power Plant Selection

The selected NPP types to which the methodology in this report is to be applied include those PWRs with U tube type steam generators and initial ECCS injection into the cold legs. The specific plant types are Westinghouse 3- and 4-loop designs, Combustion Engineering (CE) 2x4 designs and AREVA 3- and 4-loop designs all with fuel assembly lengths of 14 feet or less, and with emergency core cooling system (ECCS) injection to the cold legs. These NPP types have similar hot and cold legs, pressurizers, steam generators, and vessels. The largest difference among the NPP types is the number of hot and cold legs, and the number of steam generators. However, experience in the performance of LBLOCA analyses for these NPPs has shown that all three types behave similarly.

All of these NPP types have inverted U-tube steam generators, a pressurizer connected to a hot leg, and ECCS coolant injection into the cold legs. The steam generators in these plants include downcomer, boiler, plenum, dryer/separator, and steam dome regions. The pressurizers are essentially the same and are equipped with heaters, sprays, and a surge line connected to a hot leg.

The configuration of the vessels for all three-plant types is also essentially the same and can be modeled in the code with the same major divisions and nodalization schemes. The coolant enters the vessel through the inlet nozzles and flows into the downcomer. In the downcomer, a small fraction of the flow diverts into the upper head, but the majority of the flow goes down the downcomer (for upflow plants) into the lower head/plenum region[2]. From here the majority of the flow goes up through the active core with some flow bypassing the core through the baffle and guide tubes. From the core, the flow enters the upper plenum and exits the vessel through the hot leg nozzles. Since the hot legs pass through the vessel downcomer region into the upper plenum, they essentially provide a flow path blockage at the elevation of the hot and cold legs in all three NPP types.

The principal difference in the vessels is in the connection between the downcomer and the lower plenum/lower head. In some CE designs, there may be a flow skirt that is intended to force part of the flow to pass through the lower head before going into the lower plenum region.

As indicated above, a principal difference between these NPP types is in the number of hot and cold legs, and steam generators. The Westinghouse and AREVA 3-loop designs have three hot legs, cold legs and steam generators. The Westinghouse and AREVA 4-loop designs have four hot legs, cold legs, and steam generators. CE 2x4 designs have two hot legs, four cold legs and two steam generators.

---

[2]   For down flow baffle plants, the flow into the downcomer splits, with some flow going into the bypass region and the remainder of the flow continuing down the downcomer. In this plant configuration, the downcomer and bypass flow both enter the core.

AREVA Inc.

EMF-2103NP
Revision 3

Realistic Large Break LOCA Methodology for Pressurized Water Reactors
Topical Report

Page 4-8

Provided in Appendix B are sample problems for a Westinghouse 4-loop PWR design, a Westinghouse 3-Loop PWR design, and a CE 2x4 PWR design. Table B-7, Table B-14, and Table B-21 provide values for the most important NPP parameters. As illustrated, a major difference in the important NPP parameters is the accumulator pressure for the Westinghouse and AREVA designs, and the SITs in the CE designs. The impact of this difference is shown in the sequence of events given in Table B-11, Table B-18, and Table B-25, where the SIT flow initiation is delayed in the CE design until the pressure in the cold legs drops below the SIT pressure. Taking into account this delay in the SIT delivery, the sequence of events is similar for all three of the NPP types.

4.2 *Figures of Merit*

The figures of merit for the LOCA EM are derived from the first three acceptance criteria of 10 CFR 50.46, as presented in Section 3.0. They are Peak Clad Temperature (PCT), Maximum Local Oxidation (MLO) and Core-Wide Oxidation (CWO).

Complementary figures of merit are defined in the EM assessment process (Section 8.0) for various benchmarks where the modeling constraints do not make it possible to supply directly one of the principal figures of merit to match the physical configuration or where the alternate figure of merit makes for an easier physical interpretation. For instance, the ratio of the convective heat transfer coefficient to the global heat transfer at the time of PCT is used as figure of merit in one of the FLECHT-SEASET tests. If such alternate figures of merit are used, they are identified throughout the report where appropriate.

4.3 *References*

4-1   NUREG-0800, "Standard Review Plan, Section 15.6.5 Loss-Of-Coolant Accidents Resulting from Spectrum of Postulated Piping Breaks within the Reactor Coolant Pressure Boundary," Revision 3, U.S. NRC, March 2007.

5.0   EVALUATION MODEL REQUIREMENTS

The process of constructing a Phenomena Identification and Ranking Table (PIRT) is identified in Reference 5-1 as part of the EMDAP under Element 1- Establish Requirements for Evaluation Model Capability. As noted in Reference 5-1, Element 1 of the EMDAP process provides the application envelope for the Evaluation Model (EM) by identifying and establishing the importance of the constituent phenomena, processes and key parameters within that envelope.

The PIRT is part of the Code Scaling, Applicability, and Uncertainty (CSAU) process (Reference 5-2), and was recognized as a cost-effective method to identify and select the processes and phenomena which dominate a certain transient behavior. In subsequent applications it has been acknowledged as a generalized application to support the decision-making processes.

5.1   *Identification of Systems, Components, Phases, Geometries, Fields, and Processes That Must Be Modeled*

Identification of EM characteristics in step three of the EMDAP process is based on system hierarchical decomposition methods such as those used in the methods for scaling complex systems. Each hierarchical level can be decomposed in constituents at the next level down. A system can be divided into interacting subsystems, each subsystem into interacting modules, each module into interacting constituents, each constituent into interacting phases, each phase characterized by one or multiple geometrical configurations and described by field equations (mass, momentum and energy), and each field can be affected by several transport processes.

This step is effectively part of the PIRT process itself, which is presented in the next section with its results presented in Table 5-1.

5.2   *Identification and Ranking of Key Phenomena and Processes*

A key step in the CSAU and the EMDAP process is to identify and rank the important phenomena that should be addressed in analyzing the selected scenario. This step is performed by experts who are knowledgeable regarding LBLOCA phenomena that occur during each transient phase. The resultant PIRT provides the basis for:

1. Determining code applicability (does the code properly model the important phenomena).

2. Establishing the assessment matrix (identifying test data that contain the appropriate phenomena during each accident phase).

3. Identifying phenomenological parameters to be ranged and quantified for evaluating uncertainties.

The AREVA PIRT for the chosen scenario has evolved through multiple stages of review (including experts within AREVA and from outside the company) and adjustment. Its foundation includes an independently developed PIRT (Reference 5-3), review and development by an expert panel (including experts both within AREVA and from outside the company), and adjustments or updates to incorporate improved understanding of the phenomena. Table 5-1 provides the current version upon which Revision 3 (and implicitly Revision 2) of this methodology is based. Each phenomenon is given a ranking, where importance is proportional to the numerical value (e.g., 9 = extreme importance and 1 = least importance). High rankings indicate the important phenomena that should be simulated by a RLBLOCA evaluation model. Those phenomena with a ranking of 5 or higher are classified as important phenomena.

The following definitions apply to the PIRT in Table 5-1:

1. Blowdown: The blowdown phase of the LOCA is defined as the time period from initiation of the break until flow from the accumulators or safety injection tanks (SITs) begins.

2. Refill: The refill phase of the LOCA begins when the accumulators or SITs begin injecting and continues until the mixture level in the vessel refills the lower plenum and flow into the heated core region begins.

3. Reflood: The reflood phase of the transient begins when the lower plenum fills and emergency core cooling (ECC) begins flowing into the bottom of the active core and continues until the temperature transient throughout the core has been terminated. At that time, the LOCA stored energy and decay heat are being removed and the LOCA has been reduced to an issue of maintaining long-term cooling.

The EMF-2103(P)(A) Revision 0 final PIRT forms the basis for the Revision 3 PIRT, however the following items have been revised or added:

- [

]

- [

]
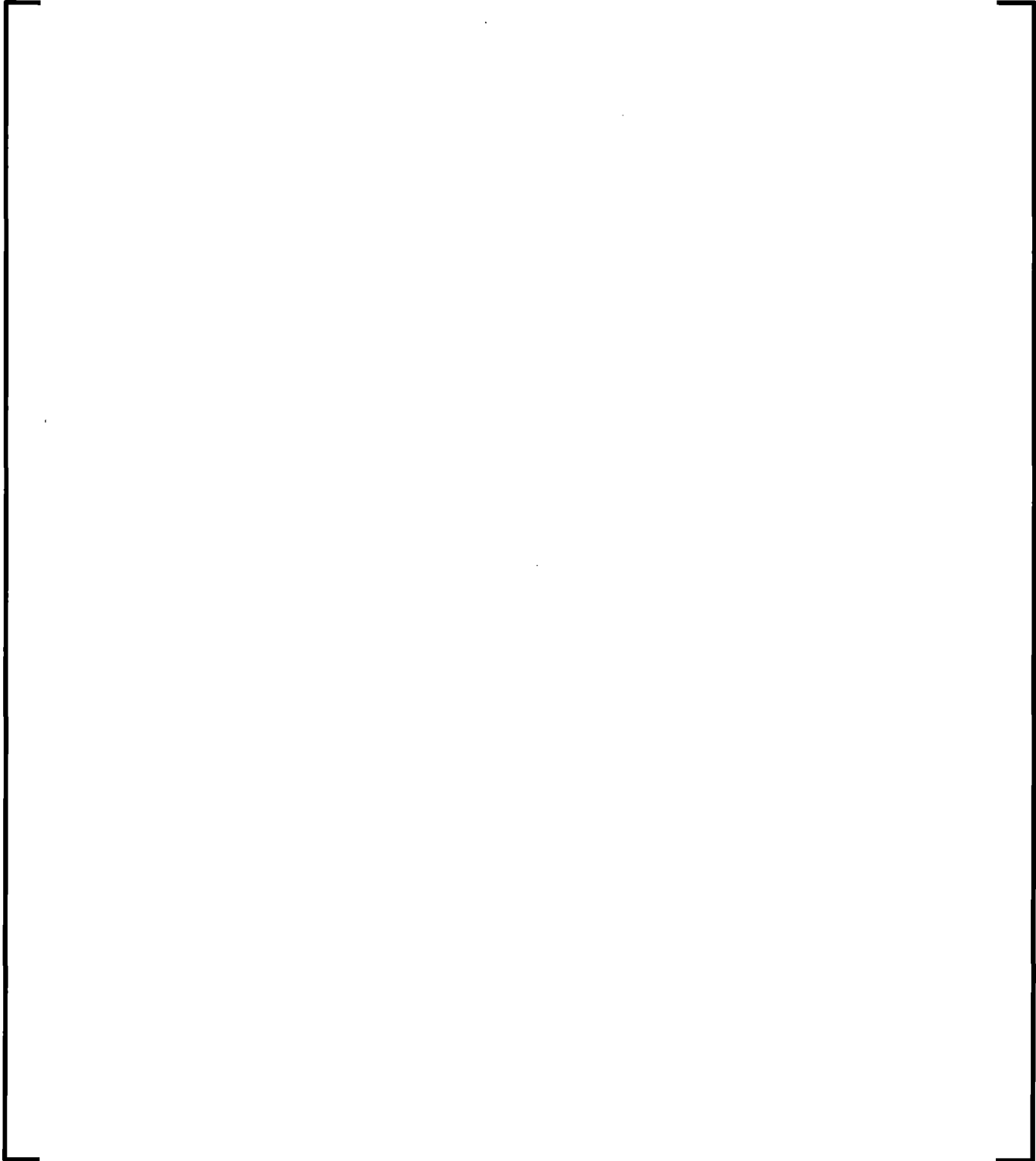
Table 5-1   Phenomena Identification and Ranking Table for PWR LBLOCA

AREVA Inc.

EMF-2103NP
Revision 3

Realistic Large Break LOCA Methodology for Pressurized Water Reactors
Topical Report

Page 5-6

AREVA Inc.

Realistic Large Break LOCA Methodology for Pressurized Water Reactors
Topical Report

EMF-2103NP
Revision 3
Page 5-7
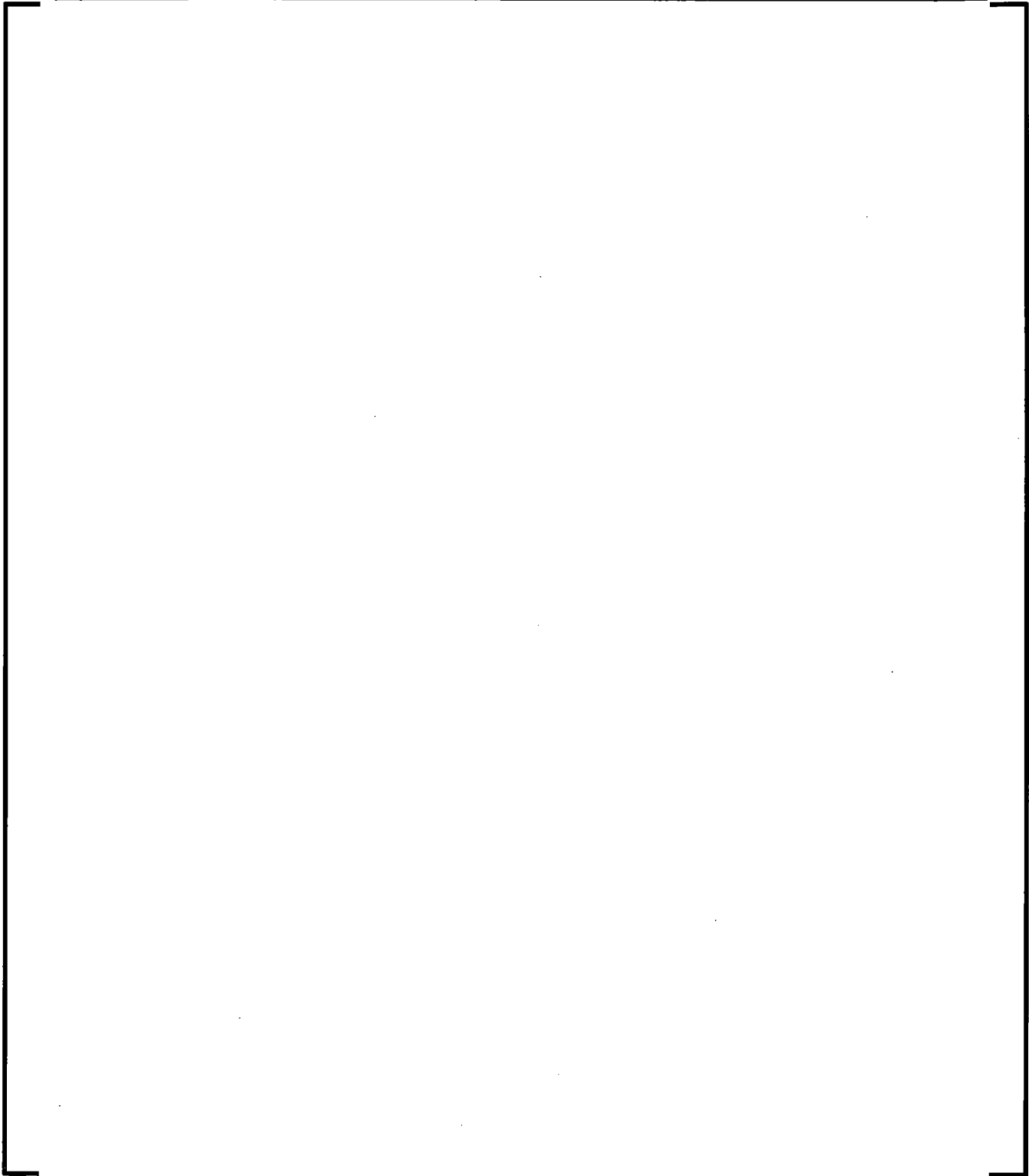
5.3   *References*

5-1   Regulatory Guide 1.203, "Transient and Accident Analysis Methods," U.S. NRC, December 2008.

5-2   NUREG/CR-5249, "Quantifying Reactor Safety Margins, Application of Code Scaling, Applicability, and Uncertainty Evaluation Methodology to a Large Break, Loss-of-Coolant Accident," U.S. NRC, December 1989.

5-3   NUREG-1230, "Compendium of ECCS Research for Realistic LOCA Analysis," December 1988.

6.0   ASSESSMENT DATA BASE SUMMARY

6.1   *Objectives for Assessment Base*

Since the EM can only approximate physical behavior for the LBLOCA, it is important to validate the calculational devices using an appropriate assessment base. The following four considerations are taken into account in establishing the assessment matrix AREVA NP used for validation.

The first consideration is the phenomena identified in the PIRT process described in Section 5.2 and presented in Table 5-1. Items ranked 5 or higher in Table 5-1 are classified as important phenomena. The assessment matrix, Table 6-1, includes the important phenomena identified in Table 5-1. Experiments are identified in Table 6-1 that address these important phenomena. The selected experiments must have sufficient data to determine code accuracy, including bias and uncertainty. For those phenomena in Table 6-1 for which an assessment is not provided, the explicit treatment and the reasons behind it are provided in the same Table 6-1.

The second consideration is that of NPP nodalization. Here experiments are selected that are representative of the types of NPPs being addressed and cover the identified phases of the selected scenario. Thus, for this application, experiments are selected that are representative of Westinghouse/AREVA 3- and 4-loop designs and CE 2x4 designs. The experiments also cover one or more of the LBLOCA phases identified in Section 4.1: blowdown, refill, and reflood.

The third consideration is to demonstrate that the code and NPP nodalization have the ability to scale from experiments of different sizes to a full size NPP for which analyses will be performed. Generally this is done by selecting a number of assessments in facilities of different scale and demonstrating that the code and NPP nodalization are capable of consistently predicting the experimental data from all the experiments.

AREVA Inc.

EMF-2103NP
Revision 3

Realistic Large Break LOCA Methodology for Pressurized Water Reactors
Topical Report

Page 6-2

The fourth and final consideration is with respect to compensating code errors. The development process embodies substantial methodology verification and validation. The use of a PIRT process and the benchmarking of the methodology, during validation against experiments chosen to measure the methodology performance regarding the PIRT phenomena, provide substantial assurance that compensating errors do not significantly impact the methodology predictions. These tests include both Separate Effects Tests (SETs) and Integral Effects Tests (IETs) dealing with the most important LOCA phenomena. With a comprehensive set of such benchmarks, Table 6-2, specifying the uncertainty ranges and providing the final assessment of the methodology, it can be concluded that if the methodology contains compensating errors, these errors do not impugn the ability of the methodology to reliably predict the course and outcome of LBLOCA transients.

6.1.1   PIRT Considerations

The PIRT presented in Section 5.2 (see Table 5-1) provides a qualitative expression of what is perceived to be the degree of importance of key phenomena present in a LBLOCA. All these phenomena are accounted for either statistically or with a bias (perhaps a null bias), and a justification for the selected treatment is provided. Within Revision 0 of this methodology, sensitivity studies were used, in part, to determine which phenomena or processes required assessment by the validation matrix. However, once a decision to validate the treatment of a phenomena or process is made, the process by which the decision was made is no longer of consequence unless the decision is changed. In that case, a revised decision process and result must be described and justified. The Revision 3 validation matrix includes all of the phenomena or processes selected for validation in Revision 0 and will not repeat the discussion of sensitivity studies for those parameters, phenomena, or processes. An accounting, including PIRT revisions made in Revision 3, of the validation matrix is made in Table 6-1. Where an item ranked 5 or higher is not included in the validation matrix, an explanation, sensitivity study or other, is provided in Table 6-1 and Section 8.5 to justify the exclusion.

Table 6-1 lists the moderate and high ranked PIRT phenomena or processes (ranked five or higher) and the processes or parameters that primarily affect them. These are then cross referenced to the decision on including them in the validation matrix or the reason for exclusion. If a sensitivity study is part of the justification, the conclusion from the study is also provided. The final entry provides a reference to the sub-section within which additional discussion is provided.

6.1.2   Nodalization Considerations

In the selection of the specific tests in each test facility to be analyzed in Revision 0, plant nodalization was an important consideration and, given the extensive experimental facility database developed, provided considerable support for that selected for plant modeling. One additional test facility was identified strictly to address nodalization effects. That test facility was the Slab Core Test Facility (SCTF), where specific assessments were performed to address core radial nodalization with variations in radial power distributions.

6.1.3   Scaling Considerations

Within the test facility database developed to support the PIRT considerations (Table 6-1) are facilities that span a scaling range of 1:1500 to 1:1. In addition, some specific tests were performed as a counterpart to tests performed in other facilities. Where data are available, these tests were added to the assessment matrix.

AREVA Inc.

Realistic Large Break LOCA Methodology for Pressurized Water Reactors
Topical Report

EMF-2103NP
Revision 3
Page 6-4

6.1.4   Compensating Errors
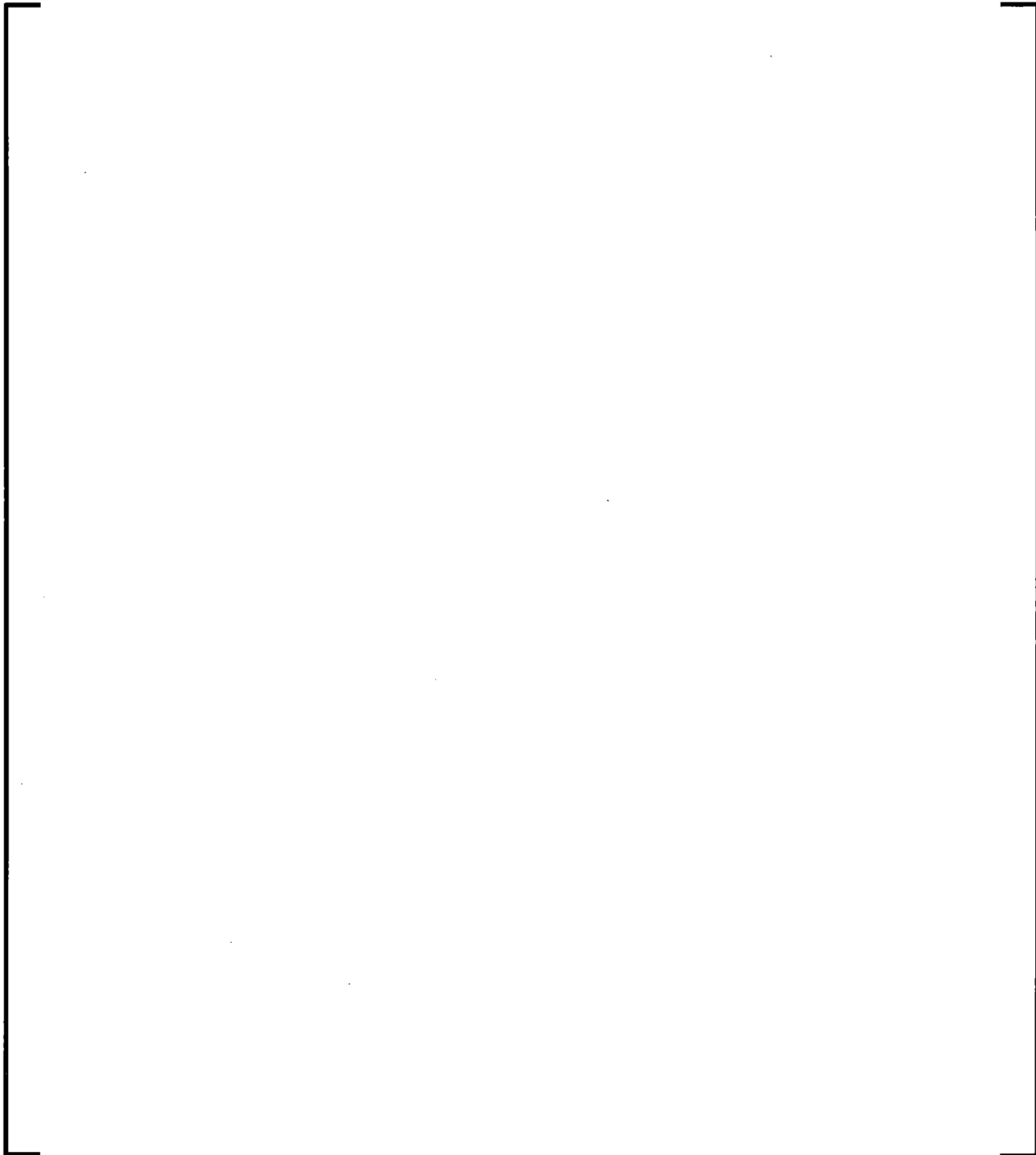
The issue of compensating errors arises primarily from the use of correlations and closure relations in the code. The interaction of the various correlations and closure relations can be such that an error in one of these models is compensated for by an error in another model. These compensating errors can result in the code being able to predict specific tests but incapable of predicting within the phenomena range of other tests. For the LBLOCA, only those compensating errors, which could function in one manner in the assessments and in an entirely different manner in the LBLOCA, are a concern. Thus, the assessment matrix must include tests that can be scaled up and that provide broad coverage of the range of the LBLOCA phenomena. The compensating error issue is addressed in the test matrix through the Full Length Emergency Core Heat Transfer - System Effects And Separate Effects (FLECHT SEASET), Slab Core Test Facility (SCTF), Cylindrical Core Test Facility (CCTF), and Thermal Hydraulic Test Facility (THTF) for the core phenomena and CCTF and Upper Plenum Test Facility (UPTF) for most of the other major RCS components. The Loss-Of-Fluid Test Facility (LOFT) and Semiscale benchmarks provide further assurance by benchmarking the methodology as an integral.

6.1.5   Summary

The main purpose of this section is to document the database of test results used to assess the EM. The selection of the database tests is a direct result of the requirements established in the PIRT based on the four considerations outlined above.

Given the four considerations previously discussed, a total EM assessment matrix documented in Table 6-2 can be recognized. Table 6-2 lists the test facilities, the actual tests analyzed from each test facility, and the associated phenomena being examined. In many cases the phenomena are involved in the benchmark or analysis and must be successfully modeled to demonstrate an effective benchmark but are not individually assessed or compared. The sum total of these comparisons is the measure of the quality of predictive capability of the EM and the computers codes employed. The models and correlations used to model these phenomena in S-RELAP5 are presented in Section 7.0. The results of the suite of code benchmarks against the tests identified in the validation matrix are presented in Section 8.0.

Table 6-1   Validation Needs for Important PIRT Entries

AREVA Inc.

Realistic Large Break LOCA Methodology for Pressurized Water Reactors
Topical Report

EMF-2103NP
Revision 3

Page 6-7

AREVA Inc.

EMF-2103NP
Revision 3

Realistic Large Break LOCA Methodology for Pressurized Water Reactors
Topical Report

Page 6-8

AREVA Inc.

EMF-2103NP
Revision 3

Realistic Large Break LOCA Methodology for Pressurized Water Reactors
Topical Report

Page 6-9

AREVA Inc.

EMF-2103NP
Revision 3

Realistic Large Break LOCA Methodology for Pressurized Water Reactors
Topical Report

Page 6-10

AREVA Inc.

Realistic Large Break LOCA Methodology for Pressurized Water Reactors
Topical Report

EMF-2103NP
Revision 3

Page 6-11

AREVA Inc.

EMF-2103NP
Revision 3

Realistic Large Break LOCA Methodology for Pressurized Water Reactors
Topical Report

Page 6-12

Table 6-2   Assessment Matrix Tests and Phenomena Addressed

AREVA Inc.

EMF-2103NP
Revision 3

Realistic Large Break LOCA Methodology for Pressurized Water Reactors
Topical Report

Page 6-13
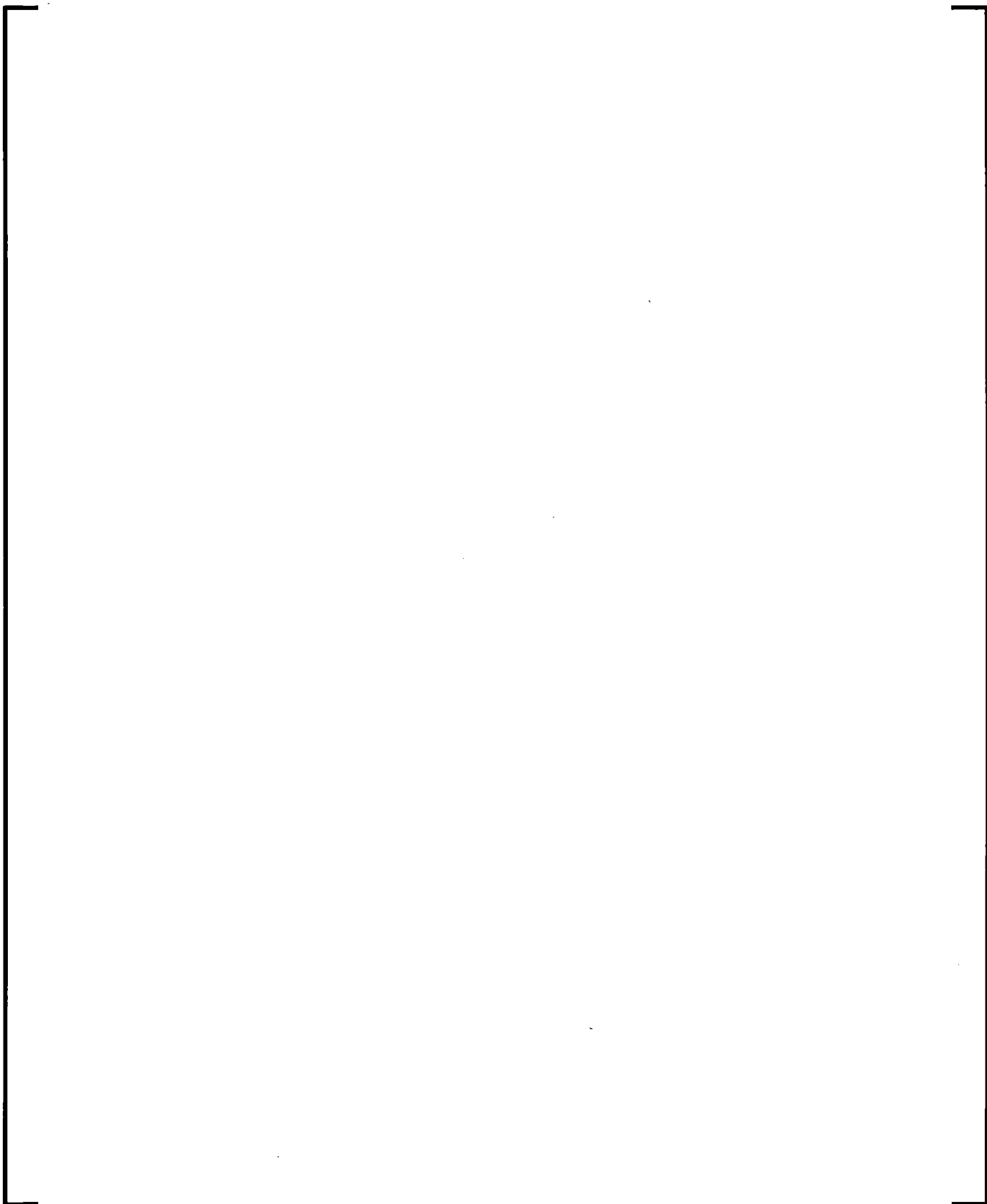
6.2   *References*

6-1   NUREG/CR-5249, "Quantifying Reactor Safety Margins, Application of
       Code Scaling, Applicability, and Uncertainty Evaluation Methodology to
       a Large Break, Loss-of-Coolant Accident," U.S. NRC, December 1989.

7.0   EVALUATION MODEL COMPUTER CODES DESCRIPTION

7.1   *Frozen Code Version Selection*

The codes selected for use in the RLBLOCA methodology include the COPERNIC
(Reference 7-1) for fuel performance, and S-RELAP5 (References 7-2, 7-3, 7-4, and 7-
5) for system analysis. The S-RELAP5 code is a RELAP5-based thermal-hydraulic
system code used for performing LOCA and non-LOCA analyses. The versions of
these codes used in the development of this methodology are UOCT09 for S-RELAP5
and UDEC02 for COPERNIC.

7.1.1   COPERNIC Fuel Rod Performance Code

A key to a RLBLOCA analysis is the model used for calculating fuel rod performance.
In particular, the initial operating temperature of the fuel pellets (stored energy), the
internal fuel rod gas pressure, and the transient gap conductance are significant
parameters which affect the calculated PCT. AREVA NP will use COPERNIC to
calculate the required fuel characteristics as a function of fuel rod exposure and power
history.

The COPERNIC fuel rod performance code was originally developed and NRC-
approved for use by AREVA NP with respect to fuel rod mechanical design. Portions of
this code were incorporated in S-RELAP5 to permit coupled calculations of fuel rod
thermal properties (thermal conductivity, heat capacity, and gap conductance) during
both the steady-state and the transient phases of an S-RELAP5 LBLOCA analysis. The
COPERNIC (Section 7.9.3) routines incorporated into S-RELAP5 were for the thermal
expansion, cladding elastic strain, gap width, and gap gas pressure, which in turn
determine the fuel rod thermal properties and gap conductance. Table 7-1 provides a
description of the models and routines incorporated into S-RELAP5.

Long-term burnup dependent "permanent" fuel rod effects such as pellet densification
and swelling, cladding creep, and fission gas release will not change appreciably during
the course of an LBLOCA transient. Calculations of these effects are performed to

initialize the fuel rod parameters, but are not altered during the transient and, thus, not included in the fuel rod model routines in S-RELAP5. The fuel pellet and cladding strains associated with these "permanent" effects are calculated in separate executions of the standalone COPERNIC code (which burns the fuel rods through the exposure histories required for the individual rods being analyzed). The results of these exposure analyses are then transferred to S-RELAP5 and used to initialize the values of the burnup dependent "permanent" effects in the COPERNIC routines.

The fuel rod analysis for an S-RELAP5-based LBLOCA calculation then proceeds in three steps:

1. The standalone fuel rod code (COPERNIC) is used to determine fuel rod properties at the end of a specified exposure history.

2. An S-RELAP5 steady-state analysis is performed using the fuel rod models in S-RELAP5, with the permanent burnup dependent fuel properties being defined by data transferred from Step 1. During this steady-state analysis, power related properties such as fuel temperatures and thermal properties are allowed to migrate to values consistent with the final steady-state power of the system. The initial transient stored energy is determined and adjusted for uncertainty and bias during this phase.

3. An S-RELAP5 transient analysis is performed using initial fuel rod thermal conditions from Step 2, and using the COPERNIC fuel rod model routines that have been incorporated in S-RELAP5 to determine fuel rod thermal properties and gap conductance during the transient.

7.1.2   S-RELAP5

AREVA Inc.

EMF-2103NP
Revision 3

Realistic Large Break LOCA Methodology for Pressurized Water Reactors
Topical Report

Page 7-3

AREVA Inc.

Realistic Large Break LOCA Methodology for Pressurized Water Reactors
Topical Report

EMF-2103NP
Revision 3

Page 7-4

AREVA Inc.

EMF-2103NP
Revision 3

Realistic Large Break LOCA Methodology for Pressurized Water Reactors
Topical Report

Page 7-5

AREVA Inc.

EMF-2103NP
Revision 3

Realistic Large Break LOCA Methodology for Pressurized Water Reactors
Topical Report

Page 7-6

[

]

Table 7-1 Models Added to S-RELAP5 from COPERNIC

[

]

7.1.3   References

7-1.   BAW-10231P-A, Revision 1, COPERNIC Fuel Rod Design Computer Code, Framatome ANP, January 2004.

7-2.   EMF-2102(P) Revision 1, S-RELAP5 Code Verification and Validation, November 2010.

7-3.   EMF-2100(P) Revision 16, S-RELAP5 Models and Correlations Code Manual, December 2011.

7-4.   EMF-2101(P) Revision 3, S-RELAP5 Programmers Guide, May 2004.

7-5.   EMF-CC-097(P) Revision 25, S-RELAP5 Input Data Requirements (User's Manual), December 2011.

7-6.   NUREG/CR-4312, EGG-2396, Revision 1, RELAP5/MOD2 code Manual, Volume I: Code Structure, Systems Models, and Solution Methods, August 1985.

7-7.   NUREG/CR-5535, INEL-95/0174, RELAP5/MOD3 Code Manual, Volume II: User's Guide and Input Requirements, June 1995.

7-8.   EMF-CC-039(P) Revision 4, ICECON: A Computer Program Used to Calculate Containment Back Pressure for LOCA Analysis (Including Ice Condenser Plants), December 2007.

7-9.   EMF-CC-039(P) Supplement 1 Revision 5, ICECON Code User's Manual: A Computer Program Used to Calculate Containment Back Pressure for LOCA Analysis (Including Ice Condenser Plants), July 2007.

7-10.   TID-4500, ANCR-1219, CONTEMPT-LT – A computer Program for Predicting Containment Pressure-Temperature Response to a Loss-Of-Coolant Accident, June 1975.

7.2   *Provision of Complete Code Documentation*

The documentation for the codes used in the development of this methodology is
provided in Reference 7-1 for COPERNIC, References 7-2, 7-3, 7-4, and 7-5 for the S-
RELAP5 code, and References 7-8 and 7-9 for the ICECON code. The documentation
describes the models and correlations used in the codes; defines the code inputs, and
provides a description of the code structure. These documents were verified against
the actual coding to ensure the documentation and coding are consistent (Section 8.0).
Revision 3 includes all the supporting documentation from these references that
pertains to the RLBLOCA EM in Section 7.0, including a comprehensive description of
the models and correlations.

The code validation for RLBLOCA from Reference 7-2, which compares the code
predictions to measured data in a number of SET and IET facilities, is included in
Section 8.0. All the benchmarks are identified in the assessment matrix (Section 6.0,
Table 6-1). In addition, AREVA NP has guidelines covering the development of
S-RELAP5 input for the NPP model and procedures for performing an actual analysis.
The input development and analysis guidelines are included in Appendix A.

7.3   *Determination of Code Applicability*

The objective of the determination and code applicability step of CSAU is to
demonstrate that the selected codes are capable of modeling the chosen event for all
NPP types. This is accomplished by comparing the event and important phenomena
identified in the PIRT with the models and correlations documents for the selected
codes. Four attributes are needed to make this comparison:

- Field equations that provide code capability to address global processes.

- Closure (constitutive) equations that support the conservation equations by providing
  code capability to model and scale specific phenomena or processes.

- Code numerics that demonstrate code capability to perform calculations efficiently
  and reliably.

- Structure and nodalization that address code capability to model the NPP geometry and components, and to provide efficient and accurate NPP predictions.

These four attributes are discussed in the following sections.

7.3.1   Field Equations

The field equations (conservation of mass, momentum, and energy) must possess the capability of simulating each of the distinct phases (blowdown, refill, and reflood) of a LBLOCA. During the refill and reflood phases, countercurrent flow occurs at various locations in the RCS, and subcooled liquid coexists with superheated steam in parts of the reactor core. Therefore, for realistic analyses, the field equations must be non-homogeneous (unequal velocity for each phase) and non-equilibrium (unequal temperature for each phase). The presence of nitrogen in the accumulator requires an additional field equation to model and track the movement of this noncondensable gas.

The required field equations are given in Table 7-2. The relationships to specific PIRT-important phenomena along with references to specific models are provided in Table 7-3. As indicated in Table 7-2 and Table 7-3, the S-RELAP5 code has the required field equations and models to address the important LBLOCA phenomena. A detailed discussion of the fluid field equations and their numerical solutions is provided in Section 7.4.

7.3.2   Closure Equations

Closure equations (constitutive models and correlations) are required to support the basic field equations. The closure equations are essential for modeling the processes and phenomena given in the PIRT (see Table 5-1). The S-RELAP5 constitutive models and correlations are presented in Reference 7-3. A detailed discussion of the constitutive models and correlations included in the EM is provided in Section 7.4. The verification and validation of the code models and correlations are given in Reference 7-2 and reiterated in Section 8.0. These two components of the present document
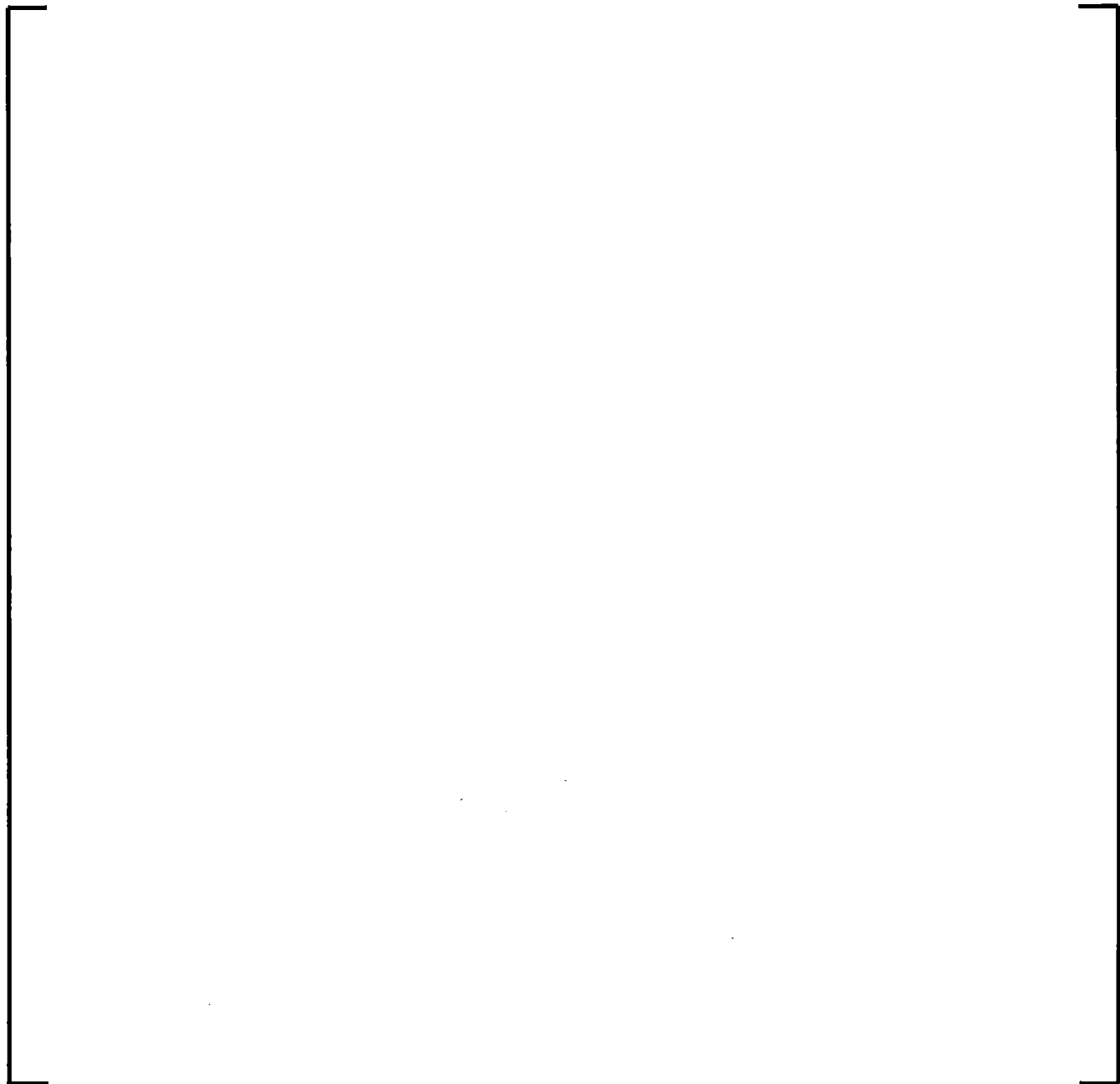
together demonstrate that the S-RELAP5 code adequately simulates LBLOCA events with a high level of confidence

The capability of the S-RELAP5 code closure equations to meet the requirements of the PIRT (see Table 5-1) is summarized in Table 7-14. The closure equations address wall friction, interphase friction, mass transfer (interphase heat transfer), wall-to-fluid heat transfer, form-losses, and similar functions. The various models require flow regime maps, boiling curves, state relationships, and fluid and material properties for completeness. As indicated in Table 7-2, the S-RELAP5 code has the required closure equations to address the important LBLOCA phenomena.

Table 7-2 Field Equations/Models in S-RELAP5

Scenario and PIRT Requirements	S-RELAP5 Model Existence	Field Equations/Model
Non-equilibrium Two-phase Flow	Yes	Six equation unequal velocity, unequal temperature
Non-condensable Gas Flow	Yes	Gas mass balance in vapor flow field
Multi-D Flow Capability	Yes	2-D components available as required
Separation Due to Gravity	Yes	Gravity pressure differential in flow field equations
Interphase Exchange Terms	Yes	Mass and energy transfer between phases, vaporization, and condensation

AREVA Inc.

EMF-2103NP
Revision 3

Realistic Large Break LOCA Methodology for Pressurized Water Reactors
Topical Report

Page 7-11

Table 7-3 Phenomena/Processes in S-RELAP5

7.3.3   Code Numerical Solutions

The numerical solutions contained in S-RELAP5 were extensively tested and checked (Reference 7-3, Section 2.6) and are discussed in Section 7.4.5. For the RLBLOCA methodology, the adequacy of S-RELAP5 numerical solutions is demonstrated in the performance of the assessments reported in Reference 7-2 and presented in Section 8.0. In addition, the adequacy of the numerical solution was also demonstrated by the time step sensitivity analysis reported in Appendix D.

7.3.4   Structure and Nodalization

To properly model an NPP, a code must be able to adequately model the important components and control systems of the NPP with respect to the chosen accident scenario. The S-RELAP5 code has the ability, as indicated in Table 7.3 of Reference 7-3, to model all the major components and associated control systems of the reference plants (listed in Section 1.0). The modeling of each of the NPP components is discussed in detail in Section 9.0. Section 9.0 also describes the studies that were performed to determine the final plant nodalization.

7.4   *Fluid Field Equations and Numerical Solutions*

The S-RELAP5 code solves a two-fluid, six equation model plus one continuity equation of noncondensable gas and a boron tracking equation for flow of a two-phase steam-water mixture which can contain a noncondensable in the vapor phase and a soluble in the liquid phase. The primary dependent variables for the eight field equations are P (pressure), U_g (gas specific internal energy), U_f (liquid specific internal energy), α_g (void fraction), X_n (noncondensable quality), ρ_B (boron density), v_g (gas velocity), and v_f (liquid velocity). The noncondensable quality is defined as the ratio of noncondensable gas mass to total gas phase mass. The phasic velocities v_g and v_f are vector variables. Other state variables, which appear in the fluid field equations, include ρ_g (gas density), ρ_f (liquid density), T_g (gas temperature), T_f (liquid temperature), and T_s (saturation temperature). These variables are related to P, U_g, and U_f through state relations. The phasic equations are coupled together via interfacial processes. The variables for

modeling the interphase processes include Γ_g (vapor generation rate per unit volume), Q_{ig} (interphase heat transfer rate per unit volume to vapor), Q_{if} (interphase heat transfer rate per unit volume to liquid), and Fl_{gf} (interphase friction force per unit volume). In addition, interaction between fluid field and heat conduction is treated through the wall vapor generation and wall heat transfer correlations.

Presented in this section are the two-fluid field equations and the solution methods for both the one-dimensional and two-dimensional formulations. The constitutive correlations describing the wall frictions, the interphase processes and the interactions between fluid and heat conduction are presented in Sections 7.6 and 7.7.

7.4.1   Vapor/Liquid Two-Fluid Field Equations

AREVA Inc.

Realistic Large Break LOCA Methodology for Pressurized Water Reactors
Topical Report

EMF-2103NP
Revision 3

Page 7-14

AREVA Inc.

EMF-2103NP
Revision 3

Realistic Large Break LOCA Methodology for Pressurized Water Reactors
Topical Report

Page 7-15

AREVA Inc.

EMF-2103NP
Revision 3

Realistic Large Break LOCA Methodology for Pressurized Water Reactors
Topical Report

Page 7-16

AREVA Inc.

EMF-2103NP
Revision 3

Realistic Large Break LOCA Methodology for Pressurized Water Reactors
Topical Report

Page 7-16

AREVA Inc.

EMF-2103NP
Revision 3

Realistic Large Break LOCA Methodology for Pressurized Water Reactors
Topical Report

Page 7-17

AREVA Inc.

EMF-2103NP
Revision 3

Realistic Large Break LOCA Methodology for Pressurized Water Reactors
Topical Report

Page 7-18

AREVA Inc.

Realistic Large Break LOCA Methodology for Pressurized Water Reactors
Topical Report

EMF-2103NP
Revision 3

Page 7-19

AREVA Inc.

Realistic Large Break LOCA Methodology for Pressurized Water Reactors
Topical Report

EMF-2103NP
Revision 3

Page 7-20

AREVA Inc.

Realistic Large Break LOCA Methodology for Pressurized Water Reactors
Topical Report

EMF-2103NP
Revision 3

Page 7-21

AREVA Inc.

Realistic Large Break LOCA Methodology for Pressurized Water Reactors
Topical Report

EMF-2103NP
Revision 3

Page 7-22

AREVA Inc.

Realistic Large Break LOCA Methodology for Pressurized Water Reactors
Topical Report

EMF-2103NP
Revision 3

Page 7-23

7.4.2   Noncondensable Gas

The basic, two-phase, single component, two-fluid field equations just discussed are extended to include a noncondensable component in the gas phase. The noncondensable component is assumed to be in mechanical and thermal equilibrium with the steam, that is $v_n = v_g$ (equal velocity) and $T_n = T_g$ (equal temperature). Here the subscript n designates the noncondensable component.

With the inclusion of a noncondensable component, all properties of the gas phase (subscript g) in the six fluid field Equations (7.1) to (7.6) are considered to be mixture properties of the steam/noncondensable mixture.[2] To track the noncondensable gas, it is necessary to add an additional mass conservation equation for the noncondensable component:

$$\frac{\partial}{\partial t}\left(\alpha_g \rho_g X_n\right) + \nabla \bullet \left(\alpha_g \rho_g X_n v_g\right) = 0 \tag{7.35}$$

---

[2]   Exceptions are the vapor enthalpies, h_g^* and h_g^s, appearing in Equation (7.6). These enthalpies are for the vapor phase (steam) alone.

AREVA Inc.

EMF-2103NP
Revision 3

Realistic Large Break LOCA Methodology for Pressurized Water Reactors
Topical Report

Page 7-24

where X_n is the mass fraction of noncondensable component based on the gaseous phase mass, that is, the ratio of noncondensable gas mass to total gas phase mass.

7.4.3   State Relationships

AREVA Inc.

EMF-2103NP
Revision 3

Realistic Large Break LOCA Methodology for Pressurized Water Reactors
Topical Report

Page 7-25

7.4.3.1 Single Component, Two-Phase Mixture

AREVA Inc.

EMF-2103NP
Revision 3

Realistic Large Break LOCA Methodology for Pressurized Water Reactors
Topical Report

Page 7-26
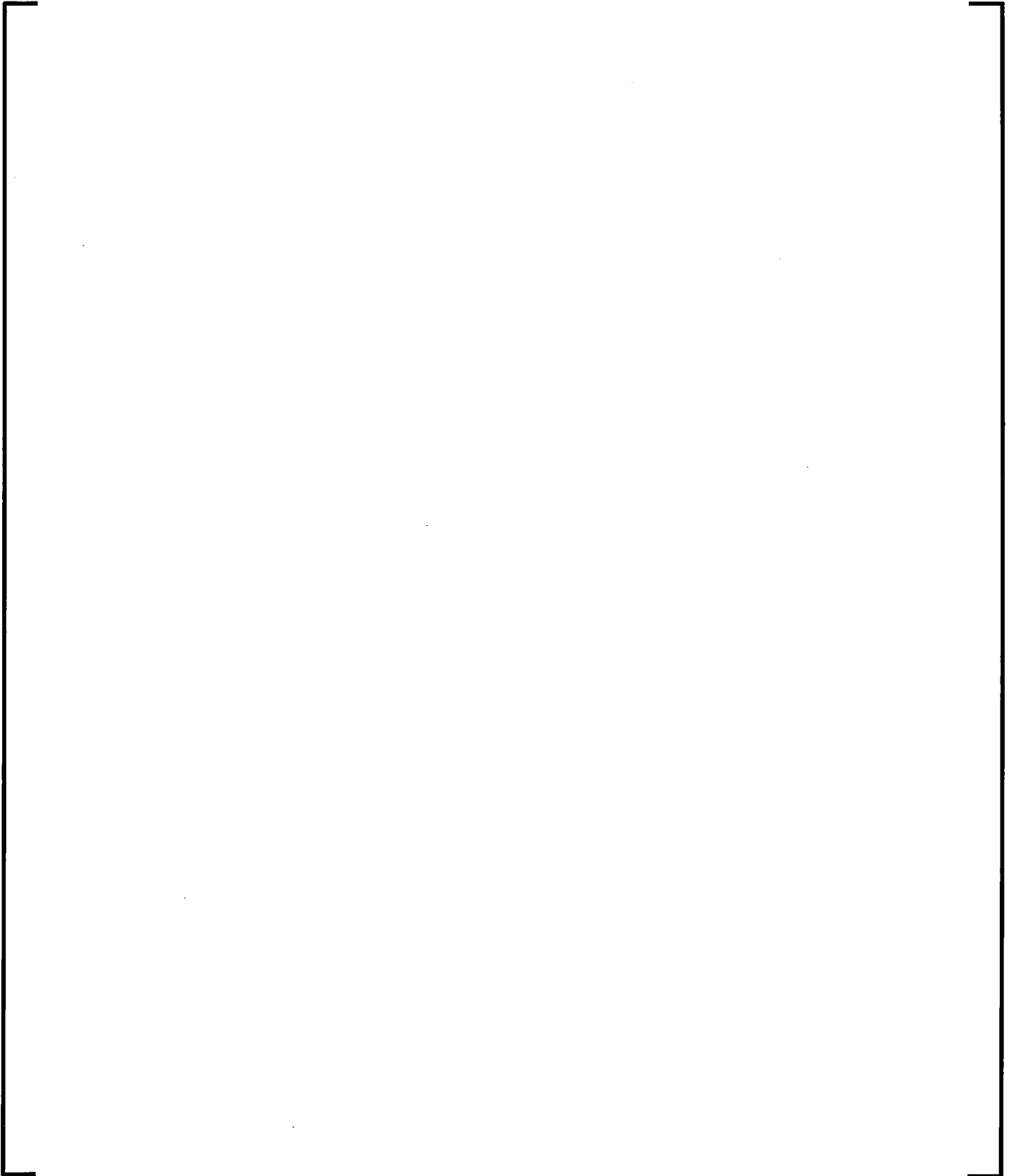
7.4.3.2   Two Component, Two-Phase Mixture

AREVA Inc.

EMF-2103NP
Revision 3

Realistic Large Break LOCA Methodology for Pressurized Water Reactors
Topical Report

Page 7-28

AREVA Inc.

EMF-2103NP
Revision 3

Realistic Large Break LOCA Methodology for Pressurized Water Reactors
Topical Report

Page 7-29

AREVA Inc.

EMF-2103NP
Revision 3

Realistic Large Break LOCA Methodology for Pressurized Water Reactors
Topical Report

Page 7-30

AREVA Inc.

EMF-2103NP
Revision 3

Realistic Large Break LOCA Methodology for Pressurized Water Reactors
Topical Report

Page 7-31

AREVA Inc.

EMF-2103NP
Revision 3

Realistic Large Break LOCA Methodology for Pressurized Water Reactors
Topical Report

Page 7-32

AREVA Inc.

EMF-2103NP
Revision 3

Realistic Large Break LOCA Methodology for Pressurized Water Reactors
Topical Report

Page 7-33

$$\left[\right]$$

7.4.4   Other Form and Modifications of Momentum Equations

Basic momentum equations for liquid and gas phases are presented in Equations (7.3) and (7.4). It is more convenient to use sum and difference momentum equations in the numerical solution scheme. Also, it is necessary to modify the difference momentum equation under horizontal stratified flow conditions.

7.4.4.1   Numerically Convenient Form

$$\left[\right]$$

AREVA Inc.

EMF-2103NP
Revision 3

Realistic Large Break LOCA Methodology for Pressurized Water Reactors
Topical Report

Page 7-34

7.4.4.2 Modifications for Horizontal Stratified Flow

AREVA Inc.

EMF-2103NP
Revision 3

Realistic Large Break LOCA Methodology for Pressurized Water Reactors
Topical Report

Page 7-35
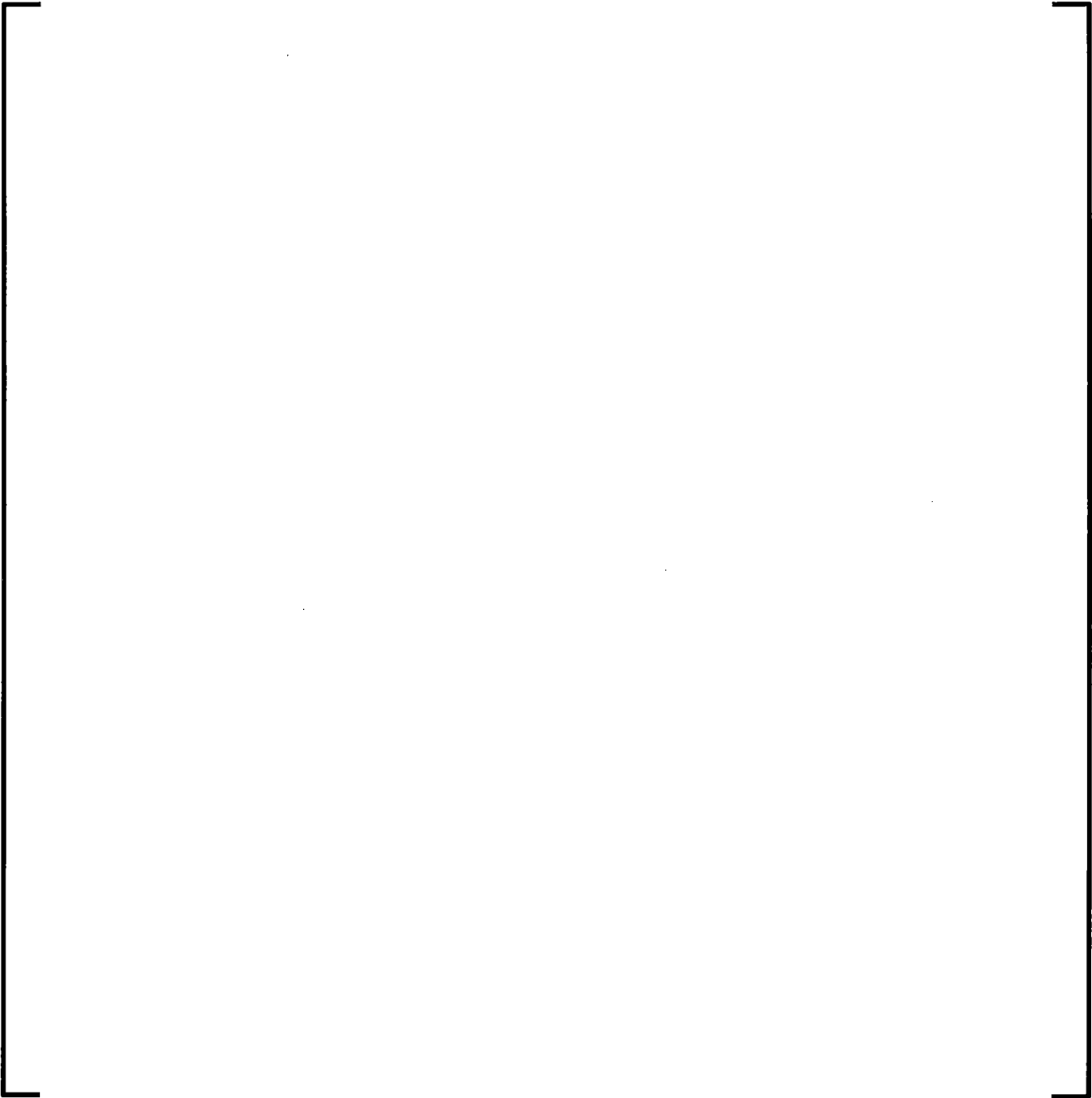
Figure 7-1 Schematic of Horizontal Stratification

$$\left[\right]$$

7.4.5   Semi-Implicit Numerical Solution Scheme

The semi-implicit numerical solution scheme replaces the system of differential equations with a system of finite-difference equations partially implicit in time. The terms evaluated implicitly are identified as the scheme is developed in the following. In all cases, the implicit terms are formulated to be linear in the dependent variables at new time. This results in a linear time-advancement matrix that is solved by direct inversion using a sparse matrix routine (Reference 7-21). An additional feature of the scheme is that implicitness is selected such that the field equations can be reduced to a single difference equation per fluid control volume (or mesh cell), which is in terms of the hydrodynamic pressure. Thus, only an N x N system of the difference equations must be solved simultaneously at each time step (N is the total number of control volumes used to simulate the fluid system).

It is well known (Reference 7-22) that the system of differential equations for two-phase, two-fluid flow constitutes an ill-posed, initial-value problem. This fact is of little concern physically since the addition of any second-order differential effect (regardless of how small) such as viscosity or surface tension results in a well-posed problem (Reference 7-23). However, the ill-posedness is of some concern numerically since it is necessary that the numerical problem be well-posed. The approximations inherent in any numerical scheme modify the solution somewhat (truncation error); these effects can be either stabilizing or destabilizing.

AREVA Inc.

Realistic Large Break LOCA Methodology for Pressurized Water Reactors
Topical Report

EMF-2103NP
Revision 3

Page 7-37

A well-posed numerical problem is obtained by several means. These include the selective implicit evaluation of spatial gradient terms at the new time, donor formulations for the mass and energy flux terms, and use of a donor-like formulation for the momentum flux terms. The term donor-like is used because the square of velocity in the momentum flux formulation is computed as a product of velocity in centered formulation and velocity in donor formulation. The well-posedness of the final numerical scheme (as well as its accuracy) has been demonstrated by extensive numerical testing during development and subsequent applications of RELAP5. Recently Shieh et al. (Reference 7-24) showed that mesh sizes and the magnitude of the interphase friction have strong effects on the stability and accuracy of the RELAP5 numerical method and that the method is capable of simulating physical instability if the mesh sizes are not too small; i.e., the ratios of mesh size to hydraulic diameter are sufficiently large.

The difference equations are based on the concept of a control volume (or mesh cell) in which mass and energy are conserved by equating accumulation to rate of influx through the cell boundaries. This model results in defining mass and energy volume average properties and requiring knowledge of velocities at the volume boundaries. The velocities at boundaries are most conveniently defined through use of momentum control volumes (cells) centered on the mass and energy cell boundaries. This approach results in a numerical scheme having a staggered spatial mesh. The scalar properties (pressure, energies, and void fraction) of the flow are defined at cell centers, and vector quantities (velocities) are defined on the cell boundaries. The resulting one-dimensional spatial noding is illustrated in Figure 7-2.

Figure 7-2 One-Dimensional Nodalization Schematic
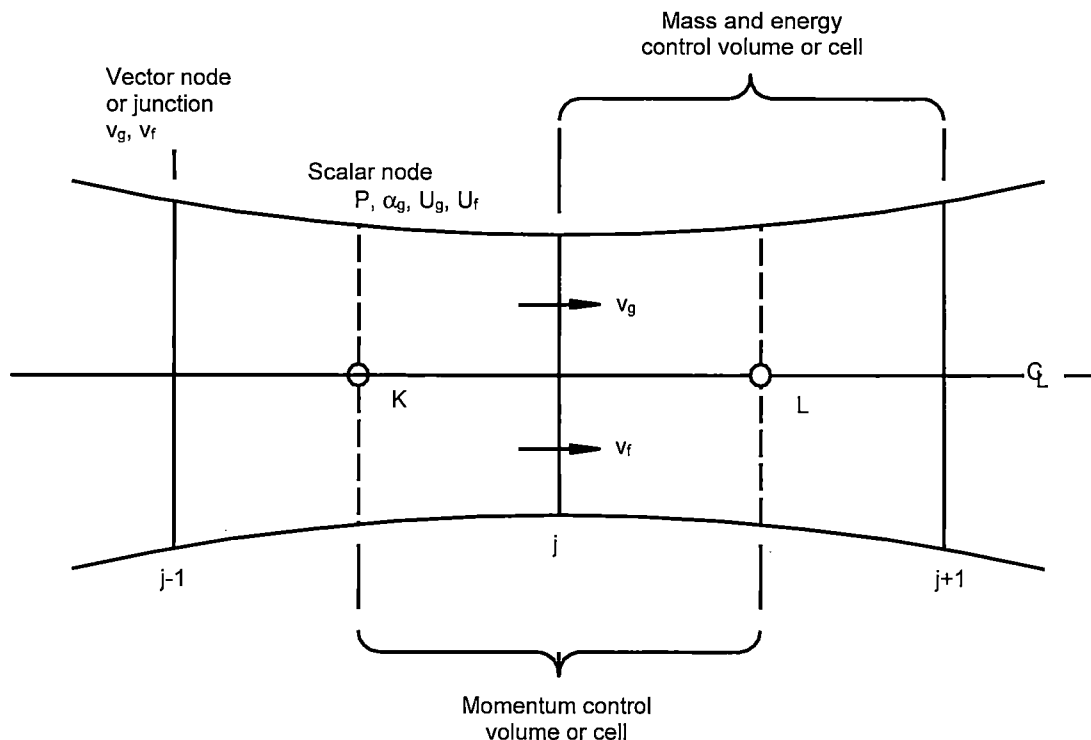
Some general guidelines for developing numerical solutions for the fluid field differential equations are summarized below.

1. Mass and energy inventories are very important quantities in water reactor safety analysis. The numerical scheme should be consistent and conservative in these quantities (a greater degree of approximation for momentum effects is considered acceptable). Both mass and energy are convected from the same cell and each is evaluated at the same time level; that is, if mass density is evaluated at old time level, energy density is also evaluated at old time.

2. To achieve fast execution speed, implicit evaluation is used only for those terms responsible for the sonic wave propagation time step limit, and those phenomena known to have small time constants. Thus, implicit evaluation is used for the velocity in mass and energy transport terms, the pressure gradient in the momentum equations, and the interphase mass and momentum exchange terms.

AREVA Inc.

EMF-2103NP
Revision 3

Realistic Large Break LOCA Methodology for Pressurized Water Reactors
Topical Report

Page 7-39

3. To further increase computing speed, time-level evaluations are selected so the resulting implicit terms are linear in the new time variables. Where it is necessary to retain non-linearities, Taylor series expansions about old time values are used to obtain a formulation linear in the new time variables (higher-order terms are neglected). Linearity results in high computing speed by eliminating the need to iteratively solve systems of nonlinear equations.

4. To allow easy degeneration to homogeneous or single-phase formulations, the momentum equations are expressed as sum and difference equations (Equations (7.83) and (7.84)).

7.4.5.1 One-Dimensional and Multi-Dimensional Formulations

AREVA Inc.

EMF-2103NP
Revision 3

Realistic Large Break LOCA Methodology for Pressurized Water Reactors
Topical Report

Page 7-40

AREVA Inc.

EMF-2103NP
Revision 3

Realistic Large Break LOCA Methodology for Pressurized Water Reactors
Topical Report

Page 7-41

AREVA Inc.

Realistic Large Break LOCA Methodology for Pressurized Water Reactors
Topical Report

EMF-2103NP
Revision 3

Page 7-42

AREVA Inc.

EMF-2103NP
Revision 3

Realistic Large Break LOCA Methodology for Pressurized Water Reactors
Topical Report

Page 7-43

7.4.5.2   Volume-Average Velocities

AREVA Inc.

EMF-2103NP
Revision 3

Realistic Large Break LOCA Methodology for Pressurized Water Reactors
Topical Report

Page 7-45

7.4.5.3 One-Dimensional, Finite-Difference Equations

AREVA Inc.

EMF-2103NP
Revision 3

Realistic Large Break LOCA Methodology for Pressurized Water Reactors
Topical Report

Page 7-46

AREVA Inc.

Realistic Large Break LOCA Methodology for Pressurized Water Reactors
Topical Report

EMF-2103NP
Revision 3

Page 7-48

AREVA Inc.

EMF-2103NP
Revision 3

Realistic Large Break LOCA Methodology for Pressurized Water Reactors
Topical Report

Page 7-49

AREVA Inc.

EMF-2103NP
Revision 3

Realistic Large Break LOCA Methodology for Pressurized Water Reactors
Topical Report

Page 7-50

7.4.5.4   Two-Dimensional, Finite-Difference Formulation

AREVA Inc.

EMF-2103NP
Revision 3

Realistic Large Break LOCA Methodology for Pressurized Water Reactors
Topical Report

Page 7-51

Figure 7-3 Momentum Cell j and Its Six Neighboring Control Volumes

AREVA Inc.

Realistic Large Break LOCA Methodology for Pressurized Water Reactors
Topical Report

EMF-2103NP
Revision 3

Page 7-52

$$\left[\phantom{\rule{0pt}{6cm}}\right]$$
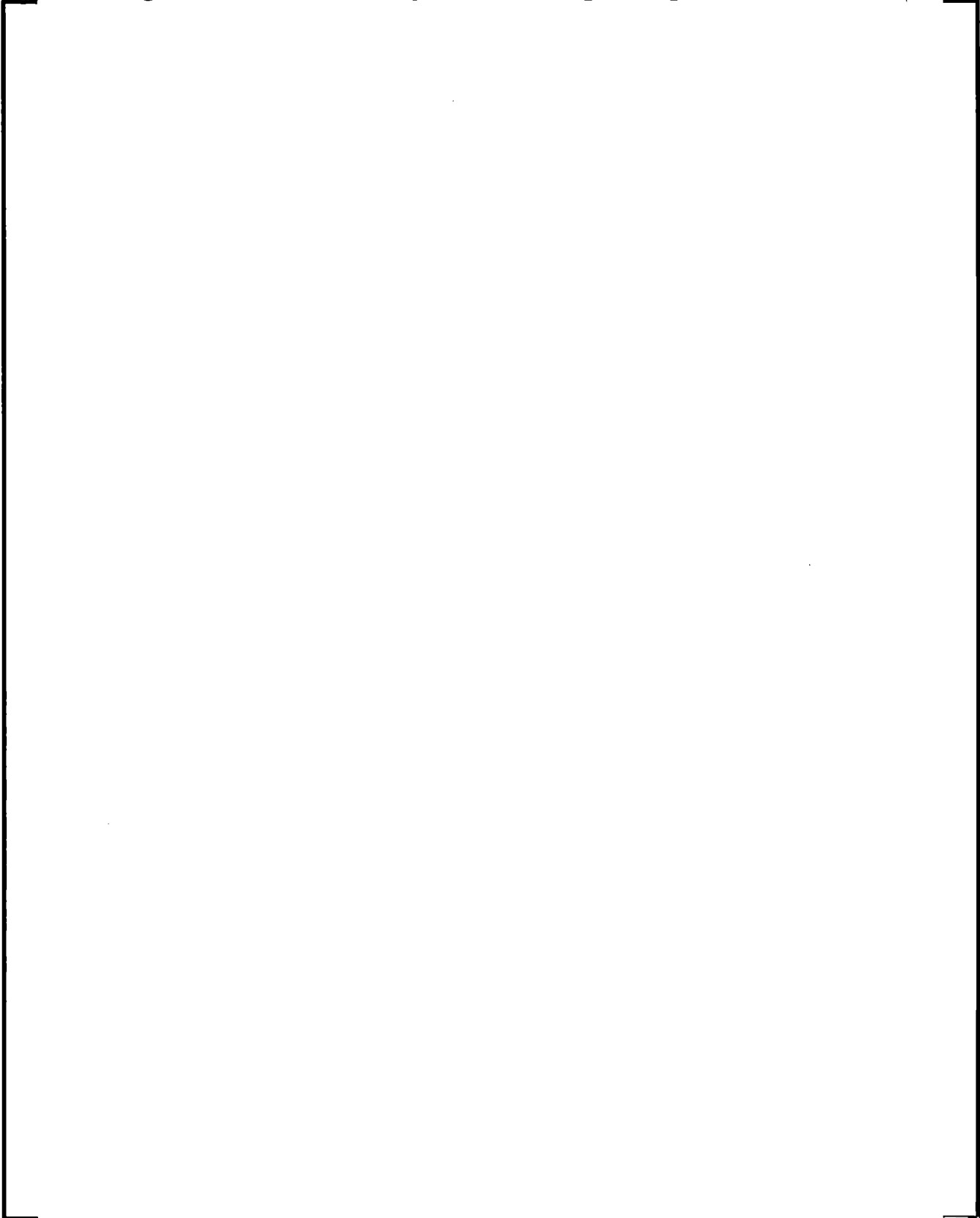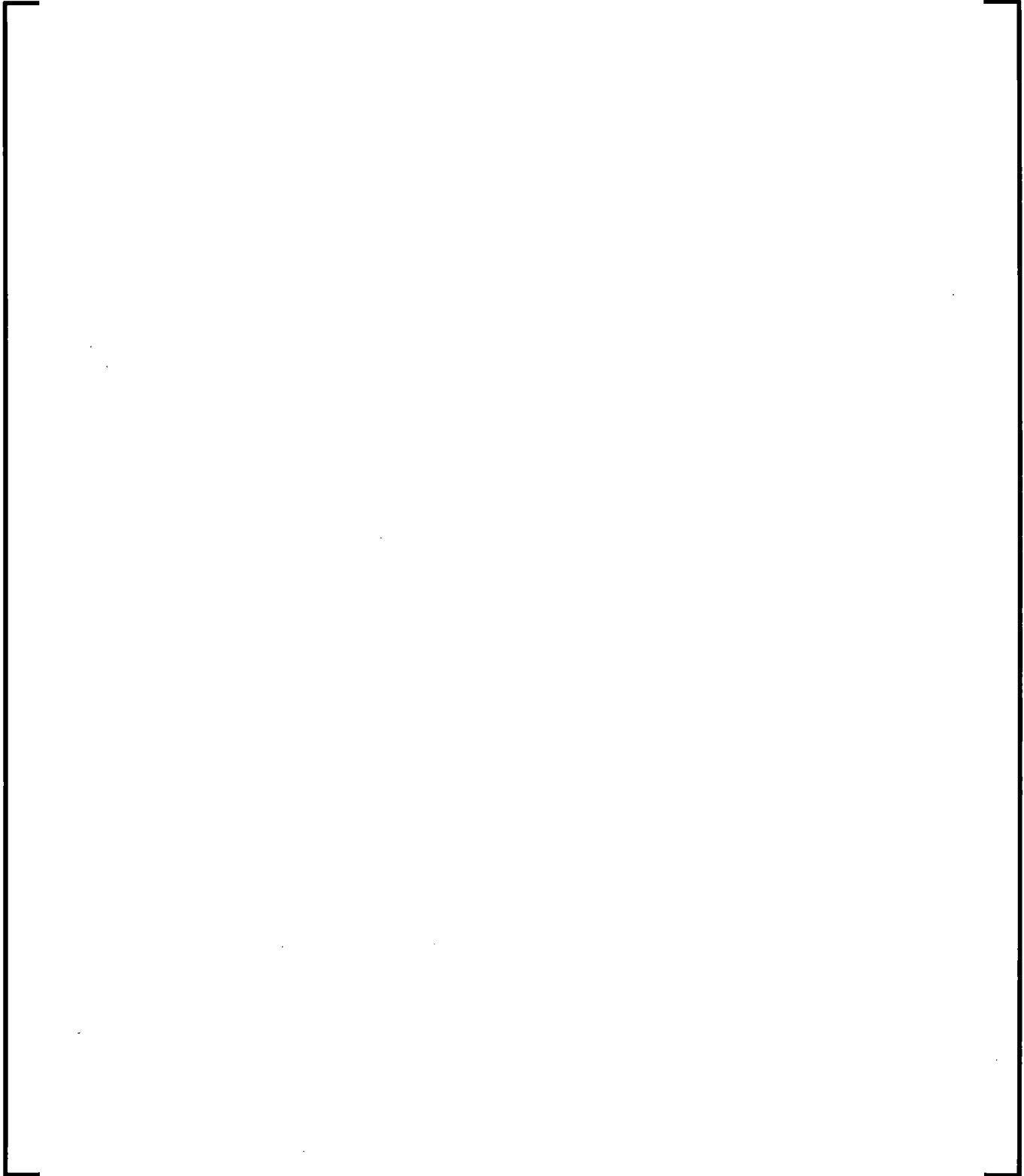
7.4.5.5   Solutions of Finite-Difference Equations

The finite-difference equations are solved numerically for the independent variables P, U_g, U_f, X_n, α_g, v_g, and v_f. There are $2N_j$ momentum equations for N_j junctions and $5N_v$ mass and energy equations for N_v (control) volumes. Once the finite-difference equations are obtained, there is no distinction between one-dimensional, two-dimensional, or cross flow junctions. Therefore, the one-dimensional finite-difference equations, Equations (7.107) through (7.111), (7.118), and (7.119), are used in the following subsections to illustrate the numerical solution scheme.

7.4.5.5.1   Momentum Equations

$$\left[\phantom{\rule{0pt}{4cm}}\right]$$

AREVA Inc.

Realistic Large Break LOCA Methodology for Pressurized Water Reactors
Topical Report

EMF-2103NP
Revision 3

Page 7-54

AREVA Inc.

EMF-2103NP
Revision 3

Realistic Large Break LOCA Methodology for Pressurized Water Reactors
Topical Report

Page 7-55

AREVA Inc.

Realistic Large Break LOCA Methodology for Pressurized Water Reactors
Topical Report

EMF-2103NP
Revision 3

Page 7-56

AREVA Inc.

EMF-2103NP
Revision 3

Realistic Large Break LOCA Methodology for Pressurized Water Reactors
Topical Report

Page 7-57

7.4.5.5.2   *Mass and Energy Balance Equations*

AREVA Inc.

Realistic Large Break LOCA Methodology for Pressurized Water Reactors
Topical Report

EMF-2103NP
Revision 3

Page 7-58

AREVA Inc.

EMF-2103NP
Revision 3

Realistic Large Break LOCA Methodology for Pressurized Water Reactors
Topical Report

Page 7-60

AREVA Inc.

Realistic Large Break LOCA Methodology for Pressurized Water Reactors
Topical Report

EMF-2103NP
Revision 3

Page 7-61

AREVA Inc.

Realistic Large Break LOCA Methodology for Pressurized Water Reactors
Topical Report

EMF-2103NP
Revision 3

Page 7-62

AREVA Inc.

EMF-2103NP
Revision 3

Realistic Large Break LOCA Methodology for Pressurized Water Reactors
Topical Report

Page 7-63

7.4.5.6 Final Solutions at Each Time-Step Advancement

AREVA Inc.

EMF-2103NP
Revision 3

Realistic Large Break LOCA Methodology for Pressurized Water Reactors
Topical Report

Page 7-64

AREVA Inc.

Realistic Large Break LOCA Methodology for Pressurized Water Reactors
Topical Report

EMF-2103NP
Revision 3

Page 7-65

AREVA Inc.

EMF-2103NP
Revision 3

Realistic Large Break LOCA Methodology for Pressurized Water Reactors
Topical Report

Page 7-66

7.4.5.7 Time Step Control

AREVA Inc.

EMF-2103NP
Revision 3

Realistic Large Break LOCA Methodology for Pressurized Water Reactors
Topical Report

Page 7-67

AREVA Inc.

EMF-2103NP
Revision 3

Realistic Large Break LOCA Methodology for Pressurized Water Reactors
Topical Report

Page 7-68

7.4.5.8   Special Techniques to Mitigate Numerical Anomalies

AREVA Inc.

EMF-2103NP
Revision 3

Realistic Large Break LOCA Methodology for Pressurized Water Reactors
Topical Report

Page 7-69

AREVA Inc.

Realistic Large Break LOCA Methodology for Pressurized Water Reactors
Topical Report

EMF-2103NP
Revision 3

Page 7-70

AREVA Inc.

EMF-2103NP
Revision 3

Realistic Large Break LOCA Methodology for Pressurized Water Reactors
Topical Report

Page 7-71

AREVA Inc.

EMF-2103NP
Revision 3

Realistic Large Break LOCA Methodology for Pressurized Water Reactors
Topical Report

Page 7-72

[ ]

7.4.6   References

7-11.   EGG-EAST-8546, Course A -- Numerical Modeling of Two-Phase
         Flows for Presentation at École d'Été d'Analyse Numérique, May
         1989.

7-12.   M. Ishii, Thermo-Fluid Dynamic Theory of Two-Phase, Collection de la
         Direction des Études et Recherches d'Électricite de France, 1975.

7-13.   D. A. Drew, "Averaging Field Equations for Two-Phase Media,"
         Studies in Applied Mathematics, L(2), pp. 133-166, 1971.

7-14.   F. H. Harlow and A. A. Amsden, "Flow of Interpenetrating Material
         Phases," Journal of Computational Physics, Volume 18, pp. 440-464,
         1975.

7-15.   NUREG/CR-5069, LA-11208-MS, TRAC-PF1/MOD1 Correlations and
         Models, December 1988.

7-16.   NUREG/CR-3046, PNL-4385M, COBRA/TRAC – A Thermal-
         Hydraulics Code for Transient Analysis of Nuclear Reactor Vessels
         and Primary Coolant Systems, Volume 1, Equations and Constitutive
         Models, March 1983.

AREVA Inc.

Realistic Large Break LOCA Methodology for Pressurized Water Reactors
Topical Report

EMF-2103NP
Revision 3
Page 7-74

7-17. D. A. Drew, L. Y. Cheng, and R. T. Lahey, Jr., "The Analysis of Virtual Mass Effects in Two-Phase Flow," International Journal of Multiphase Flow, Volume 5, pp. 233-242, 1979.

7-18. NUREG/CR-1826, EGG-2070, RELAP5/MOD1 Code Manual Volume 1: System Models and Numerical Methods, March 1982.

7-19. R. B. Bird, W. E. Stewart, and E. N. Lightfoot, Transport Phenomena, John Wiley & Sons, 1960.

7-20. U.S. Nuclear Regulatory Commission, "NRC Information Notice 92-02: RELAP5/MOD3 Computer Code Error Associated with the Conservation of Energy Equation," January 3, 1992; NRC Information Notice 92-02, "Supplement 1: RELAP5/MOD3 Computer Code Error Associated with the Conservation of Energy Equation," February 18, 1992.

7-21. A. R. Curtis and J. K. Reid, FORTRAN Subroutines for the Solution of Sparse Sets of Linear Equations, AERE-R6844, 1971.

7-22. D. Gidaspow (Chairman), "Modeling of Two-Phase Flow," Proceedings of Round Table Discussion RT-1-2 at the 5th International Heat Transfer Conference, Tokyo, Japan, September, 3-7, 1974. Also in ASME Journal of Heat Transfer, Volume 3, 1974.

7-23. J. D. Ramshaw and J. A. Trapp, "Characteristics, Stability, and Short-Wavelength Phenomena in the Two-Phase Flow Equation Systems," Nuclear Science and Engineering, Volume 66, pp. 93-102, 1978.

7-24. A. S.-L. Shieh, R. Krishnamurthy, and V. H. Ransom, "Stability, Accuracy, and Convergence of the Numerical Methods in RELAP5/MOD3," Nuclear Science and Engineering, Volume 116, pp. 227-244, 1994.

7.5   *Hydrodynamic Constitutive Models*

The hydrodynamic constitutive models for describing the interphase coupling terms and the wall friction terms in the fluid field equations shown in Section 7.4 are presented in this section. The interphase coupling terms include heat/mass transfer and interphase friction (drag and/or shear). The mass transfer term is further divided into the heat/mass transfer in the bulk fluid and the heat/mass transfer near the wall. The interphase heat/mass transfer near the wall will be discussed in Section 7.6. As presented in Section 7.4, the bulk interphase mass transfer rate is expressed in terms of interphase heat transfer rates to liquid and vapor phase.

The interphase coupling terms are formulated within the framework of the two-fluid model and are constructed from the formulations for the basic elements of flow patterns such as bubbles, droplets, vapor slugs (i.e., large bubbles), liquid slugs (i.e., large liquid drops or chunks of liquid), liquid film, and vapor film. Most formulations are semi-empirical or semi-mechanistic. All formulations have some physical meanings attached to them. For example, the dependence of interphase coupling terms on the interfacial area per unit volume makes sense. The dynamic coupling effects among all formulations and the lack of direct measuring methods make it difficult to assess each formulation individually. Consequently, the only meaningful validation of the constitutive models is to assess the whole package against the experimental data of the key parameters that can be driven by the interphase constitutive models, such as phasic temperatures, phasic velocities, phasic densities, mass flow rates, and void fraction. Code-data comparisons for these key parameters are the main sources for validating the applicability of the interphase constitutive models.

In RELAP5/MOD3 (References 7-6 and 7-7), the two-fluid formulation of interphase friction for vertical bubbly-slug flow is replaced by the drift-flux method, particularly the EPRI drift-flux correlations (Reference 7-25). The EPRI correlations are tuned mostly to the steady-state data with regular flow profiles. They perform best under steady-state or nearly steady-state conditions. There is little evidence that these fix-profile correlations are superior to the two-fluid formulation in simulating LBLOCA transients,

AREVA Inc.

Realistic Large Break LOCA Methodology for Pressurized Water Reactors
Topical Report

EMF-2103NP
Revision 3
Page 7-76

which are highly irregular and chaotic in nature. Furthermore, the EPRI correlations do not cover the entire range of two-phase flow conditions. Therefore, the RELAP5/MOD3 approach is not adopted in S-RELAP5. Assessment examples indicate that the S-RELAP5 two-fluid formulation produces code-data comparisons that are as good as those obtained by RELAP5/MOD3 for steady-state and nearly steady-state cases (References 7-26 and 7-27).

The models for interphase heat transfer, interphase friction, and wall friction are generally represented by correlations and parameters which are dependent on flow regimes. Therefore, this section begins with a description of flow regime classification.

7.5.1   Flow Regime Maps

Three principal flow-regime maps are used in S-RELAP5: (a) vertical flow map for elevation angle greater than 30 degrees, (b) horizontal flow map for elevation angle less than or equal to 30 degrees, and (c) high mixing flow map for pumps. The flow regime classification of vertical and horizontal flow maps is based heavily on the work of Taitel and Dukler (References 7-28 and 7-29), Wallis (Reference 7-30), and Ishii (References 7-31, 7-32, and 7-33), with some simplification made for efficient computation.

There are many publications on the subject of flow regime maps (References 7-34, 7-35, and 7-36). Some are relatively simple, but most are quite complex and elaborate. Selection of flow regime maps for S-RELAP5 is based on two general rules: (1) the transition criteria must be relatively simple for efficient computation, and (2) mechanistic or semi-mechanistic models are preferred. A complex flow regime map inherently has more flow regime transition lines. Since discontinuities across the transition line often produce calculational flow oscillations, there are more chances for the solution to be distorted and, thus, a less accurate solution might be obtained with an overly-complex flow regime classification. It should also be pointed out that most published data are for air-water systems. Therefore, simple semi-mechanistic approaches are expected to perform better in a system of steam-water two-phase flow with or without noncondensables. For both one- and two-dimensional components, one and only one

flow regime is defined for each control volume. If a direction-dependent parameter is required to determine the flow regime map in a two-dimensional component, the main flow direction (i.e., the x-direction, see Section 7.4.5.1) parameter value is used.

7.5.1.1   Vertical Flow Regime Map

There are seven principal flow regimes in the vertical flow map: bubbly, slug, and annular-mist for the pre-CHF or wet-wall conditions; inverted annular, inverted slug, and mist for the post-CHF or dry-wall conditions; and vertical stratification for the sharp void profile conditions. To smooth the interphase coupling terms, various transition (or interpolation) regions are inserted (they will be explained later). Jones and Zuber (Reference 7-37) defined three dominant flow patterns as bubbly, slug, and annular flow with the slug flow lying approximately between void fractions of 0.2 and 0.8. Division into bubbly, slug, and annular-mist regimes was used by Vince and Lahey (Reference 7-38) to analyze their data. One additional flow regime, churn flow, is also defined in the work of Taitel and Dukler (Reference 7-28), and Ishii (Reference 7-33). However, the churn flow is considered to be similar to the slug flow but much more chaotic and the transition line is harder to define. Therefore, the churn flow is not explicitly defined. Instead, a transition region between the slug flow and the annular-mist flow is added to implicitly account for the churn flow. Under dry-wall flow conditions, the bubbly, slug, and annular-mist regimes are, respectively, transformed to the inverted annular, inverted slug, and mist flow regimes as suggested by Ishii (References 7-31 and 7-36).

7.5.1.1.1   Wet-Wall Flow Regimes

AREVA Inc.

EMF-2103NP
Revision 3

Realistic Large Break LOCA Methodology for Pressurized Water Reactors
Topical Report

Page 7-79

AREVA Inc.

EMF-2103NP
Revision 3

Realistic Large Break LOCA Methodology for Pressurized Water Reactors
Topical Report

Page 7-81
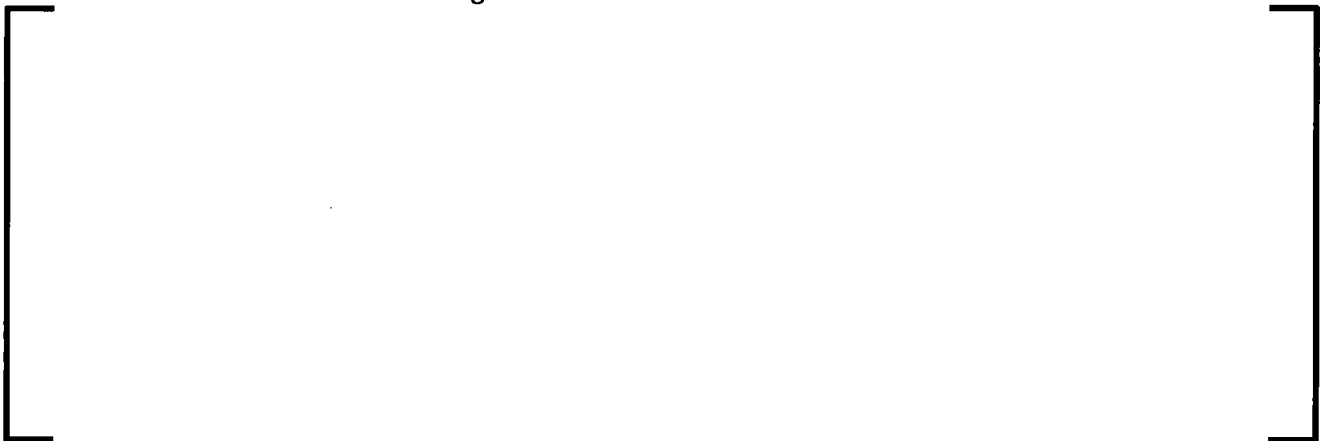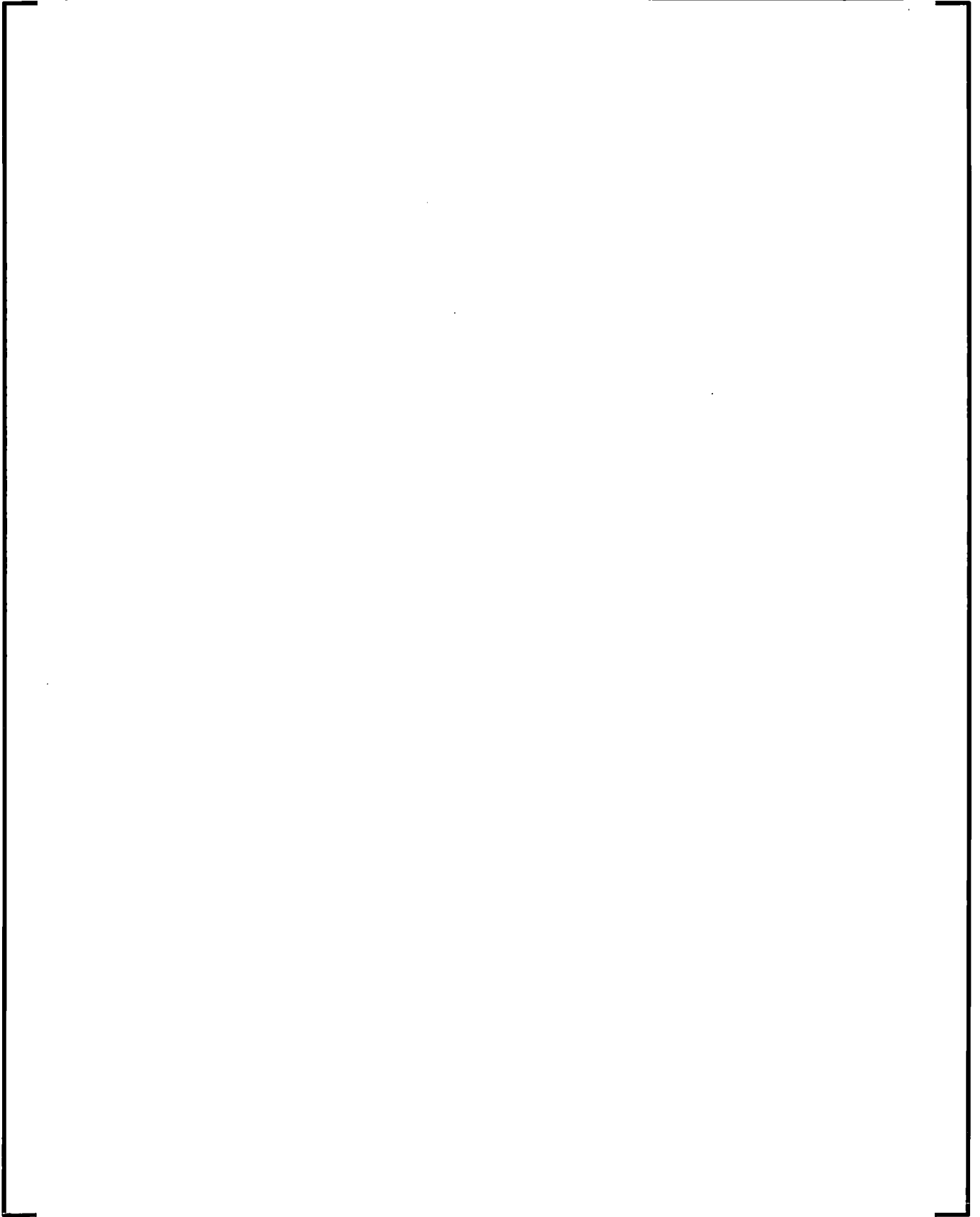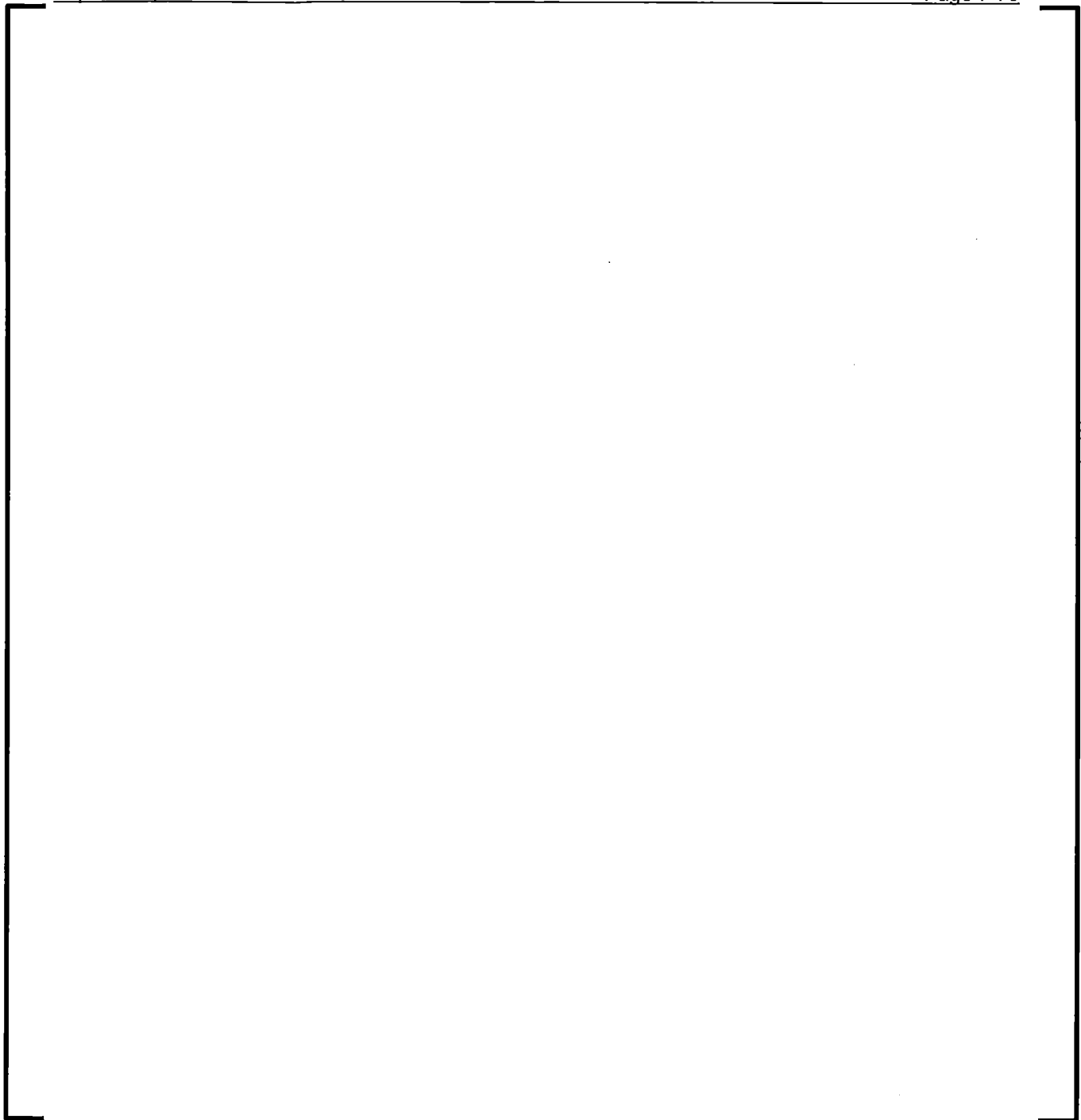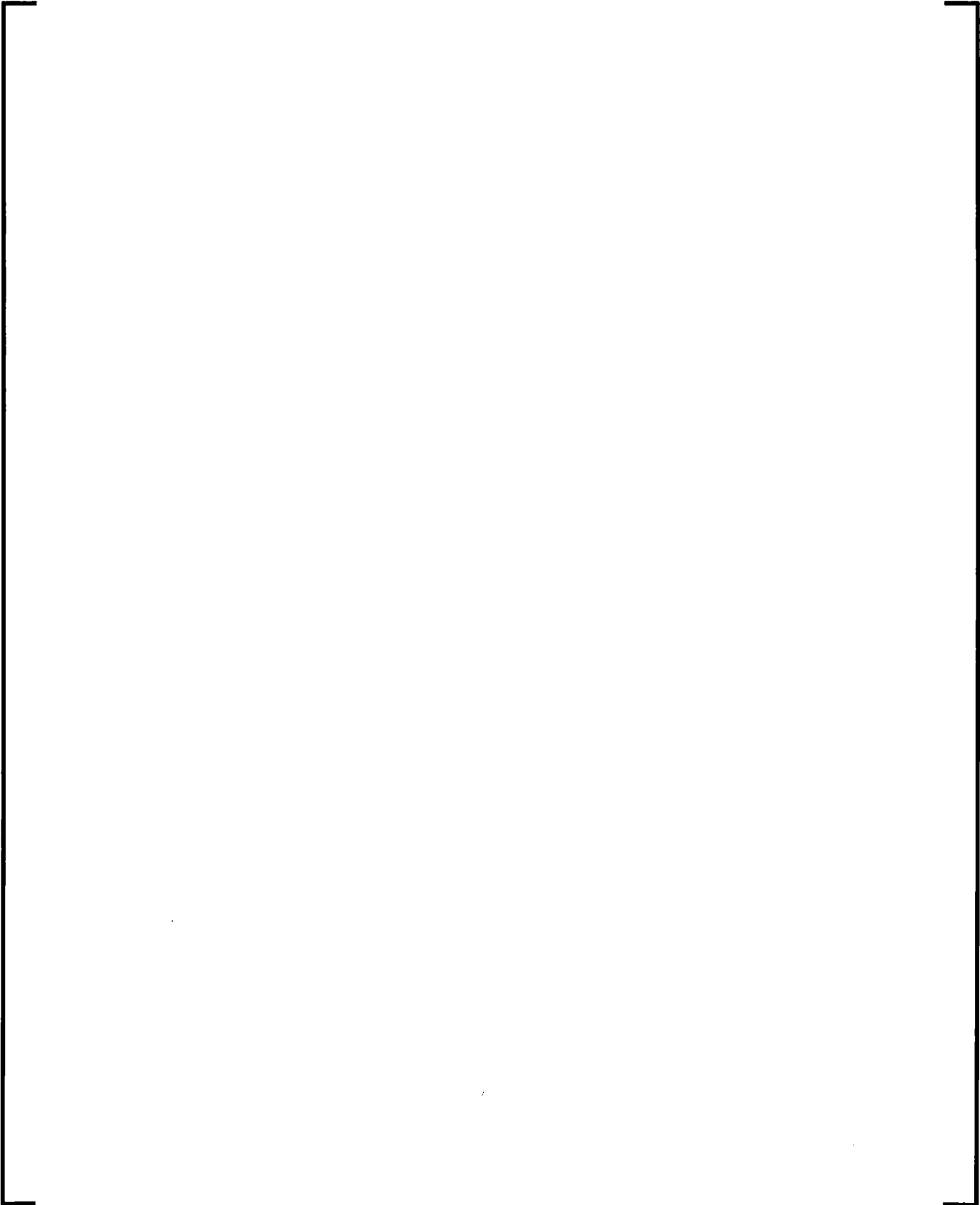
7.5.1.1.2   Dry-Wall Flow Regimes

AREVA Inc.

Realistic Large Break LOCA Methodology for Pressurized Water Reactors
Topical Report

EMF-2103NP
Revision 3

Page 7-83

7.5.1.1.3   *Vertical Stratification*

AREVA Inc.

EMF-2103NP
Revision 3

Realistic Large Break LOCA Methodology for Pressurized Water Reactors
Topical Report

Page 7-84
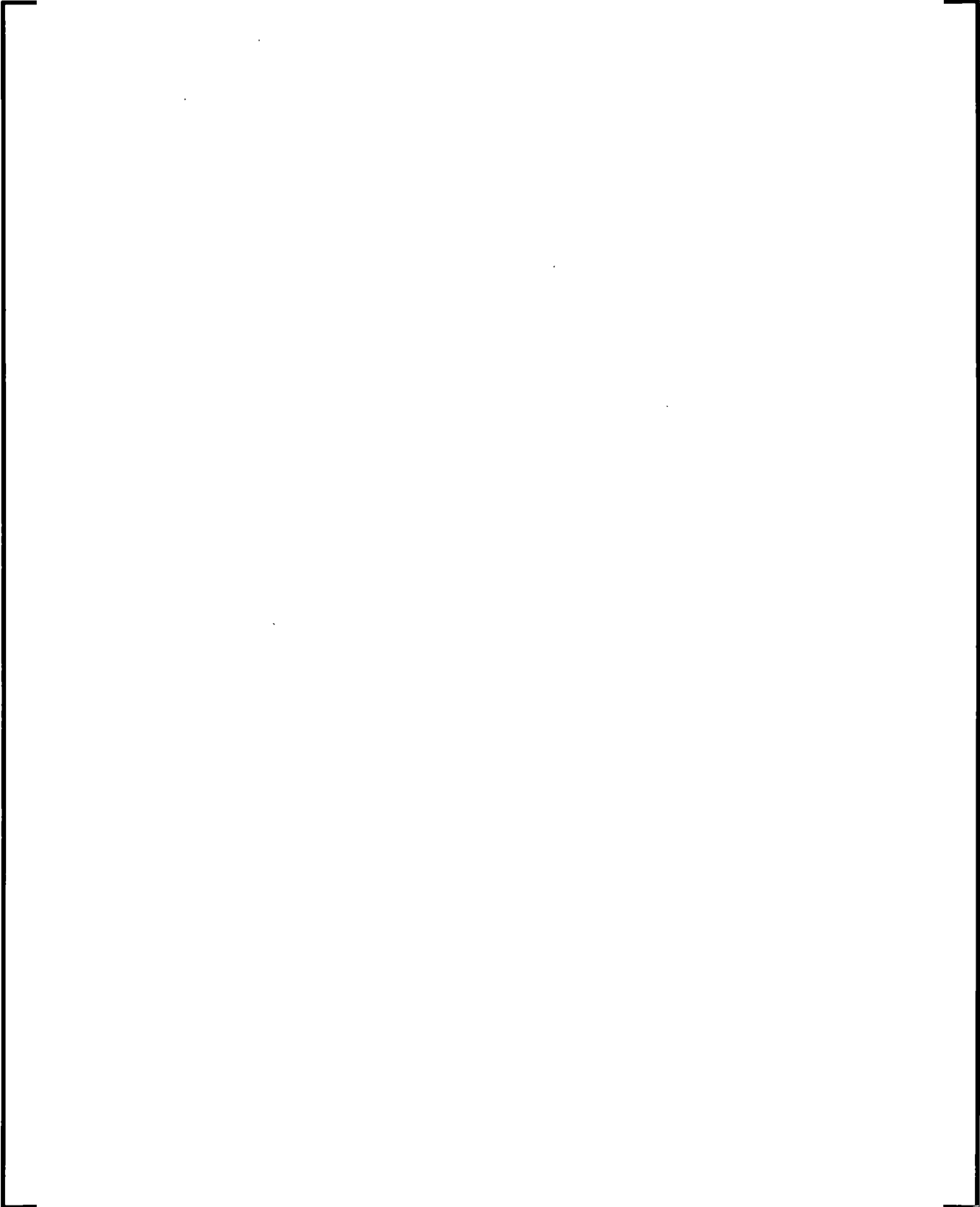
Figure 7-4 Sketch of Two-Phase Mixture Level

AREVA Inc.

EMF-2103NP
Revision 3

Realistic Large Break LOCA Methodology for Pressurized Water Reactors
Topical Report

Page 7-85

7.5.1.2 Horizontal Flow Regime Map

Four principal flow regimes are used to classify horizontal flow: stratified flow, bubbly flow, slug flow, and annular-mist flow. There is no distinction between wet-wall and dry-wall flow. This simple classification is considered to be adequate for U.S. light water reactors since vertical flow in the reactor vessel and steam generator is dominant.

Taitel and Dukler (Reference 7-28) developed the following criterion, based on the instability for a solitary wave, for stratified flow:

$$v_g \leq v_{HS} \tag{7.268}$$

where:

$$v_{HS} = \frac{1}{2}(1 - \cos\theta)\sqrt{\frac{\alpha_g A (\rho_f - \rho_g) g \cos\beta}{\rho_g D \sin\theta}} \tag{7.269}$$

Here A is the volume flow area, β is the volume vertical angle $(-30^\circ < \beta < 30^\circ)$, and θ is the angle between the vertical line and the radial line to the interface $(0^\circ \leq \theta \leq 180^\circ$, see Figure 7-1). The algebraic relation between α_g and θ is given by Equation (7.91). Also, the height of liquid level h_L (measured from the pipe bottom) is related to θ by

$$h_L = D\frac{(1 + \cos\theta)}{2} \tag{7.270}$$

Given the void fraction α_g, the angle θ can be obtained by solving Equation (7.91) iteratively. If only liquid level height is needed, then it can be computed by approximating $\cos\theta$ as $2HCL(\alpha_g)$ for $\alpha_g \leq 0.5$ and $-2HCL(\alpha_f)$ for $\alpha_g > 0.5$, where the function HCL is:

$$HCL(x) = 0.5 - 0.70269591x^{2/3} - 0.03414667x - 0.1610239111x^2 \tag{7.271}$$

The transition criterion of Equation (7.268) was applied in RELAP5/MOD2 (Reference 7-43).

To enhance the smoothness of interphase drag and interphase heat transfer terms, an interpolation or transition region between the stratified and non-stratified flow is required. For the purpose of defining the transition region, a parameter ϕ is introduced, using Equation (7.268), as follows:

$$\phi = \frac{v_g}{v_{HS}} \tag{7.272}$$

The horizontal flow is stratified if $0.9 \geq \phi$ and the transition from stratified to non-stratified occurs when $0.9 < \phi < 2.5$. Note that in the code output, the horizontal stratification flow

AREVA Inc.

EMF-2103NP
Revision 3

Realistic Large Break LOCA Methodology for Pressurized Water Reactors
Topical Report

Page 7-87

regime includes the stratification and transition regions. The large transition region is needed because the magnitude of the interphase friction term for the non-stratification flow regimes can be three orders higher than that for the stratification flow.

For non-stratified flow, the transition from bubbly flow to slug flow is given by

$$\alpha_{B-S} = 0.25 \tag{7.273}$$

Wallis (Reference 7-30) suggested that the value of $j_g{}^*$ at the boundary between slug and annular-mist flow is in the range of 0.25 to 1.0 for the pipe sizes considered by Baker (Reference 7-30). As the value of 0.9 is within this range, Equation (7.254), which is one of the two transition criteria for vertical flow, is used to define the transition boundary between the slug and annular-mist flow. Thus, the transition from slug flow to annular-mist flow occurs at the void fraction

$$\alpha_{S-A} = \frac{0.9\sqrt{gD\left(\rho_f - \rho_g\right)}}{v_g \sqrt{\rho_g}} \tag{7.274}$$

In the code implementation, the above transition void fraction is bounded between 0.8 and 0.5. Similar to the annulus component flow regime map, a slug-annular-mist transition region is defined within the slug flow regime. The transition region begins at a void fraction specified by Equation (7.258), with α_{B-S} given by Equation (7.273) and α_{S-A} given by Equation (7.274), and ends at the transition boundary specified by Equation (7.274). Thus, α_{S-A} of Equation (7.274) becomes the transition line between the slug-annular transition region and the annular regime, or α_{SA-A}.

7.5.1.3 High Mixing Flow Regime Map

AREVA Inc.

Realistic Large Break LOCA Methodology for Pressurized Water Reactors
Topical Report

EMF-2103NP
Revision 3

Page 7-88
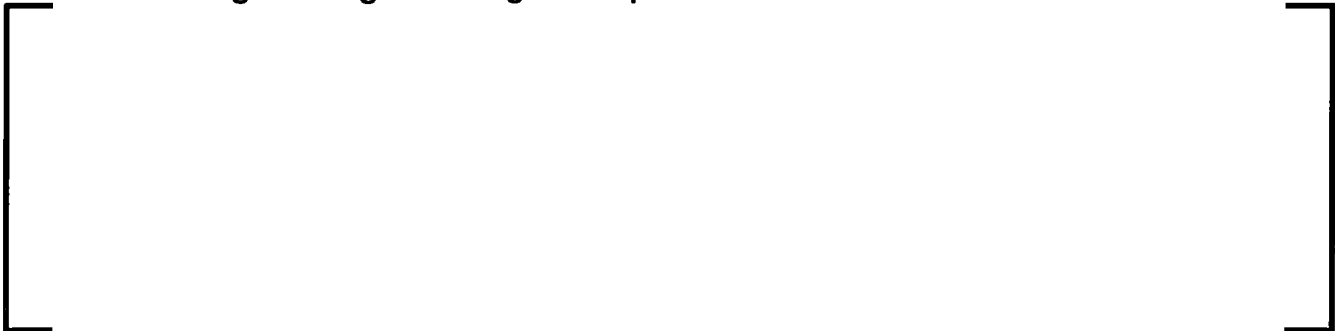
7.5.1.4 Diagrams of Flow Regimes

AREVA Inc.

Realistic Large Break LOCA Methodology for Pressurized Water Reactors
Topical Report

EMF-2103NP
Revision 3

Page 7-89

Figure 7-5 Vertical Flow Regime Map With Hatches Indicating Transition Regions

7.5.2 Interphase Friction

AREVA Inc.

EMF-2103NP
Revision 3

Realistic Large Break LOCA Methodology for Pressurized Water Reactors
Topical Report

Page 7-90

7.5.2.1   Dispersed Flow

AREVA Inc.

Realistic Large Break LOCA Methodology for Pressurized Water Reactors
Topical Report

EMF-2103NP
Revision 3

Page 7-91

AREVA Inc.

EMF-2103NP
Revision 3

Realistic Large Break LOCA Methodology for Pressurized Water Reactors
Topical Report

Page 7-92
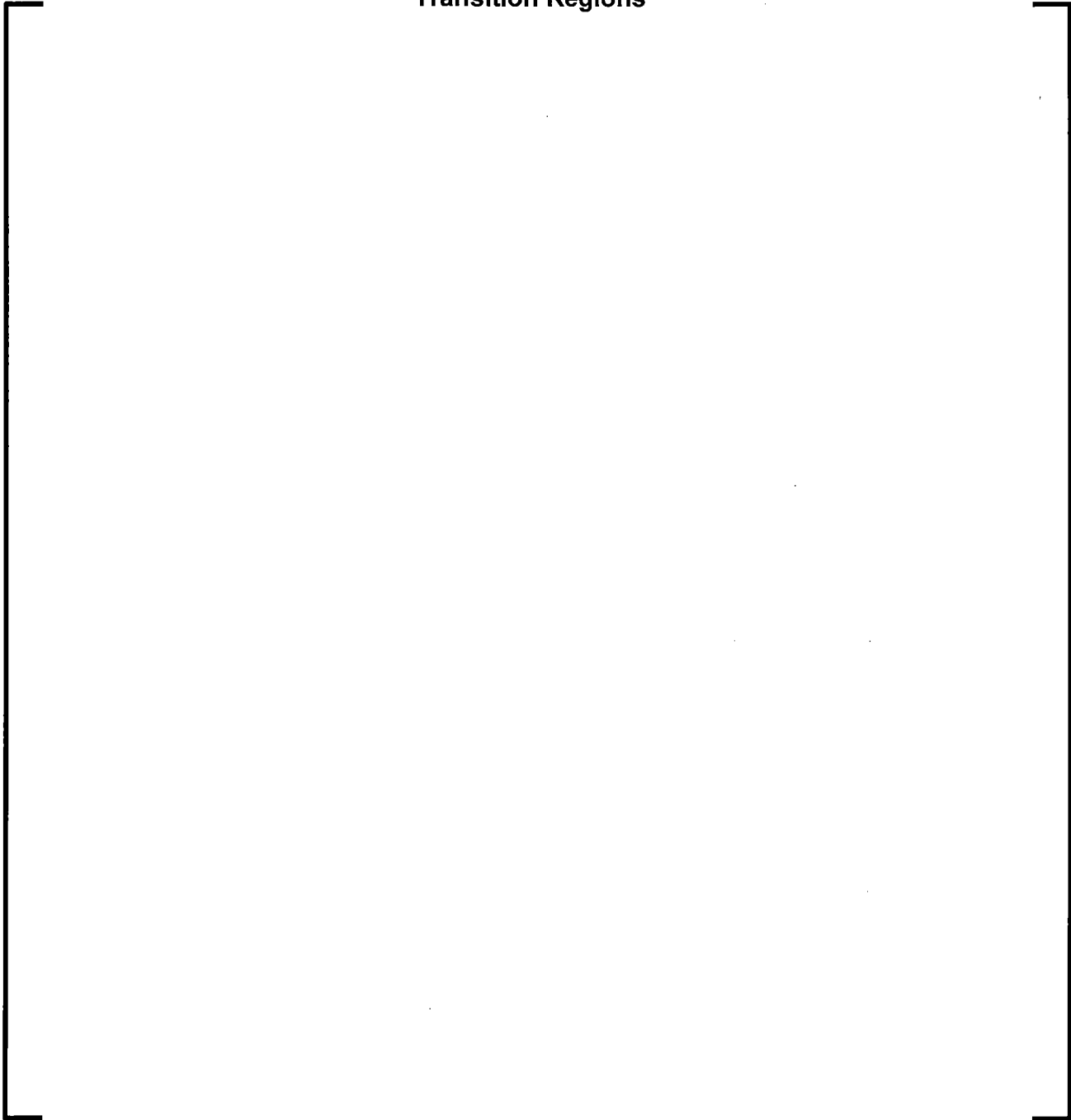
effect and system tests. The average particle diameter, d_0, computed from Equation (7.282) is limited to be between 10^{-4} m and $d_{0,max}$, where:

AREVA Inc.

EMF-2103NP
Revision 3

Realistic Large Break LOCA Methodology for Pressurized Water Reactors
Topical Report

Page 7-93

7.5.2.2   Slug Flow

AREVA Inc.

EMF-2103NP
Revision 3

Realistic Large Break LOCA Methodology for Pressurized Water Reactors
Topical Report

Page 7-94

Figure 7-7 Slug Flow Pattern

AREVA Inc.

Realistic Large Break LOCA Methodology for Pressurized Water Reactors
Topical Report

EMF-2103NP
Revision 3

Page 7-95

AREVA Inc.

Realistic Large Break LOCA Methodology for Pressurized Water Reactors
Topical Report

EMF-2103NP
Revision 3

Page 7-96

AREVA Inc.

EMF-2103NP
Revision 3

Realistic Large Break LOCA Methodology for Pressurized Water Reactors
Topical Report

Page 7-97

AREVA Inc.

Realistic Large Break LOCA Methodology for Pressurized Water Reactors
Topical Report

EMF-2103NP
Revision 3

Page 7-98

7.5.2.3   Annular-Mist Flow

AREVA Inc.

Realistic Large Break LOCA Methodology for Pressurized Water Reactors
Topical Report

EMF-2103NP
Revision 3

Page 7-99

AREVA Inc.

Realistic Large Break LOCA Methodology for Pressurized Water Reactors
Topical Report

EMF-2103NP
Revision 3

Page 7-100

AREVA Inc.

EMF-2103NP
Revision 3

Realistic Large Break LOCA Methodology for Pressurized Water Reactors
Topical Report

Page 7-101

AREVA Inc.

EMF-2103NP
Revision 3

Realistic Large Break LOCA Methodology for Pressurized Water Reactors
Topical Report

Page 7-102

7.5.2.4 Horizontal Stratified Flow

AREVA Inc.

Realistic Large Break LOCA Methodology for Pressurized Water Reactors
Topical Report

EMF-2103NP
Revision 3

Page 7-104

7.5.2.5 Inverted Annular and Inverted Slug Flow

AREVA Inc.

Realistic Large Break LOCA Methodology for Pressurized Water Reactors
Topical Report

EMF-2103NP
Revision 3

Page 7-105

AREVA Inc.

EMF-2103NP
Revision 3

Realistic Large Break LOCA Methodology for Pressurized Water Reactors
Topical Report

Page 7-106

7.5.2.6 Vertical Stratification

AREVA Inc.

EMF-2103NP
Revision 3

Realistic Large Break LOCA Methodology for Pressurized Water Reactors
Topical Report
Page 7-107

AREVA Inc.

EMF-2103NP
Revision 3

Realistic Large Break LOCA Methodology for Pressurized Water Reactors
Topical Report

Page 7-108

7.5.2.7 Junction Interphase Friction

AREVA Inc.

EMF-2103NP
Revision 3

Realistic Large Break LOCA Methodology for Pressurized Water Reactors
Topical Report

Page 7-109

AREVA Inc.

EMF-2103NP
Revision 3

Realistic Large Break LOCA Methodology for Pressurized Water Reactors
Topical Report

Page 7-110

AREVA Inc.

EMF-2103NP
Revision 3

Realistic Large Break LOCA Methodology for Pressurized Water Reactors
Topical Report

Page 7-111

AREVA Inc.

Realistic Large Break LOCA Methodology for Pressurized Water Reactors
Topical Report

EMF-2103NP
Revision 3

Page 7-112

AREVA Inc.

EMF-2103NP
Revision 3

Realistic Large Break LOCA Methodology for Pressurized Water Reactors
Topical Report
Page 7-113

AREVA Inc.

Realistic Large Break LOCA Methodology for Pressurized Water Reactors
Topical Report

EMF-2103NP
Revision 3

Page 7-115

AREVA Inc.

EMF-2103NP
Revision 3

Realistic Large Break LOCA Methodology for Pressurized Water Reactors
Topical Report

Page 7-116

7.5.2.8 Discussion of Scaling and Applicability of Interface Drag Model

AREVA Inc.

Realistic Large Break LOCA Methodology for Pressurized Water Reactors
Topical Report

EMF-2103NP
Revision 3

Page 7-117

AREVA Inc.

EMF-2103NP
Revision 3

Realistic Large Break LOCA Methodology for Pressurized Water Reactors
Topical Report

Page 7-118

AREVA Inc.

EMF-2103NP
Revision 3

Realistic Large Break LOCA Methodology for Pressurized Water Reactors
Topical Report

Page 7-119

AREVA Inc.

Realistic Large Break LOCA Methodology for Pressurized Water Reactors
Topical Report

EMF-2103NP
Revision 3

Page 7-120

7.5.3   Virtual Mass Force

The calculation of the dynamic drag due to the virtual mass effect is based on objective and symmetric formulation of the relative acceleration (Reference 7-65).

AREVA Inc.

Realistic Large Break LOCA Methodology for Pressurized Water Reactors
Topical Report

EMF-2103NP
Revision 3

Page 7-122

RELAP5/MOD1 (Reference 7-18) presented the following form of dynamic drag per unit volume, FA_{gf}:

$$FA_{gf} = -C\alpha_g\alpha_f\rho\left[\frac{\partial(v_g - v_f)}{\partial t} + v_f\left(\frac{\partial v_g}{\partial x}\right) - v_g\left(\frac{\partial v_f}{\partial x}\right)\right]$$ (7.354)

where ρ is the mixture density as given in Equation (7.8), for use in the momentum equations. As discussed in Section 2.1, the spatial derivative portion of the virtual mass term has been dropped.

The virtual mass coefficient, C, is given as

$$C = \frac{1.5}{MAX(\alpha_g, \alpha_f)} - 1.0$$ (7.355)

for all flow regimes except the horizontal stratified flow. For the horizontal stratified flow, the coefficient is set to zero as suggested by Richards and Stopher (Reference 7-66).

7.5.4　Interphase Heat Transfer

AREVA Inc.

Realistic Large Break LOCA Methodology for Pressurized Water Reactors
Topical Report

EMF-2103NP
Revision 3
Page 7-123

AREVA Inc.

EMF-2103NP
Revision 3

Realistic Large Break LOCA Methodology for Pressurized Water Reactors
Topical Report
Page 7-124

7.5.4.1 Bubbly Flow

AREVA Inc.

Realistic Large Break LOCA Methodology for Pressurized Water Reactors
Topical Report

EMF-2103NP
Revision 3

Page 7-125

AREVA Inc.

Realistic Large Break LOCA Methodology for Pressurized Water Reactors
Topical Report

EMF-2103NP
Revision 3

Page 7-126

AREVA Inc.

Realistic Large Break LOCA Methodology for Pressurized Water Reactors
Topical Report

EMF-2103NP
Revision 3

Page 7-127

AREVA Inc.

EMF-2103NP
Revision 3

Realistic Large Break LOCA Methodology for Pressurized Water Reactors
Topical Report

Page 7-128

AREVA Inc.

EMF-2103NP
Revision 3

Realistic Large Break LOCA Methodology for Pressurized Water Reactors
Topical Report

Page 7-129

7.5.4.2   Slug Flow

AREVA Inc.

EMF-2103NP
Revision 3

Realistic Large Break LOCA Methodology for Pressurized Water Reactors
Topical Report

Page 7-130

AREVA Inc.

EMF-2103NP
Revision 3

Realistic Large Break LOCA Methodology for Pressurized Water Reactors
Topical Report

Page 7-131

7.5.4.3   Mist Flow

AREVA Inc.

Realistic Large Break LOCA Methodology for Pressurized Water Reactors
Topical Report

EMF-2103NP
Revision 3

Page 7-133

AREVA Inc.

Realistic Large Break LOCA Methodology for Pressurized Water Reactors
Topical Report

EMF-2103NP
Revision 3
Page 7-134

7.5.4.4 Annular-Mist Flow

AREVA Inc.

EMF-2103NP
Revision 3

Realistic Large Break LOCA Methodology for Pressurized Water Reactors
Topical Report

Page 7-135

AREVA Inc.

Realistic Large Break LOCA Methodology for Pressurized Water Reactors
Topical Report

EMF-2103NP
Revision 3

Page 7-136

7.5.4.5   Horizontal Stratified Flow

7.5.4.6 Vertical Flow Stratification

AREVA Inc.

EMF-2103NP
Revision 3

Realistic Large Break LOCA Methodology for Pressurized Water Reactors
Topical Report

Page 7-138

7.5.4.7   Inverted Slug and Inverted Annular Flow

AREVA Inc.

Realistic Large Break LOCA Methodology for Pressurized Water Reactors
Topical Report

EMF-2103NP
Revision 3

Page 7-139

AREVA Inc.

EMF-2103NP
Revision 3

Realistic Large Break LOCA Methodology for Pressurized Water Reactors
Topical Report

Page 7-140

7.5.4.8 Equilibrium Option

7.5.4.9 Noncondensables

AREVA Inc.

EMF-2103NP
Revision 3

Realistic Large Break LOCA Methodology for Pressurized Water Reactors
Topical Report

Page 7-142

7.5.4.10 Special Treatments

AREVA Inc.

EMF-2103NP
Revision 3

Realistic Large Break LOCA Methodology for Pressurized Water Reactors
Topical Report

Page 7-143

7.5.4.10.1   Grid Spacer Droplet Shatter

AREVA Inc.

EMF-2103NP
Revision 3

Realistic Large Break LOCA Methodology for Pressurized Water Reactors
Topical Report

Page 7-144

AREVA Inc.

EMF-2103NP
Revision 3

Realistic Large Break LOCA Methodology for Pressurized Water Reactors
Topical Report

Page 7-145

Figure 7-8 Droplet Diameter Ratio vs. Weber Number[3]

AREVA Inc.

EMF-2103NP
Revision 3

Realistic Large Break LOCA Methodology for Pressurized Water Reactors
Topical Report

Page 7-146

AREVA Inc.

Realistic Large Break LOCA Methodology for Pressurized Water Reactors
Topical Report

EMF-2103NP
Revision 3

Page 7-147

AREVA Inc.

EMF-2103NP
Revision 3

Realistic Large Break LOCA Methodology for Pressurized Water Reactors
Topical Report

Page 7-148

AREVA Inc.

EMF-2103NP
Revision 3

Realistic Large Break LOCA Methodology for Pressurized Water Reactors
Topical Report

Page 7-149

AREVA Inc.

EMF-2103NP
Revision 3

Realistic Large Break LOCA Methodology for Pressurized Water Reactors
Topical Report
Page 7-150

AREVA Inc.

EMF-2103NP
Revision 3

Realistic Large Break LOCA Methodology for Pressurized Water Reactors
Topical Report

Page 7-151

AREVA Inc.

EMF-2103NP
Revision 3

Realistic Large Break LOCA Methodology for Pressurized Water Reactors
Topical Report

Page 7-152

7.5.4.10.2 Heat Transfer Smoothing

AREVA Inc.

EMF-2103NP
Revision 3

Realistic Large Break LOCA Methodology for Pressurized Water Reactors
Topical Report

Page 7-153

7.5.4.10.3   Vapor Fraction Truncation

AREVA Inc.

Realistic Large Break LOCA Methodology for Pressurized Water Reactors
Topical Report

EMF-2103NP
Revision 3

Page 7-154

AREVA Inc.

Realistic Large Break LOCA Methodology for Pressurized Water Reactors
Topical Report

EMF-2103NP
Revision 3

Page 7-155

AREVA Inc.

EMF-2103NP
Revision 3

Realistic Large Break LOCA Methodology for Pressurized Water Reactors
Topical Report

Page 7-156

7.5.4.11 Discussion of Scaling and Applicability of Interphase Heat Transfer

AREVA Inc.

EMF-2103NP
Revision 3

Realistic Large Break LOCA Methodology for Pressurized Water Reactors
Topical Report

Page 7-157

AREVA Inc.

EMF-2103NP
Revision 3

Realistic Large Break LOCA Methodology for Pressurized Water Reactors
Topical Report

Page 7-158

7.5.5   Wall Friction

The wall friction model computes the friction terms, $\alpha_f \rho_f FWF v_f$ and $\alpha_g \rho_g FWG v_g$, in the liquid and vapor momentum equations (see Equations (7.3) and (7.4)). In S-RELAP5, the friction model is essentially the same as that of RELAP5/MOD2 (Reference 7-6 and 7-69), except that the RELAP5/MOD2 approximation to the Colebrook equation of friction factor (Reference 7-92) is replaced by an explicit formula developed by Jain (Reference 7-93).

The wall friction model consists of two main parts: (1) computing the overall two-phase wall-friction pressure drop, and (2) apportioning the total wall friction into liquid and vapor components. The two-phase friction multiplier approach, with the two-phase multiplier calculated from the Heat Transfer and Fluid Flow Service (HTFS) modified Baroczy correlation (Reference 7-94), is used to obtain the total wall-friction pressure drop, which is independent of flow regimes. The phasic friction factor model, from which Chisholm (Reference 7-95) developed a theoretical basis for the Lockhart-Martinelli friction correlation (Reference 7-96), is used to develop the phasic partition factors, which depend on flow regimes.

According to the two-phase friction multiplier approach, the overall wall-friction pressure drop can be written in terms of the liquid-alone wall-friction pressure drop as

$$\left(\frac{\partial P}{\partial x}\right)_{2\phi} = \phi_f^2 \left(\frac{\partial P}{\partial x}\right)_f \tag{7.448}$$

or the vapor-alone wall-friction pressure drop

$$\left(\frac{\partial P}{\partial x}\right)_{2\phi} = \phi_g^2 \left(\frac{\partial P}{\partial x}\right)_g \tag{7.449}$$

Here ϕ_f and ϕ_g are, respectively, the liquid-alone and vapor-alone friction multipliers. The liquid- and vapor-alone friction pressure gradients are

$$\left(\frac{\partial P}{\partial x}\right)_f = \frac{\lambda'_f \rho_f \alpha_f^2 v_f^2}{2D}, \quad \left(\frac{\partial P}{\partial x}\right)_g = \frac{\lambda'_g \rho_g \alpha_g^2 v_g^2}{2D} \tag{7.450}$$

Here the primes are the liquid- and vapor-alone friction factors calculated at the respective Reynolds numbers:

$$Re_f' = \frac{\alpha_f \rho_f |v_f| D}{\mu_f}, \ Re_g' = \frac{\alpha_g \rho_g |v_g| D}{\mu_g} \tag{7.451}$$

The HTFS correlation for the two-phase friction multiplier is represented by

$$\phi_f^2 = 1 + \frac{C}{\chi} + \frac{1}{\chi^2} \tag{7.452}$$

for the liquid-alone multiplier, or

$$\phi_g^2 = 1 + C \chi + \chi^2 \tag{7.453}$$

or the vapor-alone multiplier, where C is the correlation term and χ is the Lockhart-Martinelli ratio given as

$$\chi^2 = \frac{\left(\dfrac{\partial P}{\partial x}\right)_f}{\left(\dfrac{\partial P}{\partial x}\right)_g} = \frac{\phi_g^2}{\phi_f^2} \tag{7.454}$$

The correlation term is expressed in terms of the scalar mass flux, G, and the Baroczy dimensionless property index, Λ, as

$$2 \le C = -2 + \left(28 - 0.3 G^{0.5}\right) \exp\left[-\frac{\left(\log_{10} \Lambda + 2.5\right)^2}{2.4 - 10^{-4} G} \right] \tag{7.455}$$

where:

$$\Lambda = \frac{\rho_g}{\rho_f}\left(\frac{\mu_f}{\mu_g}\right)^{0.2}, \ G = |\alpha_f \rho_f v_f + \alpha_g \rho_g v_g| \, s \tag{7.456}$$

From Equations (7.448), (7.452), and (7.454) or Equations (7.449), (7.453), and (7.454), one can obtain the overall friction pressure drop as

$$\left(\frac{\partial P}{\partial x}\right)_{2\phi} = \left(\frac{\partial P}{\partial x}\right)_f + C \sqrt{\left(\frac{\partial P}{\partial x}\right)_f \left(\frac{\partial P}{\partial x}\right)_g} + \left(\frac{\partial P}{\partial x}\right)_g \tag{7.457}$$

where the liquid- and vapor-alone pressure gradients are given in Equation (7.450) and C is given by the correlation of Equation (7.455).

In terms of RELAP5 expressions, the overall wall friction pressure loss is:

$$\alpha_f \rho_f FWF v_f + \alpha_g \rho_g FWG v_g = \left(\frac{\partial P}{\partial x}\right)_{2\phi} \tag{7.458}$$

As the total pressure drop is given by Equation (7.457), another relation is needed to partition it into phasic friction terms. Chisholm postulated that the wall shear stress could be determined using Darcy-Weisbach friction factors computed from Reynolds numbers based on phasic properties. Thus, for the liquid phase, the wall shear stress is

$$\tau_f = \frac{\lambda_f}{4} \frac{\rho_f v_f^2}{2} \tag{7.459}$$

where the friction factor λ_f is computed based on the Reynolds number for the liquid phase:

$$Re_f = \frac{\rho_f v_f D_f}{\mu_f} \tag{7.460}$$

Here the liquid hydraulic diameter is defined as

$$D_f = \frac{4 A_f}{p_f} \tag{7.461}$$

where A_f is liquid flow area and p_f is liquid wetted perimeter. Defining

$$\alpha_{fw} = \frac{p_f}{p} \tag{7.462}$$

where p is the overall wetted perimeter, and with Equation (7.461), the liquid Reynolds number can be rewritten as

$$Re_f = \frac{\alpha_f}{\alpha_{fw}} \cdot \frac{\rho_f v_f D}{\mu_f} \tag{7.463a}$$

Similar expressions can be obtained for the vapor phase:

$$\tau_g = \frac{\lambda_g}{4} \frac{\rho_g v_g^2}{2} \tag{7.463b}$$

$$\alpha_{gw} = \frac{p_g}{p} \tag{7.463c}$$

$$Re_g = \frac{\alpha_g}{\alpha_{gw}} \cdot \frac{\rho_g v_g D}{\mu_g} \tag{7.463d}$$

AREVA Inc.

EMF-2103NP
Revision 3

Realistic Large Break LOCA Methodology for Pressurized Water Reactors
Topical Report

Page 7-163

Accordingly, the ratio of phasic friction terms can be expressed as

$$\frac{\alpha_f \rho_f FWF v_f}{\alpha_g \rho_g FWG v_g} = \frac{\tau_f p_f}{\tau_g p_g} = \frac{\alpha_{fw} \lambda_f \rho_f v_f^2}{\alpha_{gw} \lambda_g \rho_g v_g^2} \qquad (7.464)$$

Solving Equations (7.458) and (7.464) for the phasic friction terms and using Equations (7.450) and (7.457) yields the following relations for the wall friction terms:

$$\alpha_f \rho_f FWF = \frac{\alpha_{fw} \rho_f \lambda_f |v_f|}{2D}\eta, \quad \alpha_g \rho_g FWG = \frac{\alpha_{gw} \rho_g \lambda_g |v_g|}{2D}\eta \qquad (7.465)$$

with

$$\eta = \frac{\lambda_f' \rho_f \alpha_f^2 v_f^2 + C\sqrt{\lambda_f' \rho_f \alpha_f^2 v_f^2 \lambda_g' \alpha_g^2 \rho_g v_g^2} + \lambda_g' \rho_g \alpha_g^2 v_g^2}{\alpha_{fw}\lambda_f \rho_f v_f^2 + \alpha_{gw}\lambda_g \rho_g v_g^2} \qquad (7.466)$$

The vapor and liquid fraction at the wall, as defined in Equations (7.463)c and (7.462), are dependent on flow regimes. [

] For bubbly and mist flow, the vapor fraction at the wall is set equal to the volume void fraction; i.e., $\alpha_{gw} = \alpha_g$. In slug flow, $\alpha_{gw} = \alpha_{gs}$, where α_{gs} is given by Equation (7.295). In annular mist flow, $\alpha_{fw} = (\alpha_{ff})^{0.25}$, where α_{ff} is given by Equation (7.308). In inverted annular flow, $\alpha_{gw} = (\alpha_g)^{0.25}$, and in inverted slug flow, $\alpha_{fw} = \alpha_{fd}$ of Equation (7.327). For horizontal stratified flow, $\alpha_{gw} = \frac{\theta}{\pi}$, where θ is the liquid level angle defined by Equation (7.270). It should be stressed that the void fraction at the wall affects only the phasic partition functions not the total wall-friction pressure gradient.

For a two-dimensional component, the wall friction factors are computed separately for each flow direction. The hydraulic diameter is defined through the user's input for each direction. The volume average phasic velocities in each direction are used separately. The volume void fraction is common for both directions.

The friction factors, λ' and λ, are functions of the Reynolds number, Re, and wall roughness, ε. For laminar flow, the friction factor is computed as

$$\lambda_L = \frac{64}{Re} , \quad 0 \le Re \le 2000 \tag{7.467}$$

For turbulent flow, the friction factor is given by the Colebrook (Reference 7-92) equation

$$\frac{1}{\sqrt{\lambda_t}} = -2\log_{10}\left(\frac{\varepsilon}{3.7D} + \frac{2.51}{Re\sqrt{\lambda_t}}\right), \quad Re \ge 4000 \tag{7.468}$$

In the laminar-turbulent transition region, $2000 \le Re \le 4000$, the friction factor is computed by the following interpolation formula

$$\lambda_{Lt} = 5.285\left[1.189 - \left(\frac{4000}{Re}\right)^{0.25}\right]\left(\lambda_{t,4000} - \lambda_{L,2000}\right) + \lambda_{L,2000} \tag{7.469}$$

where $\lambda_{L,2000}$ is the laminar friction factor at a Reynolds number of 2000 and $\lambda_{t,4000}$ is the turbulent friction factor at a Reynolds number of 4000.

The Colebrook friction factor of Equation (7.468) is of an implicit form and has to be solved numerically. The RELAP5/MOD2 numerical approximation to the Colebrook equation has been reported by Dimenna and Caraher (Reference 7-97) to yield friction factors as much as 25% larger than those of the equation itself for certain Reynolds numbers. They suggested that the approximation reported by Jain is a better one. Jain (Reference 7-93) developed the following formula for the turbulent friction factor

$$\frac{1}{\sqrt{\lambda_t}} = 1.14 - 2\log_{10}\left(\frac{\varepsilon}{D} + \frac{21.25}{Re^{0.9}}\right) \tag{7.470}$$

Jain indicated that the friction factors calculated from Equation (7.470) have a maximum deviation of ±1% from those computed with the Colebrook equation. As Equation (7.470) is simpler to implement and is more accurate than the approximation used by RELAP5/MOD2, the turbulent friction factor of Jain is implemented in S-RELAP5, replacing the old approximation.

It was suggested, after the implementation of Jain's approximation in S-RELAP5, that the approximation published by Zigrang and Sylvester (Reference 7-98) is more accurate. The Zigrang-Sylvester approximation to the Colebrook friction factor is

AREVA Inc.

EMF-2103NP
Revision 3

Realistic Large Break LOCA Methodology for Pressurized Water Reactors
Topical Report

Page 7-165

$$\frac{1}{\sqrt{\lambda_t}} = -2\log_{10}\left\{\frac{\varepsilon/D}{3.7} + \frac{2.51}{Re}\left[1.14 - 2\log_{10}\left(\frac{\varepsilon}{D} + \frac{21.25}{Re^{0.9}}\right)\right]\right\} \tag{7.471}$$

It can be seen that the above equation is much more elaborate than Equation (7.470). The Zigrang-Sylvester approximation is used in RELAP5/MOD3 (Reference 7-7). Since the Jain approximation, Equation (7.470), is sufficiently accurate for S-RELAP5 applications, there is no need to switch to the Zigrang-Sylvester approximation.

7.5.6   References

7-25.   B. Chexal and G. Lellouche, A Full-Range Drift-Flux Correlation for Vertical Flows (Revision 1), EPRI NP-3989-SR, September 1986; Void Fraction Technology for Design and Analysis, TR-106326, March 1997.

7-26.   EMF-2102(P) Revision 0, S-RELAP5: Code Verification and Validation, Sections 2.1 and 2.6, Framatome ANP, Inc., August 2001.

7-27.   EMF-2100(P) Revision 3, S-RELAP5 Models and Correlations Code Manual, Siemens Power Corporation, January 2001.

7-28.   Y. Taitel and A. E. Dukler, "A Model for Predicting Flow Regime Transitions in Horizontal and Near Horizontal Gas-Liquid Flow," American Institute of Chemical Engineering Journal Volume 22, pp. 47-55, 1976.

7-29.   Y. Taitel, D. Bornea, and A. E. Dukler, "Modeling Flow Pattern Transitions for Steady Upward Gas-Liquid Flow in Vertical Tubes," American Institute of Chemical Engineering Journal Volume 26, pp. 345-354, 1980.

7-30.   G. B. Wallis, One Dimensional Two Phase Flow, McGraw-Hill, New York, 1969.

7-31.   M. Ishii and G. DeJarlais, "Inverted Annular Flow Modeling," presented at EG&G, July 27, 1982.

7-32.   G. DeJarlais and M. Ishii, Inverted Annular Flow Experimental Study, Argonne National Laboratory Report ANL-85-31, NUREG/CR-4277, 1985.

7-33.   NUREG/CR-1873, ANL-80-111, Study of Two-Fluid Model and Interfacial Area, Argonne National Laboratory, 1980.

7-34.   S. Z. Rouhani and M. S. Sohal, "Two-Phase Flow Patterns: A Review of Research Results," Progress in Nuclear Energy Volume 11, pp.219-259, 1983.

7-35.   K. Mishima and M. Ishii, "Flow Regime Transition Criteria for Upward Two-Phase Flow in Vertical Tubes," International Journal Heat and Mass Transfer Volume 27, pp. 723-737, 1984.

7-36.   N. T. Obot and M. Ishii, "Two-Phase Flow Regime Transition Criteria in Post-Dryout Region Based on Flow Visualization Experiments," International Journal Heat and Mass Transfer Volume 31, pp. 2559-2570, 1988.

7-37.   O. C. Jones, Jr. and N. Zuber, "The Interrelation Between Void Fraction Fluctuations and Flow Patterns in Two-Phase Flow," International Journal of Multiphase Flow Volume 2, pp. 273-306, 1975.

7-38.   M. A. Vince and R. T. Lahey, Jr., "On the Development of An Objective Flow Regime Indicator," International Journal of Multiphase Flow, Volume 8, pp. 93-124, 1982.

7-39.   N. A. Radovcich and R. Moissis, The Transition from Two-Phase Bubbly Flow to Slug Flow, MIT Report 7-7673-22, June 1962.

7-40.   P. Griffith and G. A. Snyder, The Bubbly-Slug Transition in a High Velocity Two-Phase Flow, MIT Report 5003-29, TID20947, July 1964.

7-41.   M. Ishii and G. DeJarlais, "Flow Regime Transition and Interfacial Characteristics of Inverted Annular Flow," Nuclear Engineering and Design, Volume 95, pp. 171-184, 1986.

7-42.   D. D. Taylor et al., TRAC-BD1/MOD1: An Advanced Best Estimate
        Computer Program for Boiling Water Reactor Transient Analysis,
        Volume 1: Model Description, NUREG/CR-3633, EGG-2294, April
        1984.

7-43.   V. H. Ransom et al., RELAP5/MOD2 Code Manual, Volume 1: Code
        Structure, Systems Models, and Solution Methods, NUREG/CR-4312,
        EGG-2396, Revision 1, March 1987.

7-44.   A.H. Shapiro and A. J. Erickson, Transactions of ASME, Volume 79,
        p. 775, 1957.

7-45.   M. Ishii and T. C. Chawla, Local Drag Laws in Dispersed Two-Phase
        Flow, Argonne National Laboratory Report ANL79-105,
        NUREG/CR-1230, December 1979.

7-46.   S. M. Nujhawan, "Experimental Investigation of Thermal Non-
        Equilibrium in Post-Dryout Steam-Water Flow," Ph.D. Thesis, Lehigh
        University, May 1980.

7-47.   FLECHT SEASET Program, PWR FLECHT SEASET Unblocked
        Bundle, Forced and Gravity Reflood Task Data Evaluation and
        Analysis Report, NUREG/CR-2256, EPRI NP-2013, WCAP-8991,
        November 1981.

7-48.   I. Kataoka and M. Ishii, "Drift Flux Model for Large Diameter Pipe and
        New Correlation for Pool Void Fraction," International Journal Heat
        and Mass Transfer Volume 30, pp. 1927-1939, 1987.

7-49.   T. M. Anklam, R. J. Miller, and M. D. White, Experimental
        Investigations of Uncovered-Bundle Heat Transfer and Two-Phase
        Mixture-Level Swell Under High-Pressure Low Heat-Flux Conditions,
        NUREG/CR-2456, ORNL-5848, March 1982.

7-50.   I. Kataoka and M. Ishii, Mechanism and Correlation of Droplet
        Entrainment and Deposition in Annular Two-Phase Flow, Argonne
        National Laboratory Report ANL 82-44, NUREG/CR-2885, 1982.

7-51.   2D/3D Program Upper Plenum Test Facility, Test No. 11
        Countercurrent Flow in PWR Hot Leg Test, Quick Look Report,
        R515/87/08, Siemens KWU, March 1987.

7-52.   U9 316/89/2, UPTF Test No .6 Downcomer Countercurrent Flow Test,
        Quick Look Report, 2D/3D Program Upper Plenum Test Facility,
        Siemens KWU March 1989; E314/90/003, UPTF Test No. 7
        Downcomer Countercurrent Flow Test, Quick Look Report, Siemens
        KWU, March 1990.

7-53.   E314/90/19, UPTF Test No. 29 Entrainment/De-entrainment Test
        Quick Look Report, 2D/3D Program Upper Plenum Test Facility,
        November, 1990; U9 316/88/3, UPTF Test No.10 Tie Plate
        Countercurrent Flow Test, March 1988.

7-54.   A. Ohnuki, H. Adachi, and Y. Murao, "Scale Effects on Countercurrent
        Gas-Liquid Flow in Horizontal Tube Connected to Inclined Riser,"
        Nuclear Engineering and Design, Volume 107, pp. 283-294, 1988.

7-55.   J. A. Findlay, BWR Refill-Reflood Program Task 4.8 - Model
        Qualification Task Plan, NUREG/CR-1899, EPRI NP-1527,
        GEAP-24898, August 1981.

7-56.   V. H. Ransom et al., RELAP5/MOD2 Code Manual, Volume 3:
        Developmental Assessment Problems, EGG-TFM-7952, December
        1987.

7-57.   R. A. Riemke, H. Chow, and V. H. Ransom, RELAP5/MOD1 Code
        Manual Volume 3: Checkout Problems Summary, Interim Report,
        EGG-NSMD-6182, February 1983.

7-58.   H. R. Saedi and P. Griffith, "The Pressure Response of a PWR
Pressurizer During an Insurge Transient," Transactions of ANS,
Volume 44, pp. 606-607, 1983.

7-59.   D. Bharathan, H. T. Richter, and G. B. Wallis, Air-Water Counter-
Current Annular Flow in Vertical Tubes, EPRI NP-786, 1978.

7-60.   EMF-2102(P) Revision 0, S-RELAP5: Code Verification and
Validation, Framatome ANP, Inc., August 2001.

7-61.   U. S. Rohatgi, L. Y. Neymotin, J. Jo, and W. Wulff, Bias in Peak Clad
Temperature Predictions Due to Uncertainties in Modeling of ECC
Bypass and Dissolved Non-Condensible Gas Phenomena,
NUREG/CR-5254, BNL-NUREG-52168, September 1990.

7-62.   T. Iguchi et al., Data Report on Large Scale Reflood Test-43 – CCTF
Core Shakedown Test C2-SH2 (Run 54), JAERI-memo 58-155, Japan
Atomic Energy Research Institute, May 1983.

7-63.   V. H. Ransom, Course A -- Numerical Modeling of Two-Phase Flows
for Presentation at Ecole d'Ete d'Analyse Numerique,
EGG-EAST-8546, May 1989.

7-64.   J.M. Putney, "Development of a New Bubbly-Slug Interfacial Friction
Model for RELAP5", J. Nucl. Engrg. Des. 131 (1991) 223-240.

7-65.   D. A. Drew, L. Y. Cheng, and R. T. Lahey, Jr., "The Analysis of Virtual
Mass Effects in Two-Phase Flow," International Journal of Multiphase
Flow, Volume 5, pp. 233-242, 1979.

7-66.   C. G. Richards and I. Stopher, "Stratified Flow Benchmark
Calculations Using RELAP5/MOD2," presented at 1990
RELAP5/TRAC-BWR International Users Seminar, Chicago,
September 1990.

7-67. M. J. Thurgood et al., COBRA/TRAC-A Thermal-Hydraulics Code for
       Transient Analysis of Nuclear Reactor Vessels and Primary Coolant
       Systems, Volume 1, Equations and Constitutive Models,
       NUREG/CR-3046 PNL-4385, March 1983.

7-68. M. S. Plesset and S. A. Zwick, "Growth of Vapor Bubbles in
       Superheated Liquids," Journal of Applied Physics, Volume 25, pp.
       493-500, 1954.

7-69. R. A. Dimenna et al., RELAP5/MOD2 Models and Correlations,
       NUREG/CR-5194, EGG-2531, August, 1988.

7-70. K. Lee and D. J. Ryley, "The Evaporation of Water Droplets in
       Superheated Steam," Journal of Heat Transfer, pp. 445-456, 1968.

7-71. H. C. Unal, "Maximum Bubble Diameter, Maximum Bubble-Growth
       Time and Bubble-Growth Rate During the Subcooled Nucleate Flow
       Boiling of Water up to 17.7 MN/m^2," International Journal of Heat and
       Mass Transfer, Volume 19, pp. 643-649, 1976.

7-72. R. T. Lahey, Jr., "A Mechanistic Subcooled Boiling Model,"
       Proceedings of 6th International Heat Transfer Conference, Volume 1,
       pp. 293-297, 1978.

7-73. Y. M. Chen and F. Mayinger, "Measurement of Heat Transfer at the
       Phase Interface of Condensing Bubbles," Int. J. Multiphase Flow 18
       (1992) 877-890.

7-74. D. Moalem and S. Sideman, "The Effect of Motion on Bubble
       Collapse," International Journal of Heat and Mass Transfer Volume
       16, pp. 2321-2329, 1973.

7-75. LA-12031-M, TRAC-PF1/MOD2 Code Manual: Volume 3
       Programmer's Guide, NUREG/CR-5673, Los Alamos National
       Laboratory, July 1992; J. W. Spore et al., TRAC-PF1/MOD2 Volume I.
       Theory Manual, (Draft), LA-12031-M, NUREG/CR-5673, July 1993.

7-76.   S. G. Bankoff, "Some Condensation Studies Pertinent to Light Water Safety," International Journal of Multiphase Flow Volume 6, pp. 51-67, 1980.

7-77.   L. K. Brumfield, R. N. Houze, and T. G. Theofanous, "Turbulent Mass Transfer at Free, Gas-Liquid Interfaces, with Applications to Film Flows," International Journal of Heat and Mass Transfer, Volume 18, pp. 1077-1081, 1975.

7-78.   Y. A. Hassan, "Dispersed-Flow Heat Transfer During Reflood in a Pressurized Water Reactor After a Large-Break Loss-of-Coolant Accident," Transactions of ANS, Volume 53, pp. 326-328, 1986.

7-79.   M. C. Yuen and L. W. Chen, "Heat-Transfer Measurements of Evaporating Liquid Droplets," International Journal of Heat and Mass Transfer, Volume 21, pp. 537-542, 1978.

7-80.   Y. A. Hassan, "Predictions of Vapor Superheat in Rod Bundle Geometry with Modified RELAP5/MOD2," Transactions of ANS, Volume 54, pp. 212-214, 1987.

7-81.   G. Th. Analytis, "Developmental Assessment of TRAC-BF1 with Separate-Effect and Integral Reflooding Experiments," Proceedings of the 5th International Topical Meeting on Reactor Thermal Hydraulics, Volume I, pp. 287-291, September 1992; also presentation given at 4th ICAP Management Meeting, October 18-20, Bethesda, 1989.

7-82.   NUREG/CR-4356, EGG-2626, TRAC-BF1/MOD1: An Advanced Best-Estimate Computer Program for BWR Accident Analysis, Idaho National Engineering Laboratory, August 1992.

7-83.   G. Brown, "Heat Transmission of Condensation of Steam on a Spray of Water Drops," Proceedings of the General Discussion on Heat Transfer, pp. 49-52, 1951.

AREVA Inc.

EMF-2103NP
Revision 3

Realistic Large Break LOCA Methodology for Pressurized Water Reactors
Topical Report

Page 7-172

7-84.   J. G. M. Andersen, REMI/HEAT COOL, A Model for Evaluation of
Core Heat-Up and Emergency Core Spray Cooling System
Performance for Light-Water-Cooled Nuclear Power Reactors, Riso
Report No. 296, Danish Atomic Energy Commission, September
1973.

7-85.   T. G. Theofanous, "Modeling of Basic Condensation Processes," The
Water Reactor Safety Research Workshop on Condensation, Silver
Springs, MD. May 24-25, 1979.

7-86.   J. H. Linehan, M. Petrick, and M. M. El-Wakil, "The Condensation of
Saturated Vapor on a Subcooled Film During Stratified Flow,"
Chemical Engineering Symposium Series 66 (102), pp. 11-20, 1972.

7-87.   ANCR-NUREG-1335, RELAP4/MOD5 A Computer Program for
Transient Thermal-Hydraulic Analysis of Nuclear Reactors and
Related Systems, User's Manual Volume I: RELAP4/MOD5
Description, Idaho National Engineering Laboratory, September 1976.

7-88.   G. G. Sklover and M. D. Rodivilin, "Condensation on Water Jets with a
Cross Flow of Steam," Teploenergetika Volume 23, 48-51, 1976.

7-89.   J. M. Kelly and R. J. Kohrt, COBRA-TF Flow Blockage Heat Transfer
Programs, NUREG/CP-0048, pp. 211-232, January 1984.

7-90.   EMF-92-139(P), Volume 3, Supplement 3, Realistic LOCA ECCS
Evaluation Model Assessment for PWR Large Break Analysis
Assessment for LOFT Test L2-5, Siemens Power Corporation, June
1993.

7-91.   EMF-92-139(P), Volume 3, Supplement 4, Realistic LOCA ECCS
Evaluation Model Assessment for PWR Large Break Analysis
Assessment for LOFT Test L2-6, Siemens Power Corporation, June
1993.

7-92.   C. F. Colebrook, "Turbulent Flow in Pipes with Particular Reference to the Transition Region Between Smooth and Rough Pipe Laws," Journal of the Institution of Civil Engineers, Volume 11, pp. 133-156, 1939.

7-93.   A. K. Jain, "Accurate Explicit Equation for Friction Factor," ASCE J. Hydraulics Division, Volume 102, pp. 674-677, 1976.

7-94.   K. T. Chaxton, J. G. Collier, and J. A. Ward, H.T.F.S. Correlation for Two-Phase Pressure Drop and Void Fraction in Tubes, AERE-R7162, 1972.

7-95.   D. Chisholm, "A Theoretical Basis for the Lockhart-Martinelli Correlation for Two-Phase Flow," Journal of Heat Transfer, Volume 10, pp. 1767-1778, 1967.

7-96.   R. W. Lockhart and R. C. Martinelli, "Proposed Correlation of Data for Isothermal Two-Phase, Two-Component Flow in Pipes," Chemical Engineering Progress, Volume 45, pp. 39-48, 1949.

7-97.   R. A. Dimenna and D. L. Caraher, "Air-Water Hydraulics Modeling for a Mark-22 Fuel Assembly with RELAP5(U)," presented at 1990 RELAP5/TRAC-BWR International Users Seminar, Chicago, September 1990.

7-98.   D. J. Zigrang and N. D. Sylvester, "A Review of Explicit Friction Factor Equations," Transactions of ASME, Journal of Energy Resources Technology, Volume 107, pp. 280-283, 1985.

7-99.   BAW-10166PA, Revision 4, BEACH - Best Estimate Analysis Core Heat Transfer; A Computer Program for Reflood Heat Transfer During LOCA, March 1996.

7-100. J. Chiou, L.E. Hochreiter, D.B. Utton, and M.Y. Young, Spacer Grid Heat Transfer Effects during Reflood, NUREG/CP-0043, 1982.

7-101. N.T. Obot and M. Ishii, "Two-Phase Flow Regime Transition Criteria in Post-Dryout Region Based on Flow Visualization Experiments", NUREG/CR-4972, ANL-87-27, June 1987.

7-102. I. Kataoka and M. Ishii, "Mechanistic Modeling and Correlations for Pool Entrainment Phenomenon", NUREG/CR-3304, ANL-83-37, April, 1983.

7.6   *Heat Transfer Models*

The physical models, including correlations and methods, to obtain the wall-to-fluid heat transfer terms, Q_{wf}, Q_{wg}, and Γ_w, in the two-fluid field equations (see Section 7.4) are presented in this section. The partition of the total heat flux, q", into the phasic heat fluxes, q_f'' and q_g'', and the designation of a portion of heat flux for mass transfer near the wall, Γ_w, are required by a two-phase nonequilibrium code, although most experimental data may provide only information on total wall-fluid heat flux. The wall vapor generation (mass transfer) term is closely tied to the bulk interphase mass transfer terms described in Section 7.5 and is verifiable through void fraction distribution and phasic temperature measurements.

In S-RELAP5 the total heat flux q" is expressed in the general form:

$$q'' = h_{cf}\left(T_w - T_f\right) + h_{csat}\left(T_w - T_{sat}\right) + h_{cg}\left(T_w - T_g\right) \qquad (7.472)$$

where T_w, T_f, T_g, and T_{sat} are temperatures of wall (heat structure surface), liquid phase, vapor phase, and saturation, respectively. The saturation temperature corresponds to the total pressure for a boiling process and to the partial steam pressure for a condensing process. The heat transfer coefficients, h_{cf}, h_{csat}, and h_{cg}, are obtained from correlations which represent various heat transfer processes or phenomena in different heat transfer regimes. The classification of heat transfer regimes and the logic to select them will be presented in this section. Not all of the heat transfer coefficients in Equation (7.472) may be present in a particular regime. For example, in single-phase liquid flow, only h_{cf} is present. It should also be pointed out that, for computational and editing purposes, a total heat transfer coefficient is defined in S-RELAP5 as

$$h_{c,total} = h_{cf} + h_{csat} + h_{cg} \qquad (7.473)$$

The quantity $h_{c,total}$ appears as the 'heat transfer coefficient' in the set of major and minor edit variables. As each of the heat transfer coefficients in Equation (7.473) is not defined with respect to the same temperature difference, the variable $h_{c,total}$ has, in a strict sense, no physical meaning under general circumstances. It should be pointed

AREVA Inc.

Realistic Large Break LOCA Methodology for Pressurized Water Reactors
Topical Report

EMF-2103NP
Revision 3

Page 7-176

out that Equations (7.472) and (7.473) are present in the coding of RELAP5/MOD2 (Reference 7-152), although they are not explicitly stated.

The mass transfer term at the wall and apportioning of the total heat flux of Equation (7.473) into the phasic heat fluxes are formulated in accordance with the physical processes or phenomena. Different hypotheses may be used to obtain the same or similar results. Considering the film boiling under a superheated steam environment, the vaporization of liquid by the wall heat transfer can be modeled in several ways. In actuality, a portion of heat may directly or indirectly transfer to the liquid in the region near the wall and the remainder transfers to the steam. The liquid near the wall is vaporized by the heat transfer to liquid and that in the bulk is vaporized by the superheated steam. One possible assumption is that all heat goes to heating the steam and there is no wall mass transfer term. With such an approach, the vapor generation is handled by the interphase heat transfer model. Another approach is to apportion the heat to the vapor and liquid phase and set the wall vapor generation term to zero. The mass transfer is again determined by the interphase heat transfer model. The third approach is to apportion the liquid impingement or boiling heat transfer to the liquid phase and the convective heat transfer to the vapor phase and assume all the heat goes to the liquid phase for vapor generation at the wall. With an appropriate interphase heat transfer model (see Section 7.5.4.3), one can obtain good comparisons to the experimental data on the steam and wall temperatures and on the mass transfer rate with any of the above three approaches. Note, however, that the first method has a tendency to produce too high steam temperature and the second method has a high probability of producing highly superheated liquid, which causes some computational complications.

Users have the option to select the reflood model, which uses the fine-mesh rezoning scheme and two-dimensional heat conduction (see Sections 7.10.8 and 7.10.9) to efficiently compute core quenching phenomena during the reflood phase of a LBLOCA. Special considerations of the implementation of the reflood model heat transfer are discussed in Section 7.6.12.

7.6.1   Heat Transfer Regimes

AREVA Inc.

EMF-2103NP
Revision 3

Realistic Large Break LOCA Methodology for Pressurized Water Reactors
Topical Report

Page 7-178

AREVA Inc.

Realistic Large Break LOCA Methodology for Pressurized Water Reactors
Topical Report

EMF-2103NP
Revision 3

Page 7-179
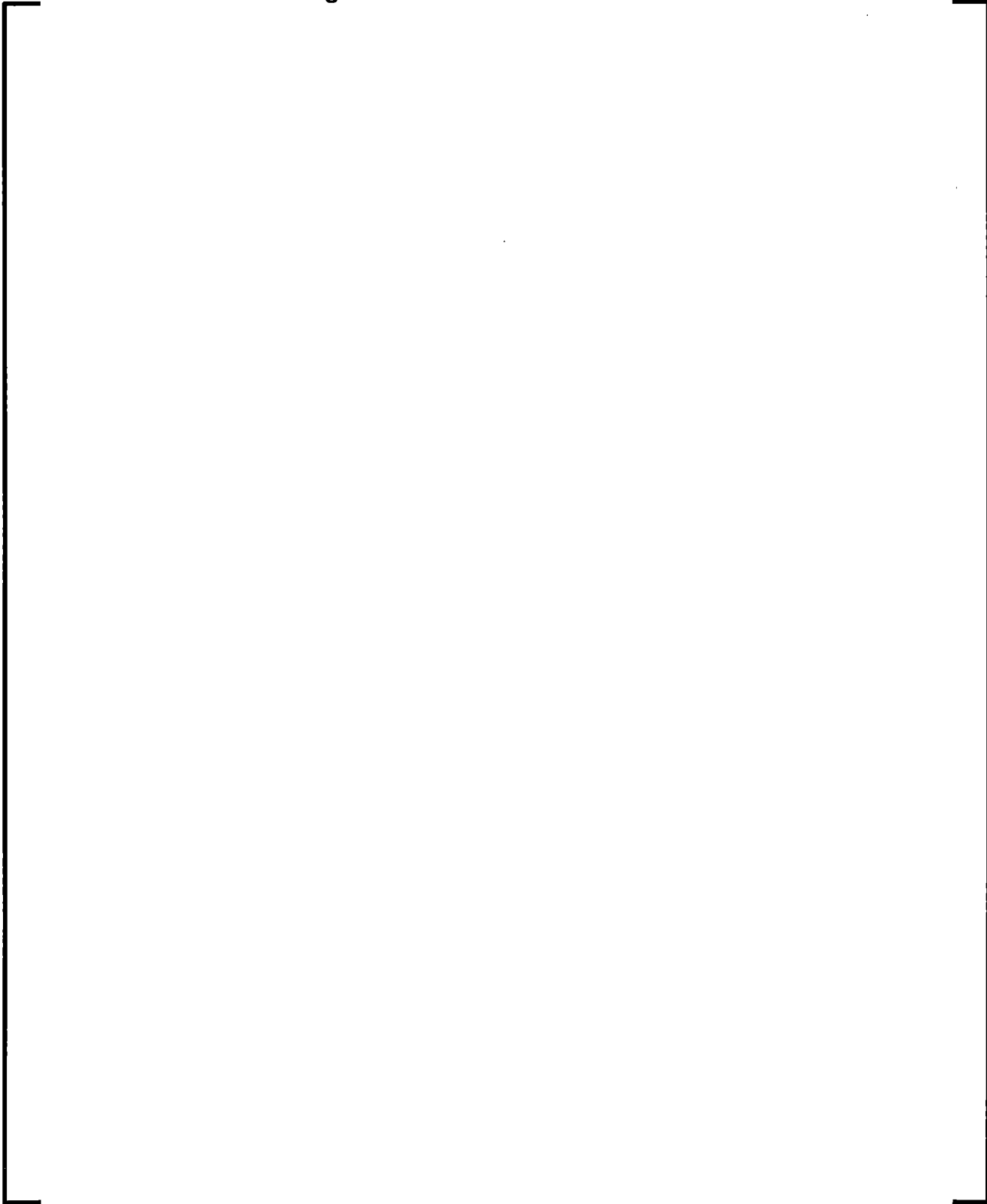
Figure 7-9 Schematic of Heat Transfer Regime Selection Logic

AREVA Inc.

EMF-2103NP
Revision 3

Realistic Large Break LOCA Methodology for Pressurized Water Reactors
Topical Report

Page 7-180

7.6.2 Single-Phase Liquid

AREVA Inc.

EMF-2103NP
Revision 3

Realistic Large Break LOCA Methodology for Pressurized Water Reactors
Topical Report

Page 7-181

AREVA Inc.

EMF-2103NP
Revision 3

Realistic Large Break LOCA Methodology for Pressurized Water Reactors
Topical Report

Page 7-182

[

].

7.6.3 Nucleate Boiling

Boiling of subcooled liquid in a heated channel begins at the point of boiling incipience, where the liquid temperature near the wall is high enough for the nucleation of small bubbles. However, a significant amount of voids appear only after the point of net vapor generation is reached. The wall temperature at the incipience of boiling, T_{IB}, is computed from a criterion published by Bergles and Rohsenow (Reference 7-158) in British units:

$$T_{IB} = T_{sat} + \left(\frac{q''}{15.6P^{1.156}}\right)^{P^{0.0234}/2.3}$$ (7.481)

The model for the point of net vapor generation was developed by Saha and Zuber (Reference 7-159). At the point of net vapor generation, the liquid subcooling, $\Delta T_{NV} = T_{sat} - T_f$, satisfies the following relations

$$\frac{q''D_h}{k_f \Delta T_{NV}} = 455$$ (7.482)

if Pe < 70000 and

$$\frac{q''}{GC_{pf}\Delta T_{NV}} = 0.0065$$ (7.483)

if Pe > 70000, where Pe is the Péclét number

$$Pe = \frac{GD_h C_{pf}}{k_f}$$ (7.484)

As shown in Figure 7-9, the determination of T_{IB} is done only when the void fraction is less than 10^{-5}. The nucleate boiling heat transfer correlations are applied from the point of boiling incipience up to the point of CHF. The computation of the wall vapor generation term begins at the point of net vapor generation. Thus, there is no wall vapor generation below the point of net vapor generation.

7.6.3.1   Heat Transfer Coefficients

The Chen correlation (Reference 7-160), developed for saturated boiling, is used for both subcooled and saturated boiling. Chen proposed, for saturated nucleate boiling, that the contributions from two mechanisms, forced convection and pool nucleate boiling, are additive. The forced convective term (or macro term) is represented by the Dittus-Boelter correlation with an F factor and the boiling term (or micro term) is represented by the Forster-Zuber correlation (Reference 7-161) with a suppression factor, S. Thus, the heat transfer coefficient for saturation boiling is the sum of macro and micro terms:

$$h_{c,CHEN} = h_{mac} + h_{mic} \qquad (7.485)$$

Extension of the Chen correlation to subcooled nucleate boiling is generally done by expressing the wall-to-fluid heat flux as

$$q'' = h_{mac}\left(T_w - T_f\right) + h_{mic}\left(T_w - T_{sat}\right) \qquad (7.486)$$

All of the heat flux in Equation (7.486) goes to the liquid and there is no heat transfer to the vapor in the nucleate boiling regime.

The 'forced convection' or 'macro' term is expressed as

$$h_{mac} = 0.023\, Re_f^{0.8}\, Pr_f^{0.4}\, \frac{k_f}{D_h} F \qquad (7.487)$$

where:

$$F = \begin{cases} 1.0 & \chi_{tt}^{-1} \le 0.1 \\[2ex] 2.35\left(\chi_{tt}^{-1} + 0.213\right)^{0.736} & \chi_{tt}^{-1} > 0.1 \end{cases} \qquad (7.488)$$

with

$$\chi_{tt}^{-1} = \left|\frac{G_g}{G_f}\right|^{0.9}\left(\frac{\rho_f}{\rho_g}\right)^{0.5}\left(\frac{\mu_g}{\mu_f}\right)^{0.1} \qquad (7.489)$$

The 'boiling' or 'micro' term is given by

AREVA Inc.

EMF-2103NP
Revision 3

Realistic Large Break LOCA Methodology for Pressurized Water Reactors
Topical Report

Page 7-184

$$h_{mic} = 0.00122 \frac{k_f^{0.79} C_{pf}^{0.45} \rho_f^{0.49}}{\sigma^{0.5} \mu_f^{0.29} \left(h_{fg} \rho_g\right)^{0.24}} \Delta T_{sat}^{0.24} \Delta P_{sat}^{0.75} S \tag{7.490}$$

where $h_{fg} = h_g^s - h_f^s$ is the latent heat of vaporization, and

$$\Delta T_{sat} = T_w - T_{sat}, \qquad \Delta P_{sat} = P_{sat}\left(T_w\right) - P \tag{7.491}$$

and the suppression factor, S, is expressed in equation form (Reference 7-162) as

$$S = \begin{cases} \left[1 + 0.12 Re_{TP}^{1.14}\right]^{-1} & Re_{TP} < 32.5 \\[2em] \left[1 + 0.42 Re_{TP}^{0.78}\right]^{-1} & 32.5 \leq Re_{TP} < 70 \\[2em] 0.0797 & Re_{TP} \geq 70 \end{cases} \tag{7.492}$$

with

$$Re_{TP} = 10^{-4} Re_f F^{1.25} \tag{7.493}$$

For subcooled boiling, the extension of the Chen correlation, as defined in Equation (7.486), requires that F = 1. Moles and Shaw (Reference 7-163) reported satisfactory agreement for water at low to moderate subcoolings in comparing the (extended) Chen correlation to subcooled boiling data for several fluids. To avoid abrupt change in the magnitude of the F factor, the code defines a transition region of 5K subcooling. Within the transition region, the F factor decreases from the computed saturation value at zero subcooling to 1 at 5K subcooling. This makes the computed forced convection term smoother when the heat transfer mode changes from single-phase liquid to subcooled nucleate boiling and then to saturated nucleate boiling. Smooth transition of the boiling or micro term is also made by increasing the micro term from zero at T_{IB} to the computed value at 2K above T_{IB} or from zero at 2K below T_{NV} to the computed value at T_{NV}, whichever is applicable. These smoothing procedures are physically appropriate and are necessary in order to reduce the chances of computing sudden jumps in flow or heat transfer solutions.

AREVA Inc.

EMF-2103NP
Revision 3

Realistic Large Break LOCA Methodology for Pressurized Water Reactors
Topical Report

Page 7-185

7.6.3.2 Wall Vapor Generation

AREVA Inc.

Realistic Large Break LOCA Methodology for Pressurized Water Reactors
Topical Report

EMF-2103NP
Revision 3

Page 7-186

AREVA Inc.

Realistic Large Break LOCA Methodology for Pressurized Water Reactors
Topical Report

EMF-2103NP
Revision 3

Page 7-187

Figure 7-10 Diagram of pre-CHF Heat Transfer Correlations Selection Logic

7.6.4   Critical Heat Flux

As explained in Section 7.6.1, critical heat flux (CHF) determines the boundary between nucleate boiling and transition boiling. In general, correlations are used to compute critical heat flux. The RLBLOCA EM uses the set of CHF correlations installed in S-RELAP5 from RELAP5/MOD2 (Reference 7-152) and is composed of the Biasi correlation (Reference 7-166) for high flow rate, and the modified Zuber correlation (Reference 7-167) for low flow rate.

7.6.4.1   Biasi and Zuber Correlations

AREVA Inc.

EMF-2103NP
Revision 3

Realistic Large Break LOCA Methodology for Pressurized Water Reactors
Topical Report

Page 7-189

AREVA Inc.

Realistic Large Break LOCA Methodology for Pressurized Water Reactors
Topical Report

EMF-2103NP
Revision 3

Page 7-191
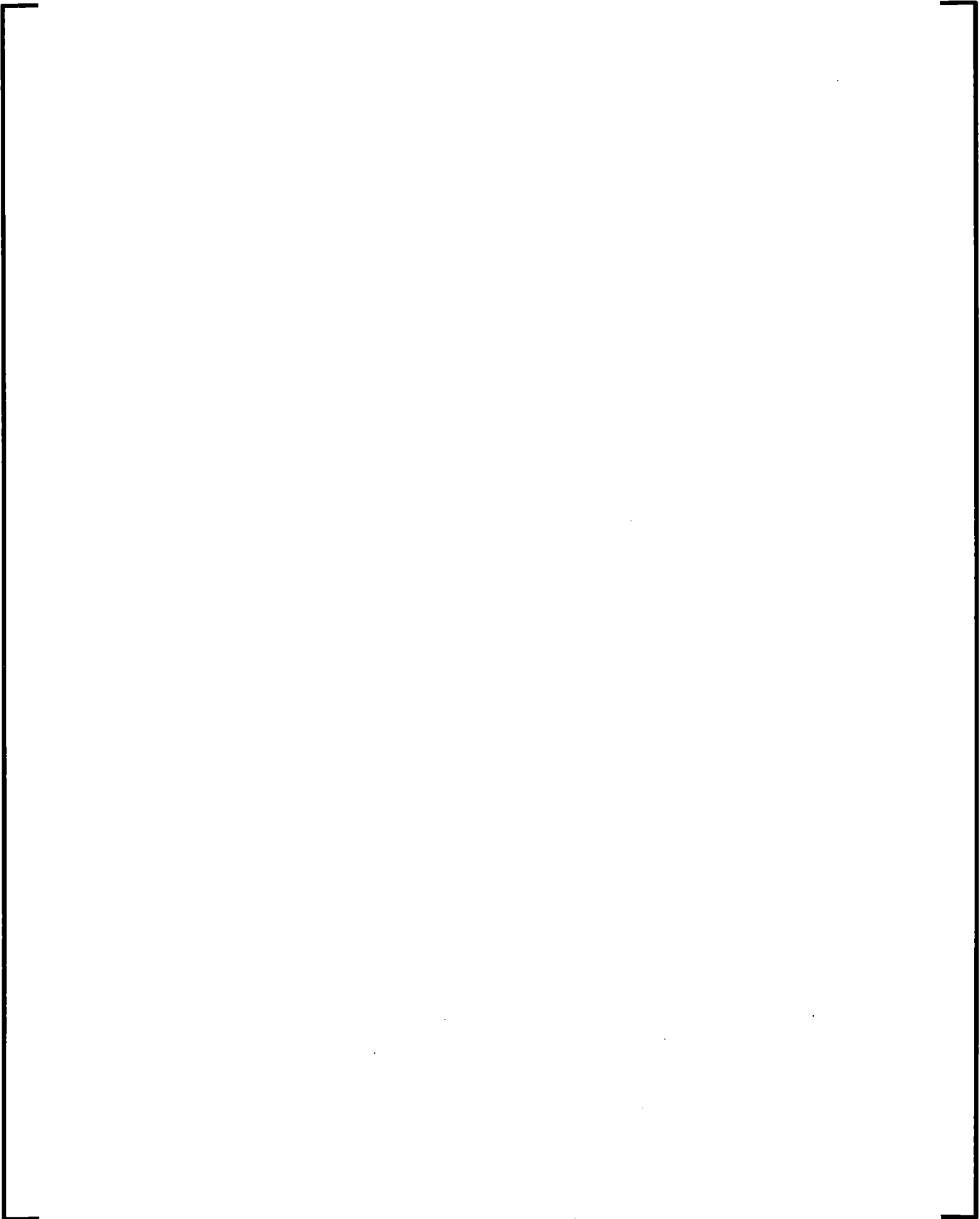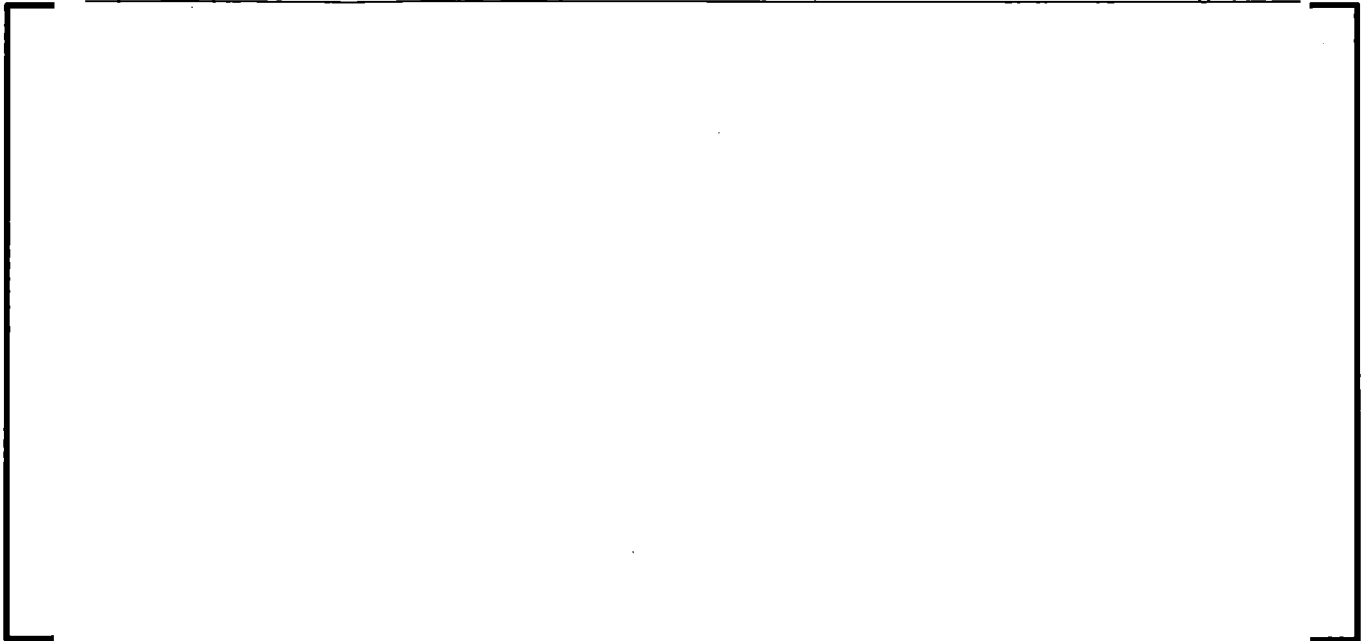
Figure 7-11 Diagram of Critical Heat Flux Correlation Selection Logic

AREVA Inc.

EMF-2103NP
Revision 3

Realistic Large Break LOCA Methodology for Pressurized Water Reactors
Topical Report

Page 7-192

7.6.5 Single-Phase Vapor

7.6.5.1 Single-Phase Vapor for Non-Core Heat Structures

AREVA Inc.

EMF-2103NP
Revision 3

Realistic Large Break LOCA Methodology for Pressurized Water Reactors
Topical Report

Page 7-193

AREVA Inc.

Realistic Large Break LOCA Methodology for Pressurized Water Reactors
Topical Report

EMF-2103NP
Revision 3

Page 7-194
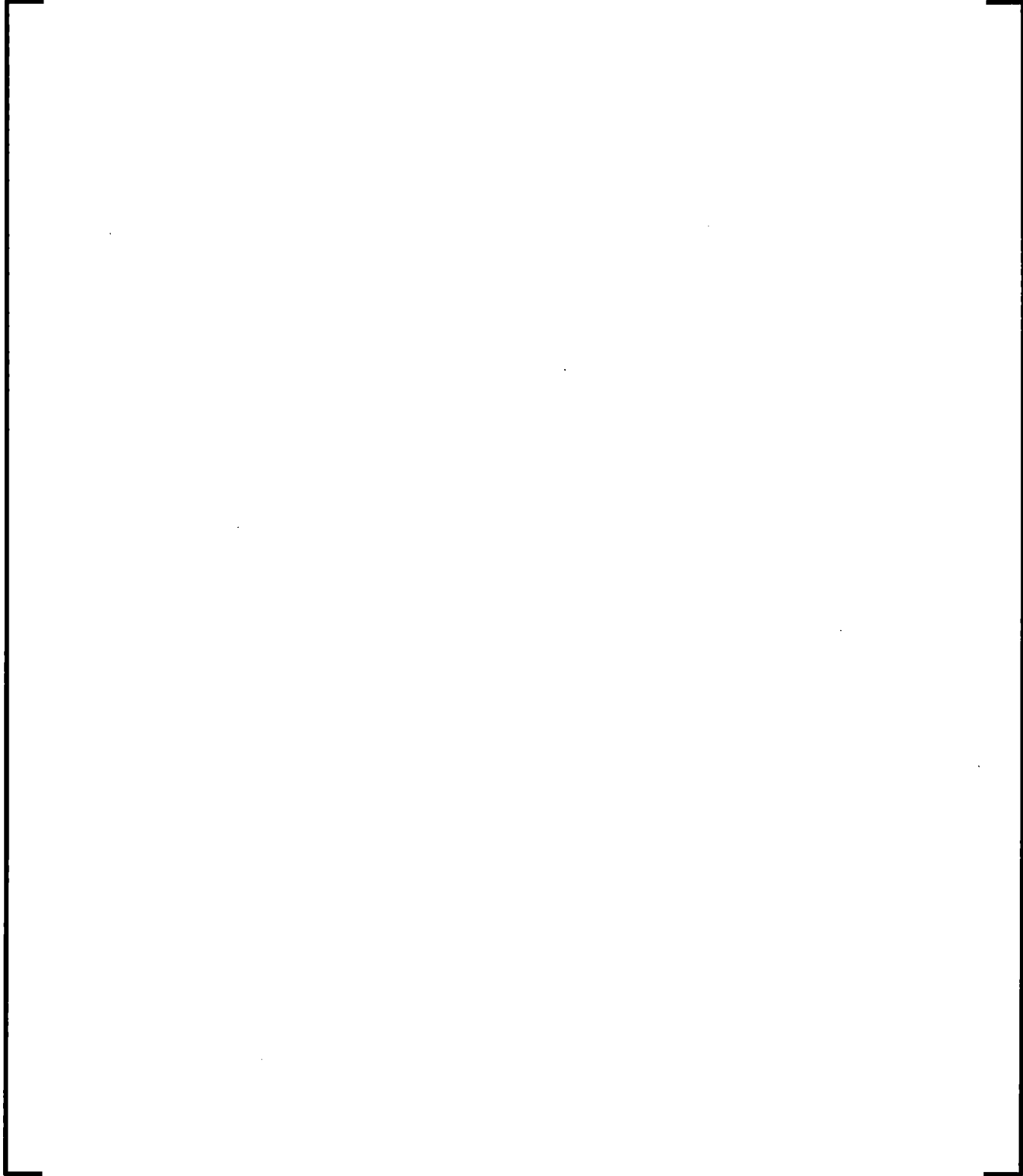
Figure 7-12 Diagram of Single Phase Vapor Heat Transfer Correlation Selection Logic

7.6.6   Transition Boiling

In the transition boiling region, the heat transfer mainly consists of two parts: the boiling heat transfer to liquid, q_f'', and the convective heat transfer to vapor, q_g''. The heat fluxes are computed based essentially on the modified form of Chen's transition heat transfer correlation (References 7-172 and 7-152) as

$$q_f'' = q_{CHF}'' F_f \tag{7.512}$$

and

$$q_g'' = h_{cg}\left(T_w - T_g\right)\left(1 - F_f\right)$$

where F_f is the fractional liquid wetted wall area.

The fractional liquid wetted wall area is given by the following correlation:

$$F_f = \exp\left[-\lambda\left(\sqrt{T_w - T_{sat}} - a\sqrt{T_{CHF} - T_{sat}}\right)\right] \tag{7.513}$$

where:

$$\lambda = \mathrm{MAX}\left[C_1 - 10^{-5}C_2 G, 10^{-5}C_3 G\right]$$

$$C_2 = 0.075\alpha_g + \frac{0.05}{\left(1 - \alpha_g^{40}\right)} \tag{7.514}$$

$$C_1 = 2.4C_2, \quad C_3 = 0.2C_2$$

and

$$a = \mathrm{MAX}\left\{0.0, \mathrm{MIN}\left[1.0, 0.25\left(4.0 - T_w + T_{CHF}\right)\right]\right\} \tag{7.515}$$

The temperatures in Equation (7.513) are in °F and the mass flux G in Equation (7.514) is in $lb_m/h - ft^2$.

The C_1 and C_2 coefficients are in the modified form of RELAP5/MOD2 (Reference 7-152) and MOD3 (Reference 7-173), and are different from the original correlation (Reference 7-172). The factor of $a\sqrt{T_{CHF} - T_{sat}}$ in Equation (7.513) is not present in the original correlation and is included to bring the heat flux at the CHF point to the CHF.

AREVA Inc.

EMF-2103NP
Revision 3

Realistic Large Break LOCA Methodology for Pressurized Water Reactors
Topical Report

Page 7-196

The CHF, q''_{CHF}, in Equation (7.512) was introduced in RELAP5/MOD2 (Reference 7-152) to replace the "average liquid contact heat flux," which is too complex to code efficiently, in the original correlation.

For the convective heat transfer, the correlation of the heat transfer coefficient proposed by Chen is replaced by Equation (7.506). Note that the liquid mass flux is not included in the computation of the Reynolds number, Equation (7.511), for the heat transfer coefficient to vapor.

An illustration of the calculation logic for the transition boiling heat transfer is provided in Figure 7-13.

AREVA Inc.

Realistic Large Break LOCA Methodology for Pressurized Water Reactors
Topical Report

EMF-2103NP
Revision 3
Page 7-197

Figure 7-13 Diagram of Transition Boiling Heat Transfer Calculation Logic
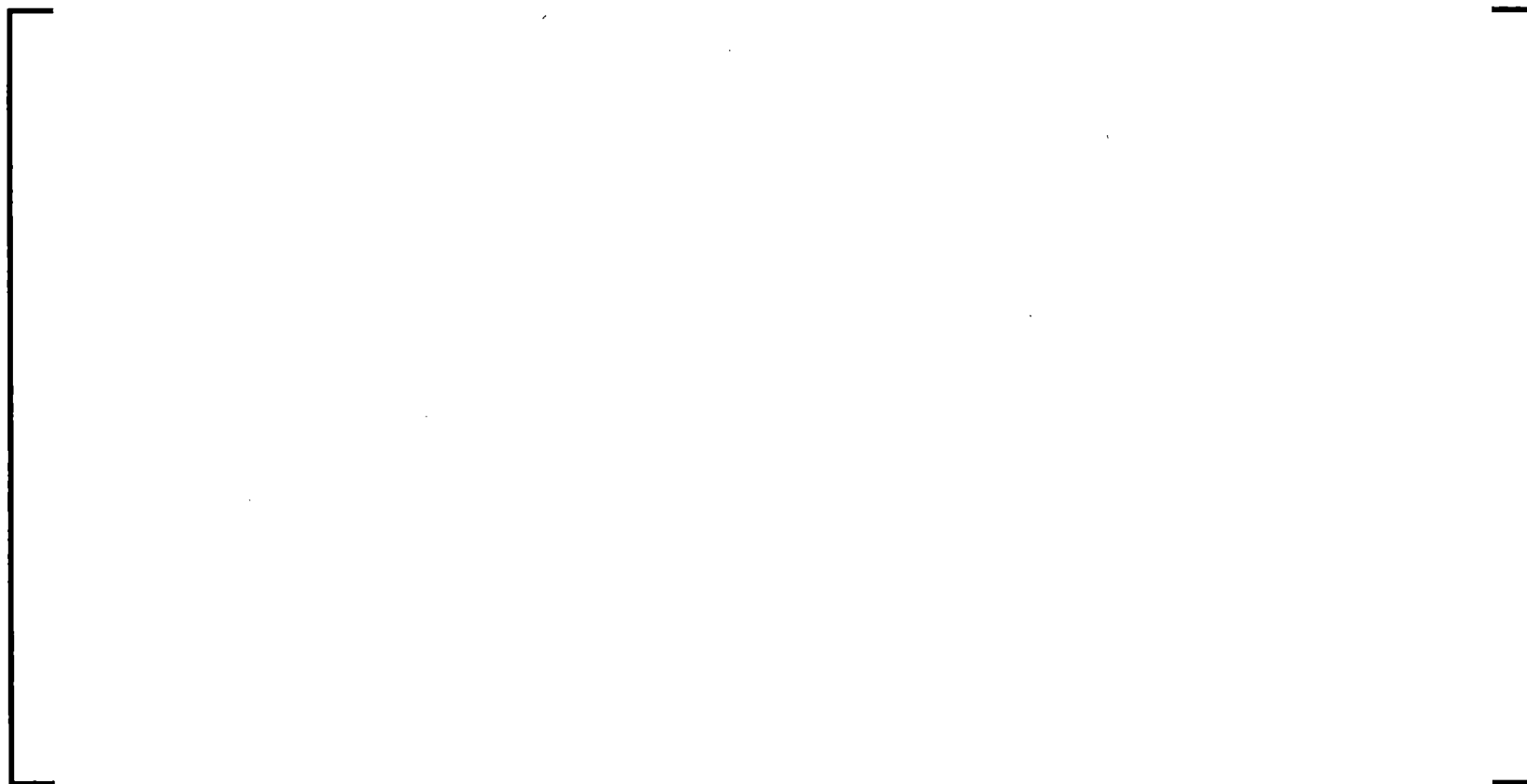
7.6.7   Film Boiling

7.6.7.1   Film Boiling for Non-Core Heat Structures

AREVA Inc.

Realistic Large Break LOCA Methodology for Pressurized Water Reactors
Topical Report

EMF-2103NP
Revision 3

Page 7-200

AREVA Inc.

Realistic Large Break LOCA Methodology for Pressurized Water Reactors
Topical Report

EMF-2103NP
Revision 3

Page 7-202
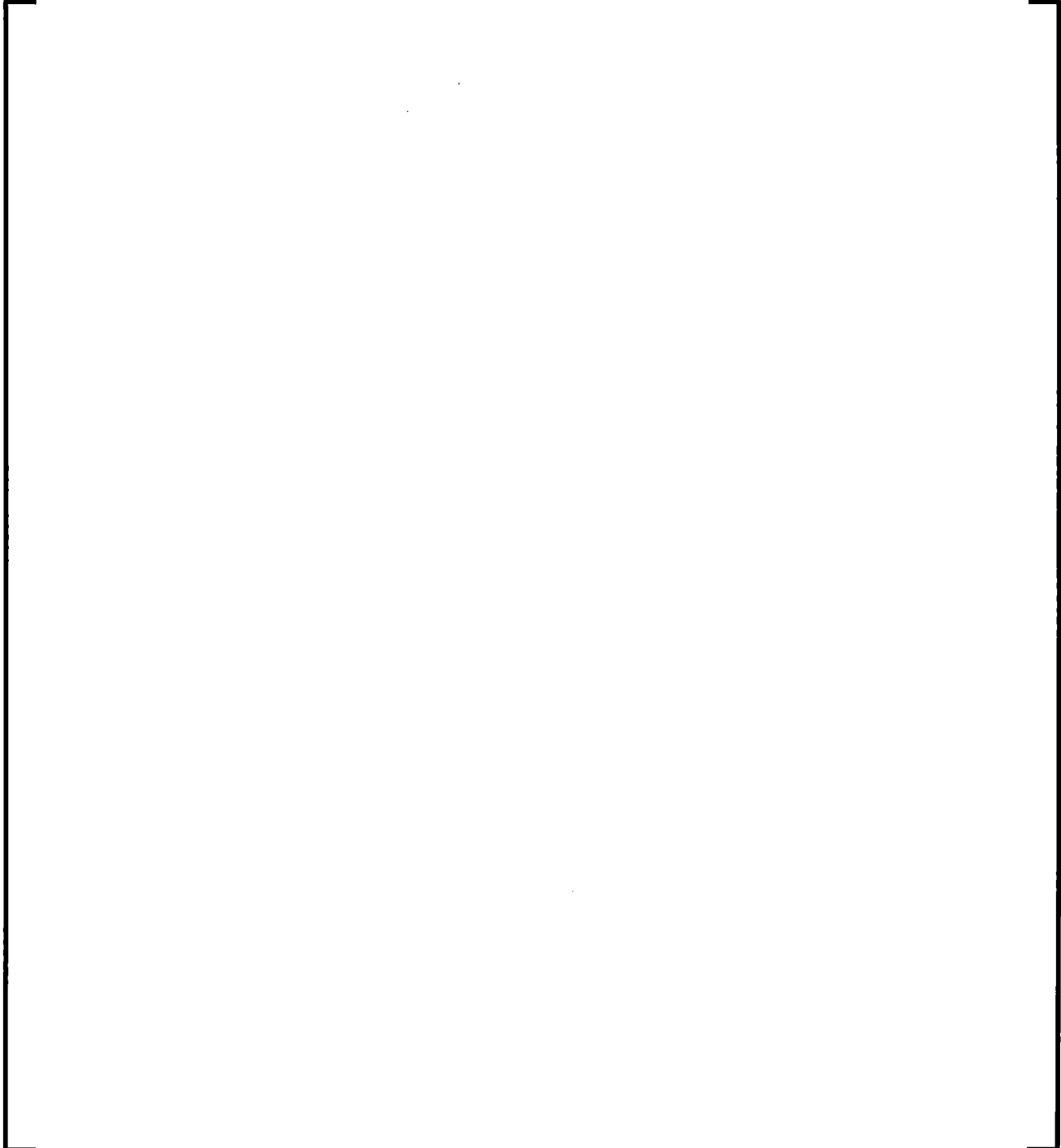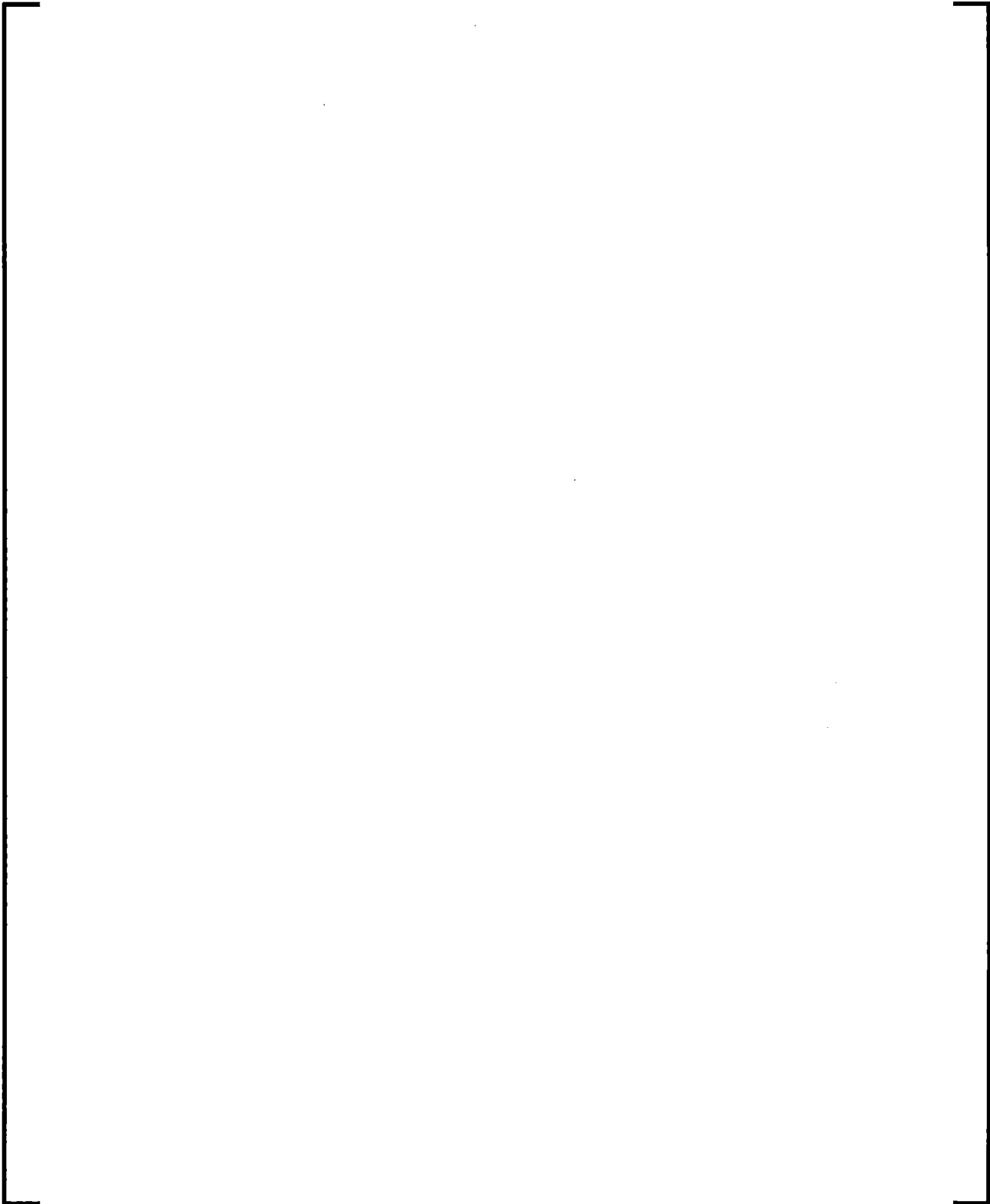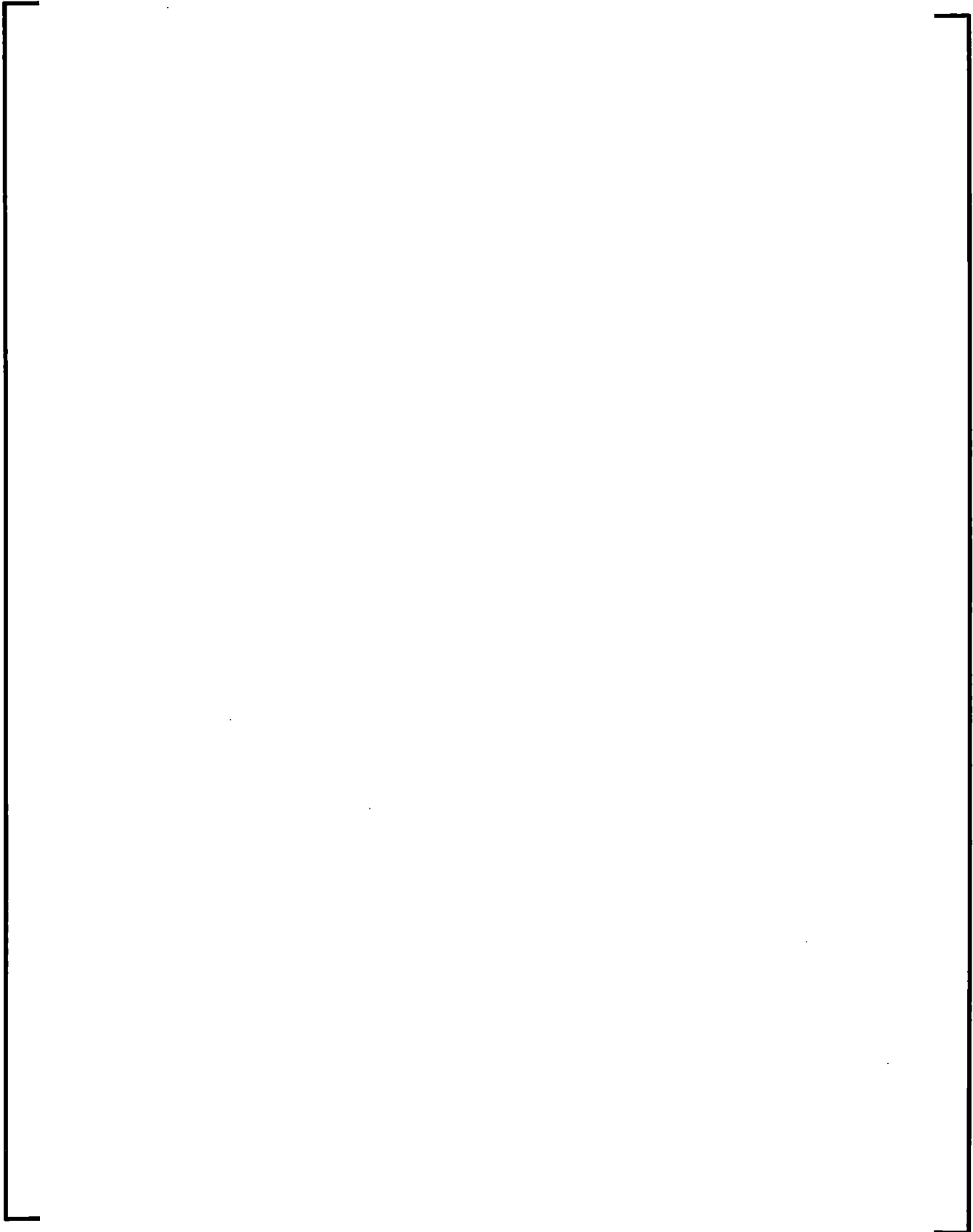
Figure 7-14 Diagram of Film Boiling Heat Transfer Calculation Logic for Non-Core Heat Structures

AREVA Inc.

Realistic Large Break LOCA Methodology for Pressurized Water Reactors
Topical Report

EMF-2103NP
Revision 3
Page 7-203

7.6.7.2 Film Boiling for Core Bundle Heat Structures

The core bundle model is designed to be exclusively used in the core region for LOCA scenarios and is activated through user input. The model is used in conjunction with the reflood model for large break LOCA. The model replaces the use of Sleicher-Rouse and Forslund-Rohsenow in dispersed flow film boiling with a modified version of the Wong-Hochreiter (Reference 7-183) correlation for laminar and turbulent flow convective heat transfer. Also, the transition from inverted annular film boiling to dispersed flow film boiling is modified.

The Wong-Hochreiter correlation, given by

$$\frac{Nu}{Pr_g^{1/3}} = \begin{cases} 7.86 & Re_g \leq 2000 \\ 0.0162\,Re_g - 24.55 & 2000 < Re_g < 2500 \\ 0.0797\,Re_g^{0.6774} & 2500 \leq Re_g \leq 25200 \\ 0.023\,Re_g^{0.8} & 25200 < Re_g \end{cases} \tag{7.525}$$

uses four different heat transfer coefficients based on the magnitude of the vapor Reynolds number. It is first modified by replacing the region between laminar and turbulent flow with the previously described natural convection heat transfer correlation by Holman, Equation (7.510) (Reference 7-202a). It is further modified by taking the maximum of the heat transfer coefficients instead of the Reynolds Number based switching. The Dittus-Boelter correlation is used in the high Reynolds Number region. Although the Dittus-Boelter correlation typically under-predicts the heat transfer in bundles, the premise of the Wong-Hochreiter work, it has been successfully used in conjunction with the two-phase turbulent heat transfer enhancement for rod bundles by Drucker and Dhir (Reference 7-184) and, hence, motivated the final form of the bundle heat transfer model where the heat transfer coefficient is defined as the maximum of Wong-Hochreiter and Dittus-Boelter with two phase turbulent enhancements. Finally, an overall heat transfer enhancement for rod bundles with grid spacers under laminar and turbulent flow conditions has been included with the bundle model.

Thus, for the bundle model, the convective heat transfer coefficient, h_{cg}, is given by

$$h_{cg} = MAX(h_{cg,lam}, h_{cg,nc}, \psi h_{cg,wh}, \psi h_{cg,db})F \tag{7.526}$$

where the laminar region is

$$h_{cg,lam} = 7.86 Pr_g^{0.3333} \frac{k_g}{D_h} \tag{7.527}$$

and, as previously mentioned, the natural convection is given by Holman [Equation (7.510) and Reference 7-7-202a]. From the Wong-Hochreiter correlation, the low Reynolds number region that was fitted to steam cooling data is used:

$$h_{cg,wh} = 0.0797 Re_g^{0.6774} Pr_g^{0.3333} T_{cf} \frac{k_g}{D_h} \tag{7.528}$$

The Dittus-Boelter correlation is modified to account for variable properties across the boundary layer when large temperature differences exist:

$$h_{cg,db} = 0.023 Re_g^{0.8} Pr_g^{0.3333} T_{cf} \frac{k_g}{D_h} \tag{7.529}$$

The form used is by Sleicher-Rouse and only considers the situation where the wall is heating the steam. The temperature correction factor T_{cf} has the same formulation as given for the Sleicher-Rouse correlation and presented in Equation (7.508). Although the turbulent two-phase enhancement by Drucker and Dhir was developed for wet and dry walls, only the dry-wall form is used:

$$\psi = MIN\left(U_{limit}, 1 + 3.25\sqrt{\frac{\alpha_f Gr}{Re_g^2}}\right) \tag{7.530}$$

$$Gr = g\rho_g(\rho_f - \rho_g)\frac{D^3}{\mu_g^2}$$

Also, its influence is restricted by U_{limit} to a maximum value of 5.0 and its affect is diminished linearly as void fraction varies from 0.90 to 0.70, inclusive.

Finally, two optional grid spacer effects and a laminar flow heat transfer enhancement are given by a three factor multiplier to the convective heat transfer. The first two

factors, the optional grid spacer effects, are given by Yao, Hochreiter, and Leech (Reference 7-185), while the third factor is Reynolds Number dependent and was developed by Meholic et al. (Reference 7-186) using recent high void low flow data from the Rod Bundle Heat Transfer (RBHT) facility at Pennsylvania State University. The convective enhancement is given by:

$$F = F_1 F_2 F_3 \tag{7.531}$$

where

$$F_1 = \left(1 + 5.55 \varepsilon^2 \, e^{-0.13\frac{x}{D}} \right) \tag{7.532}$$

$$F_2 = \left(1 + \beta^2 \tan^2 \varphi \, e^{-0.034\frac{x}{D}} \right)^{0.4} \tag{7.533}$$

$$F_3 = \begin{cases} 1.75 & Re_g < 736 \\ 11.008 \, Re_g^{-0.2788} & 736 \leq Re_g \leq 5450 \\ 1.0 & 5450 < Re_g \end{cases} \tag{7.534}$$

and where

ε is the blockage ratio of the spacer to flow channel when looking from upstream,

x is the axial distance from the downstream end of the spacer,

D is the hydraulic diameter of the flow channel;

β is the fraction of area of the vane to the flow cross-section, viewing from upstream,

φ is the angle of swirling vane with respect to axial flow direction.

The factors F1 and F2 are user input, while F3 is implemented into the S-RELAP5 coding and active for all calculations.

In the bundle model, the transition between dispersed flow film boiling and steady film boiling is made by using a quadratic or cubic exponential decay to the Modified Bromley

correlation, Equation (7.520), over the void fraction range of 0.6 to 0.9. The initial decay

uses an exponent of three that transitions to two over the range of Reynolds numbers

from 2000 to 4000. The purpose of the exponent transition is to capture the effects of

the change in quality above the quench front as it moves through a volume, as indicated

by the increased vapor Reynolds number during this same period. The Bromley

attenuation is given by:

$$F_{Br} = \left(\frac{0.90 - \alpha_g}{0.90 - 0.60} \right)^{f(Re_g)}, \quad f(Re_g) = \begin{cases} 3 & Re_g \leq 2000 \\ 4 - 5x10^{-4} Re_g & 2000 < Re_g < 4000 \\ 2 & 4000 \leq Re_g \end{cases} \quad (7.535)$$

AREVA Inc.

Realistic Large Break LOCA Methodology for Pressurized Water Reactors
Topical Report

EMF-2103NP
Revision 3

Page 7-207

Figure 7-15 Diagram of Film Boiling Heat Transfer Calculation Logic for Active Core Heat Structures

7.6.8 Radiation Heat Transfer

7.6.8.1 Wall to Fluid Radiation

At high wall temperatures, the radiation heat transfer from wall to fluid is treated using a model developed by Sun (Reference 7-187). The wall-to-fluid radiation model considers the vapor-droplet mixture as an optically thin medium and uses an electric network analogy to analyze the radiation energy exchange among three nodes: wall, liquid droplets, and vapor. The resultant radiation fluxes among the three nodes are expressed as

$$q''_{wg} = F_{wg}\sigma_B \left(T_w^4 - T_g^4 \right)$$

$$q''_{wf} = F_{wf}\sigma_B \left(T_w^4 - T_{sat}^4 \right) \tag{7.536}$$

$$q''_{gf} = F_{gf}\sigma_B \left(T_g^4 - T_{sat}^4 \right)$$

Here σ_B is the Stefan-Boltzman constant, 5.668×10^{-8} W/m^2-K^4, and the Fs are the gray body factors:

$$F_{wg} = \frac{1}{R_w + R_g + \left(\dfrac{R_w R_g}{R_f} \right)}$$

$$F_{wf} = \frac{1}{R_w + R_f + \left(\dfrac{R_w R_f}{R_g} \right)} \tag{7.537}$$

$$F_{gf} = \frac{1}{R_g + R_f + \left(\dfrac{R_g R_f}{R_w} \right)}$$

The resistance terms in the above gray factors are given in terms of emissivities as

$$R_g = \frac{1-\varepsilon_g}{\varepsilon_g\left(1-\varepsilon_g\varepsilon_f\right)}$$

$$R_f = \frac{1-\varepsilon_f}{\varepsilon_f\left(1-\varepsilon_f\varepsilon_g\right)} \qquad (7.538)$$

$$R_w = \frac{1}{1-\varepsilon_g\varepsilon_f} + \frac{1-\varepsilon_w}{\varepsilon_w}$$

The emissivities for vapor and droplets are computed from the following formulas:

$$\varepsilon_g = 1-\exp\left(-a_g L_m\right)$$

$$(7.539)$$

$$\varepsilon_f = 1-\exp\left(-a_f L_m\right)$$

where L_m is a mean path length and a_g and a_f are, respectively, the absorption coefficients of vapor and droplets. Sun et al. (Reference 7-187) used a value of $\varepsilon_w = 0.7$ in their analysis of core cooling for BWR (boiling water reactor) rod bundles. This value of wall emissivity is implemented in the code.

The mean path length is taken as $L_m = 0.85\ D_h$ for a rod bundle geometry from a FLECHT SEASET data evaluation and analysis report (Reference 7-188), [

] The absorption coefficient of vapor is given by the following relation:

$$a_g = 1.814\text{x}10^{-4}\, P\left(\frac{555.56}{T_g}\right)^2\left[1-0.054\left(\frac{555.56}{T_g}\right)^2\right]\alpha_g \qquad (7.540)$$

where P is pressure in Pa and T_g is the vapor phase temperature in K. The particular form of Equation (7.540), i.e., the dependency on P and T_g, and the constant are from the FLECHT SEASET report (Reference 7-188). The void fraction factor is added to account for the two-phase condition. The absorption coefficient of liquid droplets is expressed as

$$a_f = 1.11 \frac{\alpha_f}{d_{od}} \qquad (7.541)$$

where α_f is the liquid volume fraction and d_{od} is the average droplet diameter. The above equation is obtained from the formulation given by Sun (Reference 7-187) by expressing the number density of droplets in terms of average droplet diameter. For liquid fractions above 0.35, the droplet diameter is approximated as 0.9 D_h (hydraulic diameter). For liquid fractions below 0.1, the droplet diameter is calculated according to formulas described in Section 3.2.1 with the minimum diameter value limited to 5×10^{-4} m. For liquid fractions between 0.35 and 0.1, the value of ε_f on the two limits are used for interpolation.

The radiation heat transfer from vapor to liquid is immaterial as far as the total wall-to-fluid heat flux is concerned. Thus the radiation heat flux from wall to fluid is

$$q''_{rad} = q''_{wf} + q''_{wg} \qquad (7.542)$$

For single-phase vapor, $F_{wf} = F_{gf} = 0$, the wall-to-fluid radiation heat flux becomes

$$q''_{rad} = \frac{\varepsilon_g \sigma_B}{1 + \varepsilon_g \dfrac{(1 - \varepsilon_w)}{\varepsilon_w}} \left(T_w^4 - T_g^4 \right) \qquad (7.543)$$

The wall-to-fluid radiation heat transfer is significant only at sufficiently high wall temperatures; hence the radiation is computed only when the surface temperature is above the vapor temperature and is greater than 650K. Furthermore, the heat transfer contribution from the wall-to-fluid radiation is neglected (set to zero) when the void fraction is below 0.65. This restriction may not significantly affect the results since the wall temperature is likely low under the condition of high liquid fraction.

7.6.8.2 Surface to Surface Radiation

The model for wall to wall thermal radiation is the one used in RELAP5/MOD3.3 (Reference 7-191). It is a simplistic approach that assumes the surfaces have a line of sight or a reflection path through which they can communicate with each other in the same enclosure. The computation method is a lumped-system approximation for gray diffuse surfaces contained in an enclosure. The assumptions are:

The fluid in the enclosure neither emits nor absorbs radiant thermal energy.

Reflectance from a surface is neither a function of incident nor reflected direction nor of radiation frequency.

Temperature, reflectance, and radiosity are constant over each surface.

The radiosity of a surface is the total radiant energy leaving the surface (i.e., the emitted energy plus the reflected energy). Mathematically this is written for the i-th surface as:

$$R_i = \varepsilon_i \sigma T_i^4 + \rho_i \sum_{j=1}^{n} R_j F_{ij} \tag{7.544}$$

where

R = radiosity

ε = emissivity

σ = Stefan-Boltzmann constant

T = temperature

ρ = $1 - \varepsilon$; reflectivity

F_{ij} = view factor from surface i to surface j

The net heat flux, Q, at surface i is the difference between the radiosity for i and the radiosity of all surfaces times their view factor to surface i:

AREVA Inc.

Realistic Large Break LOCA Methodology for Pressurized Water Reactors
Topical Report

EMF-2103NP
Revision 3

Page 7-212

$$Q_i = R_i - \sum_{j=1}^{n} R_j F_{ij} \qquad (7.545)$$

The above two equations can be combined to yield:

$$Q_i = \frac{\varepsilon_i}{\rho_i} \left(\sigma T_i^4 - R_i \right) \qquad (7.546)$$

Thus, it only remains to solve for R_i to obtain the heat flux at surface i. Equation (7.546) represents a set of n simultaneous linear equations which can be written in a matrix form as:

$$\left(\delta_{ij} - \rho_i F_{ij} \right) R_i = \varepsilon_i \sigma T_i^4 \qquad (7.547)$$

where the Kronecker delta function is defined as:

$$\delta_{ij} = \quad 0, \quad i \neq j$$

$$\delta_{ij} = \quad 1, \quad i = j$$

The solution of Equation (7.547) involves a matrix inversion written as:

$$R_i = \left(\delta_{ij} - \rho_i F_{ij} \right)^{-1} \varepsilon_i \sigma T_i^4 \qquad (7.548)$$

The matrix inversion need only be performed once during the initialization since it does not involve variables that change with time.

Inclusion of thermal radiation changes the conduction solution boundary condition to the form:

$$-k \left. \frac{\partial T}{\partial r} \right|_{i} = h_i \left(T_i - T_r \right) + Q_i \qquad (7.549)$$

where

$\quad$ k $\quad = \quad$ surface conductivity

$\quad$ r $\quad = \quad$ radius

$\quad$ h $\quad = \quad$ convective heat transfer coefficient

AREVA Inc.

Realistic Large Break LOCA Methodology for Pressurized Water Reactors
Topical Report

EMF-2103NP
Revision 3
Page 7-213

T_r = reference temperature

Note that the radiation term is not implicit in surface temperature, which can cause solution instabilities for thin surfaces and large time steps unless convection dominates radiation.

View factors are computed external to S-RELAP5 and, thus, are not discussed here. However, verification of the view factors is performed by requiring the view factors sum to 1.0 and reciprocity is checked:

$$\sum_{i=1}^{n} F_{ij} = 1.0 \tag{7.550}$$

$$A_i F_{ij} = A_j F_{ji} \tag{7.551}$$

If Equations (7.550) and (7.551) are not satisfied to within 0.1 percent, appropriate error messages are included in the output file and problem execution is terminated.

7.6.9 Wall Vapor Generation in Post-CHF Regimes

Transition boiling and film boiling are commonly referred to as post-CHF heat transfer regimes. In the post-CHF regimes, the wall vapor generation term is evaluated according to the following formulation:

$$\Gamma_w = \frac{q''_{wv} \dfrac{A_w}{V}}{h_{fg} + C_{pf} MAX(T_{sat} - T_f, 0)} \tag{7.552}$$

with

$$q''_{wv} = q''_f + q''_{rad}\alpha_f \tag{7.553}$$

where V is the volume of a cell (control volume), A_w is the heat surface area, and h_{fg} is the latent heat of vaporization. The boiling heat transfer to liquid drops, q''_f, is given in Sections 7.6.6 and 7.6.7 and the radiation heat flux, q''_{rad}, is given in Section 7.6.8.

In the post-CHF region, the steam is superheated, therefore the bulk mass transfer term is usually positive (i.e., vapor is generated). As both the wall and bulk vapor generation terms are positive, the partition between the two terms is less critical in determining void

AREVA Inc.

Realistic Large Break LOCA Methodology for Pressurized Water Reactors
Topical Report

EMF-2103NP
Revision 3
Page 7-214

distribution. This is in contrast with the situation in nucleate boiling (see Section 7.6.3.2), where the bulk term is usually negative (condensing) and the void distribution is strongly dependent on the wall vapor generation term. Numerically, the wall vapor generation term is required in the post-CHF region to keep liquid from becoming superheated. Physically, the void distribution is determined by the total vapor generation from the wall and bulk terms and the liquid phase temperature in the post-CHF region is mainly controlled by the wall vapor generation term.

7.6.10   Noncondensable-Water Mixture

The correlations for the convective heat transfer in an air-water mixture are the same as RELAP5/MOD2 (Reference 7-152) without any modifications, as this heat transfer regime is seldom encountered in LWR (Light Water Reactor) applications. For void fractions less than or equal to 0.3, the heat transfer coefficient is expressed as

$$h_{a-w} = h_{cf,db} \alpha_f^{-0.33} \qquad Re_f < 2000$$

$$h_{a-w} = h_{cf,db} \alpha_f^{-0.8} \qquad Re_f \geq 2000$$

(7.554)

where $h_{cf,db}$ is given in Equation (7.474), and Re_f is defined in Equation (7.475). For void fractions between 0.3 and 0.8, the heat transfer coefficient is

$$h_{a-w} = h_{cf,db} \left(\frac{10^5}{P} \right)^{0.17}$$

(7.555)

where P is pressure in Pa.

For void fractions greater than or equal to 0.8, the heat transfer coefficient is

$$h_{a-w} = \alpha_f h_{cf,db} + \alpha_g h_{cg}$$

(7.556)

where h_{cg} is given in Equation (7.506).

7.6.11   Condensation

AREVA Inc.

EMF-2103NP
Revision 3

Realistic Large Break LOCA Methodology for Pressurized Water Reactors
Topical Report

Page 7-215

AREVA Inc.

EMF-2103NP
Revision 3

Realistic Large Break LOCA Methodology for Pressurized Water Reactors
Topical Report

Page 7-216

AREVA Inc.

EMF-2103NP
Revision 3

Realistic Large Break LOCA Methodology for Pressurized Water Reactors
Topical Report

Page 7-217

AREVA Inc.

EMF-2103NP
Revision 3

Realistic Large Break LOCA Methodology for Pressurized Water Reactors
Topical Report

Page 7-218

AREVA Inc.

Realistic Large Break LOCA Methodology for Pressurized Water Reactors
Topical Report

EMF-2103NP
Revision 3

Page 7-219

7.6.12   Special Treatments for Core-Reflood

AREVA Inc.

EMF-2103NP
Revision 3

Realistic Large Break LOCA Methodology for Pressurized Water Reactors
Topical Report

Page 7-220

AREVA Inc.

Realistic Large Break LOCA Methodology for Pressurized Water Reactors
Topical Report

EMF-2103NP
Revision 3
Page 7-221
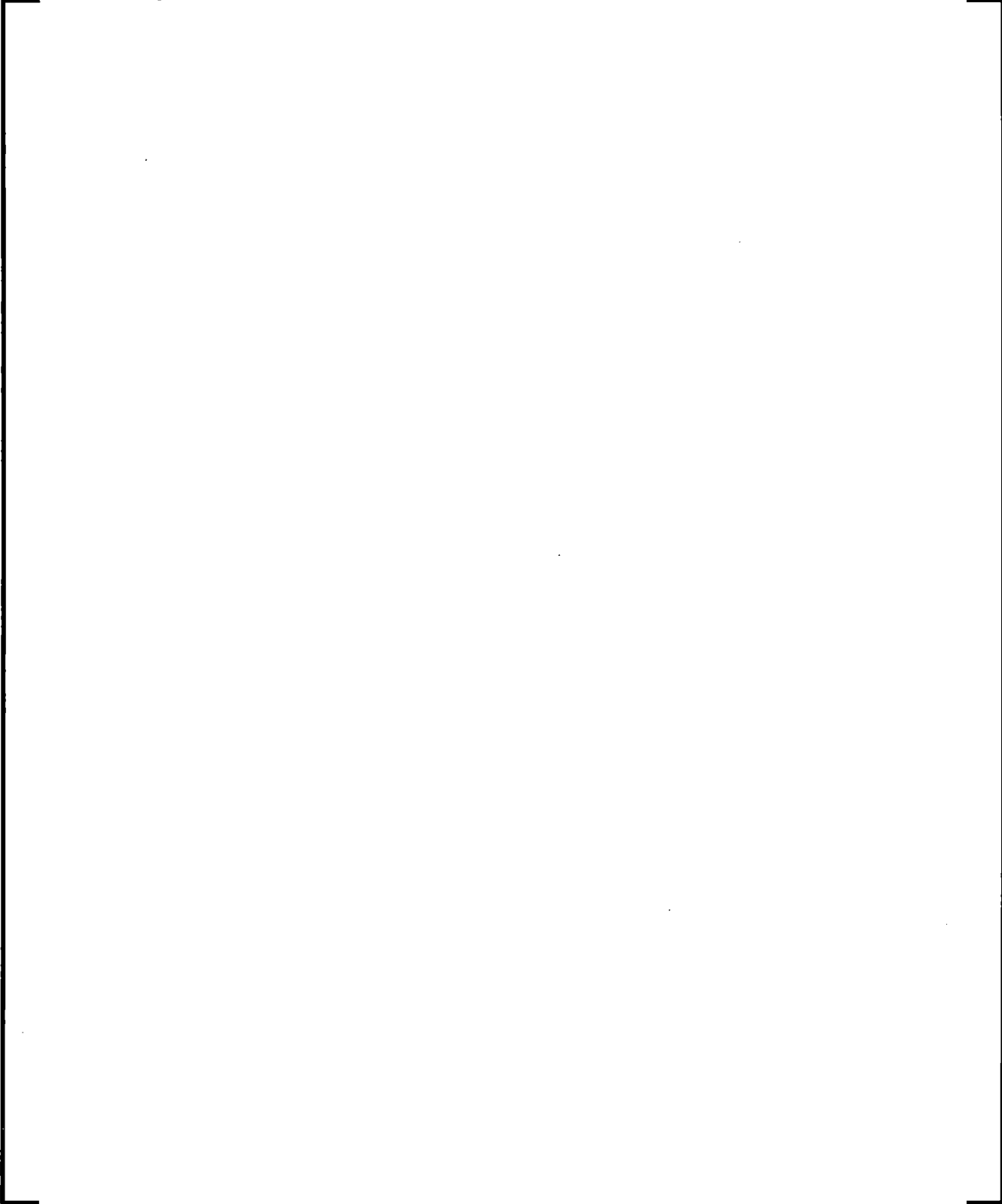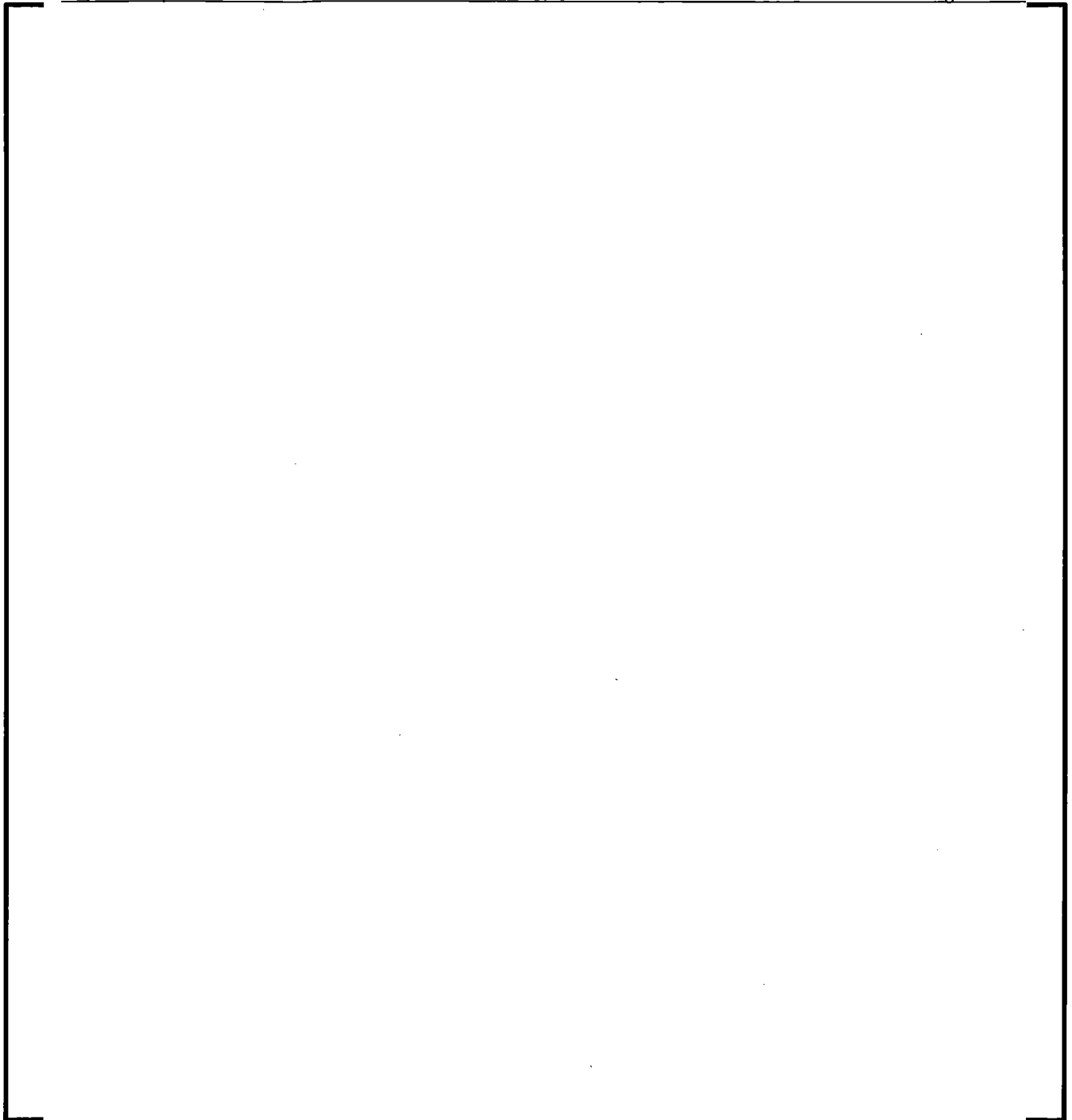
7.6.13 Discussion of Scaling and Applicability of Heat Transfer Models

AREVA Inc.

EMF-2103NP
Revision 3

Realistic Large Break LOCA Methodology for Pressurized Water Reactors
Topical Report

Page 7-222
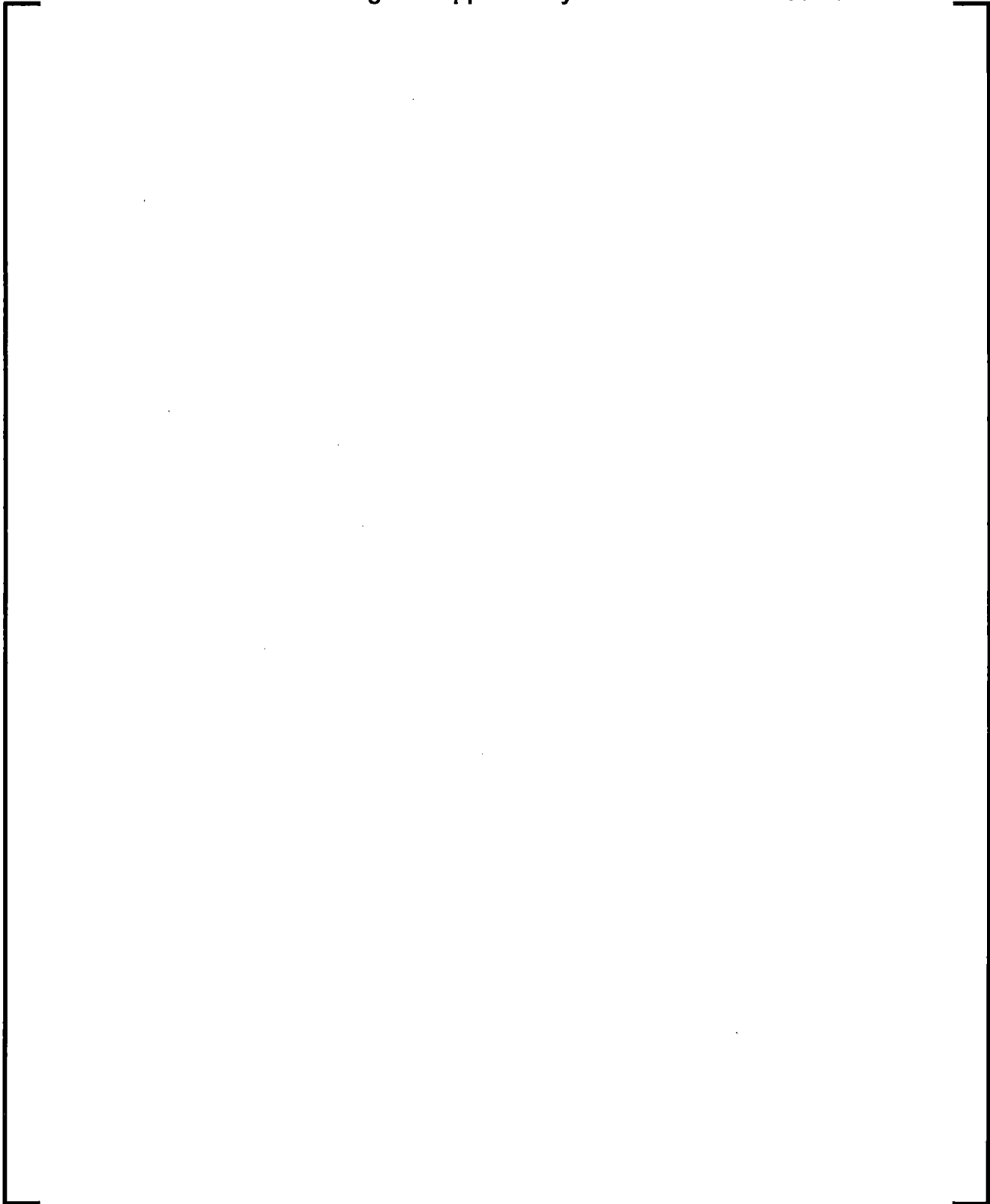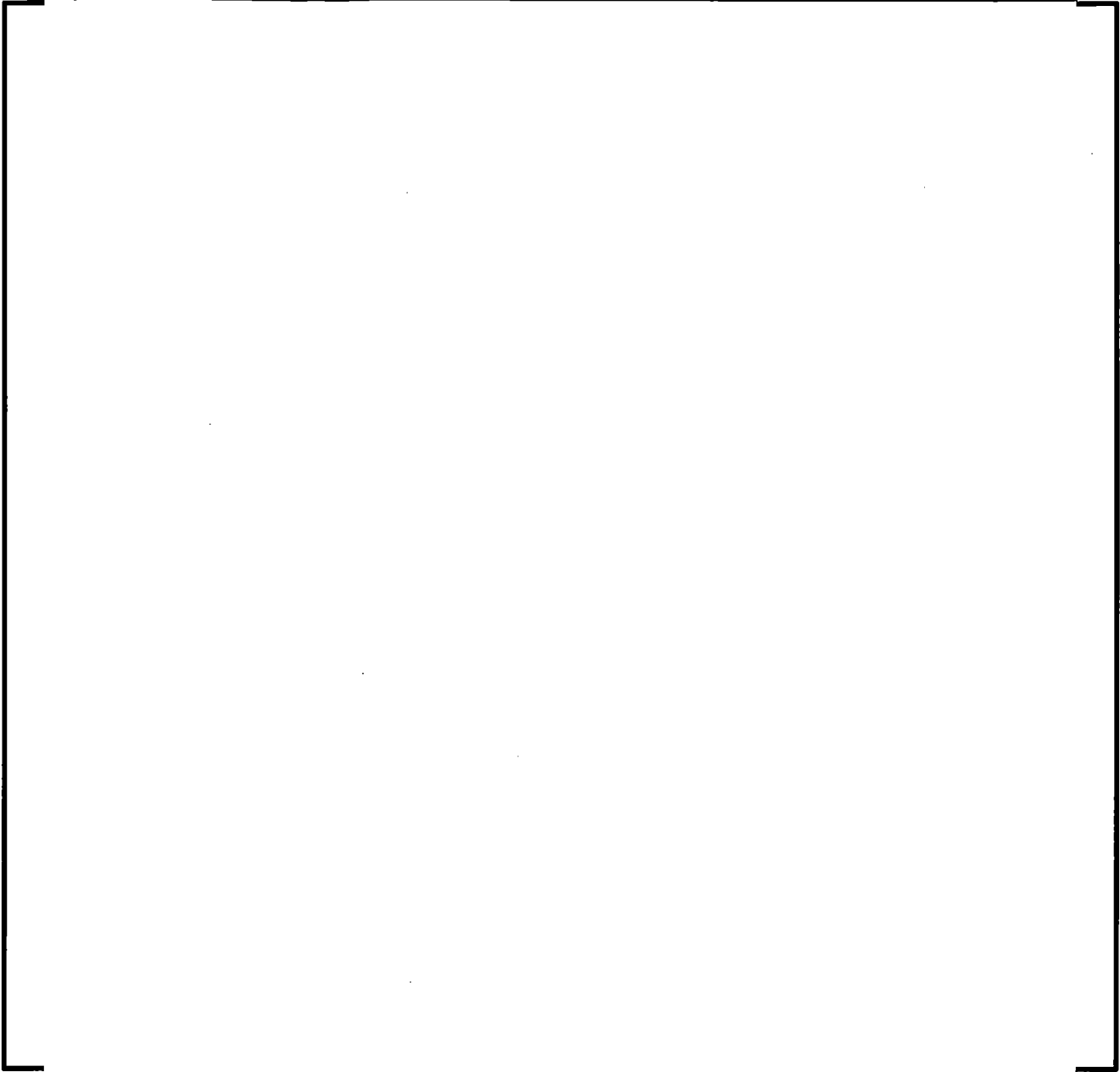
7.6.14   References

7-103. J. M. Kelley, "Quench Front Modeling and Reflood Heat Transfer in COBRA-TF," ASME Winter Annual Meeting, New York, NY, 1979, 79-WA/HT-63.

7-104. BAW-10227P-A, Evaluation of Advanced Cladding and Structural Material (M5) in PWR Reactor Fuel, Framatome ANP, February 2000.

7-105. BAW-10164P, Rev. 4, RELAP5/MOD2 B&W An Advanced Computer Program for Light Water Reactor LOCA and Non-LOCA Transient Analysis, September 1999.

7-106. FTG-32-1266194-02, M5 Swelling 7 Rupture Model, September 1999.

AREVA Inc.

EMF-2103NP
Revision 3

Realistic Large Break LOCA Methodology for Pressurized Water Reactors
Topical Report
Page 7-224

7-107. BAW-10231P-A, Revision 1, COPERNIC Fuel Rod Design Computer Code, Framatome ANP, January 2004.

7-108. J. V. Cathcart, et al., Reaction Rate Studies, IV, Zirconium Metal-Water Oxidation Kinetics, ORNL/NUREG-17, August 1977.

7-109. Fuel Material Manual Basic Properties of M5 Cladding Tube, FTG Document Number 38-1287806-00, Internal Identification Number TFJC DC 1241 E0.

7-110. D. L. Hagrman, G. A. Reymann, and R. E. Mason, MATPRO-11 (Revision 2) A Handbook of Material Properties for Use in the Analysis of Light Water Reactor Fuel Rod Behavior, NUREG-CR-0497, TREE-1280, Rev. 2, EG&G Idaho, Inc., Idaho Falls, ID, August 1981.

7-111. EMF-CC-39(P), Revision 3, ICECON: A Computer Program Used to Calculate Containment Back Pressure for LOCA Analysis (Including Ice Condenser Plants), Siemens Power Corporation, July 2004.

7-112. "Minimum Containment Pressure Model for PWR ECCS Performance Evaluation," U.S. Nuclear Regulatory Commission Branch Technical Position, CSB 6-2, March 2007.

7-113. Pump Two-Phase Performance Program, EPRI NP-1556, Volumes 1-8, September 1980.

7-114. The RELAP5 Development Team, RELAP5/MOD3 Code Manual Volume 1: Code Structure, System Models, and Solution Methods, NUREG/CR-5535, INEL-95/0174, June, 1995.

7-115. EG&G Idaho, Inc., RELAP4/MOD6: A Computer Program for Transient Thermal-Hydraulic Analysis of Nuclear Reactors and Related Systems, Users Manual, CDAP-TR-003, May 1978.

7-116. W. Kastner and G. J. Seeberger, "Pump Behavior and its Impact on a Loss-of-Coolant Accident in a Pressurized Water Reactor," Nuclear Technology, Volume 60, February 1983, pp. 268-277.

7-117. EMF-CC-039(P), Revision 4, Supplement 1, ICECON Code Users
        Manual: A Computer Program Used to Calculate Containment Back
        Pressure for LOCA Analysis (Including Ice Condenser Plants), AREVA
        NP Inc.

7-118. J. A. Trapp and V. H. Ransom, "A Choked-Flow Calculation Criterion
        for Nonhomogeneous, Nonequilibrium Two-Phase Flows,"
        International Journal of Multiphase Flow, Volume 8, pp. 669-681,
        1992.

7-119. P. R. Garabedian, Partial Differential Equations, John Wiley and Sons,
        New York, 1964.

7-120. G. B. Whitham, Linear and Nonlinear Waves, John Wiley and Sons,
        New York, 1974.

7-121. A. H. Shapiro, The Dynamics and Thermodynamics of Compressible
        Fluid Flow, II, Ronald, New York, 1954.

7-122. D. A. Drew, L. Y. Cheng, and R. T. Lahey, Jr., "The Analysis of Virtual
        Mass Effects in Two-Phase Flow," International Journal of Multiphase
        Flow, Volume 5, pp. 233-242, 1979.

7-123. P. S. Anderson, P. Astrop, L. Eget, and O. Rathman, "Numerical
        Experience with the Two-Fluid Model RISQUE," Proceedings from
        Topical Meeting on Thermal Reactor Safety, Sun Valley, ID, July 31-
        August 4, 1997.

7-124. D. Gidaspow (Chairman), "Modeling of Two-Phase Flow,"
        Proceedings of Round Table Discussion RT-1-2 at the 5th
        International Heat Transfer Conference, Tokyo, Japan, September 3-
        7, 1974: also in ASME Journal of Heat Transfer, Volume 3, 1974.

7-125. J. D. Ramshaw and J. A. Trapp, "Characteristics, Stability, and Short-
        Wavelength Phenomena in Two-Phase Flow Equation Systems,"
        Nuclear Science and Engineering, Volume 66, pp. 93-102, 1978.

AREVA Inc.

EMF-2103NP
Revision 3

Realistic Large Break LOCA Methodology for Pressurized Water Reactors
Topical Report

Page 7-226

7-126. N. Zuber, "On the Dispersed Two-Phase Flow in the Laminar Flow Regime," Chemical Engineering Science, Volume 19, pp.897-917, 1964.

7-127. K. E. Carlson et al., RELAP5/MOD3 Code Manual Volume IV: Models and Correlations (Draft), NUREG/CR-5535, June 1990.

7-128. V. H. Ransom et al., RELAP5/MOD2 Code Manual Volume I: Code Structure, Systems Models, and Solution Methods, NUREG/CR-4312, EGG-2396, Revision 1, March 1987.

7-129. M. D. Alamgir and J. H. Lienhard, "Correlation of Pressure Undershoot During Hot Water Depressurization," ASME Journal of Heat Transfer, Volume 103, pp. 52-73, 1981.

7-130. N. Abuaf, O. C. Jones, Jr., and B. J. C. Wu, Critical Flashing Flow in Nozzles with Subcooled Inlet Conditions, BNL-NUREG-27512, 1980.

7-131. XN-NF-82-49(P)(A), Revision 1, Supplement 1, Exxon Nuclear Company Evaluation Model Revised EXEM PWR Small Break Model, Siemens Power Corporation, October 1994.

7-132. J. K. Vennard, Elementary Fluid Mechanics, 4th edition, John Wiley and Sons, New York, 1965.

7-133. E. Janssen and J. A. Kervinen, Two-Phase Pressure Drop Across Contractions and Expansions: Water-Steam Mixtures at 600 to 1400 PSIA, GEAP-4622, General Electric Company, AEC Research and Development Report, June 1964.

7-134. V. Ransom et al., RELAP5/MOD2 Code Manual, Volume 3: Developmental Assessment Problems, EGG-TFM-7952, December 1987.

7-135. J. A. Trapp and V. H. Ransom, RELAP5 Hydrodynamic Model Progress Summary – Abrupt Area Changes and Parallel Branching, PG-R-77-92, November 1977.

7-136. J. G. Collier, "Advanced Study Institute on Two-Phase Flows and Heat Transfer," ASI Proceedings, Istanbul, Turkey, August 1976.

7-137. M. M. El-Wakil, Nuclear Heat Transport, International Textbook Company, Scranton, PA 1971.

7-138. P. A. Lottes, "Expansion Losses in Two-Phase Flows," Nuclear Science and Energy, Volume 9, pp. 26-31, 1961.

7-139. G. B. Wallis, One-Dimensional Two-Phase Flow, McGraw-Hill, New York, 1969.

7-140. S. S. Kutateladze, Heat Transfer in Condensation and Boiling, USAEC Report, AEC-tr-3770, 1952.

7-141. XN-NF-82-49 (P)(A), Revision 1, Exxon Nuclear Company Evaluation Model EXEM PWR Small Break Model, Exxon Nuclear Company, April 1989.

7-142. D. D. Taylor et al., TRAC-BD1/MOD1: An Advanced Best Estimate Computer Program for Boiling Water Reactor Transient Analysis, Volume 1: Model Description, NUREG/CR-3633, EGG-2294, April 1984.

7-143. S. G. Bankoff, R. S. Tankin, M. C. Yuen, and C. L. Hsieh, "Countercurrent Flow of Air/Water and Steam/Water Through a Horizontal Perforated Plate," International Journal of Heat and Mass Transfer, Volume 24, pp. 1381-1395, 1981.

7-144. D. R. Liles et al., NUREG/CR-5069, LA-11208-MS, TRAC-PF1/MOD1 Correlations and Models, December 1988.

7-145. C. L. Tien, K. S. Chung, and C. P. Liu, Flooding in Two-Phase Countercurrent Flows, EPRI NP-1283, December 1979.

7-146. C. J. Crowley et al., Downcomer Effects in a 1/15 Scale PWR
        Geometry - Experimental Data Report, Creare, NUREG-0281, May
        1977; 1/5 Scale Countercurrent Flow Data Presentation and
        Discussion, Creare, NUREG/CR-2106, November 1981.

7-147. R. A. Cudnik et al., Topical Report on Penetration Behavior in a 1/15
        Scale Model of a Four-Loop Pressurized Water Reactor, Battelle
        Columbus Laboratories, BMI-NUREG-1973, June 1977; W. A.
        Carbiener et al., Steam-Water Mixing and System Hydrodynamics
        Program, Quarterly Progress Report, Battelle Columbus Laboratories,
        BMI-NUREG-1972, May 1977.

7-148. MPR Associates, Inc., Summary of Results from UPTF Downcomer
        Separate Effects Tests, Comparison to Previous Scaled Tests, and
        Application to U.S. Pressurized Water Reactors, MPR-1163, July
        1990.

7-149. 2D/3D Program Upper Plenum Test Facility, UPTF Test No. 6
        Downcomer Countercurrent Flow Test, Quick Look Report, U9
        316/89/2, Siemens AG, March 1989; UPTF Test No. 7 Downcomer
        Countercurrent Flow Test, Quick Look Report, E314/90/003, Siemens
        AG, March 1990.

7-150. H. Glaeser, "Analysis of Downcomer and Tie Plate Countercurrent
        Flow in The Upper Plenum Test Facility (UPTF)," Proceedings of 4th
        International Topical Meeting on Reactor Thermal Hydraulics, Volume
        1, pp. 75-81, October 1989.

7-151. EMF-2102(P) Revision 0, S-RELAP5: Code Verification and
        Validation, Section 3.5, Framatome ANP, Inc., August 2001.

7-152. V. H. Ransom et al., RELAP5/MOD2 Code Manual, Volume 1: Code
        Structure, Systems Models, and Solution Methods, NUREG/CR-4312,
        EGG-2396, Revision 1, March 1987.

AREVA Inc.

EMF-2103NP
Revision 3

Realistic Large Break LOCA Methodology for Pressurized Water Reactors
Topical Report

Page 7-229

7-153.   F. W. Dittus and L. M. K. Boelter, "Heat Transfer in Automobile Radiators of the Tubular Type," Publications in Engineering, Volume 2, pp. 443-461, University of California, Berkeley, 1930.

7-154.   W. H. McAdams, Heat Transmission, 3rd edition, McGraw-Hill, New York, 1954.

7-155.   M. J. Thurgood et al., COBRA/TRAC-A Thermal-Hydraulics Code for Transient Analysis of Nuclear Reactor Vessels and Primary Coolant Systems, Volume 1, Equations and Constitutive Models, NUREG/CR-3046 PNL-4385, March 1983.

7-156.   E. M. Sparrow, A. L. Loeffler, and H. A. Hubbard, "Heat Transfer to Longitudinal Laminar Flow Between Cylinders," Journal of Heat Transfer Volume 83, 415, 1961.

7-157.   D. R. Liles et al., TRAC-PF1/MOD1 Correlations and Models, NUREG/CR-5069, LA-11208-MS, December 1988.

7-158.   A. E. Bergles and W. M. Rohsenow, "The Determination of Forced-Convection Surface-Boiling Heat Transfer," Journal of Heat Transfer, Transactions of ASME, Volume 86, p. 365, 1964.

7-159.   P. Saha and N. Zuber, "Point of Net Vapor Generation and Vapor Void Fraction in Subcooled Boiling," Proceedings of 5th International Heat Transfer Conference, Volume IV, pp.175-179, 1974.

7-160.   J. C. Chen, "A Correlation for Boiling Heat Transfer to Saturated Fluids in Convective Flow," Process Design and Development, Volume 5, pp. 322-327, 1966.

7-161.   H. K. Forster and N. Zuber, "Bubble Dynamics and Boiling Heat Transfer," American Institute of Chemical Engineering Journal, Volume 1, pp. 532-535, 1955.

7-162. R. Viskanta and A. K. Mohanty, TMI-2 Accident: Postulated Heat Transfer Mechanisms and Available Data Base, NUREG/CR-2121, ANL-81-26, April 1981.

7-163. F. D. Moles and J. R. G. Shaw, "Boiling Heat Transfer to Subcooled Liquids Under Conditions of Forced Convection," Transactions Institution of Chemical Engineers, Volume 50, pp. 76-84, 1972.

7-164. R. T. Lahey, Jr., "A Mechanistic Subcooled Boiling Model," Proceedings of 6th International Heat Transfer Conference, Volume 1, pp. 293-297, 1978.

7-165. Z. Rouhani, Void Measurements in the Region of Subcooled and Low Quality Boiling, Part 2, AE-239 (1966).

7-166. Biasi et al., "Studies on Burnout Part 3 - A New Correlation for Round Ducts and Uniform Heating and Its Comparison with World Data," Energia Nucleare, Volume 14, pp. 530-536, 1967.

7-167. P. Griffith, J. F. Pearson, and R. J. Lepkowski, "Critical Heat Flux During a Loss-of Coolant Accident," Nuclear Safety Volume 18, pp. 298-309, 1977.

7-168. J. G. Collier, Convective Boiling and Condensation, 2nd edition, McGraw-Hill, New York, 1981.

7-169. N. Zuber, M. Tribus, and J. W. Westwater, "Hydrodynamic Crisis in Pool Boiling of Saturated and Subcooled Liquid," 2nd International Heat Transfer Conference, Denver, Colorado, 1961.

7-170. R. A. Dimenna et al., RELAP5/MOD2 Models and Correlations, NUREG/CR-5194, EGG-2531, August, 1988.

7-171. C. A. Sleicher and M. W. Rouse, "A Convenient Correlation for Heat Transfer to Constant and Variable Property Fluids in Turbulent Pipe Flow," International Journal of Heat and Mass Transfer, Volume 18, pp. 677-683, 1975.

7-172. J. C. Chen, R. K. Sundaram, F. T. Ozkaynak, A Phenomenological Correlation for Post-CHF Heat Transfer, NUREG-0237, June 1977.

7-173. The RELAP5 Development Team, RELAP5/MOD3 Code Manual Volume 4: Models and Correlations, NUREG/CR-5535, INEL-95/0174, Idaho National Engineering Laboratory, August,1995, see footnote on Page 4-80.

7-174. V. H. Sanchez-Espinoza, E. Elias, C. Homann, W. Hering, and D. Struwe, Development and Validation of a Transition Boiling Model for the RELAP5/MOD3 Reflood Simulation, FZKA 5954, Forschungszentrum Karlsruhe, September 1997.

7-175. R. P. Forslund and W. M. Rohsenow, "Dispersed Flow Film Boiling," Journal of Heat Transfer Volume 90 (6), pp. 399-407, 1968.

7-176. L. A. Bromley, "Heat Transfer in Stable Film Boiling," Chemical Engineering Progress Volume 46, pp. 221-227, 1950.

7-177. P. J. Berenson, "Film Boiling Heat Transfer from a Horizontal Surface," Journal of Heat Transfer, pp. 351-358, 1961.

7-178. Y. Y. Hsu and R. W. Graham, Transport Processes in Boiling and Two-Phase Systems, McGraw-Hill, New York, 1976.

7-179. R. W. Shumway, TRAC-PF1 Post-CHF Heat Transfer Coefficient Variation for CSAU, Appendix O to Quantifying Reactor Safety Margins: Application of Code Scaling, Applicability, and Uncertainty Evaluation Methodology to a Large-Break, Loss-of-Coolant Accident, NUREG/CR-5249, EGG-2552, December 1989.

7-180. G. Th. Analytis, M. Richner, and S. N. Aksan, Assessment of Interfacial Shear and Wall Heat Transfer of RELAP5/MOD2/36.02 During Reflooding, EIR-Bericht Nr. 624, May 1987.

7-181. Y. Murao and J. Sugimoto, "Correlation of Heat Transfer Coefficient for Saturated Film Boiling During Reflood Phase Prior to Quenching," Journal of Nuclear Science and Technology, Volume 18(4), pp. 275-284, 1981.

7-182. M. S. Dougall and W. M. Rohsenow, Film Boiling on the Inside of Vertical Tubes with Upward Flow of a Fluid at Low Qualities, MIT-ME 9079-26, 1963.

7-183. Wong, S. and Hochreiter, L. E., "Analysis of the FLECHT-SEASET Unblocked Bundle Steam Cooling and Boil-off Tests", January 1981, NUREG/CR-1533.

7-184. M. Drucker and V. K. Dhir, "Studies of Single and Two Phase Heat Transfer in a Blocked Four Rod Bundle," EPRI-NP 3485, Electric Power Research Institute, 1984.

7-185. S. C. Yao, L. E. Hochreiter, and W. J. Leech, Heat Transfer Augmentation in Rod Bundles Near Grid Spacers, J. Heat Transfer, 104, pp. 76-81, February 1982.

7-186. M. J. Meholic, L. E. Hochreiter, J. H. Mahaffy, and J. Spring, "Increased Convective Heat Transfer Caused by Spacer Grids in Laminar High Void Fraction Flows," 2008 ANS Winter Meeting, Reno, NV.

7-187. K. H. Sun, J. M. Gonzales-Santalo, and C. L. Tien, "Calculations of Combined Radiation and Convection Heat Transfer in Rod Bundles Under Emergency Cooling Conditions," Journal of Heat Transfer, pp. 414-420, 1976.

7-188. FLECHT SEASET Program, PWR FLECHT SEASET Unblocked Bundle, Forced and Gravity Reflood Task Data Evaluation and Analysis Report, NUREG/CR-2256, EPRI NP-2013, WCAP-8991, November 1981.

AREVA Inc.
EMF-2103NP
Revision 3
Realistic Large Break LOCA Methodology for Pressurized Water Reactors
Topical Report
Page 7-233

7-189. D.K. Edwards, "On the Use of Total Radiation Properties of Gases," ANL/RAS 75-12, April 1975.

7-189a. S.S. Penner, "Quantitative Molecular Spectroscopy and Gas Emissivities," Addison-Wesley Publishing Company Inc., Reading, Massachusetts, USA, 1959.

7-190. E. F. Carpenter and A. P. Colburn, "The Effect of Vapor Velocity on Condensation Inside Tubes," Proceedings of General Discussion on Heat Transfer, Institute Mechanical Engineering/American Society of Mechanical Engineers, pp. 20-26, 1951.

7-191. RELAP5/MOD3.3 Code Manual Volume 1: Code Structure, System Models, and Solution Methods, NUREG/CR-5535/Rev 1-Vol 1, December, 2001.

7-192. L. Arrieta and G. Yadigaroglu, Analytic Model for Bottom Reflooding and Heat Transfer in Light Water Reactors, EPRI Report NP-756, 1978.

7-193. D. C. Groeneveld, S. C. Cheng, and T. Doan, "1986 AECL-UO Critical Heat Flux Lookup Table," Heat Transfer Engineering, Volume 7, pp. 46-62, 1986.

7-194. A. W. Bennett, G. F. Hewitt, H. A. Kearsey, and R. K. F. Keeys, Heat Transfer to Steam-Water Mixtures Flowing in Uniformly Heated Tubes in Which the Critical Heat Flux Has Been Exceeded, UKAEA Research Group Report, AERE-R 5373, October 1967.

7-195. EMF-2102(P) Revision 0, S-RELAP5: Code Verification and Validation, Framatome ANP, Inc., August 2001.

7-196. EMF-92-139(P), Volume 3, Supplement 3, Realistic LOCA ECCS Evaluation Model Assessment for PWR Large Break Analysis Assessment for LOFT Test L2-5, Siemens Power Corporation, June 1993.

7-197. EMF-92-139(P), Volume 3, Supplement 4, Realistic LOCA ECCS
        Evaluation Model Assessment for PWR Large Break Analysis
        Assessment for LOFT Test L2-6, Siemens Power Corporation, June
        1993.

7-198. EMF-92-139(P), Volume 3, Supplement 6, Realistic LOCA ECCS
        Evaluation Model Assessment for PWR Large Break Analysis
        Westinghouse 3-Loop PWR Sample Problem, Siemens Power
        Corporation, May 1993.

7-199. EMF-92-139(P), Volume 3, Supplement 7, Realistic LOCA ECCS
        Evaluation Model Assessment for PWR Large Break Analysis
        Westinghouse 4-Loop PWR Example Problem, Siemens Power
        Corporation, June 1993.

7-200. J. C. M. Leung, "Transient Critical Heat Flux and Blowdown Heat
        Transfer Studies," Ph.D. dissertation, Northwestern University, June
        1980.

7-201. S. Wang, Y. K. Kao, and J. Weisman, "Studies of Transition Boiling
        Heat Transfer with Saturated Water at 1-4 Bar," Nuclear Engineering
        Design, Volume 70, pp.223-243, 1982.

7-202. J. Zhang, S. M. Bajorek, R. M. Kemper, and L. E. Hochreiter,
        "WCOBRA/TRAC Analysis of ORNL High Flow Rod Bundle Film
        Boiling Tests," 1997 National Heat Transfer Conference, August 10-
        12, Baltimore, MD.

7-202a. J. P. Holman, "Heat Transfer," 5th edition, McGraw-Hill, New York,
        1981.

7.7   *Hydrodynamic Process Models*

Certain models in RELAP5 have been developed to simulate special hydrodynamic processes. These models are presented in the following subsections.

7.7.1   Choked Flow

The choked-flow model is used to predict if the flow is choked at a break or nozzle and, if it is, to establish the discharge boundary condition. Generally, the flow at the break or nozzle is choked until the system pressure nears the containment pressure. In addition, the choked-flow model can be used to predict existence of and calculate choked flow at internal points in the system.

7.7.1.1   Choked Flow Theory

The RELAP5 choked flow model is based on the choking theory developed by Ransom and Trapp (Reference 7-118). Choking is defined as the condition wherein the mass flow rate becomes independent of the downstream conditions (that point at which further reduction in the downstream pressure does not change the mass flow rate). The fundamental reason that choking occurs is that acoustic signals can no longer propagate upstream. This occurs when the fluid velocity equals or exceeds the propagation velocity. The choked-flow model is based on a definition that is established by a characteristic analysis using time-dependent differential equations.

Consider a system of n first-order, quasi-linear, partial differential equations of the form

$$A(U) \frac{\partial U}{\partial t} + B(U) \frac{\partial U}{\partial x} + C(U) = 0 \qquad (7.569)$$

The characteristic directions (or characteristic velocities) of the system are defined (References 7-119 and 7-120) as the roots[4], λ_i (i ≤ n), of the characteristic polynomial

$$(A\lambda - B) = 0 \qquad (7.570)$$

---

[4]   The number n is the number of differential equations comprising the system defined by Equation (7.569), and the number i designates any of the corresponding n roots.

The real part of any root, λ_i, gives the velocity of signal propagation along the corresponding characteristic path in the space/time plane. The imaginary part of any complex root, λ_i, gives the rate of growth or decay of the signal propagating along the respective path. For a hyperbolic system in which all the roots of Equation (7.570) are real and nonzero, the number of boundary conditions required at any boundary point equals the number of characteristic lines entering the solution region as time increases. If we consider the system (Equation (7.569)) for a particular region $0 \le x \le L$ and examine the boundary conditions at $x = L$, as long as any λ_i is less than zero, we must supply some boundary information to obtain the solution. If all λ_i are greater than or equal to zero, no boundary conditions are needed at $x = L$; and the interior solution is unaffected by conditions beyond this boundary.

A choked condition exists when no information can propagate into the solution region from the exterior. Such a condition exists at the boundary point, $x = L$, when

$$\lambda_j = 0 \qquad \text{for some } j \le n$$

$$\tag{7.571}$$

$$\lambda_i \ge 0 \qquad \text{for all } i \ne j$$

These are the mathematical conditions satisfied by the equations of motion for a flowing fluid when reduction in downstream pressure ceases to result in increasing flow rate. It is well known (Reference 7-121) that the choked condition for single-phase flow occurs when the fluid velocity just equals the local sound speed. For this case, one of the λ_is is just equal to zero. For the two-phase case, it is possible for all λ_is to be greater than zero under special conditions which can exist during discharge of a subcooled liquid.

Extensive investigation was carried out to determine a two-phase choked-flow criterion under two assumed conditions[5]: (a) thermal equilibrium between phases, and (b) adiabatic phases without phase change (frozen). The frozen assumption was in poor agreement with data compared to the thermal equilibrium assumption. Therefore, the

---

[5] The hydrodynamic model is not based on either of these assumptions. However, the purpose of this analysis is simply to establish a criterion for choked flow; thus, there is no conflict with the basic hydrodynamic model.

thermal equilibrium assumption with slip is used as the basis for the RELAP5 choked-flow criterion when two-phase conditions exist.

7.7.1.1.1   Two-Phase Flow Choking

The two-fluid model for the conditions of thermal equilibrium (equilibrium interphase mass transfer) is described by the overall mass continuity equation, two-phasic momentum equations, and the mixture entropy equation. This system of equations is

$$\frac{\partial\left(\alpha_g\rho_g + \alpha_f\rho_f\right)}{\partial t} + \frac{\partial\left(\alpha_g\rho_g v_g + \alpha_f\rho_f v_f\right)}{\partial x} = 0 \tag{7.572}$$

$$\alpha_g\rho_g\left[\frac{\partial v_g}{\partial t} + v_g\frac{\partial v_g}{\partial x}\right] + \alpha_g\frac{\partial P}{\partial x} + C\alpha_g\alpha_f\rho\left[\frac{\partial v_g}{\partial t} + v_f\frac{\partial v_g}{\partial x} - \frac{\partial v_f}{\partial t} - v_g\frac{\partial v_f}{\partial x}\right] = 0 \tag{7.573}$$

$$\alpha_f\rho_f\left[\frac{\partial v_f}{\partial t} + v_f\frac{\partial v_f}{\partial x}\right] + \alpha_f\frac{\partial P}{\partial x} + C\alpha_f\alpha_g\rho\left[\frac{\partial v_f}{\partial t} + v_g\frac{\partial v_f}{\partial x} - \frac{\partial v_g}{\partial t} - v_f\frac{\partial v_g}{\partial x}\right] = 0 \tag{7.574}$$

$$\frac{\partial\left(\alpha_g\rho_g S_g + \alpha_f\rho_f S_f\right)}{\partial t} + \frac{\partial\left(\alpha_g\rho_g S_g v_g + \alpha_f\rho_f S_f v_f\right)}{\partial x} = 0 \tag{7.575}$$

The momentum equations include the interphase force terms due to relative acceleration (Reference 7-122). These force terms have a significant effect on wave propagation velocity and consequently on the choked flow velocity. The particular form chosen is frame invariant and symmetrical; and the coefficient of virtual mass, $C\alpha_g\alpha_f\rho$, is chosen to ensure a smooth transition between pure vapor and pure liquid. For a dispersed flow, the constant, C, has a theoretical value of 0.5; whereas, for a separated flow, the value may approach zero. The energy equation is written in terms of mixture entropy, which is constant for adiabatic flow. (The energy dissipation associated with interphase mass transfer and relative phase acceleration is neglected.)

The nondifferential source terms, C(U), in Equation (7.569) do not enter into the characteristic analysis or affect the propagation velocities. For this reason, the source terms associated with wall friction, interphase drag, and heat transfer are omitted for brevity in Equations (7.572) through (7.575).

AREVA Inc.

Realistic Large Break LOCA Methodology for Pressurized Water Reactors
Topical Report

EMF-2103NP
Revision 3
Page 7-238

In the thermal equilibrium case, ρ_g, ρ_f, S_g, and S_f are known functions of the pressure only (the vapor and liquid values along the saturation curve). The derivatives of these variables are designated by an asterisk as follows

$$\rho_f^* = \frac{d\rho_f^S}{dP}, \quad \rho_g^* = \frac{d\rho_g^S}{dP} \tag{7.576}$$

$$S_f^* = \frac{dS_f^S}{dP}, \quad S_g^* = \frac{dS_g^S}{dP} \tag{7.577}$$

The system of governing equations (Equations (7.572) through (7.575)) can be written in terms of the four dependent variables, α_g, P, v_g, and v_f, by application of the chain rule and the property derivatives (Equations (7.576) and (7.577)). Thus, the system of equations can be written in the form of Equation (7.569) where the A and B are fourth-order square coefficient matrices.

The characteristic polynomial that results is fourth-order in λ, and factorization can only be carried out approximately to obtain the roots for λ and establish the choking criterion. The first two roots are

$$\lambda_{1,2} = \frac{\left(\left\{ \alpha_f \rho_g + \frac{\rho C}{2} \pm \left(\left(\frac{\rho C}{2} \right)^2 - \alpha_g \alpha_f \rho_g \rho_f \right)^{1/2} \right\} v_g + \left\{ \alpha_g \rho_f + \frac{\rho C}{2} \mp \left(\left(\frac{\rho C}{2} \right)^2 - \alpha_g \alpha_f \rho_g \rho_f \right)^{1/2} \right\} v_f \right)}{\left(\alpha_f \rho_g + \frac{\rho C}{2} \right) + \left(\alpha_g \rho_f + \frac{\rho C}{2} \right)} \tag{7.578}$$

These two roots are obtained by neglecting the fourth-order factors relative to the second-order factors in $(\lambda - v_g)$ and $(\lambda - v_f)$. There are no first- or third-order factors. Inspection of Equation (7.578) shows that $\lambda_{1,2}$ have values between v_g and v_f; thus, the fourth-order factors in $(\lambda - v_g)$ and $(\lambda - v_f)$ are small (i.e., neglecting these terms is justified). The values for $\lambda_{1,2}$ may be real or complex depending on the sign of the

quantity $\left(\left(\frac{\rho C}{2} \right)^2 - \alpha_g \alpha_f \rho_g \rho_f \right)$.

The remaining two roots are obtained by dividing out the quadratic factor containing $\lambda_{1,2}$, neglecting the remainder, and factoring the remaining quadratic terms.   [

] The remaining roots are

$$\lambda_{3,4} = v + D\left(v_g - v_f\right) \pm a \tag{7.579}$$

where:

$$v = \frac{\left(\alpha_g \rho_g v_g + \alpha_f \rho_f v_f\right)}{\rho} \tag{7.580}$$

$$a = a_{HE} \left\{ \frac{C\rho^2 + \rho\left(\alpha_g \rho_f + \alpha_f \rho_g\right)}{C\rho^2 + \rho_g \rho_f} \right\}^{1/2} \tag{7.581}$$

and

$$D = 0.5\left[\frac{\alpha_g \rho_f - \alpha_f \rho_g}{\rho\,C + \alpha_f \rho_g + \alpha_g \rho_f} + \frac{\rho_g \rho_f\left(\alpha_f \rho_f - \alpha_g \rho_g\right)}{\rho\left(\rho_g \rho_f + C\,\rho^2\right)} - a_{HE}^2\, \frac{\rho\left(\alpha_g \rho_g^2 S_g^* + \alpha_f \rho_f^2 S_f^*\right)}{\rho_g \rho_f\left(S_g - S_f\right)} \right] \tag{7.582}$$

The quantity, a_{HE}, is the homogeneous equilibrium speed of sound. The roots, $\lambda_{3,4}$, have only real values.

The general nature and significance of these roots is revealed by applying the characteristic consideration. The speed of propagation of small disturbances is related to the values of the characteristic roots. In general, the velocity of propagation corresponds to the real part of a root, and the growth or attenuation is associated with the complex part of the root. Choking will occur when the signal, which propagates with the largest velocity relative to the fluid, is just stationary, i.e.,

$$\lambda_j^R = 0 \quad \text{for some } j \le 4 \tag{7.583}$$

and

$$\lambda_i^R \ge 0 \quad \text{for all } i \ne j \tag{7.584}$$

The existence of complex roots for $\lambda_{1,2}$ makes the initial boundary value problem ill-posed. This problem has been discussed by many investigators (References 7-123

and 7-124), and the addition of any small, second-order viscous effects renders the
problem well-posed (References 7-123 and 7-125). The whole phenomenon of systems
with mixed orders of derivatives and a first-order system with the addition of a small,
second-order term has been discussed and analyzed by Whitham (Reference 7-120).
He has shown that the second-order viscous terms give infinite characteristic velocities.
However, very little information is propagated along these characteristic lines; and the
bulk of the information is propagated along characteristic lines defined by the first-order
system. We conclude that the ill-posed nature of Equations (7.572) through (7.575) can
be removed by the addition of small, second-order viscous terms that have little effect
upon the propagation of information. Therefore, the choking criterion for the two-phase
flow system analyzed here is established from Equation (7.583).

The explicit character of the choking criterion for the two-phase flow model defined by
Equations (7.572) through (7.575) is examined. Since the two roots, $\lambda_{1,2}$, are between
the phase velocities, v_f and v_g, the choking criterion is established from the roots, $\lambda_{3,4}$,
and Equation (7.583). The choking criterion is

$$v + D\left(v_g - v_f\right) = \pm a \tag{7.585}$$

The choking criterion can be rewritten in terms of the mass mean and relative Mach
numbers

$$M_v = \frac{v}{a}, \qquad M_r = \frac{\left(v_g - v_f\right)}{a} \tag{7.586}$$

as

$$M_v + D M_r = \pm 1 \tag{7.587}$$

This relation is similar to the choking criterion for single-phase flow where only the mass
average Mach number appears and choking corresponds to a Mach number of unity.

The choking criterion (Equation (7.587)) is a function of the two parameters, D and a. In
Figure 7-16, a is plotted as a function of the void fraction, α_g, for a typical steam/water
system at 7.5 MPa, with C equal to zero (the stratified equilibrium sound speed), C
equal to 0.5 (the typical value for a dispersed flow model), and in the limiting case

AREVA Inc.

EMF-2103NP
Revision 3

Realistic Large Break LOCA Methodology for Pressurized Water Reactors
Topical Report

Page 7-241

where C becomes infinite (homogeneous equilibrium sound speed). From Figure 7-16, it is evident that the virtual mass coefficient has a significant effect upon the choked-flow dynamics in two-phase flow (Reference 7-126).

To establish the actual choked-flow rate for two-phase flow with slip, the relative velocity term in Equation (7.587) must also be considered. The relative Mach number coefficient, D, is shown plotted in Figure 7-17 for values of C equal to 0, 0.5, and infinity. It is evident from these results that the choked-flow velocity can differ appreciably from the mass mean velocity when slip occurs. It is significant that the variation of the choked-flow criterion from the homogeneous result is entirely due to velocity nonequilibrium, since these results have been obtained under the assumption of thermal equilibrium.

Figure 7-16 Equilibrium Speed of Sound as a Function of Void Fraction and Virtual Mass Coefficient
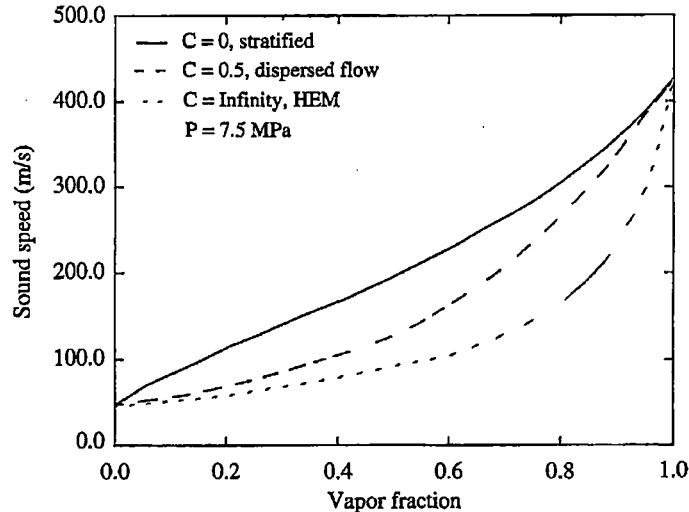
**Figure 7-17 Coefficient of Relative Mach Number for Thermal
Equilibrium Flow as a Function of Void Fraction and
Virtual Mass Coefficient**
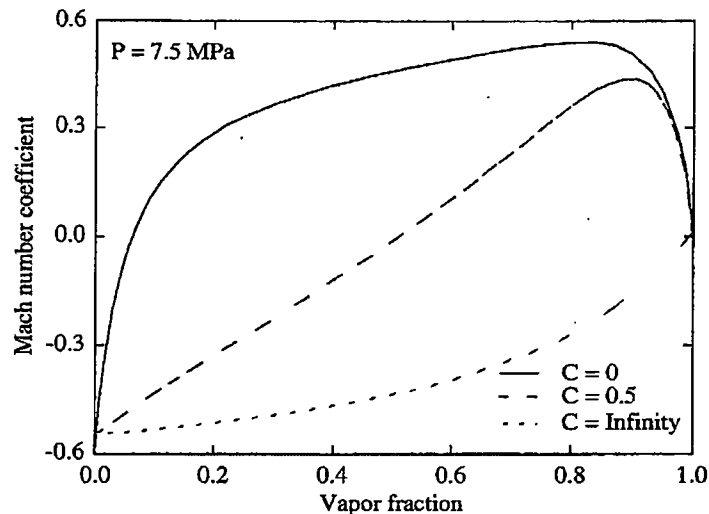
7.7.1.1.2 Subcooled Choking

The previous analysis assumes two-phase conditions exist throughout the break flow process. However, initially and in the early phase of blowdown, the flow approaching the break or break nozzle will be subcooled liquid. Under most conditions of interest in LWR (Light Water Reactor) systems, the fluid undergoes a phase change at the break. The transition from single- to two-phase flow is accompanied by a discontinuous change in the fluid bulk modulus. This is especially true for the liquid-to-liquid/vapor transition. For example, at 600 kPa, the ratio of the single- to two-phase sound speed at the liquid boundary is 339.4. Thus, considerable care must be exercised when analyzing a flow having transitions to or from a pure phase. (A discontinuity is also present at the vapor boundary, but the ratio is only 1.069.)

To understand the physical process that occurs for subcooled upstream conditions, consider the flow through a converging/diverging nozzle connected to an upstream plenum with subcooled water at a high pressure. For a downstream pressure only slightly lower than the upstream pressure, subcooled liquid flow will exist throughout the nozzle. Under these conditions, the flow can be analyzed using Bernoulli's equation,

AREVA Inc.

EMF-2103NP
Revision 3

Realistic Large Break LOCA Methodology for Pressurized Water Reactors
Topical Report

Page 7-243

which predicts a minimum pressure, P_t, at the throat.[6] As the downstream pressure is lowered further, a point is reached where the throat pressure equals the local saturation pressure, P_{sat}. If the downstream pressure is lowered further, vaporization will take place at the throat.[7] When this happens, the fluid sound speed lowers drastically; but continuity considerations dictate that the velocity, v_t, of the two-phase mixture (at the point of minuscule void fraction) just equals the velocity of the subcooled water slightly upstream of the throat. When this occurs, v_t in the subcooled region is less than the water sound speed; but in the two-phase region, v_t can be greater than the two-phase sound speed. Hence, the subcooled water has a Mach number less than 1, $M < 1$, whereas the two-phase mixture at the throat has a Mach number greater than 1. Under these conditions (Mach numbers greater than 1 in the two-phase region), downstream pressure effects are not propagated upstream and the flow is choked. In particular, the supersonic two-phase fluid at the throat must increase in velocity and the pressure must drop as it expands in the diverging section.[8] (Transition back to subsonic flow can occur in the nozzle as a result of a shock wave.) This choked condition is shown as case (a) in Figure 7-18. Contrary to the usual single-phase choked flow in a converging/diverging nozzle, there is no point in the flow field where $M = 1$. This is because in the homogeneous equilibrium model the fluid undergoes a discontinuous change in sound speed from single-phase subcooled conditions to two-phase conditions, although the fluid properties are continuous through the transition point.

When this condition prevails, the flow rate can be established from application of Bernoulli's equation $\left[\frac{1}{2}\rho \left(v_t^2 - v_{up}^2 \right) = P_{up} - P_{sat} \right]$. For further decreases in the downstream pressure, no further increase in upstream fluid velocity will occur as long as the upstream conditions are maintained constant.

---

[6] For all practical cases of choking, the subcooled water can be considered incompressible with infinite sound speed.

[7] An idealized one-dimensional homogeneous equilibrium model is assumed.

[8] In a supersonic flow, a diverging nozzle implies an increase in velocity.

AREVA Inc.

EMF-2103NP
Revision 3

Realistic Large Break LOCA Methodology for Pressurized Water Reactors
Topical Report

Page 7-244

Now consider the process where subcooled choked flow, as described above, initially exists (with a very low downstream pressure) and the upstream pressure is lowered as shown in cases (b) and (c) in Figure 7-18. As the upstream pressure decreases, the pressure at the throat will remain at P_{sat}, and Bernoulli's equation will give a smaller subcooled water velocity (v_t) at the throat. As P_{up} is lowered further, a point is reached where $v_t = a_{HE}$ and M = 1 on the two-phase side of the throat. (The Mach number in the subcooled portion upstream of the throat is much less than 1.) This situation is shown schematically in Figure 7-18 as case (b).

As the upstream pressure is lowered further, the point where the pressure reaches P_{sat} must move upstream of the throat. This is shown as case (c) in Figure 7-18. The subcooled water velocity at the P_{sat} location is smaller than the two-phase sound speed, and the flow is subsonic. In the two-phase region between the point at which P_{sat} is reached and the throat, the Mach number is less than 1 but increases to M = 1 at the throat; that is, the two-phase sonic velocity is reached at the throat (as in the case of choked flow having a continuous variation of sound speed with pressure). As P_{up} is lowered still further, the P_{sat} point moves upstream until the flow becomes completely two-phase.

Figure 7-18 Subcooled Choking Process

$$v_t = \left[v_{up}^2 + 2\left(P_{up(a)} - P_{sat}\right)/\rho \right]^{1/2} \qquad v_t = \left[v_{up}^2 + 2\left(P_{up(b)} - P_{sat}\right)/\rho \right]^{1/2} = a_{HE} \qquad v_t = a_{HE} > \left[v_{up}^2 + 2\left(P_{up(c)} - P_{sat}\right)/\rho \right]^{1/2}$$
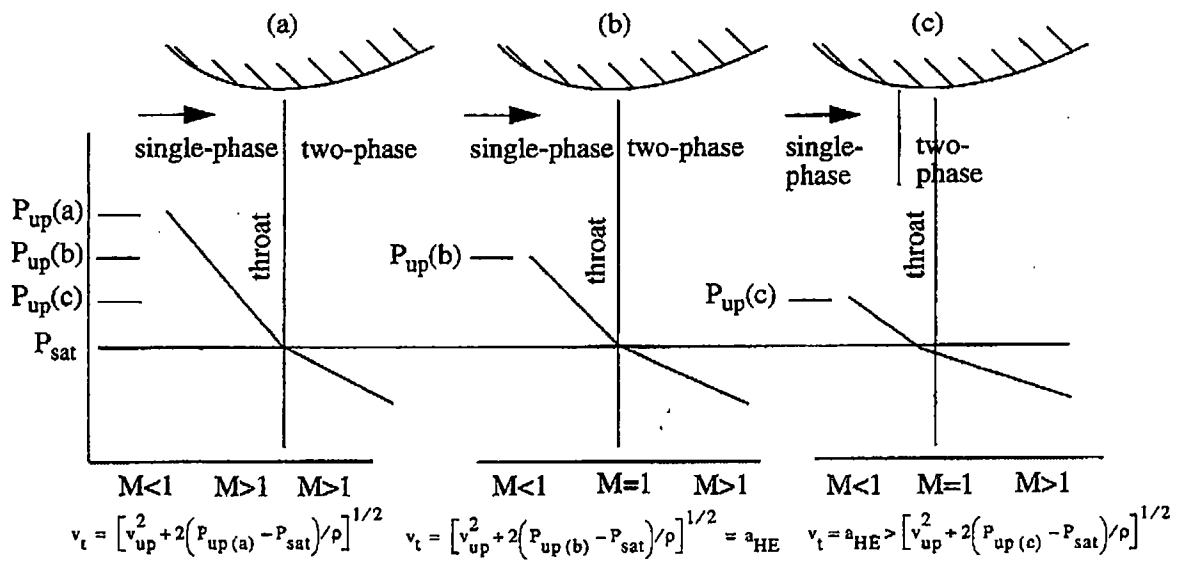
7.7.1.2   Implementation of Choked Flow Model

AREVA Inc.

EMF-2103NP
Revision 3

Realistic Large Break LOCA Methodology for Pressurized Water Reactors
Topical Report

Page 7-246

7.7.1.2.1 Subcooled Choking Computation

AREVA Inc.

EMF-2103NP
Revision 3

Realistic Large Break LOCA Methodology for Pressurized Water Reactors
Topical Report

Page 7-247
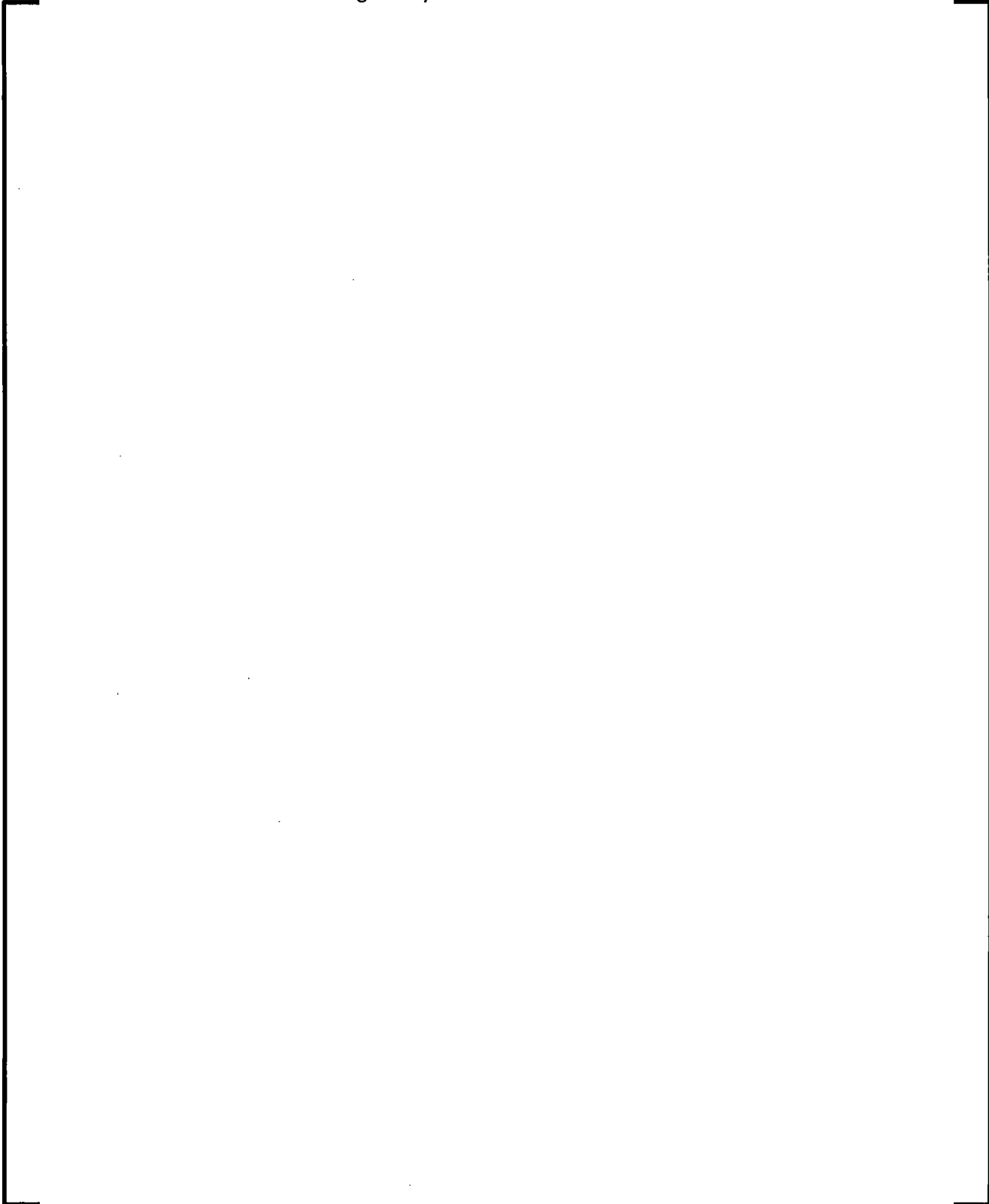
7.7.1.2.2   Two-Phase Choking Computation

AREVA Inc.

Realistic Large Break LOCA Methodology for Pressurized Water Reactors
Topical Report

EMF-2103NP
Revision 3

Page 7-248

AREVA Inc.

Realistic Large Break LOCA Methodology for Pressurized Water Reactors
Topical Report

EMF-2103NP
Revision 3

Page 7-249

AREVA Inc.

EMF-2103NP
Revision 3

Realistic Large Break LOCA Methodology for Pressurized Water Reactors
Topical Report

Page 7-251

AREVA Inc.

Realistic Large Break LOCA Methodology for Pressurized Water Reactors
Topical Report

EMF-2103NP
Revision 3

Page 7-252

7.7.1.2.3   Numerical Implementation

AREVA Inc.

EMF-2103NP
Revision 3

Realistic Large Break LOCA Methodology for Pressurized Water Reactors
Topical Report

Page 7-253

AREVA Inc.

Realistic Large Break LOCA Methodology for Pressurized Water Reactors
Topical Report

EMF-2103NP
Revision 3

Page 7-254

AREVA Inc.

Realistic Large Break LOCA Methodology for Pressurized Water Reactors
Topical Report

EMF-2103NP
Revision 3

Page 7-255

Summarizing, the main steps in the computation of critical mass flow rate are: (1) determining the thermodynamic state at the throat, (2) computing the critical flow criterion, (3) solving the momentum equations for choked flow if the choking criterion is satisfied, and (4) applying special treatments for the subcooled to two-phase transition. As the iteration solution method is used in calculating the state properties at the throat and the choking criterion, it is suggested that for computational efficiency the choking option should be selected only at those junctions where choking is expected to occur.

7.7.2   Abrupt Area Change

The general reactor system contains piping networks with many sudden area changes and orifices. The basic hydrodynamic model is formulated for slowly varying (continuous) flow area variations; therefore, a special model is required for handling the flow through sudden area changes and orifices.

The abrupt area change model, discussed here, is based on the Bourda-Carnot (Reference 7-132) formulation for a sudden enlargement and standard pipe flow relations, including the vena-contracta effect for a sudden contraction or an orifice or both. It does not include the case where an enlargement, a contraction, or an orifice is rounded or beveled. Quasi-steady continuity and momentum balances are employed at points of abrupt area change. The numerical implementation of these balances is such that hydrodynamic losses are independent of upstream and downstream nodalization. In effect, the quasi-steady balances are employed as jump conditions that couple fluid components having abrupt changes in cross-sectional area. This coupling process is achieved without change to the basic linear semi-implicit and nearly-implicit numerical time-advancement schemes.

7.7.2.1 Abrupt Area Change Modeling Assumptions

The basic assumption used for the transient calculation of two-phase flow in flow passages with points of abrupt area change is: the transient flow process can be approximated as a quasi-steady flow process that is instantaneously satisfied by the upstream and downstream conditions (that is, transient inertia, mass, and energy

storage are neglected at abrupt area changes). However, the upstream and downstream flows are treated as fully transient flows.

There are several bases for the above assumption. A primary consideration is that available loss correlations are based on data taken during steady flow processes; however, transient investigations (Reference 7-132) have verified the adequacy of the quasi-steady assumption. The volume of fluid and associated mass, energy, and inertia at points of abrupt area change is generally small compared with the volume of upstream and downstream fluid components. The transient mass, energy, and inertia effects are approximated by lumping them into upstream and downstream flow volumes. Finally, the quasi-steady approach is consistent with modeling of other important phenomena in transient codes (that is, heat transfer, pumps, and valves).

7.7.2.2   Review of Single-Phase Abrupt Area Change Models

The modeling techniques used for dynamic pressure losses associated with abrupt area change in single-phase flow are reviewed briefly before discussing the extension of these methods to two-phase flows. In a steady incompressible flow, losses at an area change are modeled by the inclusion of an appropriate dynamic head loss term, h_L, in the one-dimensional modified Bernoulli equation

$$\left(\frac{v^2}{2}+\frac{P}{\rho}\right)_1 = \left(\frac{v^2}{2}+\frac{P}{\rho}\right)_2 + h_L$$

(7.622)

The particular form of the dynamic head loss is obtained by employing the Bourda-Carnot (Reference 7-132) assumption for calculating losses associated with the expansion part of the flow process at points of abrupt area change.

7.7.2.2.1   Expansion

Consider a steady and incompressible flow undergoing a sudden increase in cross-sectional area (expansion) as shown in Figure 7-19. Here the flow is assumed to be from left to right with the upstream conditions denoted by the subscript 1 and the downstream conditions by 2. Here the upstream and downstream conditions are assumed to be far enough remote from the point of area change that flow is one-

dimensional; i.e., none of the two-dimensional effects of the abrupt area change exist. These locations can range from several diameters upstream to as many as 30 diameters downstream. However, for purposes of modeling the overall dynamic pressure loss, the entire process is assumed to occur as a discontinuous jump in flow condition at the point of abrupt area change. In this context, Stations 1 and 2 refer to locations immediately upstream and downstream of the abrupt area change.

The dynamic head loss for the abrupt expansion shown in Figure 7-19 can be obtained using the Bourda-Carnot (Reference 7-132) assumption; i.e., the pressure acting on the washer shaped area, $A_2 - A_1$, is the upstream pressure, P_1. When this assumption is employed in an overall momentum balance, the head loss is

$$h_L = \frac{1}{2}\left(1 - \frac{A_2}{A_1}\right)^2 v_2^2$$

(7.623)

By defining $e = \dfrac{A_2}{A_1}$ as the expansion area ratio, the loss in the dynamic pressure associated with the area of change is related to the head by

$$\Delta P = \rho h_L = \frac{1}{2}\rho\left(1 - \varepsilon\right)^2 v_2^2$$

(7.624)

Figure 7-19 Abrupt Expansion
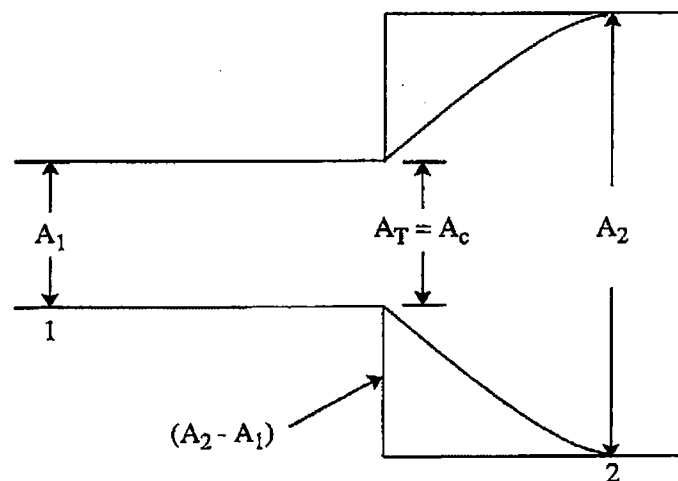
7.7.2.2.2 Contraction

The flow process at a point of abrupt reduction in flow area (contraction) is idealized in much the same manner as for the expansion, except that an additional process must be considered. The flow continues to contract beyond the point of abrupt area reduction and forms a vena contracta, as depicted in Figure 7-21. The point of vena-contracta is designated by c. The far-upstream and far-downstream conditions are designated by 1 and 2, respectively.

Consider a sudden contraction in a steady incompressible flow. The loss in dynamic pressure from the upstream station to the vena-contracta is usually neglected. Measurements indicate that the contracting flow experiences a loss no larger than $\Delta P_L \sim 0.05 \left(\frac{1}{2} \rho v_c^2 \right)$ (Reference 7-132), where v_c is the velocity at the contracta. The dynamic pressure loss associated with the new expansion from the area at vena-contracta to the downstream area is modeled using the Bourda-Carnot assumption with the condition at vena-contracta as the upstream condition, that is

$$\Delta P_L = \frac{1}{2} \rho \left(1 - \frac{A_c}{A_2} \right)^2 v_c^2 \qquad (7.625)$$

where from continuity considerations for incompressible flow,

$$v_c = \frac{A_2 v_2}{A_c} \qquad (7.626)$$

The contraction ratio $\frac{A_c}{A_2}$ is an empirical function of $\frac{A_2}{A_1}$. The function is

$\frac{A_c}{A_2} = 0.62 + 0.38 \left(\frac{A_2}{A_1} \right)^3$ and it is an approximation to the table in Reference 7-132.

Figure 7-20 shows the comparison between the table and the function. The comparison is quite good. Combining Equations (7.625) and (7.626) leads to

$$\Delta P_L = \frac{1}{2} \rho \left(1 - \frac{A_2}{A_c} \right)^2 v_2^2 \qquad (7.627)$$

AREVA Inc.

Realistic Large Break LOCA Methodology for Pressurized Water Reactors
Topical Report

EMF-2103NP
Revision 3

Page 7-260

as the dynamic pressure loss for a contraction (Reference 7-132).

Figure 7-20 Comparison of RELAP5 Function Equation and Table for Contraction Ratio
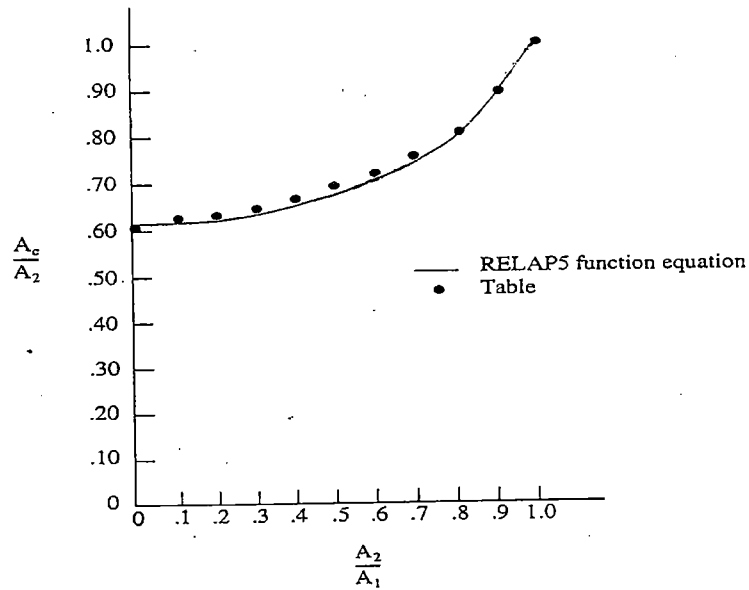
Figure 7-21 Abrupt Contraction

AREVA Inc.

EMF-2103NP
Revision 3

Realistic Large Break LOCA Methodology for Pressurized Water Reactors
Topical Report

Page 7-261
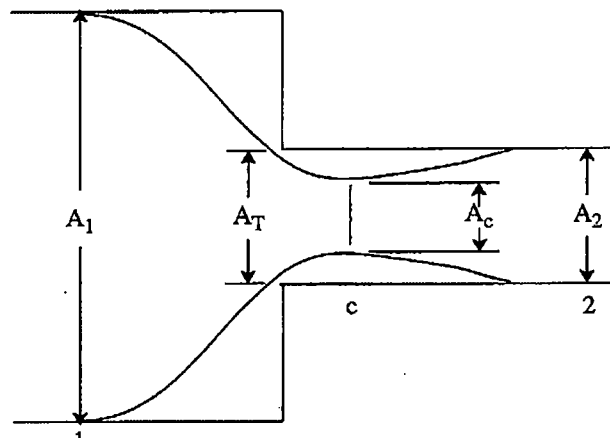
7.7.2.2.3 Abrupt Area Change With an Orifice

The most general case of an abrupt area change is a contraction with an orifice at the point of contraction. Such a configuration is shown in Figure 7-22. In this case, an additional flow area, the orifice flow area, must be specified. Conditions at the orifice throat station will be designated by a subscript T. Three area ratios are used throughout this development. The first is the contraction area ratio at the vena contracta relative to the minimum physical area, $\varepsilon_c = \dfrac{A_c}{A_T}$. The second is the ratio of the minimum physical area to the upstream flow area, $\varepsilon_T = \dfrac{A_T}{A_1}$. The third is the ratio of the downstream to upstream area, $\varepsilon = \dfrac{A_2}{A_1}$.

Figure 7-22 Orifice at Abrupt Area Change
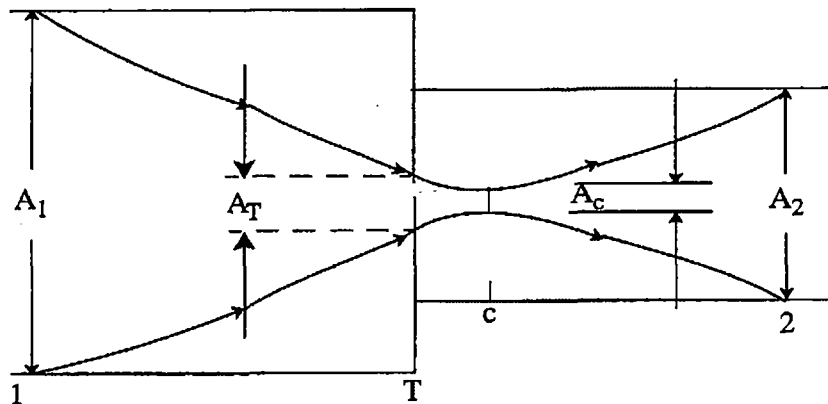
The dynamic pressure loss (ΔP_L) for an abrupt area contraction combined with an orifice is analyzed in a manner parallel to that for a simple contraction. The loss associated with the contracting fluid stream from Station 1 to c (the point of vena contracta) is neglected. The dynamic pressure loss associated with the expansion from the vena contracta to the downstream section is given by

$$\Delta P_L = \frac{1}{2}\rho \left(1 - \frac{A_c}{A_2}\right)^2 v_c^2 \qquad (7.628)$$

AREVA Inc.

EMF-2103NP
Revision 3

Realistic Large Break LOCA Methodology for Pressurized Water Reactors
Topical Report

Page 7-262

The contraction ratio, $\varepsilon_c = \dfrac{A_c}{A_T}$, is an empirical function of $\varepsilon_T = \dfrac{A_T}{A_1}$. The code uses the

same function equation as is used for a contraction. The function is $\varepsilon_c = 0.62 +$

$0.38(\varepsilon_T)^3$. Using the continuity equations, $v_c = \dfrac{A_T v_T}{A_c} = v_T \varepsilon_c$ and $v_T = \dfrac{A_T v_T}{A_T} = \dfrac{\varepsilon}{\varepsilon_T} v_2$,

Equation (7.628) can be written as

$$\Delta P_L = \frac{1}{2}\rho\left(1 - \frac{\varepsilon}{\varepsilon_c \varepsilon_T}\right)^2 v_2^2 \qquad (7.629)$$

Equation (7.629) is a generalization applicable to all the cases previously treated. For a

pure expansion, $\varepsilon_T = 1$, $\varepsilon_c = 1$, and $\varepsilon > 1$; for a contraction, $\varepsilon_T = \varepsilon < 1$ and $\varepsilon_c < 1$. Each of

these is a special case of Equation (7.629). The two-phase dynamic pressure loss

model is based on an adaptation of the general single-phase head loss give by

Equation (7.629).

7.7.2.3 Two-Phase Abrupt Area Change Model

The two-phase flow through an abrupt area change is modeled in a manner very similar

to that for single-phase flow by defining phasic flow areas. The two phases are coupled

through the interphase drag, a common pressure gradient, and the requirement that the

phases coexist in the flow passage.

The one-dimensional phasic stream-tube momentum equations can be deduced from

the multi-dimensional form given in Section 7.4.1. The flow at points of abrupt area

change is assumed to be quasi-steady and incompressible. In addition, the terms in the

momentum equations due to body force, wall friction, and mass transfer are assumed to

be small in the region affected by the area change. The interphase drag terms are

retained, since the gradient in relative velocity can be large at points of abrupt area

changes.

Equations (7.3) and (7.4) in one-dimensional form can be integrated approximately for a

steady, incompressible, smoothly varying flow to obtain modified Bernoulli-type

equations for each phase

$$\left(\frac{1}{2}\rho_f v_f^2 + P\right)_1 = \left(\frac{1}{2}\rho_f v_f^2 + P\right)_2 + \left(\frac{FI'}{\alpha_f}\right)_1 (v_{f,1} - v_{g,1})L_1 + \left(\frac{FI'}{\alpha_f}\right)_2 (v_{f,2} - v_{g,2})L_2 \qquad (7.630)$$

and

$$\left(\frac{1}{2}\rho_g v_g^2 + P\right)_1 = \left(\frac{1}{2}\rho_g v_g^2 + P\right)_2 + \left(\frac{FI'}{\alpha_g}\right)_1 (v_{g,1} - v_{f,1})L_1 + \left(\frac{FI'}{\alpha_g}\right)_2 (v_{g,2} - v_{f,2})L_2 \qquad (7.631)$$

where L_1 and L_2 are the lengths from the upstream condition to the throat and from the throat to the downstream condition respectively and where $FI' = \alpha_f \alpha_g \rho_f \rho_g FI$. The interphase drag is divided into two parts associated with the upstream and downstream parts of the flow affected by the area change.

The interphase drag is increased for horizontal, stratified, abrupt area changes in order to ensure more homogeneous flow when the flow becomes more increasingly co-current. Reference 7-133 discusses the observation of a strong mixing action as the flow contracts so that the two-phase mixture is well homogenized at the vena contracta. The interphase drag is increased by adding an extra interphase term ($f_{gf,extra}$) to the normal interphase drag (f_{gf}) from Equation (7.276). The extra interphase drag has the form

$$f_{gf,extra} = f_{gf,abrupt}^{scrah} \bullet f_{gf}^{1-scrah} \qquad (7.632)$$

where:

$$f_{gf,abrupt} = MAX\left\{f_{gf}, 8 \times 10^5 \bullet \exp\left[-14(1 - \alpha_{f,j})^2 + 2.5\, MAX(0, \alpha_{f,down})\right]^{0.33}\right\} \qquad (7.633)$$

$$scrah = 1.0 - \frac{|v_{g,j} - v_{f,j}|}{MAX(10^{-30}, |v_{g,j} + v_{f,j}|)} \qquad (7.634)$$

and $\alpha_{f,down}$ is the downstream liquid volume fraction. The term ($f_{gf,extra}$) is normally set to f_{gf}, but when scrah >0, then ($f_{gf,extra}$) is calculated from Equation (7.632). The form of this extra interphase drag was determined during the RELAP5/MOD2 development assessment (Reference 7-134) for the LOFT-Wyle small break test.

7.7.2.3.1   General Model

Consider the application of Equations (7.630) and (7.631) to the flow of a two-phase fluid through a passage having a generalized abrupt area change (the flow passage shown in Figure 7-23[9]). Here the area A_T is the throat or minimum area associated with an orifice located at the point of the abrupt area change. Since each phase is governed by a modified Bernoulli-type equation, it is reasonable to assume that losses associated with changes in the phasic flow area can be modeled by separate dynamic pressure loss terms for both the liquid and gas phases. Hence, we assume that the liquid sustains a loss as if it alone (except for interphase drag) were experiencing an area change from $\alpha_{f,1}A_1$ to $\alpha_{f,T}A_T$ to $\alpha_{f,2}A_2$; and the gas phase experiences a loss as if it alone were flowing through an area change from $\alpha_{g,1}A_1$ to $\alpha_{g,T}A_T$ to $\alpha_{g,2}A_2$. The area changes for each phase are the phasic area changes (see Figure 7-23). When the losses for these respective area changes, based on the Bourda-Carnot model and given by Equation (7.629), are added to Equations (7.630) and (7.631), the following phasic momentum equations are obtained:

$$\left(\frac{1}{2}\rho_f v_f^2 + P\right)_1 = \left(\frac{1}{2}\rho_f v_f^2 + P\right)_2 + \frac{1}{2}\rho_f\left(1 - \frac{\alpha_{f2}\varepsilon}{\alpha_{f,T}\varepsilon_{fc}\varepsilon_T}\right)^2 \left(v_{f,2}\right)^2$$
$$+ \left(\frac{FI'}{\alpha_f}\right)_1 \left(v_{f,1} - v_{g,1}\right)L_1 + \left(\frac{FI'}{\alpha_f}\right)_2 \left(v_{f,2} - v_{g,2}\right)L_2 \tag{7.635}$$

$$\left(\frac{1}{2}\rho_g v_g^2 + P\right)_1 = \left(\frac{1}{2}\rho_g v_g^2 + P\right)_2 + \frac{1}{2}\rho_g\left(1 - \frac{\alpha_{g,2}\varepsilon}{\alpha_{g,T}\varepsilon_{g,c}\varepsilon_T}\right)^2 \left(v_{g,2}\right)^2$$
$$+ \left(\frac{FI'}{\alpha_g}\right)_1 \left(v_{g,1} - v_{f,1}\right)L_1 + \left(\frac{FI'}{\alpha_g}\right)_2 \left(v_{g,2} - v_{f,2}\right)L_2 \tag{7.636}$$

The above two equations lead to the following form-loss factors for liquid and vapor:

---

[9]   In Figure 7-23, the liquid and vapor phases are shown as separated flow for clarity. The models developed are equally applicable to separated and dispersed flow regimes, as evidenced by the calculations performed when the abrupt area change model was incorporated into RELAP5 (Reference 7-135). The model was verified on single phase expansions, contractions, and orifices. Three two-phase problems were also run: (1) expansion case with the interphase drag equal to zero, which simulates separated flow, (2) expansion case with the interphase drag appropriate for dispersed flow, and (3) contraction case with the interphase drag appropriate for dispersed flow.

$$K_f = \left(1 - \frac{\alpha_{f,2}\varepsilon}{\alpha_{f,T}\varepsilon_{f,c}\varepsilon_T}\right)^2$$

$$(7.637)$$

$$K_g = \left(1 - \frac{\alpha_{g,2}\varepsilon}{\alpha_{g,T}\varepsilon_{g,c}\varepsilon_T}\right)^2$$

Figure 7-23 Schematic Flow of Two-Phase Mixture at Abrupt Area Change
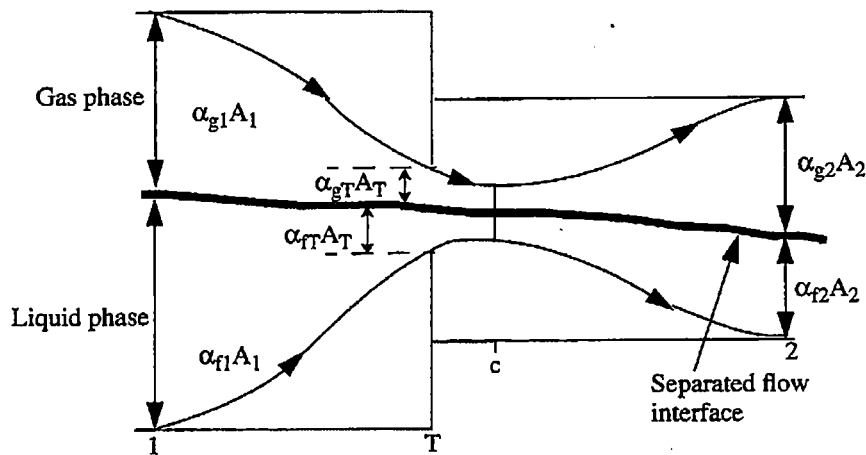
These phasic momentum equations are used across an abrupt area change. In Equations (7.635) and (7.636), $\varepsilon_{f,c}$ and $\varepsilon_{g,c}$ are the same tabular function of area ratio as in the single-phase case, except the area ratios used are the phasic area ratios

$$\varepsilon_{f,T} = \frac{\alpha_{f,T}}{\alpha_{f,1}}\varepsilon_T$$

$$(7.638)$$

and

$$\varepsilon_{g,T} = \frac{\alpha_{g,T}}{\alpha_{g,1}}\varepsilon_T$$

$$(7.639)$$

respectively. The area ratios, $\varepsilon = \dfrac{A_2}{A_1}$ and $\varepsilon_T = \dfrac{A_T}{A_1}$, are the same as for single-phase flow.

The interphase drag effects in Equations (7.635) and (7.636) are important. These terms govern the amount of slip induced by an abrupt area change; and if they are omitted, the model will always predict a slip at the area of change appropriate to a completely separated flow situation and give erroneous results for a dispersed flow.

7.7.2.3.2   Model Application

A few remarks concerning the way Equations (7.635) and (7.636) are applied to expansions and contractions, both with and without an orifice, are necessary. In a single-phase, steady flow situation and given the upstream conditions v_1 and P_1, one can solve v_2 and P_2 by using the continuity equation ($v_1 A_1 = v_2 A_2$) and Equation (7.622). Equations (7.635) and (7.636), along with the two phasic continuity equations, can be used in a similar manner except that now the downstream void fraction is an additional unknown which must be determined.

Expansion

For the purpose of explanation, consider the case of an expansion ($\alpha_{f,T} = \alpha_{f,1}$, $\alpha_{g,T} = \alpha_{g,1}$, $\varepsilon > 1$, $\varepsilon_T = 1$, $\varepsilon_{f,c} = \varepsilon_{g,c} = 1$, $L_1 = 0$) for which Equations (7.635) and (7.636) reduce to

$$\left(\frac{1}{2}\rho_f v_f^2 + P\right)_1 = \left(\frac{1}{2}\rho_f v_f^2 + P\right)_2 + \frac{1}{2}\rho_{f,2}\left(1 - \frac{\alpha_{f,2}\varepsilon}{\alpha_{f,1}}\right)^2 \left(v_{f,2}\right)^2 + \left(\frac{FI'}{\alpha_f}\right)_2 \left(v_{f,2} - v_{g,2}\right)L_2 \qquad (7.640)$$

$$\left(\frac{1}{2}\rho_g v_g^2 + P\right)_1 = \left(\frac{1}{2}\rho_g v_g^2 + P\right)_2 + \frac{1}{2}\rho_{g,2}\left(1 - \frac{\alpha_{g,2}\varepsilon}{\alpha_{g,1}}\right)^2 \left(v_{g,2}\right)^2 + \left(\frac{FI'}{\alpha_g}\right)_2 \left(v_{g,2} - v_{f,2}\right)L_2 \qquad (7.641)$$

These two equations with the incompressible continuity equations

$$\alpha_{f,1}v_{f,1}A_1 = \alpha_{f,2}v_{f,2}A_2 \qquad (7.642)$$

and

$$\alpha_{g,1}v_{g,1}A_1 = \alpha_{g,2}v_{g,2}A_2 \qquad (7.643)$$

are a system of four equations having four unknowns, $\alpha_{f,2}$ ($\alpha_{g,2} = 1 - \alpha_{f,2}$, $v_{f,2}$), $v_{g,2}$ and P_2, given the upstream conditions, $\alpha_{f,1}$ ($\alpha_{g,1} = 1 - \alpha_{f,1}$), $v_{f,1}$, $v_{g,1}$ and P_1. (The interphase drag, FI', is a known function of the flow properties.) It is important to note that the

downstream value of the liquid fraction ($\alpha_{f,2}$) is an additional unknown compared with the single-phase case and is determined (with the downstream velocities and pressure) by simultaneous solution of Equations (7.640) through (7.643) without additional assumptions. By taking a proper linear combination of Equations (7.635) and (7.636), the usual overall momentum balance can be obtained using the Bourda-Carnot (Reference 7-132) assumption (References 7-136 and 7-137).

If, as in the cited literature (References 7-136 and 7-138), only the overall momentum balance is used at an expansion, there will be an insufficient number of equations to determine all the downstream flow parameters, $\alpha_{f,2}$, $v_{f,2}$, $v_{g,2}$, and P_2. The indeterminacy has been overcome in cited works by means of several different assumptions concerning the downstream void fraction.[10] In the model developed here (Equations (7.640) and (7.641)), division of the overall loss into liquid and gas parts, respectively, results in sufficient conditions to determine all downstream flow variables, including $\alpha_{f,2}$. In addition, the present model includes force terms due to interphase drag in Equations (7.640) and (7.641), which are necessary to predict the proper amount of slip and void redistribution that occurs at points of area change.

Contraction

Consider the application of Equations (7.635) and (7.636) to a contraction. To determine both the downstream conditions and throat conditions from the upstream values of $\alpha_{f,1}$, $v_{f,1}$, $v_{g,1}$, and P_1, an additional consideration needs to be made. To obtain the throat values, apply the momentum equations valid for the contracting section of flow. (Here, the L_1 portion of the interphase force is associated with the contraction.)

$$\left(\frac{1}{2}\rho_f v_f^2 + P\right)_1 = \left(\frac{1}{2}\rho_f v_f^2 + P\right)_T + \left(\frac{FI'}{\alpha_f}\right)_1 \left(v_{f,1} - v_{g,1}\right)L_1 \tag{7.644}$$

$$\left(\frac{1}{2}\rho_g v_g^2 + P\right)_1 = \left(\frac{1}{2}\rho_g v_g^2 + P\right)_T + \left(\frac{FI'}{\alpha_g}\right)_1 \left(v_{g,1} - v_{f,1}\right)L_1 \tag{7.645}$$

---

[10] J. G. Collier (Reference 7-136) mentions three different assumptions that have been used: (1) $\alpha_{f,2} = \alpha_{f,1}$, (2) $\alpha_{f,2}$ is given by a homogeneous model, and (3) $\alpha_{f,2}$ is given by the Hughmark void fraction correlation.

$$\alpha_{f,1}\, v_{f,1}\, A_1 = \alpha_{f,T}\, v_{f,T}\, A_T \tag{7.646}$$

$$\alpha_{g,1}\, v_{g,1}\, A_1 = \alpha_{g,T}\, v_{g,T}\, A_T \tag{7.647}$$

These four equations are solved simultaneously for the values of $\alpha_{f,T}$ ($\alpha_{g,T} = 1 - \alpha_{f,T}$), $v_{f,T}$, $v_{g,T}$, P_T at the throat section (the minimum physical area). No additional or special assumptions are made concerning the throat conditions, since they follow as a direct consequence of the unique head loss models for each phase. After the throat values have been obtained, the conditions at the point of vena-contracta are established, assuming the void fraction is the same as at the throat. Thus, $\varepsilon_{f,c}$ and $\varepsilon_{g,c}$ are established using the tabular function in Appendix A of Reference 7-135 and the throat area ratios, $\varepsilon_{f,T}$ and $\varepsilon_{g,T}$, are defined by Equations (7.646) and (7.647). The functions are $\varepsilon_{f,c} = 0.62 + 0.38(\varepsilon_{f,T})^3$ and $\varepsilon_{g,c} = 0.62 + 0.38(\varepsilon_{g,T})^3$. To determine the downstream values, Equations (7.635) and (7.636) can be applied directly from Stations 1 to 2 with the throat values known, or the expansion loss equations can be used from the throat section to Station 2. Both approaches produce identical downstream solutions. As in the case of an expansion, because the proper upstream and downstream interphase drag is included, this modeling approach establishes the phase slip and resulting void redistribution. An orifice at an abrupt area change is treated exactly as the contraction explained above (that is, with two separate calculations to establish first the throat and then the downstream flow variables).

Countercurrent Flow

The preceding development implicitly assumed a co-current flow. For countercurrent flow, Equations (7.635) and (7.636) are applied exactly as in co-current flow except that the upstream sections for the respective phases are located on different sides of the abrupt area change. The difference appears in how the throat and downstream voids are determined. To determine the throat properties, equations similar to Equations (7.644) through (7.647) are used with the upstream values appropriate for each phase. These four equations are then solved for $\alpha_{f,T}$, $v_{f,t}$, $v_{g,t}$, and P_T. To determine the downstream values for each phase, only the head loss terms are needed for the downstream voids. (The downstream v_f, v_g, and P do not appear.) For countercurrent

flow, these voids are set such that the downstream void of each phase plus the upstream void of the opposite phase adds to 1. (Both phases together must fill the flow channel.) With the throat and downstream voids now known, Equations (7.635) and (7.636) can be used directly to determine the total loss for each phase at the abrupt area change.

Numerical Implementation

The implementation will be described for the co-current expansion case only; the co-current contraction, countercurrent expansion, and countercurrent contraction cases are similar.

Consider Equations (7.640) and (7.641) without the interphase drag term, since it is not needed to show the implementation method. Using the incompressible continuity Equations (7.642) and (7.643) in the second term on the right hand side of (7.640) and (7.641), and neglecting the interphase drag yields,

$$\left(\frac{1}{2}\rho_f v_f^2 + P\right)_1 = \left(\frac{1}{2}\rho_f v_f^2 + P\right)_2 + \frac{1}{2}\rho_f \left(1 - \frac{\alpha_{f,1}}{\alpha_{f,2}\varepsilon}\right)^2 v_{f,1}^2 \tag{7.648}$$

$$\left(\frac{1}{2}\rho_g v_g^2 + P\right)_1 = \left(\frac{1}{2}\rho_g v_g^2 + P\right)_2 + \frac{1}{2}\rho_g \left(1 - \frac{\alpha_{g,1}}{\alpha_{g,2}\varepsilon}\right)^2 v_{g,1}^2 \tag{7.649}$$

Subtracting Equation (7.649) from Equation (7.648), solving Equations (7.642) and (7.643) for $v_{f,2}$ and $v_{g,2}$, and substituting these into the resulting equation yields

$$\alpha_{f,1}\rho_f v_{f,1}^2 \left(\frac{1}{\alpha_{f,2}\varepsilon}\right)\left[\left(\frac{\alpha_{f,1}}{\alpha_{f,2}\varepsilon}\right) - 1\right] = \alpha_{g,1}\rho_g v_{g,1}^2 \left(\frac{1}{\alpha_{g,2}\varepsilon}\right)\left[\left(\frac{\alpha_{g,1}}{\alpha_{g,2}\varepsilon}\right) - 1\right] \tag{7.650}$$

where incompressibility implies $\rho_{f,1} = \rho_{f,2} = \rho_f$ and $\rho_{g,1} = \rho_{g,2} = \rho_g$.

Multiplying by $\alpha_{f,2}\alpha_{g,2}\varepsilon^2$ and performing algebraic manipulations yields

$$\alpha_{f,1}\rho_f v_{f,1}^2 \left(\alpha_{f,1} - \alpha_{f,2}\varepsilon\right)\left(1 - 2\alpha_{f,2} + \alpha_{f,2}^2\right) = \alpha_{g,1}\rho_g v_{g,1}^2 \left[\alpha_{g,1} - \left(1 - \alpha_{f,2}\right)\varepsilon\right]\alpha_{f,2}^2 \tag{7.651}$$

AREVA Inc.

EMF-2103NP
Revision 3

Realistic Large Break LOCA Methodology for Pressurized Water Reactors
Topical Report

Page 7-270

This is a cubic equation which is then solved for $\alpha_{f,2}$ using donor phasic densities for ρ_f and ρ_g. Then Equations (7.642), (7.643), and (7.648) are used to obtain the remaining variables $v_{f,2}$, $v_{g,2}$, and P_2.

7.7.2.4 Modifications to Momentum Equations

AREVA Inc.

Realistic Large Break LOCA Methodology for Pressurized Water Reactors
Topical Report

EMF-2103NP
Revision 3
Page 7-271
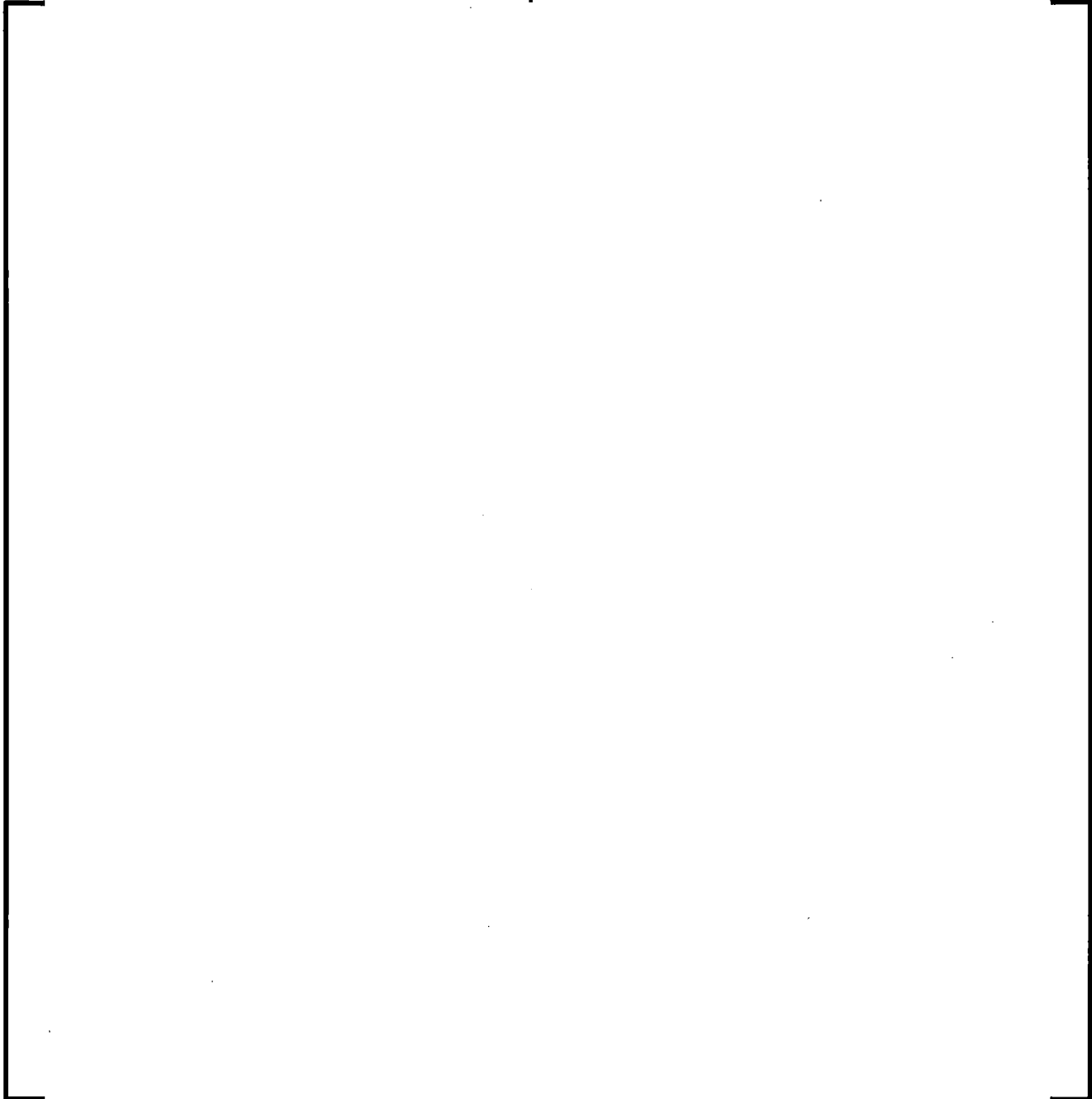
7.7.3 Countercurrent Flow Limiting Model

Countercurrent flow limiting model determines the amount of downflow liquid against upflow vapor. In principle, the countercurrent flow phenomena, including the countercurrent flow limitation (CCFL), can be properly treated through the interphase friction model. For flow through restrictions, however, it is difficult to properly model the interphase friction at a junction with a strong abrupt area change, since the donor properties do not truly represent the state properties at the junction. One could model the flow restriction as a (control) volume of short length and small size. But such a nodalization scheme may cause computational difficulties such as instabilities and excessive computation time. Therefore, a CCFL model is implemented to improve the computation of countercurrent flow phenomena.

There are several PWR internal structures where countercurrent flow is vital to core coolability under LOCA conditions. Some of them are the upper core tie plate, the downcomer annulus, and the steam generator inlet plenum region. CCFL in the steam generator inlet plenum region determines the liquid drainage from the steam generator to the hot leg. CCFL at the upper tie plate limits the liquid fallback to the core region. Downflow of ECC water in the downcomer to the lower plenum determines the amount of ECC water available for core reflood.

Two forms of CCFL correlations are commonly used: the Wallis type (Reference 7-139) and the Kutateladze (Reference 7-140) type. In the Exxon EM small break methodology (Reference 7-141), a Kutateladze-type CCFL correlation was used in the upper core tie plate region to limit the penetration of the upper plenum liquid, which partly originates from steam generators and hot legs, into the core region. The Kutateladze form was also used in TRAC-BD1 (Reference 7-142) for BWR tie plates and side entry orifices. Bankoff et al. (Reference 7-143) proposed a general form, which combines the Wallis and Kutateladze forms. The Bankoff general form was used by TRAC-PF1 (Reference 7-144) and RELAP5/MOD3 (Reference 7-127).

AREVA Inc.

Realistic Large Break LOCA Methodology for Pressurized Water Reactors
Topical Report

EMF-2103NP
Revision 3

Page 7-272

7.7.3.1　Formulation and Implementation

AREVA Inc.

Realistic Large Break LOCA Methodology for Pressurized Water Reactors
Topical Report

EMF-2103NP
Revision 3

Page 7-273

AREVA Inc.

EMF-2103NP
Revision 3

Realistic Large Break LOCA Methodology for Pressurized Water Reactors
Topical Report

Page 7-274

AREVA Inc.

EMF-2103NP
Revision 3

Realistic Large Break LOCA Methodology for Pressurized Water Reactors
Topical Report

Page 7-275

7.7.3.2   Downcomer ECC Water Penetration

AREVA Inc.

EMF-2103NP
Revision 3

Realistic Large Break LOCA Methodology for Pressurized Water Reactors
Topical Report

Page 7-277
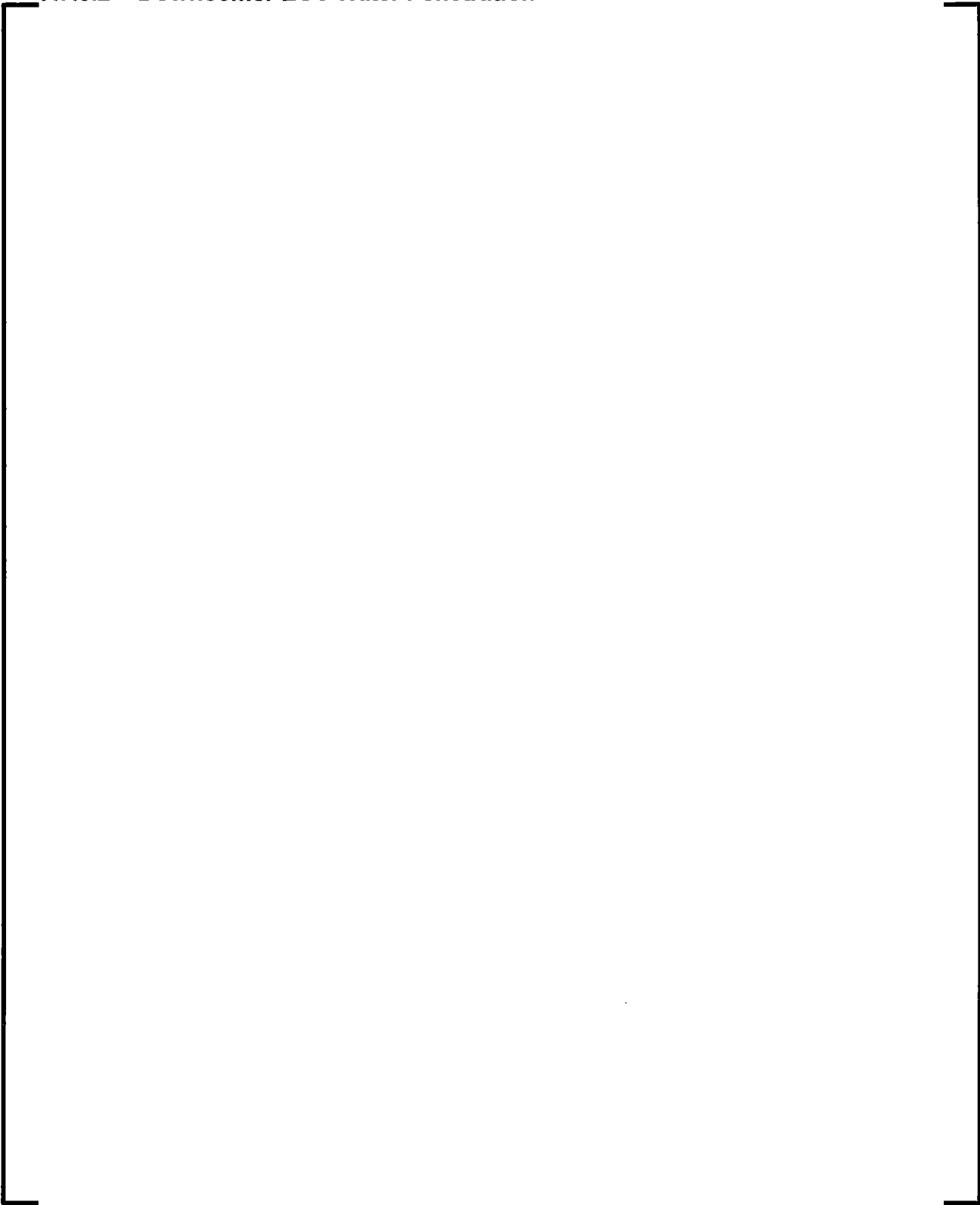
Figure 7-24 Downcomer 2-D Nodalization for Vapor Velocity Profile Calculation

Figure 7-25 Gas Velocity Profiles for Air Injection of 300 kg/s

$$\begin{bmatrix} & & \\ & & \\ & & \end{bmatrix}$$
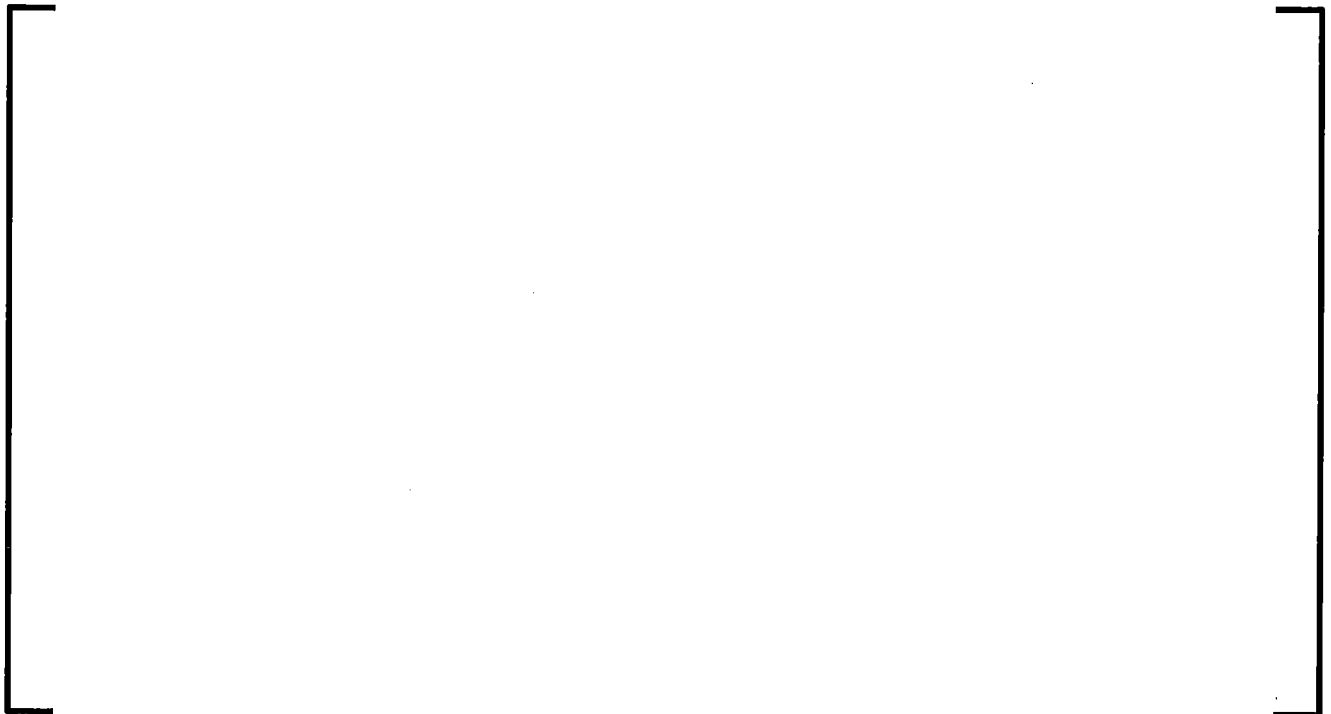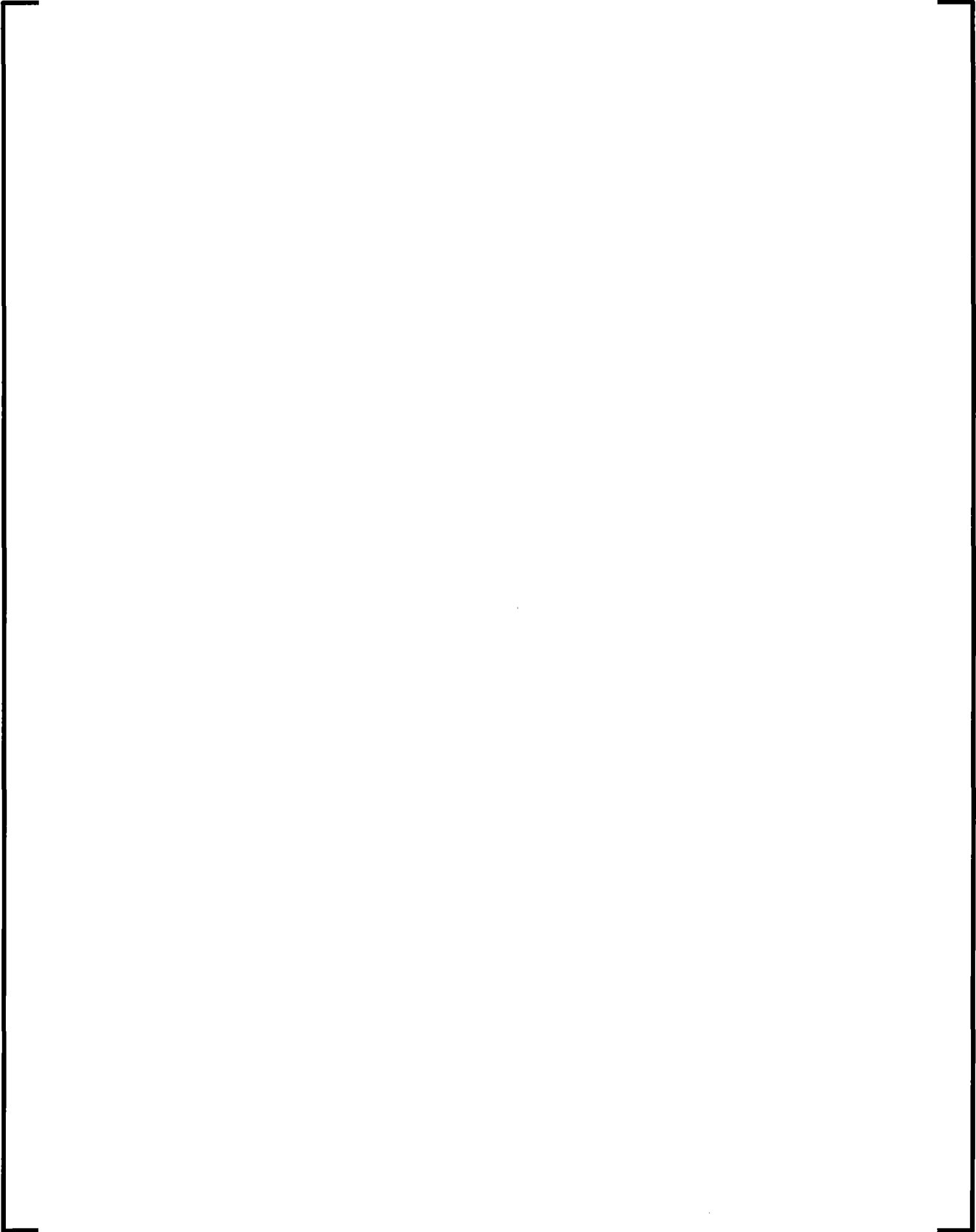
7.8   *Special Component Models*

S-RELAP5 contains models for subsystem components such as containment, pump, valve and separator. A discussion of these special component models is presented here.

7.8.1   Pump Model

The S-RELAP5 PUMP component model has been modified to apply two-phase pump performance degradation data which is available from EPRI (Reference 7-113). The EPRI pump data is more appropriate for use in PWR pump analysis than is the Semiscale pump data traditionally used for this purpose. With the exception of the two-phase degradation model, the S-RELAP5 PUMP component model is the same as that of RELAP5/MOD3 (Reference 7-114).

The basic approach to pump modeling is to superimpose a quasi-static model for pump performance on the RELAP5 volume-junction flow path representation. The pump is a volume-oriented component, and the head developed by the pump is apportioned equally between the suction and discharge junctions that connect the pump volume to the system. The pump model is interfaced with the two-fluid hydrodynamic model by assuming the head developed by the pump is similar to a body force. Thus, the head term appears in the mixture (sum) momentum equation; but like the gravity body force, it does not appear in the difference momentum equation used in RELAP5. The term that is added to the sum momentum is $\frac{1}{2}\rho gH$, where H is the total head rise of the pump (m), ρ is the volume fluid density (kg/m^3), and g is the acceleration due to gravity (m/s^2). The factor $\frac{1}{2}$ is needed because the term is applied at both the suction and discharge junctions. Numerical treatment of the head term is described in Section 2.6.5.1, in particular, Equations (7.135) through (7.142).

The pump energy term described in the RELAP5/MOD3 Code Manual (Reference 7-114) includes phasic velocity terms. These velocity terms come from the substitution of the phasic mechanical energies into the total energy equations. They disappear in the S-RELAP5 formulation of energy equations, since total energy equations are used. Thus, the pump energy is simply the product of pump torque and pump angular speed. The phasic partition of the pump energy is weighted by $(\alpha_f \rho_f C_{pf})$ and $(\alpha_g \rho_g C_{pg})$.

7.8.1.1 Centrifugal Pump Performance Model

The basic pump performance data must be generated experimentally. Analytical programs have been developed that are reasonably successful in predicting near-design pump performance for single-phase fluids. However, for off-design operation or for operation with a two-phase fluid, the problems of analytical pump performance prediction are nearly insurmountable. The basic parameters that characterize the pump performance are the rotational speed, ω or N, the volumetric flow, Q, the head rise, H, and the shaft torque, τ. The relationship between these four parameters can be uniquely displayed by a four-quadrant representation of such data. A typical four-quadrant curve is shown in Figure 7-26. Both positive and negative values for each of the four parameters are represented. The disadvantages in using such a data map for numerical purposes are the need for two-dimensional interpolation, the large number of points needed to define the entire range, and the fact that the map is infinite in extent. These objections can be largely overcome by use of a homologous transformation based on the centrifugal pump similarity relationships. Such a transformation collapses the four-quadrant data onto a single, bounded, dimensionless curve having eight octants. Typical homologous curves for the head and torque are illustrated in Figures 7-27 and 7-28, respectively, where ω_R, Q_R, H_R, and τ_R are the rated values for the pump speed, volumetric flow rate, head, and torque, respectively. The homologous transformation is not unique, and not all points of Figure 7-26 lie on the curves of Figures 7-27 and 7-28. However, the data are closely grouped, and the single curve is a good approximation for pump performance. The pump model allows the user the option of accounting for two-phase degradation effects on pump performance.

The two-phase degradation model is based on experimental data. Available pump data for the 1½ Loop Model Semiscale and Westinghouse Canada Limited (WCL) experiments were used in developing the two-phase pump model. The single-phase pump head (dimensionless) curve for the Semiscale pump is shown in Figure 7-29, and the fully degraded two-phase pump head curves are shown in Figure 7-30. These represent complete pump characteristics (except for the reverse pump fully degraded region) for the Semiscale pump operating under two-phase conditions, with the average of the void fractions of the pump inlet and outlet mixtures between 0.2 and 0.9. The lines drawn through the data were determined by least-squares polynomial fits to the data using known constraints.

A comparison of the two-phase data in Figure 7-30 with the single-phase data in Figure 7-29 shows that the two-phase dimensionless head ratio ($\frac{h}{v^2}$ or $\frac{h}{\alpha^2}$) is significantly less than the single-phase dimensionless head ratio for the normal pump operation region (HAN and HVN). For negative ratios of $\frac{v}{\alpha}$, such as those that occur in the HAD region, the pump flow becomes negative. When the pump flow is negative, the two-phase dimensionless head ratio is greater than the single-phase dimensionless head ratio. Two-phase flow friction losses are generally greater than single-phase losses, and friction is controlling in this energy dissipation region (HAD). The other regions of two-phase dimensionless head ratio data show similar deviations from single-phase data.

AREVA Inc.

EMF-2103NP
Revision 3

Realistic Large Break LOCA Methodology for Pressurized Water Reactors
Topical Report

Page 7-282

Figure 7-26 Typical Pump Characteristic Four-Quadrant Curves

AREVA Inc.

EMF-2103NP
Revision 3

Realistic Large Break LOCA Methodology for Pressurized Water Reactors
Topical Report

Page 7-283
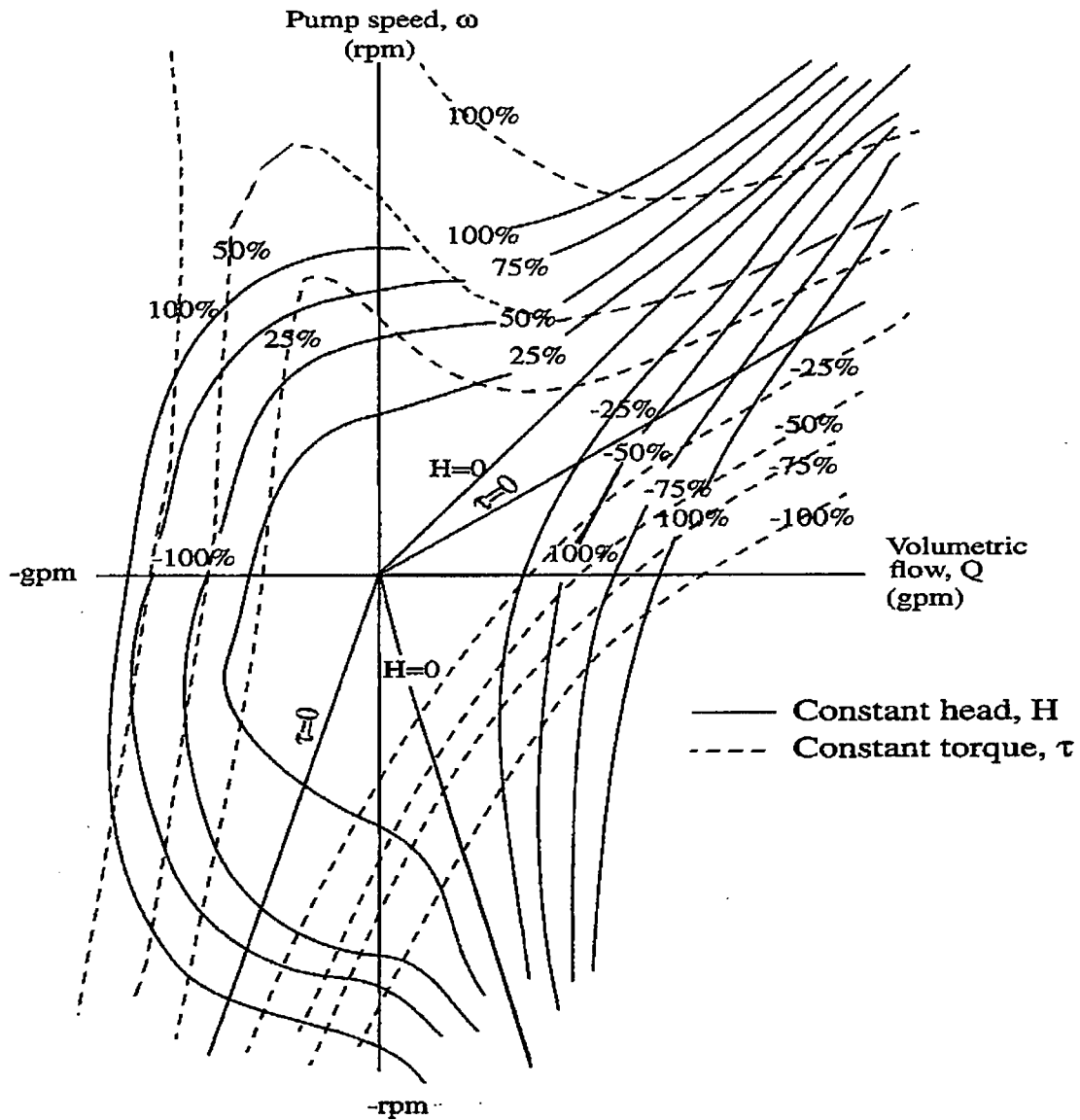
Figure 7-27 Typical Pump Homologous Head Curves

AREVA Inc.

Realistic Large Break LOCA Methodology for Pressurized Water Reactors
Topical Report

EMF-2103NP
Revision 3

Page 7-284
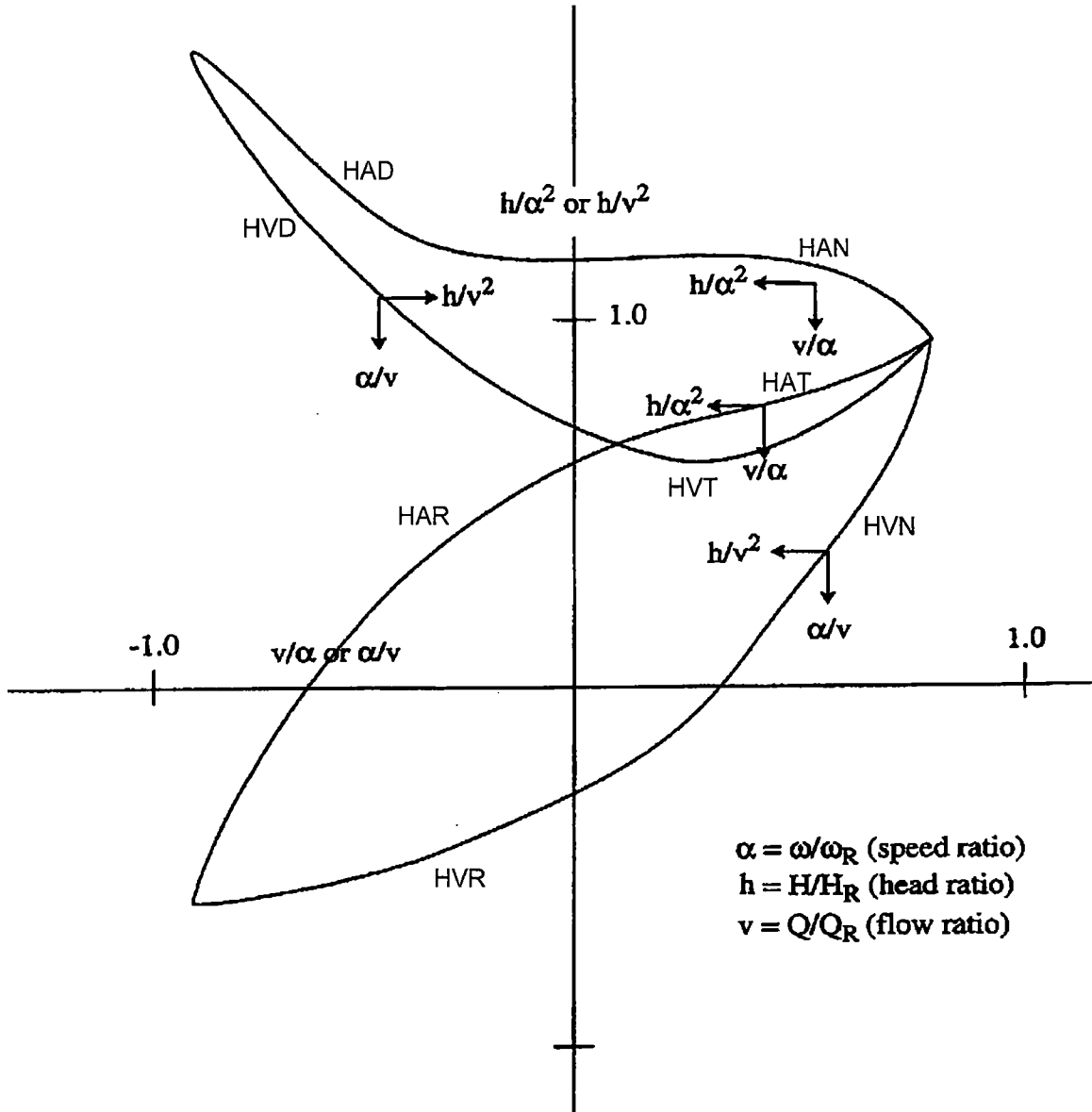
Figure 7-28 Typical Pump Homologous Torque Curves

β/α^2 or β/v^2

BVD

$\beta 1 v^2$

1.0

BVT

BAN

α/v

β/α^2

BVN

v/α

BAD

β/v^2

β/α^2

v/α or α/v

α/v

v/α

-1.0

1.0

$\alpha = \omega/\omega_R$ (speed ratio)
$\beta = \tau/\tau_R$ (torque ratio)
$v = Q/Q_R$ (flow ratio)

BAT

BVR

-1.0

BAR

AREVA Inc.

Realistic Large Break LOCA Methodology for Pressurized Water Reactors
Topical Report

EMF-2103NP
Revision 3

Page 7-285
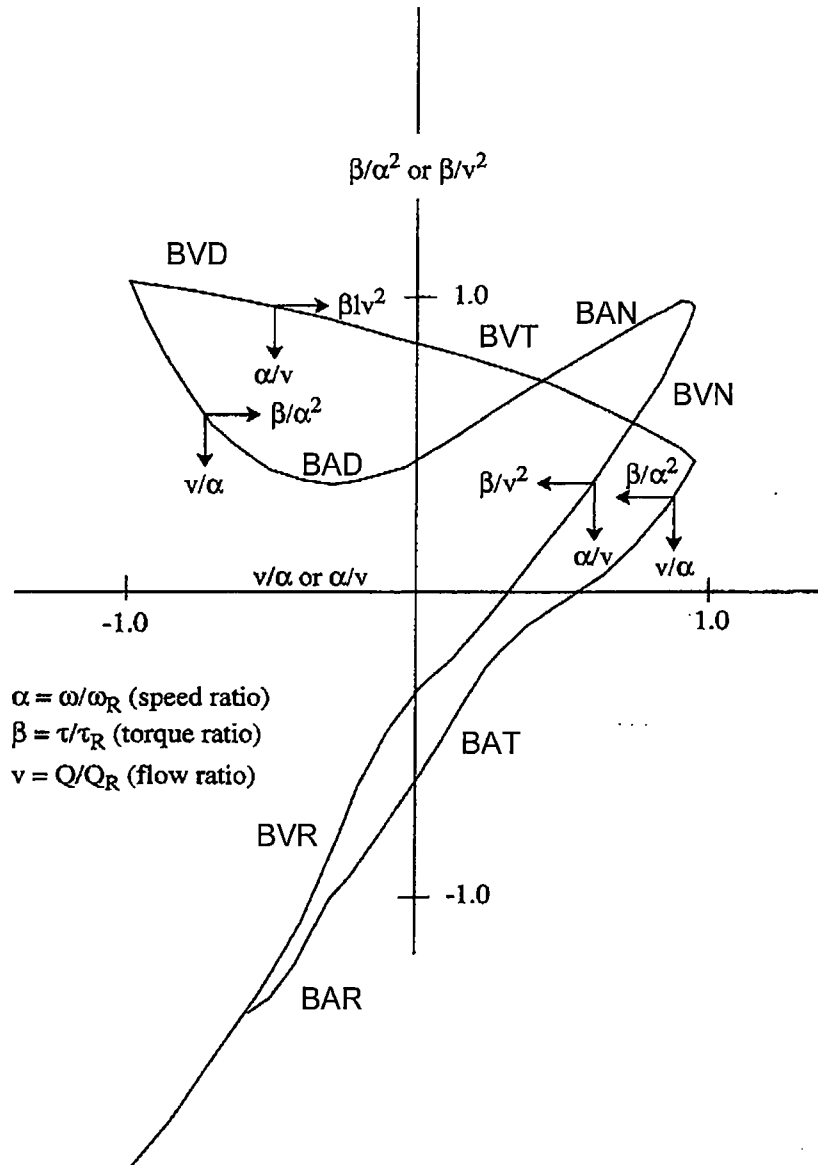
Figure 7-29 Single-Phase Homologous Head Curves for 1-½ Loop
MOD1 Semiscale Pumps

Normal pump $(+Q, +\alpha)$ {HAN / HVN

Energy dissipation $(-Q, +\alpha)$ {HAD / HVD

Normal turbine $(-Q, -\alpha)$ {HAT / HVT

Reverse pump $(+Q, -\alpha)$ {HAR / HVR
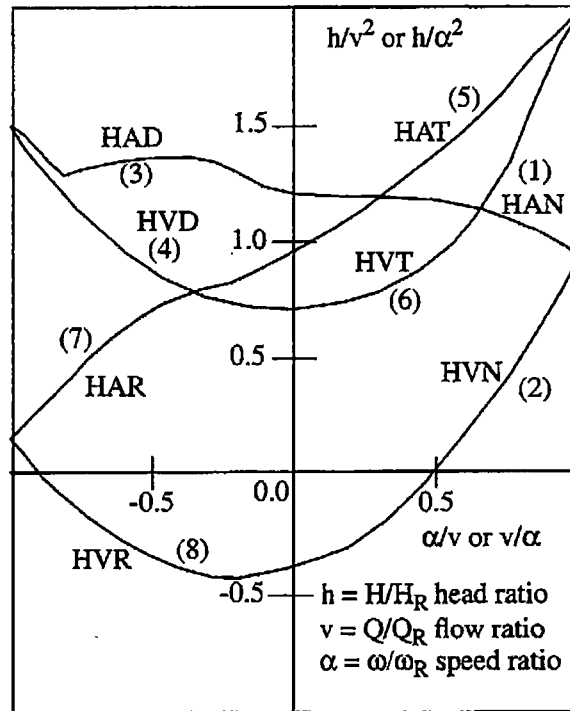
**Figure 7-30 Fully Degraded, Two-Phase Homologous Head Curves
for 1-½ Loop MOD1 Semiscale Pumps**
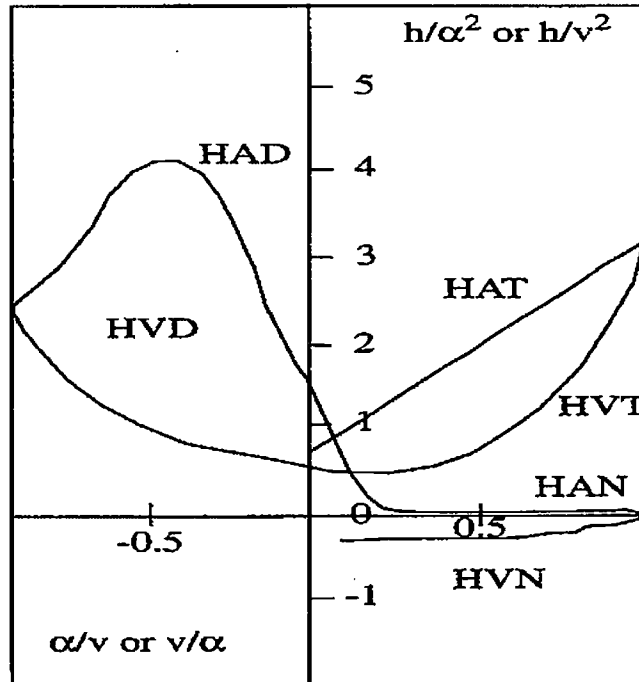
Table 7-4 presents the difference between the single- and two-phase dimensionless

head ratio data as a function of $\dfrac{v}{\alpha}$ and $\dfrac{\alpha}{v}$ for the various pumping regions shown in

Figures 7-29 and 7-30 where:

$$x = \frac{v}{\alpha} \quad \text{or} \quad \frac{\alpha}{v}$$

(7.670)

$$y = \left(\left. \frac{h}{\alpha^2} \right|_{1\phi} - \left. \frac{h}{\alpha^2} \right|_{2\phi} \right) \quad \text{or} \quad \left(\left. \frac{h}{v^2} \right|_{1\phi} - \left. \frac{h}{v^2} \right|_{2\phi} \right)$$

The differences shown in Table 7-4 are for the eight curve types used for determining

pump head.

Table 7-4 SEMISCALE Dimensionless Head Ratio Difference Data
(Single-Phase Minus Two-Phase)

Curve Type	x	y	Curve Type	x	y
1(HAN)	0.00	0.00	4(HVD)	-1.00	-1.16
	0.10	0.83		-0.90	-0.78
	0.20	1.09		-0.80	-0.50
	0.50	1.02		-0.70	-0.31
	0.70	1.01		-0.60	-0.17
	0.90	0.94		-0.50	-0.08
	1.00	1.00		-0.35	0.00
				-0.20	0.05
2(HVN)	0.00	0.00		-0.10	0.08
	0.10	-0.04		0.00	0.11
	0.20	0.00			
	0.30	0.10	5(HAT)	0.00	0.00
	0.40	0.21		0.20	-0.34
	0.80	0.67		0.40	-0.65
	0.90	0.80		0.60	-0.93
	1.00	1.00		0.80	-1.19
				1.00	-1.47
3(HAD)	-1.00	-1.16			
	-0.90	-1.24	6(HVT)	0.00	0.11
	-0.80	-1.77		0.10	0.13
	-0.70	-2.36		0.25	0.15
	-0.60	-2.79		0.40	0.13
	-0.50	-2.91		0.50	0.07
	-0.40	-2.67		0.60	-0.04
	-0.25	-1.69		0.70	-0.23
	-0.10	-0.50		0.80	-0.51
	0.00	0.00		0.90	-0.91
				1.00	-1.47
			7(HAR)	-1.00	0.00
				0.00	0.00
			8(HVR)	-1.00	0.00
				0.00	0.00

AREVA Inc.

EMF-2103NP
Revision 3

Realistic Large Break LOCA Methodology for Pressurized Water Reactors
Topical Report

Page 7-288

The head multiplier, $M_H(\alpha_g)$, and void fraction data shown in Table 7-5 were obtained in the following manner. The Semiscale and WCL pump data (Reference 7-115) were converted to dimensionless head ratios of $\dfrac{h}{\alpha^2}$ or $\dfrac{h}{v^2}$. Values of the dimensionless head ratios were obtained for pump speeds and volumetric flow rates within 50% of the rated speed and flow rate for the pumps. The difference between the single- and two-phase dimensionless ratios was developed as a function of the average void fractions for the pump inlet and outlet mixtures. The difference between the single- and two-phase dimensionless ratios was then normalized to a value between 0 and 1.0. The normalized result was tabulated as a function of the void fraction.

Table 7-5 Head Multiplier and Void Fraction Data

α_g	$M_H(\alpha_g)$
0.000	0.00
0.070	0.00
0.080	0.74
0.165	1.00
0.900	1.00
1.000	0.00

If the two-phase option is selected, the pump head and torque are calculated from

$$H = H_{1\phi} - M_H\left(\alpha_g\right)\left(H_{1\phi} - H_{2\phi}\right) \tag{7.671}$$

$$\tau = \tau_{1\phi} - M_\tau\left(\alpha_g\right)\left(\tau_{1\phi} - \tau_{2\phi}\right) \tag{7.672}$$

where:

$1\phi \;=\;$ single-phase value;

$2\phi \;=\;$ two-phase, fully degraded value, $0.2 < \alpha_g < 0.9$; and

$M \;=\;$ multiplier on difference curve as a function of α_g.

Assumptions inherent in the pump model for two-phase flow include:

- The head multiplier, $M_H(\alpha_g)$, determined empirically for the normal operating region of the pump, is also valid as an interpolating factor in all other operating regions.

- The relationship of the two-phase to the single-phase behavior of the Semiscale pump is applicable to large reactor pumps. This assumes that the pump model for two-phase flow is independent of pump-specific speed.

7.8.1.2 Centrifugal Pump Drive Model

The pump torque is used to calculate the pump speed after the pump has been shut off by the input trip signal. The speed is calculated by the deceleration equation

$$I\frac{d\omega}{dt} = \tau \tag{7.673}$$

The finite difference approximation of this equation is

$$\omega_{t+\Delta t} = \omega_t + \frac{\tau\Delta t}{I} \tag{7.674}$$

where:

τ =   net torque;

I =   moment of inertia;

t =   time;

Δt =   time step; and

ω =   angular velocity.

The rate of energy addition to the pump system is given by $\tau\omega$ and is added to the energy equations for the pump component.

The total pump torque is calculated by considering the hydraulic torque from the homologous curves and the pump frictional torque. The net torque with the drive motor shut off is

$$\tau = \tau_{hy} + \tau_{fr} \qquad (7.675)$$

where:

τ_{hy} =   hydraulic torque; and

τ_{fr} =   frictional torque.

The frictional torque is in the form of a cubic equation. The value of the frictional torque is also dependent on the sign of the pump speed. An option is available to specify whether reverse rotation of the pump is allowed.

The hydraulic torque is calculated from the homologous curves using the density ratio

$$\tau_{hy} = \tau_{ho} \frac{\rho}{\rho_R}$$

where:

τ_{ho} =   homologous torque;

ρ =   fluid density; and

ρ_R =   rated fluid density.

The electric drive motor will affect the speed behavior of the pump while the motor remains connected to its power source. The net torque with the drive motor on is incorporated into the pump model by adding the value of motor torque, τ_m, to the torque summation

$$\tau = \tau_{hy} + \tau_{fr} - \tau_m \qquad (7.676)$$

where the sign of the motor torque is the same as that of the hydraulic and frictional torque for steady operating conditions, that is, zero net torque.

AREVA Inc.

Realistic Large Break LOCA Methodology for Pressurized Water Reactors
Topical Report

EMF-2103NP
Revision 3

Page 7-291

Induction motors are used to drive primary coolant pumps. At constant voltage, the motor torque is an explicit function of speed. This torque/speed relationship is normally available from the motor manufacturer.

Motor torque is supplied to the pump model as a tabular function of torque versus speed as given by the manufacturer's data. A typical torque/speed curve for an induction motor is shown in Figure 7-31:

Figure 7-31 Typical Torque vs. Speed Curve

Percent synchronous speed (1200 rpm)
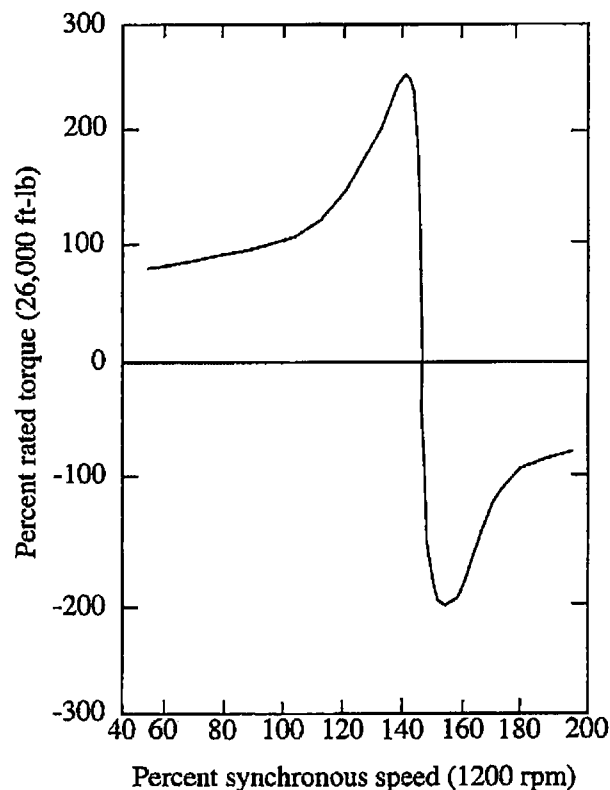
The capability to simulate a locked-rotor condition of the pump is included in RELAP5. This option provides for simulation of the pump rotor lockup as a function of input elapsed time, maximum forward speed, or maximum reverse speed. At the time the rotor locks (and at all times thereafter), the pump speed is set equal to zero.

AREVA Inc.

EMF-2103NP
Revision 3

Realistic Large Break LOCA Methodology for Pressurized Water Reactors
Topical Report

Page 7-292

7.8.1.3   EPRI Pump Two-Phase Head Degradation Model

AREVA Inc.

EMF-2103NP
Revision 3

Realistic Large Break LOCA Methodology for Pressurized Water Reactors
Topical Report

Page 7-293

7.8.1.4 Two-Phase Head Difference Multiplier

AREVA Inc.

Realistic Large Break LOCA Methodology for Pressurized Water Reactors
Topical Report

EMF-2103NP
Revision 3

Page 7-294
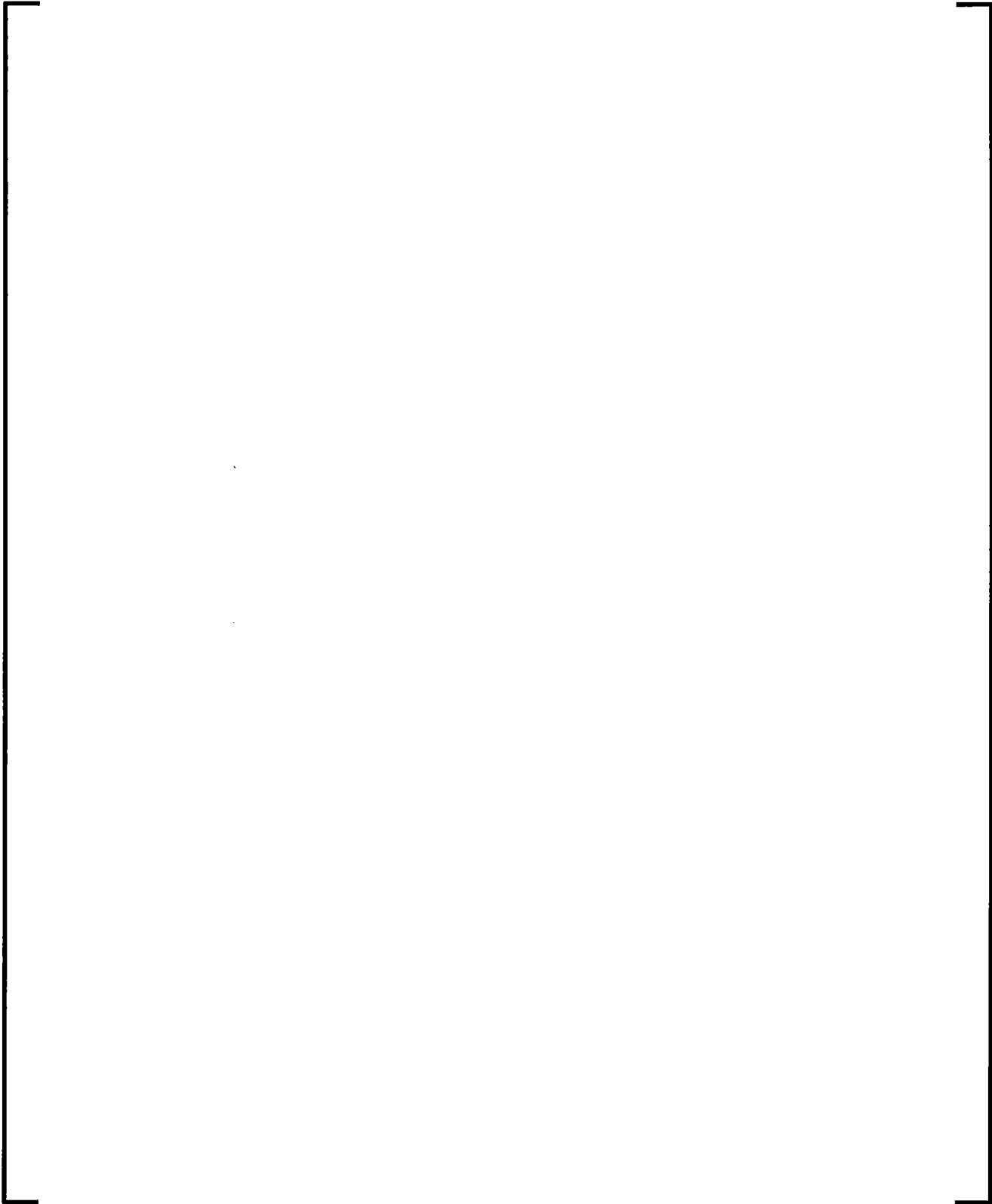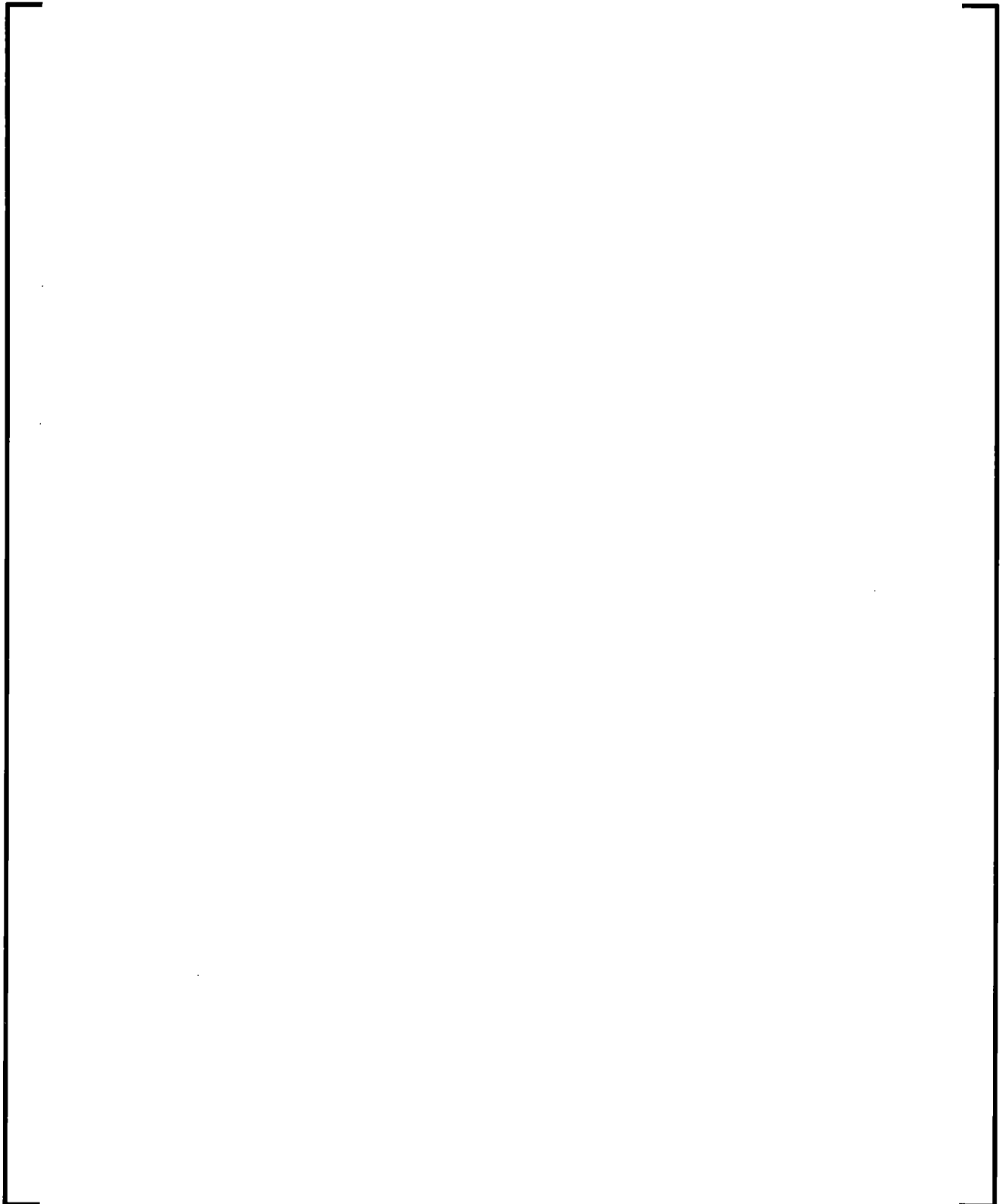
Head Difference Multiplier in AN Region

In the AN octant, head difference multipliers derived from the EPRI data are seen to depend primarily on pump void fraction, hence an analytical expression has been derived which accurately reproduces the EPRI data at a $\frac{v}{a}$ ratio of 1.0. In S-RELAP5, the following curve fit for M_H is used throughout the AN octant, independent of the $\frac{v}{a}$ ratio.

for $0.0 < \alpha \leq 0.1478$:

$$M_H = 0.0 \qquad\qquad (7.677)a$$

for $0.1478 < \alpha < 0.73$:

$$M_H = -0.5888 + 4.4455\alpha - 3.1193\alpha^2 \qquad\qquad (7.677)b$$

for $0.73 < \alpha \leq 0.95$:

$$M_H = -5.7515 + 17.6679\alpha - 11.5444\alpha^2 \qquad\qquad (7.677)c$$

for $\alpha > 0.95$:

$$M_H = 12.284(1-\alpha) \qquad\qquad (7.678)$$

A plot of this analytical function is shown in Figure 7-32. The curve labeled a/v_1.0 represents the combination of Equations (7.677) through (7.678). The above equations are applied to all regions except the HVN region, which is described in the next subsection.

Figure 7-32 AN and VN Octant Head Difference Multipliers
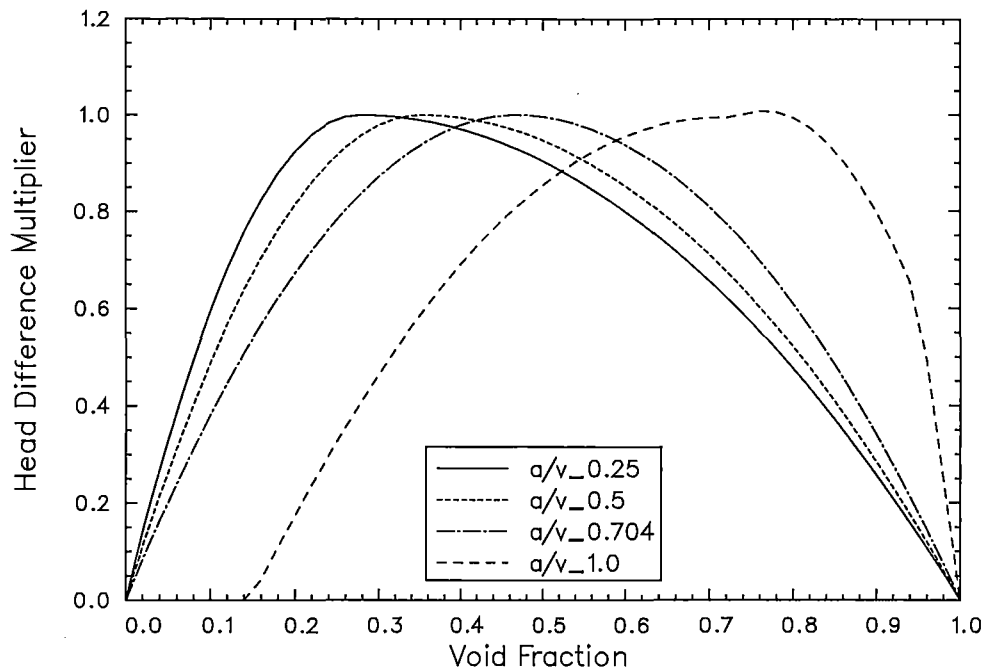
Head Difference Multiplier in VN Region

The EPRI data indicate that in the VN octant, the void fraction for maximum degradation

is a function of the ratio $\dfrac{a}{v}$, moving toward lower void fractions as $\dfrac{a}{v}$ decreases. A curve

fit to the EPRI data allows the void fraction for maximum degradation to be expressed
as follows

$$\alpha_{MAX} = 0.2752 - 0.1474\left(\frac{a}{v}\right) + 0.5978\left(\frac{a}{v}\right)^2 \qquad (7.679)$$

Using the above expression for α_{MAX}, the head difference multiplier in the VN octant
may be approximated analytically by the following quadratic functions

$$\text{for } \alpha \le \alpha_{MAX} \qquad M_H = 1.0 - \left[\frac{\alpha_{MAX} - \alpha}{\alpha_{MAX}}\right]^2 \qquad (7.680)$$

$$\text{for } \alpha > \alpha_{MAX} \qquad M_H = 1.0 - \left[\frac{\alpha - \alpha_{MAX}}{1.0 - \alpha_{MAX}}\right]^2 \qquad (7.681)$$

In order to smoothly merge the multiplier formulations used in the AN and VN octants,

Equations (7.679) and (7.680) are used in the VN octant for $\frac{a}{v}$ values between 0.0 and

0.9. Between $\frac{a}{v} = 0.9$ and 1.0, both the AN region (Equation (7.677)a) and the VN

region (Equation (7.680)) multipliers are calculated, and a linear interpolation (based on

$\frac{a}{v}$) between these two values is used to obtain the actual multiplier to be used.

Plots of Equations (7.680) and (7.681) for various $\frac{a}{v}$ ratios are also shown in Figure

7-32. The curve labeled a/v_1.0 represents both the $\frac{a}{v} = 1.0$ value for the VN octant

and the $\frac{v}{a} = 1.0$ value for the AN octant.

7.8.1.4.1   Pressure Dependence of Pump Head Degradation

The EPRI data show that the magnitude of two-phase degradation effects is dependent
on pump inlet pressure. Two-phase degradation effects tend to become more
significant at lower pressures, presumably because of the greater difference in phase
densities at lower pressures. Kastner and Seeberger (Reference 7-116) indicate the
range of pump pressures and void fractions that might be encountered in hypothetical
LOCA analyses. Pressures significantly below 850 psia (59 bar) are encountered only
at void fractions above 0.8, where degradation effects are becoming insignificant. The
EPRI data show very little difference between 1000 psia and 850 psia head degradation
in the AN region near rated operating conditions. At off-rated conditions, Kastner and
Seeberger (Reference 7-116) show a significant difference (approx. 33%) between
low-flow AN region head degradation at 1000 psia and at 850 psia. EPRI results reveal
an approximate 33% difference between 1000 psia and 850 psia head degradation in
the high-flow VN region.

The head difference multiplier formulations presented in Equations (7.677)a through (7.678) and (7.680) through (7.681) are based on EPRI data at 1000 psia. In S-RELAP5, these equations are used for all pressures above 1000 psia. At pressures between 1000 psia and 850 psia, an adjustment factor increasing linearly from 1.0 to 1.33 is applied to the two-phase head multiplier. This pressure correction factor is given by

for P_{inlet} > 1000 psia:

$$f_{PCORR} = 1.0 \tag{7.682}$$

for $850 \le P_{inlet} \le 1000$ psia:

$$f_{PCORR} = 1 + 0.33\frac{1000 - P_{inlet}}{1000 - 850} \tag{7.683}$$

for P_{inlet} < 850 psia:

$$f_{PCORR} = 1.33 \tag{7.684}$$

where P_{inlet} is the pump inlet pressure (psia).

7.8.1.4.2   Implementation of EPRI Based Two-Phase Degradation Model

Equations (7.677)a through (7.684) have been included in a new S-RELAP5 subroutine PHMULT. The pump volume conditions, instead of the inlet conditions, are used in the implementation. The use of these models specifies only the pump two-phase head difference multiplier formulation, and it is important to note that this multiplier option is intended for use with head difference curves derived from the EPRI data. Table 7-6 shows the appropriate head difference curves. The head difference dh used in Table 7-6 is defined as follows:

$dh = h_{1\phi} - h_{2\phi}$ where $h = \dfrac{H_{actual}}{H_{rated}}$ and H is the pump head.

7.8.1.4.3   Pump Two-Phase Torque Degradation Model

The EPRI data also include torque degradation data and present a more realistic means of treating two-phase torque degradation in PWR reactor coolant pumps than do Semiscale torque degradation data. The methodology given by Equation (7.672) is adequate for representing the torque EPRI degradation data, i.e., the torque multiplier is a function of void fraction only, and this data can be implemented in an S-RELAP5 model simply through input deck modifications, replacing Semiscale based data with EPRI based data. Table 7-7 shows torque difference homologous curves based on EPRI data, while Table 7-8 shows a torque difference multiplier curve derived from the EPRI data and intended for use with the data in Table 7-7. The torque difference db used in Table 7-7 is defined as follows:

$$db = b_{1\phi} - b_{2\phi}$$

where $b = \dfrac{\tau_{actual}}{\tau_{rated}}$ and τ is pump torque.

Table 7-6 Head Difference Homologous Curves Based on EPRI Data

AN Octant		VN Octant		AD Octant		VD Octant	
$\frac{v}{a}$	$\frac{dh}{a^2}$	$\frac{a}{v}$	$\frac{dh}{v^2}$	$\frac{v}{a}$	$\frac{dh}{a^2}$	$\frac{a}{v}$	$\frac{dh}{v^2}$
0.0	0.91	0.0	0.05	-1.0	-0.98	-1.0	-0.98
0.1	0.89	0.1	0.27	-0.9	-1.02	-0.9	-1.08
0.2	0.88	0.2	0.41	-0.8	-1.05	-0.8	-1.11
0.3	0.84	0.3	0.44	-0.7	-1.01	-0.7	-1.12
0.4	0.80	0.4	0.37	-0.6	-0.95	-0.6	-1.05
0.5	0.78	0.5	0.28	-0.5	-0.85	-0.5	-0.95
0.6	0.77	0.6	0.25	-0.4	-0.72	-0.4	-0.85
0.7	0.77	0.7	0.29	-0.3	-0.59	-0.3	-0.71
0.8	0.77	0.8	0.40	-0.2	-0.43	-0.2	-0.54
0.9	0.77	0.9	0.55	-0.1	-0.26	-0.1	-0.35
1.0	0.74	1.0	0.74	-0.0	0.91	-0.0	-0.24

AT Octant		VT Octant		AR Octant		VR Octant	
$\frac{v}{a}$	$\frac{dh}{a^2}$	$\frac{a}{v}$	$\frac{dh}{v^2}$	$\frac{v}{a}$	$\frac{dh}{a^2}$	$\frac{a}{v}$	$\frac{dh}{v^2}$
0.0	-0.16	0.0	-0.24	-1.0	0.0	-1.0	0.0
0.1	-0.16	0.1	-0.23	0.0	0.0	0.0	0.0
0.2	-0.16	0.2	-0.22				
0.3	-0.14	0.3	-0.22				
0.4	-0.13	0.4	-0.21				
0.5	-0.13	0.5	-0.22				
0.6	-0.12	0.6	-0.21				
0.7	-0.14	0.7	-0.21				
0.8	-0.16	0.8	-0.21				
0.9	-0.16	0.9	-0.22				
1.0	-0.18	1.0	-0.18				

AREVA Inc.
EMF-2103NP
Revision 3

Realistic Large Break LOCA Methodology for Pressurized Water Reactors
Topical Report
Page 7-300

Table 7-7 Torque Difference Homologous Curves Based on EPRI Data

AN Octant		VN Octant		AD Octant		VD Octant	
$\frac{v}{a}$	$\frac{db}{a^2}$	$\frac{a}{v}$	$\frac{db}{v^2}$	$\frac{v}{a}$	$\frac{db}{a^2}$	$\frac{a}{v}$	$\frac{db}{v^2}$
0.0	0.01	0.0	0.05	-1.0	0.00	-1.0	0.00
0.1	0.04	0.1	0.25	-0.1	0.00	0.0	0.00
0.2	0.07	0.2	0.35	0.0	0.01		
0.3	0.09	0.3	0.34				
0.4	0.12	0.4	0.23				
0.5	0.14	0.5	0.15				
0.6	0.17	0.6	0.13				
0.7	0.20	0.7	0.13				
0.8	0.23	0.8	0.16				
0.9	0.25	0.9	0.24				
1.0	0.28	1.0	0.28				

AT Octant		VT Octant		AR Octant		VR Octant	
$\frac{v}{a}$	$\frac{db}{a^2}$	$\frac{a}{v}$	$\frac{db}{v^2}$	$\frac{v}{a}$	$\frac{db}{a^2}$	$\frac{a}{v}$	$\frac{db}{v^2}$
0.0	0.00	0.0	0.00	-1.0	0.00	-1.0	0.00
1.0	0.00	1.0	0.00	0.0	0.00	0.0	0.00

Table 7-8 Torque Difference Multiplier Table Based on EPRI Data

Void Fraction	M_T	Void Fraction	M_T
0.0	0.000	0.5	0.8299
0.1	0.2743	0.6	0.6317
0.2	0.7707	0.7	0.4492
0.3	0.9808	0.8	0.2314
0.33	1.000	0.9	0.00893
0.4	0.9686	1.0	0.000

7.8.2   Valves

Valves are quasi-steady models that are used either to specify an option in a system model or to simulate control mechanisms in a hydrodynamic system. The valve models can be classified into two categories: valves that open or close instantly and valves that open or close gradually. Either type can be operated by control systems or by flow dynamics.

Valves in the first category are trip valves and check valves. The model for these valves does not include valve inertia or momentum effects. If the valve is used as a junction with an abrupt area change, then the abrupt area change model is used to calculate kinetic loss factors when the valve is open.

Valves in the second category are the inertial swing check valve, the motor valve, the servo valve, and the relief valve. The inertial valve and relief valve behavior is modeled using Newton's second law of motion. The abrupt area change model controls losses through these valves as the cross-sectional flow area varies with valve assembly movement. The motor and servo valve use differential equations to control valve movement. These two valves include the options to use the abrupt area change model to calculate losses across the valve or to use flow coefficients (C_v) specified by the user. The C_vs are converted to energy loss coefficients within the numerical scheme (see Equation (7.697)).

Valves are modeled as junction components. The types of valves are defined as follows.

7.8.2.1   Trip Valve

The operation of a trip valve is solely dependent on the trip selected. With an appropriate trip, an abrupt full opening or full closing of the valve will occur. A latch option is also included for latching the valve in the open or closed position.

AREVA Inc.

Realistic Large Break LOCA Methodology for Pressurized Water Reactors
Topical Report

EMF-2103NP
Revision 3

Page 7-302

7.8.2.2 Check Valve

The operation of a check valve can be specified to open or close by static differential pressure, to open by static differential pressure and close by flow reversal, or to open by static differential pressure and close by dynamic differential pressure.

All of the check valves will be opened based on static differential pressure across the junction according to

$$
\begin{aligned}
\left(P_K + \Delta P_{K_g}\right) - \left(P_L + \Delta P_{L_g}\right) - PCV &> 0, \text{ valve opens} \\
&= 0, \text{ remains as previously defined}
\end{aligned}
\tag{7.685}
$$

where:

P_K, P_L =   junction from and to volume thermodynamic pressures;

$\Delta P_{K_g}, \Delta P_{L_g}$ =   static pressure head due to gravity; and

PCV   =   back pressure required to close the valve (user input).

For a static pressure controlled check valve, the valve will open if Equation (7.685) becomes positive and will close if Equation (7.685) becomes negative. If Equation (7.685) is zero, the valve will remain as previously defined.

For a flow controlled check valve, the valve will open if Equation (7.685) is positive and will close only if a flow reversal occurs such that

$$
\left(\alpha_f \rho_f v_f + \alpha_g \rho_g v_g\right)_j < 0
\tag{7.686}
$$

The terms α_f and α_g are the junction liquid and vapor volume fractions, respectively; ρ_f and ρ_g are the junction liquid and vapor densities, respectively; and v_f and v_g are the junction liquid and vapor velocities, respectively.

For a dynamic pressure controlled check valve, the valve opens if Equation (7.685) is greater than zero. Once the valve is open, the forces due to pressure differential and momentum hold the valve open until

$$\left(P_K + \Delta P_{K_g}\right) - \left(P_L + \Delta P_{L_g}\right) + GC - PCV \quad < 0, \text{ valve closes}$$

$$= 0, \text{ remains as previously defined}$$

where:

$$GC = \frac{1}{2}\left(\alpha_f \rho_f v_f \left|v_f\right| + \alpha_g \rho_g v_g \left|v_g\right|\right)_j \qquad (7.687)$$

Flow and dynamic pressure controlled valves exhibit a hysteresis effect with respect to the forces opening and closing the valve. The static pressure controlled valve, however, has no hysteresis effect.

All check valves may be initialized as either open or closed. Leakage is also allowed if the valve is closed, and the abrupt area change model may be used to calculate the valve form losses.

7.8.2.3   Inertial Valve

This valve models the motion of the valve flapper assembly in an inertial-type check valve. The abrupt area change model is used to calculate kinetic form losses, assuming that the area between the flapper and the valve seat behaves as an orifice whose area changes in time as a function of the inertial valve geometry.

The motion of the flapper about the shaft axis is given by Newton's second law (angular version) as

$$\Sigma \tau = I \dot{\omega} \qquad (7.688)$$

where:

τ = torque;

I = moment of inertia;

$\dot{\omega}$ = angular acceleration;

ω = angular velocity = $\dot{\Theta}$, counter-clockwise motion is positive; and

Θ = disc angular position, $\Theta = 0$ is fully closed.

Torque is defined as r times F; the cross product of a force F and the distance from the hinge pivot point, r, to the force. Each particle of a rotating body has kinetic energy. Kinetic energy is defined as $0.5mV^2$ where m is the mass and V is the velocity. Since $V = r\omega$ where r is the distance to the particle and ω is the angular velocity, the kinetic energy of the particle is $0.5mr^2\omega^2$. The total kinetic energy of a rotating body is the sum of the kinetic energy of all its particles. Since the angular velocity of all particles is the same, ω can be factored out to give:

$$\text{Kinetic Energy} = 0.5(\Sigma m_i r_i^2)\omega^2 \tag{7.689}$$

The term in parentheses is known as the moment of inertia, I.

A diagram of an inertial valve is shown in Figure 7-33. The valve flapper disc resides in a pipe and swings on a hinge pin. The valve is used to prevent backflow. The flapper position depends on factors such as: flapper mass, gravity vector, moment of inertia, distance from the hinge pin to the center of mass, flapper area, pressure difference across the valve, viscous and Coulomb friction between the flapper and the pin, and lift and drag forces on the flapper. Only torque due to differential pressure, T_{DP}, Coulomb friction, T_F, and weight, T_W, are included in this model, where:

$$\tau_{DP} = (P_K - P_L)A_P L \tag{7.690}$$

$$\tau_F = \Delta P_F A_R L \tag{7.691}$$

$$\tau_W = -MgL\sin\Theta \tag{7.692}$$

P_K = pressure in the hydraulic cell on the left;

P_L = pressure in the hydraulic cell on the right;

A_P = projected area of the disc;

L   =   user-input flapper moment arm length from the hinge to the center of inertia;

A_R =   area of disc $= \pi R_v^2$;

R_v =   user-input disc radius;

ΔP_F =   user-input value of minimum pressure difference across the valve required to initiate motion (cracking pressure);

g   =   acceleration due to gravity; and

M   =   mass of the flapper.

Figure 7-33 Diagram of Inertial Valve
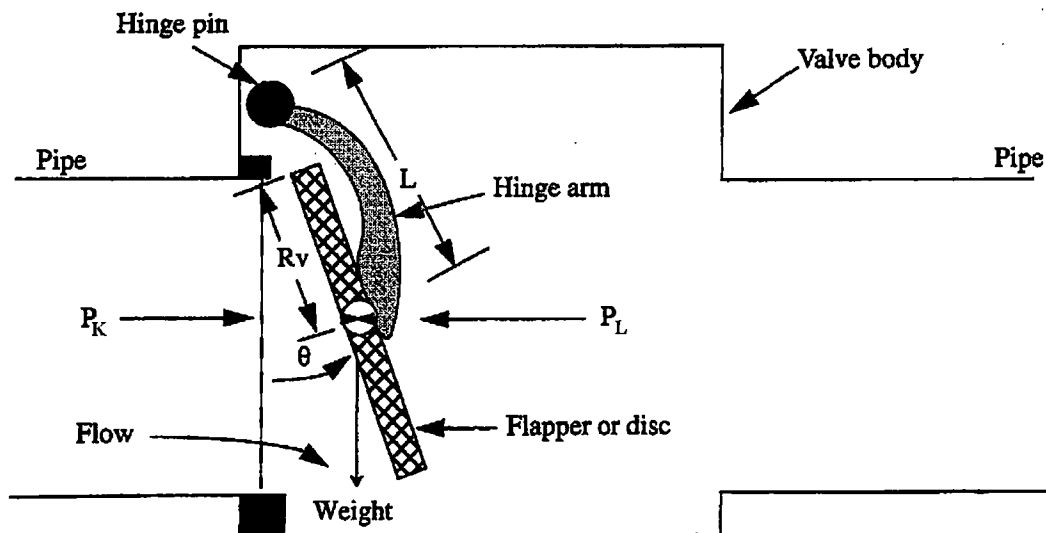
The differential pressure across the flapper faces decreases as the valve flapper swings into the hydraulic cell on the right. To approximate this decrease, the projected area is used in the T_{DP} term (see Figure 7-34). The projected area of a circle is an ellipse with an area of $\pi R_v b$, since $b = R_v \sin(\phi)$ where ϕ is 90 − Θ.

Figure 7-34 Two Views of a Partially Open Flapper Valve

Front view   Side view

$$A_P = \pi R_v^2 \sin(90 - \Theta) = \pi R_v^2 \cos\Theta \tag{7.693}$$

The angular acceleration is solved from Equation (7.688):

$$\dot\omega^n = \frac{\sum \tau}{I} \tag{7.694}$$

and the new time flapper velocity and angle are:

$$\omega^n = \omega^{n-1} + \dot\omega^n \Delta t \tag{7.695}$$

The new time angle is calculated from the angle at the previous time step and the average velocity during the time step.

$$\Theta^n = \Theta^{n-1} + 0.5\left(\omega^{n-1} + \omega^n\right)\Delta t \tag{7.696}$$

where superscript n stands for new time and n–1 indicates the previous time step value.

In order to obtain the correct velocity to compare with the sonic speed at the valve the vena-contracta is considered. The effective flow area is C_c times the actual open area.

C_c =   contraction coefficient effective area/actual open area.

Table 7-9 gives the table of contraction coefficients. C_c is less than one and has the effect of increasing the code calculated velocity in the valve opening. Also shown is the loss coefficient which the abrupt area change model should automatically calculate for the code users.

Table 7-9 Contraction Coefficient Table

Area Fraction Open	0.0	0.1	0.2	0.3	0.4	0.5	0.6	0.7	0.8	0.9	1.0
C_c	0.617	0.624	0.632	0.643	0.659	0.681	0.712	0.755	0.813	0.892	1.0
K_{LOSS}	0.38	0.36	0.34	0.31	0.27	0.22	0.16	0.10	0.005	0.02	0.0

Several options are allowed with the use of this valve, such as specifying minimum and maximum flapper angular positions when the valve is closed, specifying latch or no latch options, and specifying leakage area.

7.8.2.4 Motor Valve

This valve model has the capability of controlling the junction flow area between two control volumes as a function of time. The operation of the valve is controlled by two trips; one for opening the valve and a second for closing the valve. A constant rate parameter controls the speed at which valve area changes. The motor valve area variation can also be specified using a general table. When the general table is specified, the constant rate parameter controls the valve stem position and the general table relates the stem position to the valve flow area. Conversely, when the general table is not specified, the constant rate parameter controls the rate of change in valve area.

The abrupt change model is used to calculate kinetic form losses with respect to the valve area. However, if the normalized valve flow area has a value less than 1.0×10^{-10}, the valve is assumed to be closed.

A second option allowed for the motor valve is the specification of valve flow coefficients, C_v. These coefficients may be specified using a general table of C_v versus normalized stem position and the smooth junction option must be specified. The conversion of C_v to an energy loss coefficient, K, is done in the numerical scheme using the formula

$$K = 2\frac{A_{valve}^2}{C_v^2 \rho_o} \tag{7.697}$$

where A_{valve} is the input value of junction area, and $\rho_o = 999.09$ kg/m^3 is the density of water at 288.71 K (60.0 °F).

7.8.2.5   Servo Valve

The servo valve operation is similar to that for the motor valve. However, the valve area or stem position is controlled by a control variable rather than by a specified rate parameter. The servo valve also has the same options as the motor valve.

7.8.2.6   Relief Valve

For thermal-hydraulic analysis of overpressure transients, it is necessary to simulate the effects of relief valves. In particular, it is desirable to model the valve dynamic behavior, including simulation of valve flutter and hysteresis effects.

To assist in understanding the relief valve model, three schematics of a typical relief valve are shown in Figures 7-35 through 7-37. The three schematics represent the valve in the closed (Figure 7-35), partially open (Figure 7-36), and fully open (Figure 7-37) modes, respectively. In the schematics the seven main components of a relief valve are shown, which are the valve housing, inlet, outlet, piston, rod assembly, spring, bellows, and valve adjusting ring assembly.

The numerical model of the valve simply approximates the fluid forces acting on the valve piston and the valve reaction to these forces. The model of the fluid forces is based on a quasi-steady-state form of the impulse momentum principle, and the valve reaction force is based on Newton's second law of motion.

A qualitative understanding of the operation of the relief valve can be gained by referring again to Figures 7-35 through 7-37. If the valve inlet pressure is low, the valve is closed, as shown in Figure 7-35. As the inlet pressure increases, the valve piston will remain closed until the force of the upstream pressure on the valve exceeds the set point forces. The set point forces are the combined forces of the piston and rod assembly weight, the valve spring, the atmospheric pressure inside the bellows, and the downstream back pressure around the outside of the bellows. Once the set point forces

are exceeded, the valve piston will begin to lift. Upon opening, the upstream fluid will begin to expand through the opening into the valve ring region. This initial expansion occurs through the angle α_o, and the flow changes direction through an average angle, Θ_o, as shown in Figure 7-35. As the flow accelerates, the momentum effects of the expansion and change in flow direction exert a thrust on the valve piston, causing the valve to open further. As the valve partially opens, the angle of expansion decreases to α_1 and the change in flow direction increases to Θ_1, as shown in Figure 7-36. This effect, in turn, further increases the thrust on the valve piston, causing it to fully open, as shown in Figure 7-37. As these processes occur, the valve reaction forces and fluid momentum forces vary in such a manner that the valve will not close until the upstream pressure decreases significantly below the valve set point pressure. In this respect, a hysteresis effect is observed that is characteristic of relief valves.

The relief valve model consists of a set of equations designed to approximate the behavior described above. In implementing the model, the dynamic behavior of the fluid is calculated at each time step by the hydrodynamic solution scheme. The resultant phasic velocities and thermodynamic properties are then used to solve a quasi-steady equation approximating the fluid forces on the valve piston. The valve dynamic reaction forces are then calculated, and the new time valve piston speed and position are estimated.

AREVA Inc.

EMF-2103NP
Revision 3

Realistic Large Break LOCA Methodology for Pressurized Water Reactors
Topical Report

Page 7-310

Figure 7-35 Schematic of a Typical Relief Valve in the Closed Position
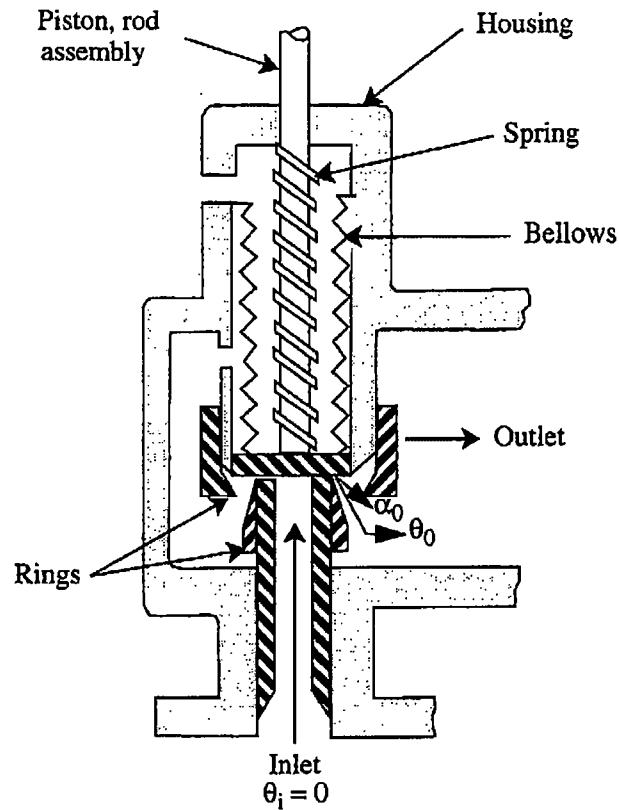
The relief valve model is formulated, applying D'Alembert's principle in which the forces acting on the face of the valve piston are balanced, for which the valve reaction forces can be written as

$$\text{(reaction forces)} = F_R = m_v a_{v,x} + B(v_{v,x} - v_{housing}) + K_s x \tag{7.698}$$

where:

m_v = mass of the valve mechanism that is in motion (i.e., the valve piston, rod assembly combined with the spring and bellows);

$a_{v,x}$ = valve assembly acceleration in the x direction;

B = damping coefficient;

$v_{v,x}$ = velocity of the valve mechanism in the x direction;

$V_{housing}$ = velocity of the valve housing = 0;

K_s = spring constant; and

x = piston position (i.e., x coordinate).

The positive x direction is assumed to be in the direction of fluid flow at the valve inlet. The fluid forces, F_F, can be formulated by summing the forces acting over the surfaces of the fluid flow channel such that

$$F_F = \left(P_i A_D\right)_x - \left(P_a A_{Ba}\right)_x - \left(P_o A_{Bo}\right) - \left(P_e A_e\right)_x - F_R \tag{7.699}$$

where:

FR = reaction forces;

Pi = valve inlet pressure;

AD = valve piston face area exposed to the inlet flow stream;

Pa = atmospheric pressure inside the bellows;

ABa = valve piston area inside the bellows;

Po = valve back pressure outside the bellows;

ABo = valve piston area outside the bellows;

Ae = valve ring exit area; and

Pe = valve ring exit pressure.

and where the subscript x denotes that the force component is in the x direction.

AREVA Inc.
EMF-2103NP
Revision 3
Realistic Large Break LOCA Methodology for Pressurized Water Reactors
Topical Report
Page 7-312

Figure 7-36 Schematic of a Typical Relief Valve in the Partially Open Position
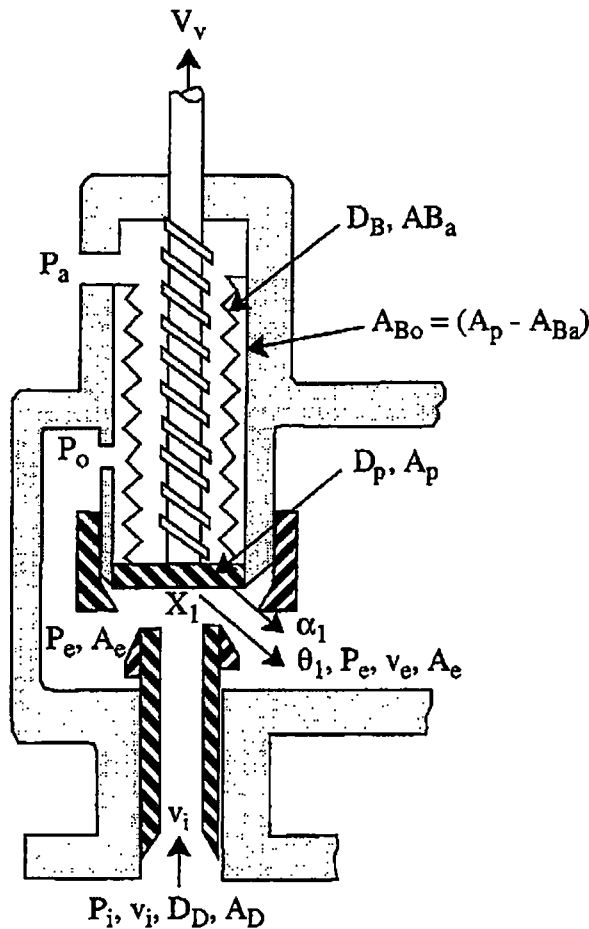
Figure 7-37 Schematic of a Typical Relief Valve in the Fully Open Position
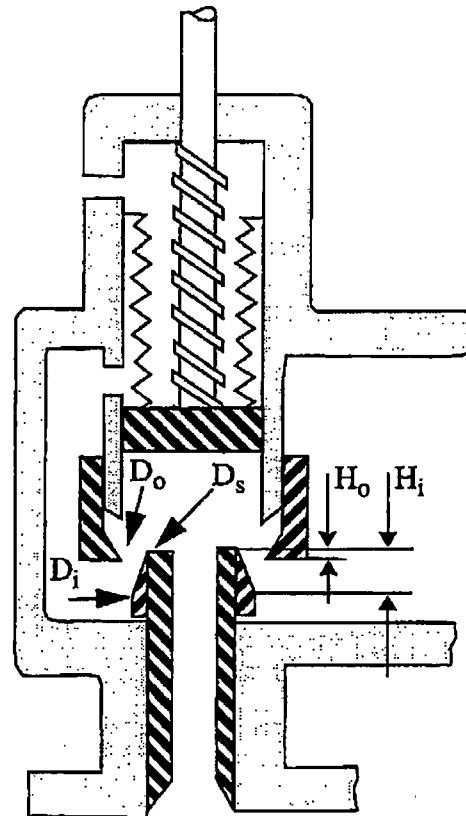
The valve back pressure outside the bellows and valve ring exit pressure are calculated from the density change from the throat to the outlet and ring exit.

The sonic speed (a) is expressed by

$$a^2 = \left(\frac{dP}{d\rho}\right)_s \tag{7.700}$$

The pressure variation is related to the density variation as

$$dP = a^2 dr \tag{7.701}$$

Since the isentropic compressibility is expressed by

$$\kappa_s = \frac{1}{\rho}\left(\frac{d\rho}{dP}\right)_s \tag{7.702}$$

the pressure variation is related to the density variation as

$$d\rho = \kappa_s \rho dP \tag{7.703}$$

The Bernoulli equation gives

$$dP = -\frac{\rho}{2}d\mathbf{v}^2 \tag{7.704}$$

The mass flux is expressed as

$$G = \rho v \tag{7.705}$$

Consequently,

$$dG^2 = \rho^2 dv^2 + v^2 d\rho^2 \tag{7.706}$$

Algebraic manipulations result in

$$d\rho = \frac{\kappa_s}{2}\left[dG^2 - 2v^2\rho d\rho\right] \tag{7.707}$$

Thus, it is obtained

$$d\rho = -\left[\frac{\kappa_s}{1.0 - \kappa_s \rho v^2}\right]\frac{dG^2}{2} \tag{7.708}$$

From the above equation and using $G = \rho v$, the variations of density from the throat to the outlet and to the ring exit can be calculated as

$$\Delta\rho_o = -\left[\frac{\kappa_s}{1.0 - \kappa_s G_{th} v_{th}}\right]\frac{\left(G_o^2 - G_{th}^2\right)}{2} \tag{7.709}$$

$$\Delta\rho_e = -\left[\frac{\kappa_s}{1.0 - \kappa_s G_{th} v_{th}}\right]\frac{\left(G_e^2 - G_{th}^2\right)}{2} \tag{7.710}$$

The pressures at the outlet and ring exit can be obtained as

$$P_o = P_{th} - a^2\left[\frac{\kappa_s}{1.0 - \kappa_s G_{th} v_{th}}\right]\frac{\left(G_o^2 - G_{th}^2\right)}{2} \tag{7.711}$$

$$P_e = P_{th} - a^2 \left[\frac{\kappa_s}{1.0 - \kappa_s G_{th} v_{th}} \right] \frac{\left(G_e^2 - G_{th}^2 \right)}{2} \tag{7.712}$$

The pressure at the throat is obtained from the Bernoulli equation using the inlet pressure and flow conditions.

Since the fluid is flowing through a channel that both expands and changes direction, the fluid undergoes a change in momentum expressed by the impulse momentum principle as

$$F_F = \Delta \left(m v \right) = \dot{m}_F \left(v_{e,x} - v_{i,x} \right) \tag{7.713}$$

where:

$\dot{m}_F$ =   mass flow rate of the fluid through the valve;

$v_{e,x}$ =   fluid velocity exiting through the rings; and

$v_{i,x}$ =   fluid velocity entering the valve inlet.

Balancing the forces by combining Equations (7.698) through (7.713) gives

$$m_v a_{v,x} + B v_{v,x} + K_s x = -P_a A_{Ba} - P_o A_{Bo} - P_e A_e \cos\Theta - \dot{m}_F \left(v_e \cos\Theta - v_i \right) + P_i A_D \tag{7.714}$$

The valve acceleration can be expressed in terms of the valve velocity as

$$a_{v,x} = \frac{dv_{v,x}}{dt} + g \tag{7.715}$$

where g is the acceleration of gravity.

Combining Equations (7.714) and (7.715), treating the velocity damping term and spring force position terms implicitly, and integrating over the time step gives

$$m_v \left(v_{v,x}^{n+1} - v_{v,x}^n \right) + B v_{v,x}^{n+1} dt + K_s x^{n+1} dt + m_v g dt = \left[P_i^n A_D - P_a A_{Ba} - P_o^n A_{Bo} \right.$$
$$\left. - P_e^n A_e \cos\Theta_e^n - \dot{m}_F \left(v_e^n \cos\Theta_e^n - v_i^n \right) \right] dt \tag{7.716}$$

where n and n+1 represent the old and new time terms, respectively.

The position term, x^{n+1}, can be written in terms of the valve velocity by considering that

$$v_{v,x} = \frac{dx}{dt} \tag{7.717}$$

If Equation (7.717) is integrated over the time step, then

$$x^{n+1} = x^n + v_{v,x}^{n+1} dt \tag{7.718}$$

If the valve set point pressure is equated to $K_s x_o$, then combining Equations (7.716) and (7.718) and both adding and subtracting the term $K_s x_o$ gives the numerical form of the relief valve model,

$$\begin{aligned}
m_v \left(v_{v,x}^{n+1} - v_{v,x}^n\right) + \left[(B + K_s dt) v_{v,x}^{n+1} + K_s \left(x^n - x_o\right) + m_v g\right] dt \\
= -K_s x_o dt + \left[P_i^n A_D - P_a A_{Ba} - P_e^n A_{Bo} - P_e^n A_e \cos \Theta_e^n - \dot{m}_F^n \left(v_e^n \cos \Theta_e^n - v_i^n\right)\right] dt
\end{aligned} \tag{7.719}$$

where the sign of the gravity term, g, is dependent on the valve orientation. For example, if the valve is oriented upward (i.e., +x is upward), then the gravity term is expressed as $g = -|g|$.

In the numerical scheme, Equation (7.719) is solved for the new time valve piston velocity, v_v^{n+1}, in terms of the current time terms with superscript n. The terms required to model the valve geometry and the valve damping, spring, and back pressure forces are input to the code.

The characteristic relief valve hysteresis effects are inherent in the formulation of Equation (7.719). For example, if the valve is closed, then all velocity terms are zero and $x = x_o$. Therefore, acceleration of the valve piston in the positive x direction cannot occur until the upstream force $P_i A_D$ exceeds the spring set point and valve weight. Once the valve opens and the fluid accelerates, the forces due to the change in fluid momentum aid in holding the valve open. Therefore, the valve cannot close until the combined fluid pressure and momentum terms decrease significantly below the set point forces. Hence, the desired hysteresis is incorporated in the model.

7.8.2.7   Pilot Operated Safety Valve
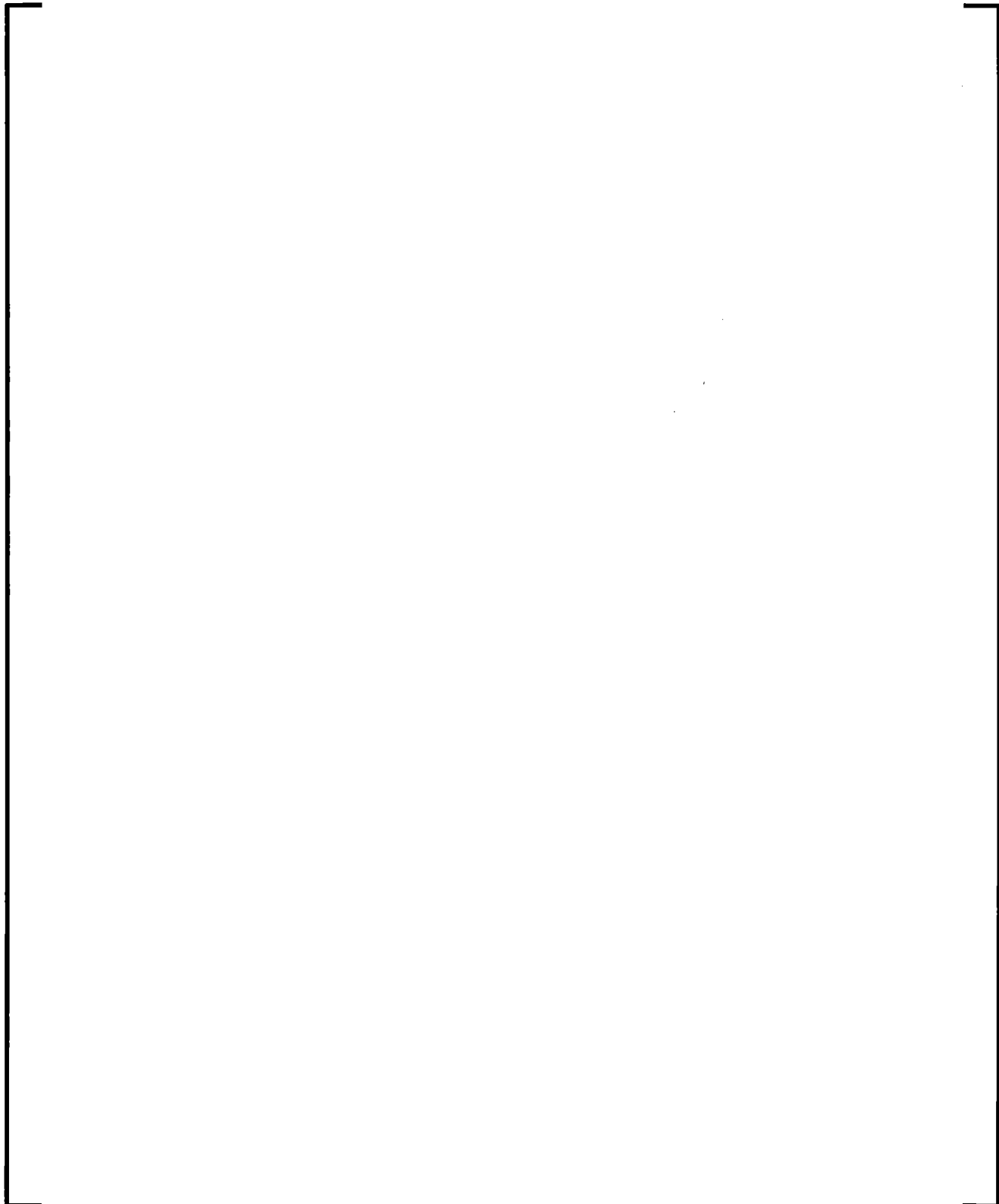
7.8.3   Separator

The ideal separator component model is from RELAP5/MOD3 (Reference 7-114). It is a non-mechanistic or black-box model consisting of a special volume with junction flows, as pictured in Figure 7-38. A steam-water inflowing mixture is separated by defining the quality of the outflow streams using empirical functions. No attempt is made to model the actual separation process from first principles.

Figure 7-38 Typical Separator Volume and Junctions

J_1-Vapor outlet junction

Volume K

J_3-Separator inlet junction

J_2-Liquid fall back junction
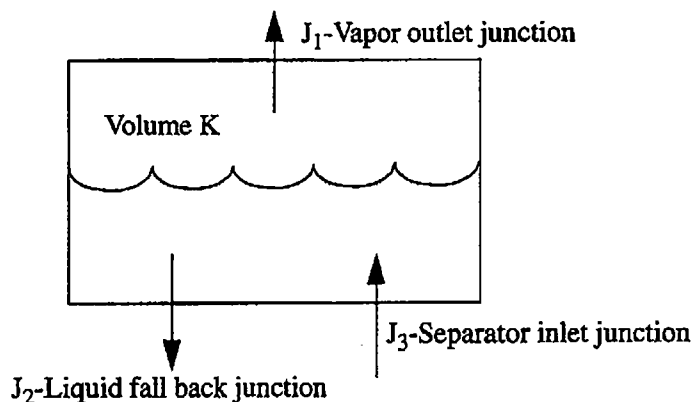
The separator vapor outlet performance is defined by means of a special function for the vapor void fraction at J_1. The donored junction vapor void fraction used to flux mass through the steam outlet is related to the vapor void fraction in the separator volume using the curve in Figure 7-39. For separator volume void fractions above the value of VOVER (an input parameter), perfect separation is assumed and pure vapor is fluxed out junction J_1. For separator volume void fractions less than VOVER, a two-phase mixture is fluxed out. The VOVER parameter governs the vapor void fraction of the outflow. If VOVER is small, the vapor outflow corresponds to an ideal separator. If VOVER equals 1.0, the vapor outlet junction behaves as a normal junction; and the

vapor outlet junction void fraction is equal to the separator volume average void fraction. A limit is placed on the vapor void fraction of the outflow, in that at most 90% of the vapor present in the separator volume can be fluxed out junction J_1. This limit is used to prevent over extraction of vapor.

The flow of separator liquid through the fallback junction is modeled in a manner similar to the steam outlet except that pure liquid outflow is assumed when the volume liquid fraction is greater than the value of VUNDER (see Figure 7-39). As with the steam outlet, a 90% extraction limit is placed on the liquid drain. Normal donored fluxes are used for the separator inlet junction. Although the void fractions used to flux mass and energy from the separator volumes are modified, the normal junction momentum equations are used to calculate the flow velocities.

Figure 7-39 Donor Junction Voids for Outflow
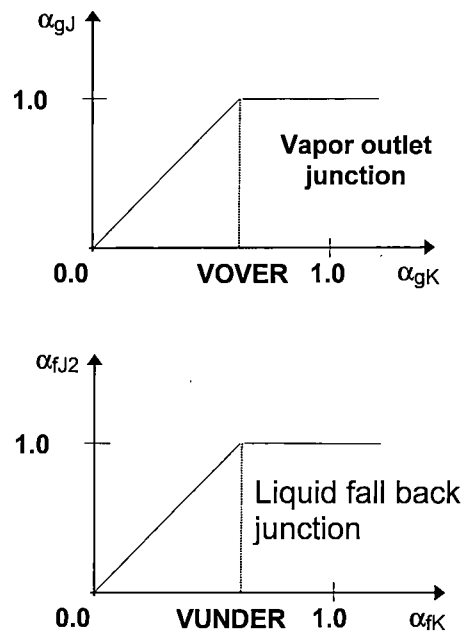
7.9   S-RELAP5 Fuel Models

Revision 3 of the RLBLOCA EM uses only the COPERNIC fuel model in Reference 7-107, which is presented in this document.

AREVA Inc.

EMF-2103NP
Revision 3

Realistic Large Break LOCA Methodology for Pressurized Water Reactors
Topical Report

Page 7-319

7.9.1   General Features of Fuel Rod Model Implementation

AREVA Inc.

EMF-2103NP
Revision 3

Realistic Large Break LOCA Methodology for Pressurized Water Reactors
Topical Report

Page 7-320

AREVA Inc.

EMF-2103NP
Revision 3

Realistic Large Break LOCA Methodology for Pressurized Water Reactors
Topical Report

Page 7-321
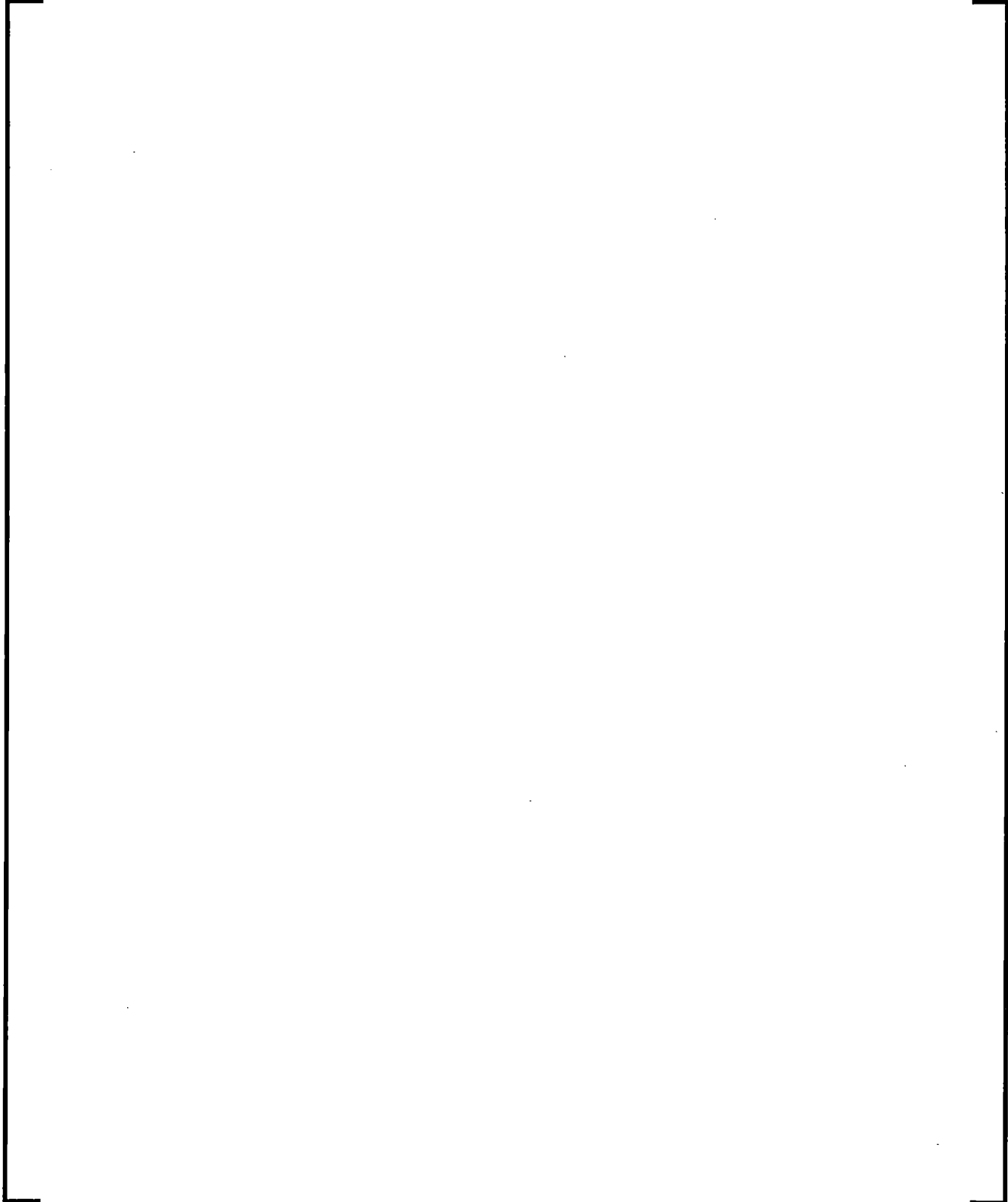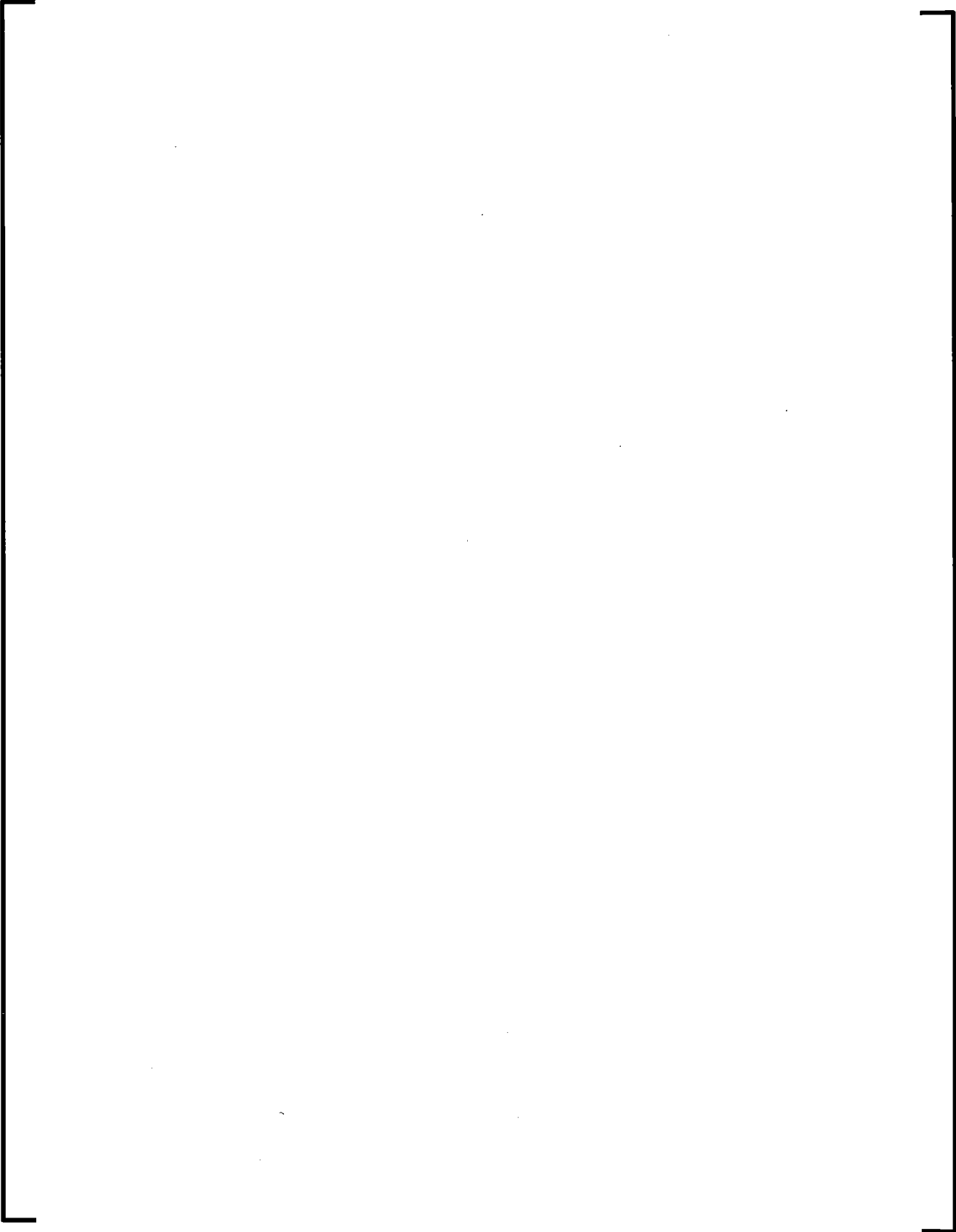
7.9.2   Fuel Rod Model Common Output Features

AREVA Inc.

EMF-2103NP
Revision 3

Realistic Large Break LOCA Methodology for Pressurized Water Reactors
Topical Report

Page 7-322

7.9.2.1   Fuel Rod Related Minor Edit Plot Variables

AREVA Inc.

EMF-2103NP
Revision 3

Realistic Large Break LOCA Methodology for Pressurized Water Reactors
Topical Report

Page 7-323

AREVA Inc.

Realistic Large Break LOCA Methodology for Pressurized Water Reactors
Topical Report

EMF-2103NP
Revision 3
Page 7-324
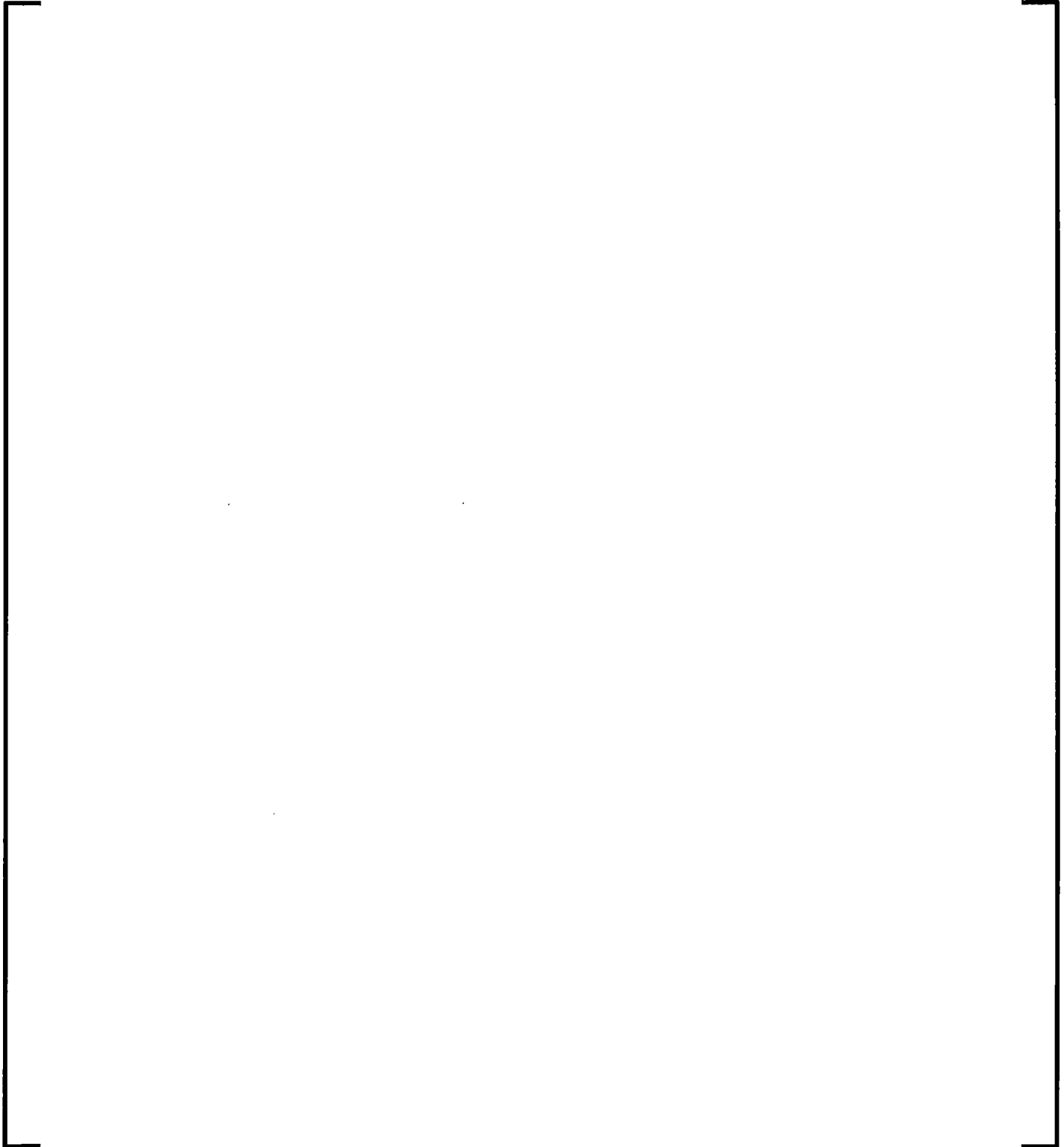
7.9.2.2 Fuel Rod Related Major Edit Summary Output Quantities

AREVA Inc.

EMF-2103NP
Revision 3

Realistic Large Break LOCA Methodology for Pressurized Water Reactors
Topical Report

Page 7-325

7.9.2.3 Fuel Rod Related Uncertainty Multipliers

7.9.3 S-RELAP5/COPERNIC Fuel Model
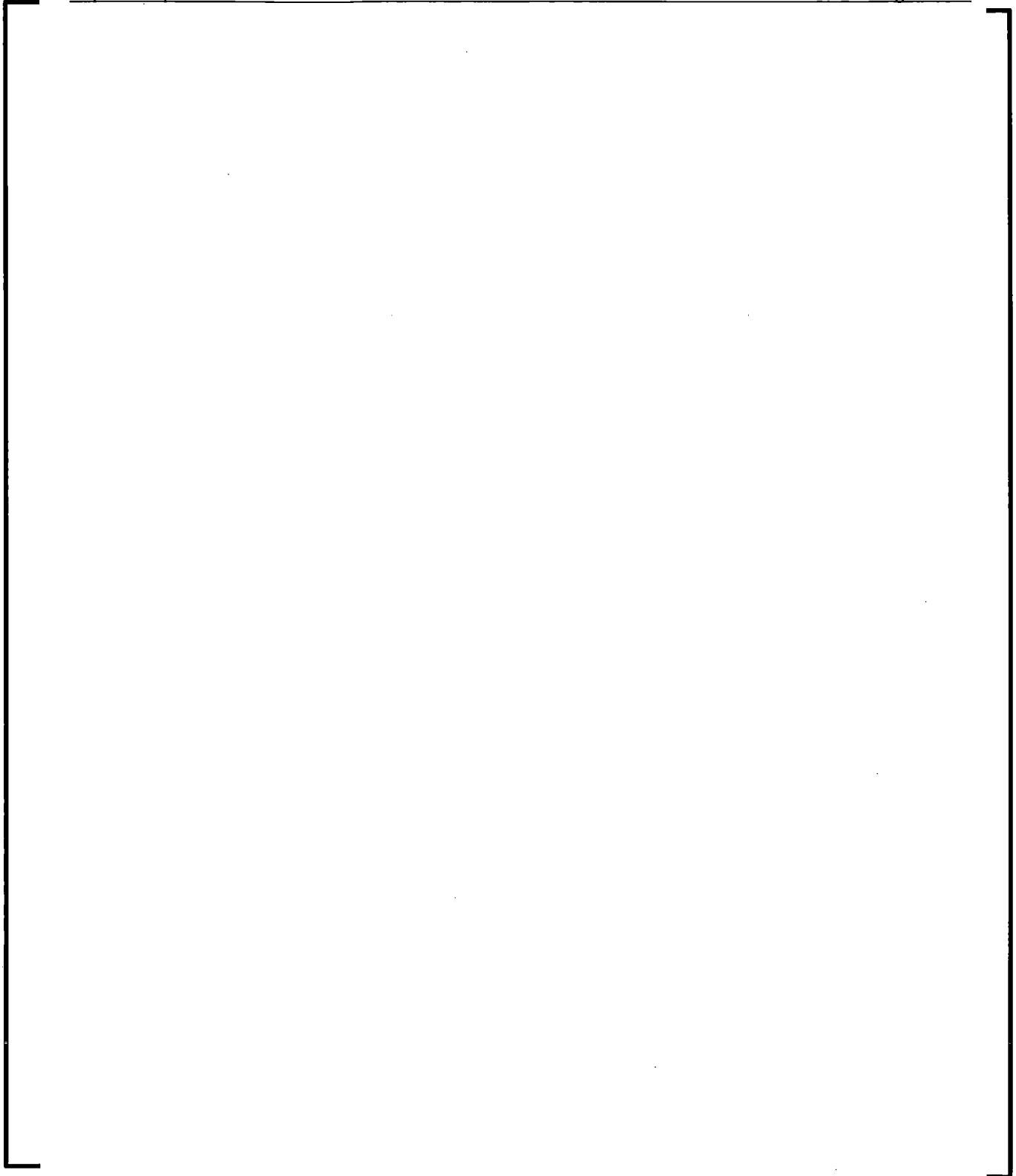
7.9.3.1   COPERNIC Fuel Deformation Models

7.9.3.2   COPERNIC Gap Conductance Model

AREVA Inc.

EMF-2103NP
Revision 3

Realistic Large Break LOCA Methodology for Pressurized Water Reactors
Topical Report

Page 7-328

7.9.3.3 Clad Ballooning, Rupture and Area Adjustment Models

AREVA Inc.

EMF-2103NP
Revision 3

Realistic Large Break LOCA Methodology for Pressurized Water Reactors
Topical Report

Page 7-329
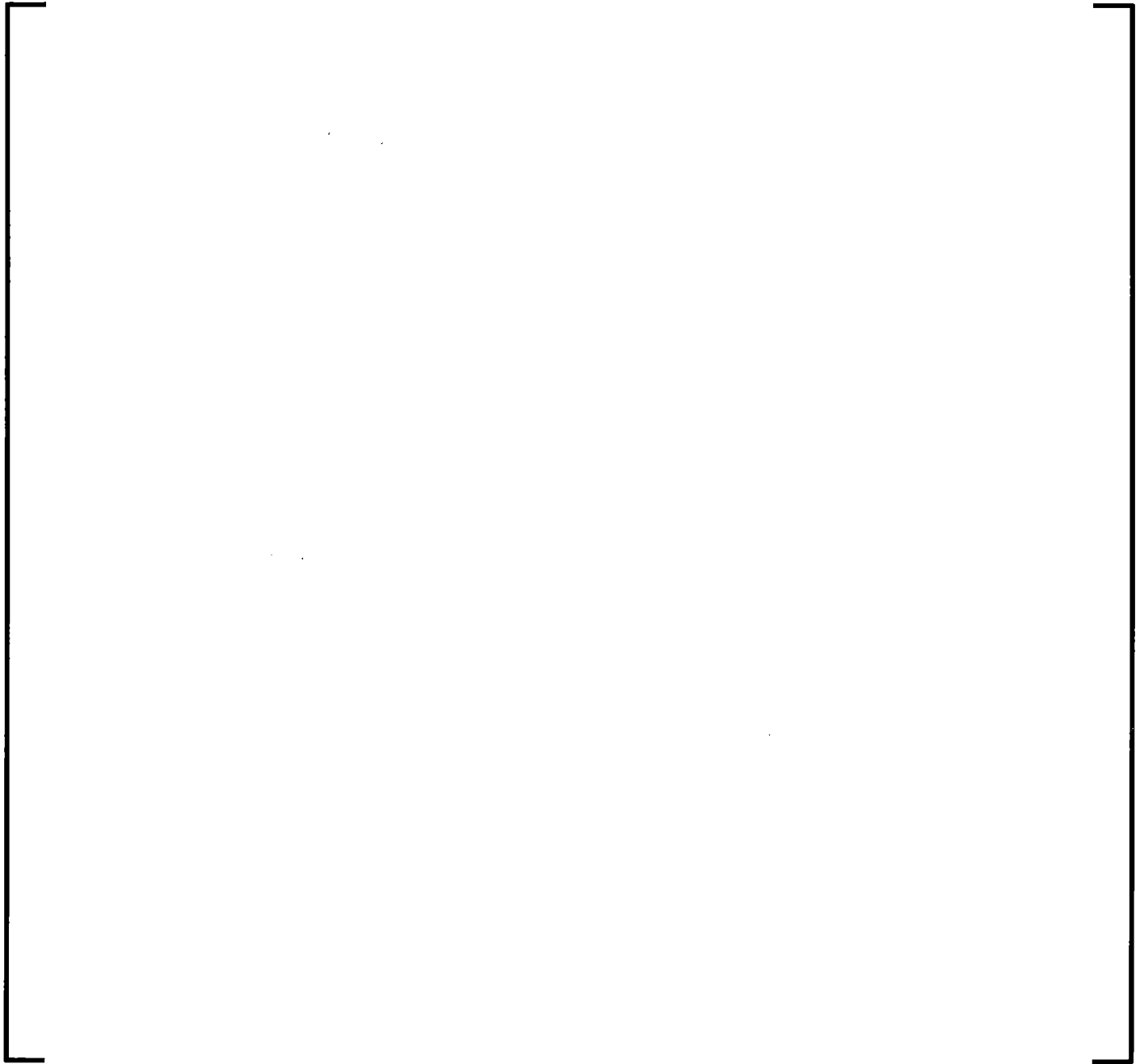
7.9.3.3.1   Statistical Treatment of M5 Radial Swelling, Rupture, and Fuel Relocation

AREVA Inc.

Realistic Large Break LOCA Methodology for Pressurized Water Reactors
Topical Report

EMF-2103NP
Revision 3

Page 7-330

AREVA Inc.

Realistic Large Break LOCA Methodology for Pressurized Water Reactors
Topical Report

EMF-2103NP
Revision 3

Page 7-331

AREVA Inc.

EMF-2103NP
Revision 3

Realistic Large Break LOCA Methodology for Pressurized Water Reactors
Topical Report

Page 7-332

Figure 7-40 Packing Factor Data with Quadratic Fitting Function

AREVA Inc.

EMF-2103NP
Revision 3

Realistic Large Break LOCA Methodology for Pressurized Water Reactors
Topical Report

Page 7-334

Table 7-10 Packing Factors and Sources

AREVA Inc.

EMF-2103NP
Revision 3

Realistic Large Break LOCA Methodology for Pressurized Water Reactors
Topical Report

Page 7-335

AREVA Inc.

EMF-2103NP
Revision 3

Realistic Large Break LOCA Methodology for Pressurized Water Reactors
Topical Report

Page 7-336
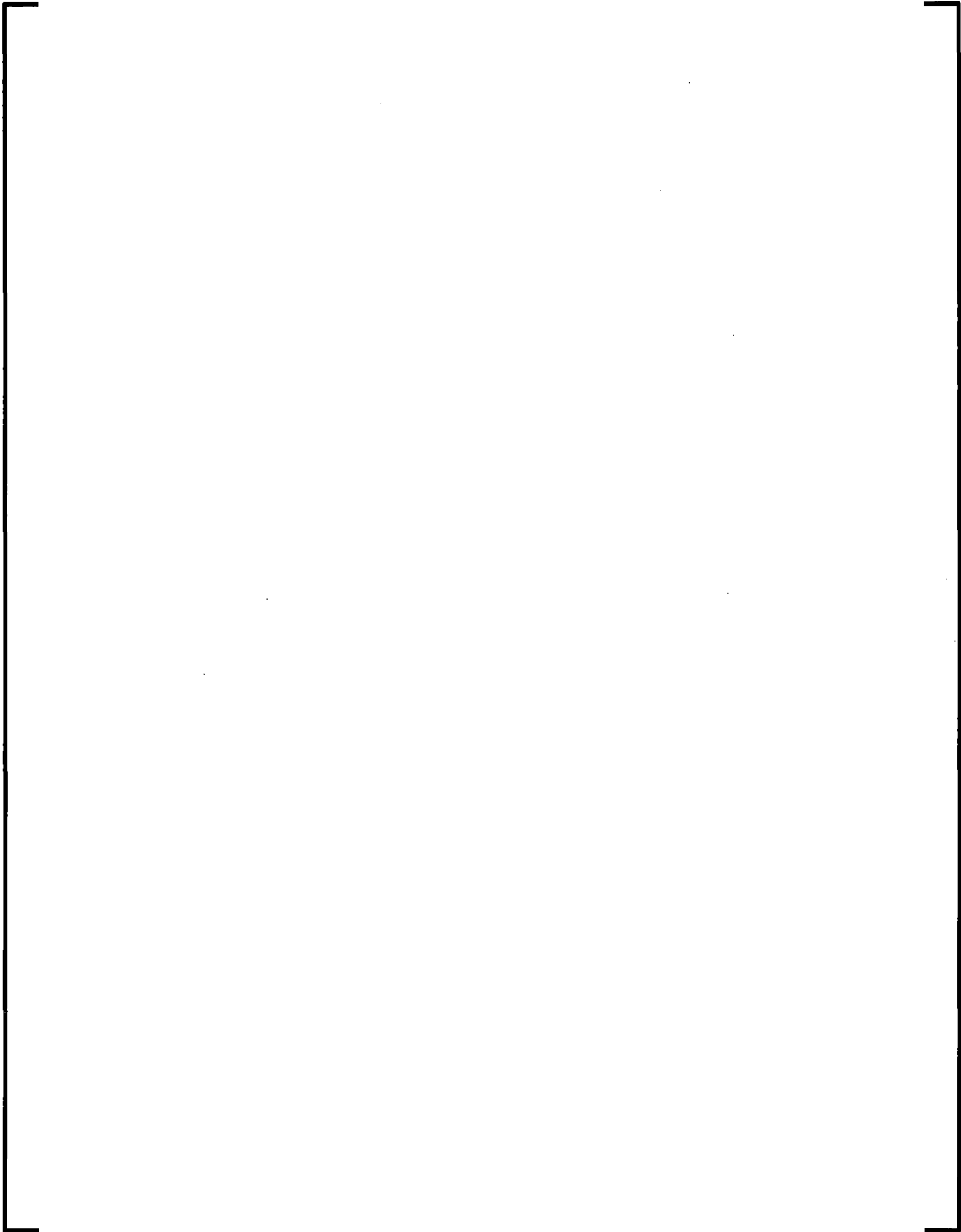
7.9.3.3.2 Subchannel Flow and Heat Transfer Evaluations for the Ballon and Rupture Region

AREVA Inc.

EMF-2103NP
Revision 3

Realistic Large Break LOCA Methodology for Pressurized Water Reactors
Topical Report

Page 7-337

[

]

AREVA Inc.

Realistic Large Break LOCA Methodology for Pressurized Water Reactors
Topical Report

EMF-2103NP
Revision 3

Page 7-339
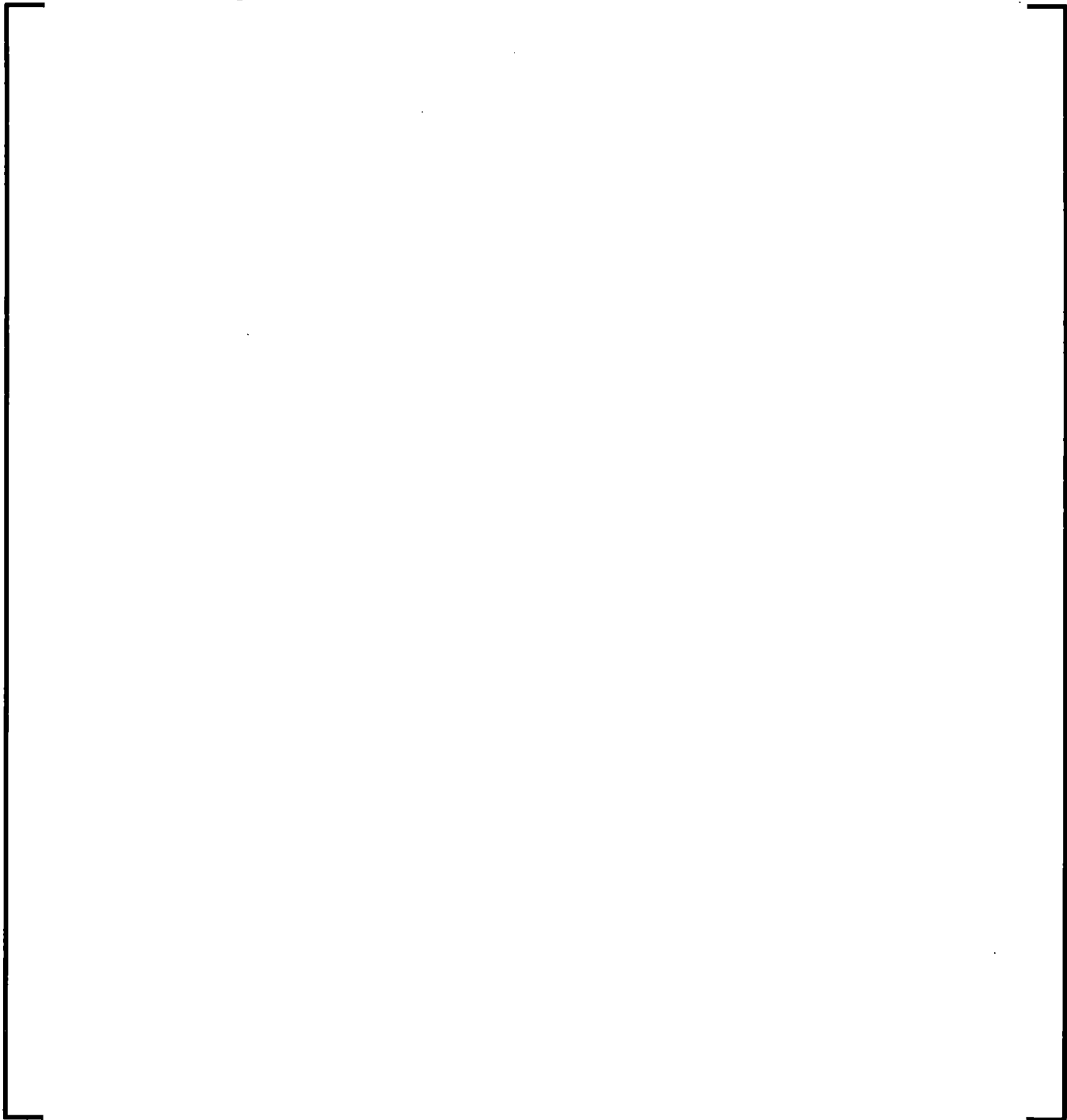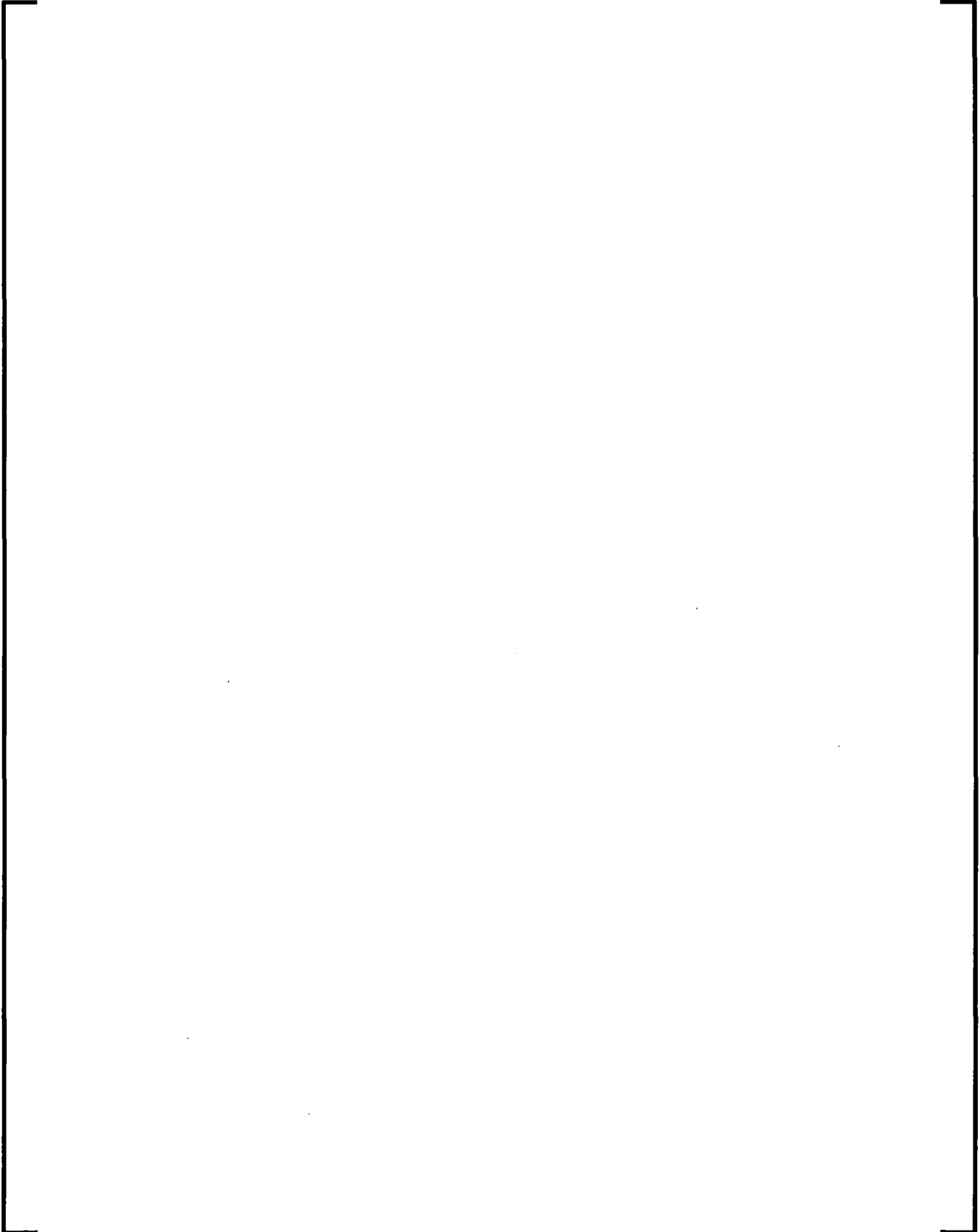
Figure 7-41 A schematic of the sub-channel cooling model

AREVA Inc.

EMF-2103NP
Revision 3

Realistic Large Break LOCA Methodology for Pressurized Water Reactors
Topical Report

Page 7-340

AREVA Inc.

EMF-2103NP
Revision 3

Realistic Large Break LOCA Methodology for Pressurized Water Reactors
Topical Report

Page 7-340

AREVA Inc.

EMF-2103NP
Revision 3

Realistic Large Break LOCA Methodology for Pressurized Water Reactors
Topical Report

Page 7-341

Figure 7-42 Comparison of Cladding Temperatures with (ruptured rod) and without (unruptured rod) SCC Model Applied

7.9.3.4   Material Thermal Properties
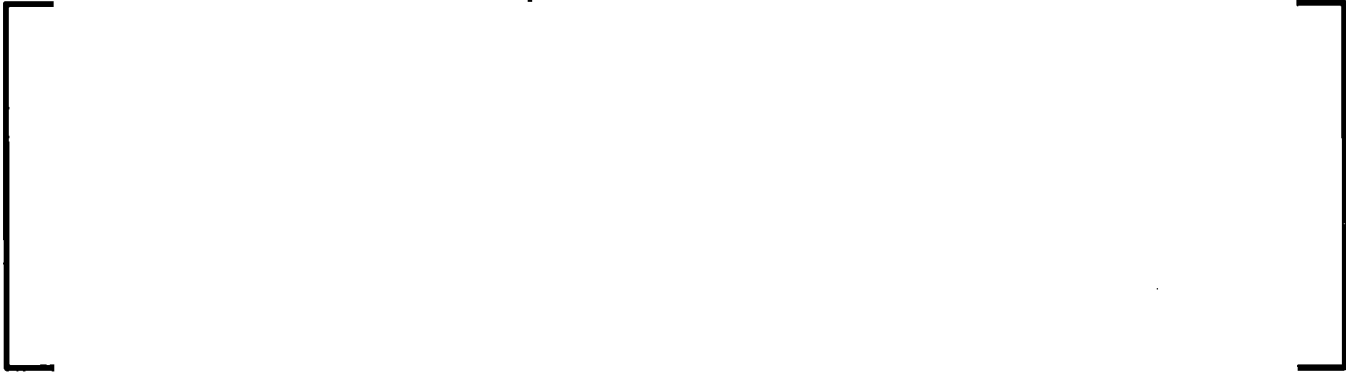
7.9.3.5   Zirconium/Steam Reaction Kinetics

AREVA Inc.

EMF-2103NP
Revision 3

Realistic Large Break LOCA Methodology for Pressurized Water Reactors
Topical Report

Page 7-344

AREVA Inc.

Realistic Large Break LOCA Methodology for Pressurized Water Reactors
Topical Report

EMF-2103NP
Revision 3

Page 7-345

AREVA Inc.

EMF-2103NP
Revision 3

Realistic Large Break LOCA Methodology for Pressurized Water Reactors
Topical Report

Page 7-346

7.9.3.6 Material Properties of M5 Clad

AREVA Inc.

EMF-2103NP
Revision 3

Realistic Large Break LOCA Methodology for Pressurized Water Reactors
Topical Report

Page 7-347

7.9.3.6.2 Thermal Conductivity

AREVA Inc.

EMF-2103NP
Revision 3

Realistic Large Break LOCA Methodology for Pressurized Water Reactors
Topical Report

Page 7-348

7.9.3.6.3   Elastic Modulus

7.9.3.6.4   Thermal Expansion

7.9.3.6.5   Emissivity

AREVA Inc.

EMF-2103NP
Revision 3

Realistic Large Break LOCA Methodology for Pressurized Water Reactors
Topical Report

Page 7-350

7.9.3.6.6　M5 Clad Radial Ballooning and Rupture Deformations

AREVA Inc.

Realistic Large Break LOCA Methodology for Pressurized Water Reactors
Topical Report

EMF-2103NP
Revision 3

Page 7-351

AREVA Inc.

Realistic Large Break LOCA Methodology for Pressurized Water Reactors
Topical Report

EMF-2103NP
Revision 3

Page 7-352

AREVA Inc.

EMF-2103NP
Revision 3

Realistic Large Break LOCA Methodology for Pressurized Water Reactors
Topical Report

Page 7-353

Table 7-11   Rupture Strain for M5 Clad

AREVA Inc.

EMF-2103NP
Revision 3

Realistic Large Break LOCA Methodology for Pressurized Water Reactors
Topical Report

Page 7-354

AREVA Inc.

EMF-2103NP
Revision 3

Realistic Large Break LOCA Methodology for Pressurized Water Reactors
Topical Report

Page 7-355
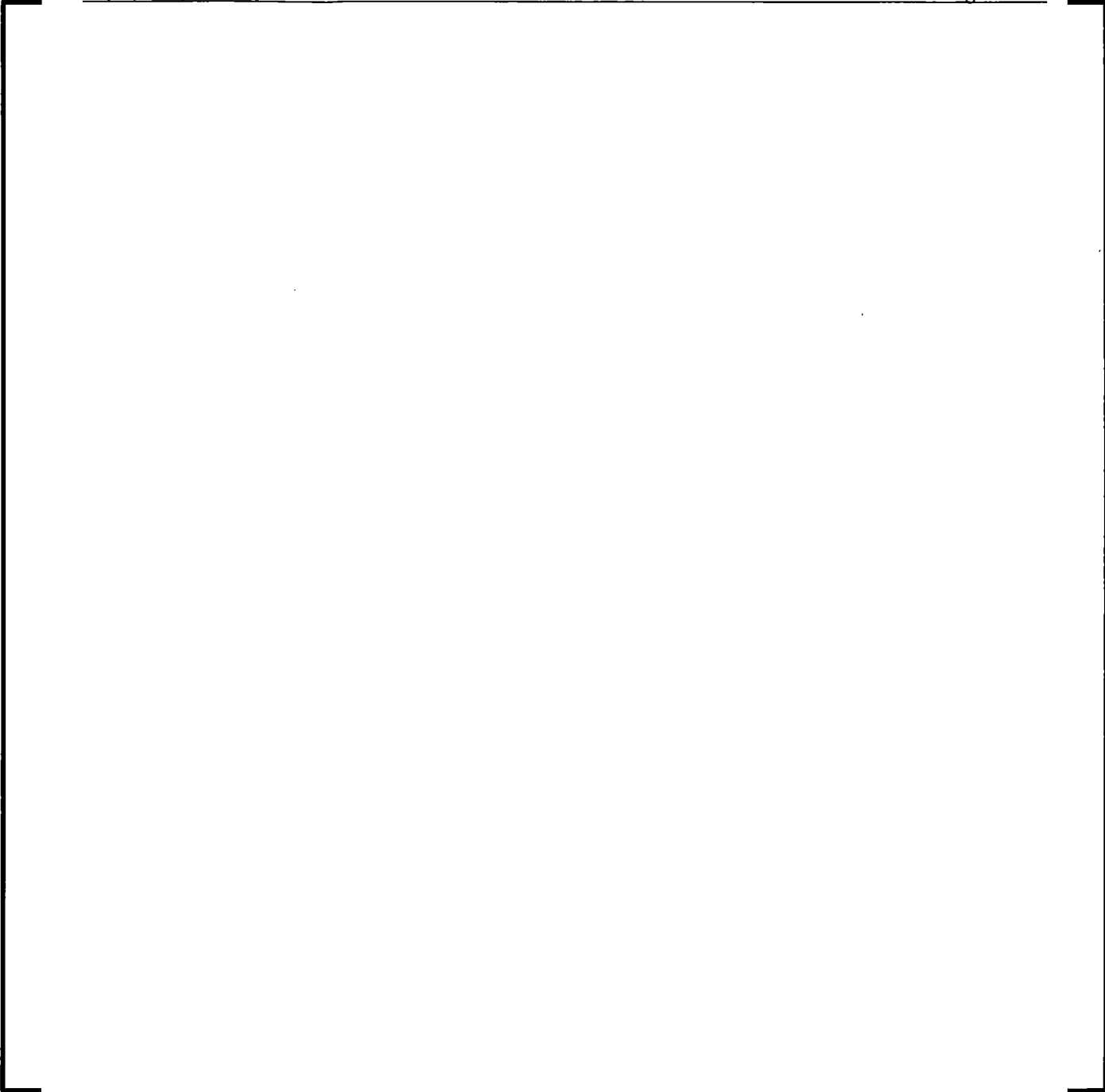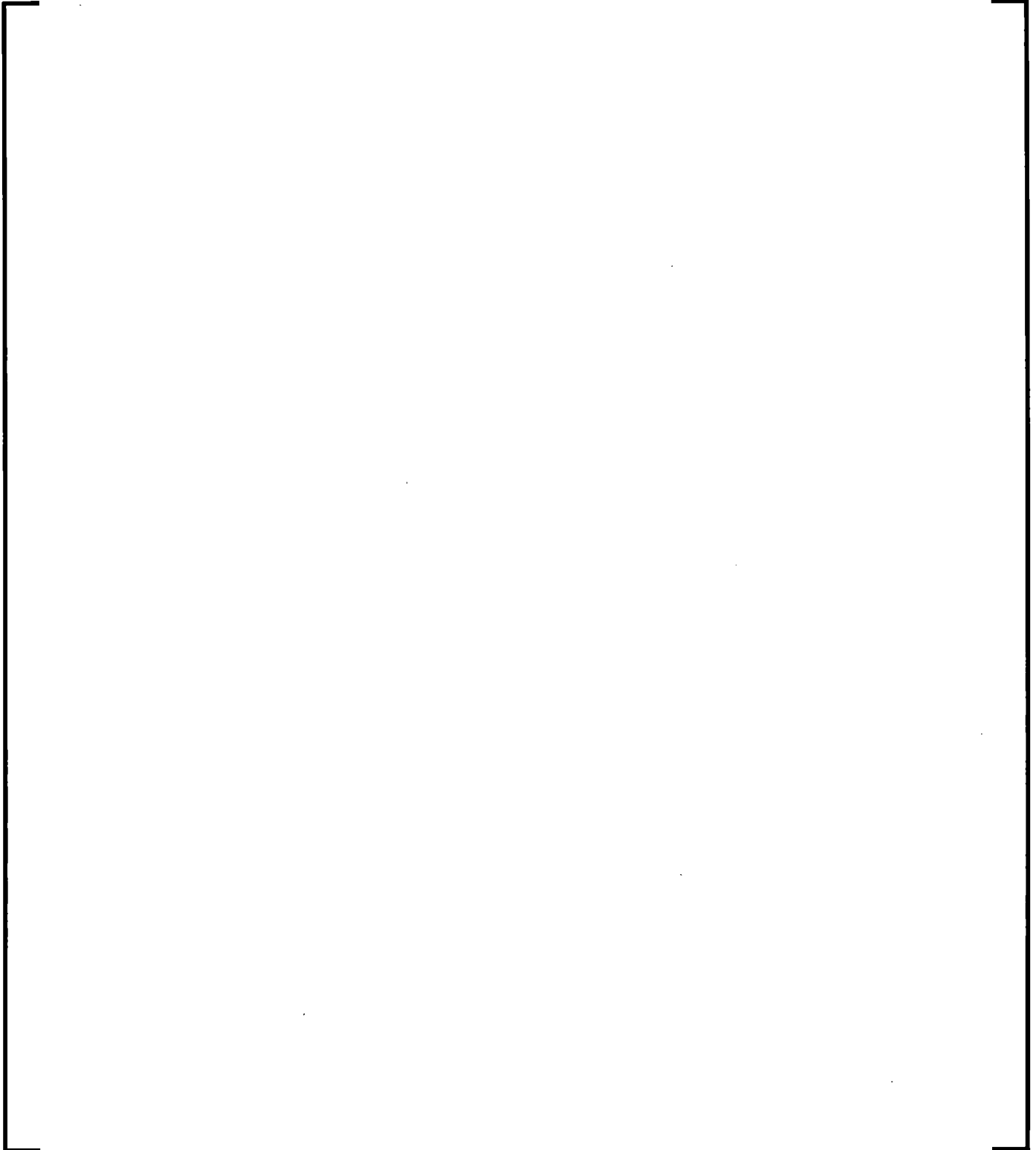
Table 7-12   Pre-Rupture Strain for M5 Clad

AREVA Inc.

EMF-2103NP
Revision 3

Realistic Large Break LOCA Methodology for Pressurized Water Reactors
Topical Report

Page 7-356
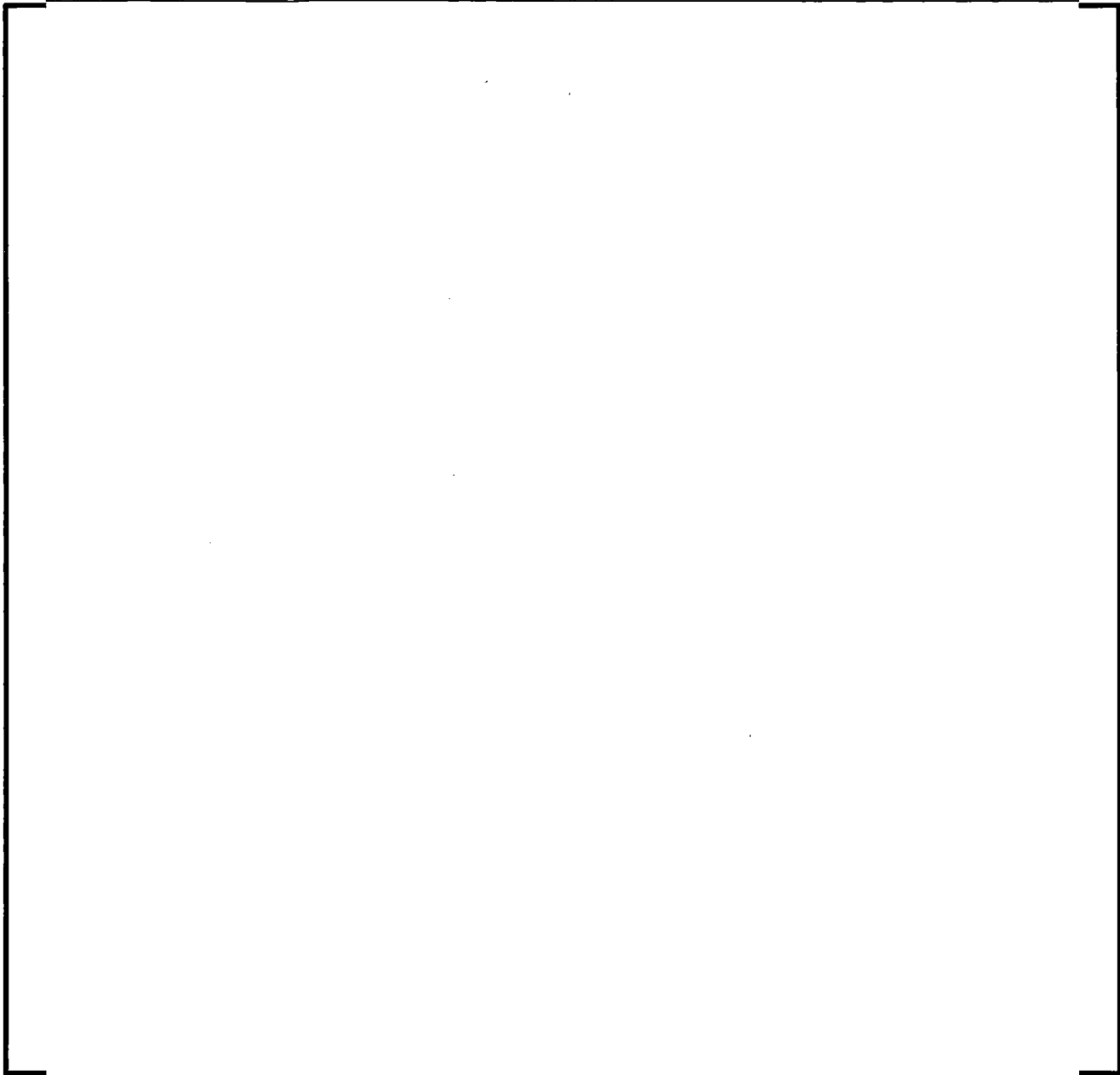
7.9.4   References

7-203. Technical Report SEMCA-2005-313, STATE-OF-THE-ART REVIEW OF PAST PROGRAMS DEVOTED TO FUEL BEHAVIOR UNDER LOCA CONDITIONS Part One. Clad Swelling and Rupture-Assembly Flow Blockage, Claude Grandjean,, IRSN, Saint-Paul-Lez-Durance, France, December 2005.

7-204. L. J. Siefken, Axial Fuel Relocation in Ballooning Fuel Rods, Transactions of the 7th International Conference on Structural Mechanics in Reactor Technology, Chicago, Illinois, August 1983.

7-205. NEA/CSNI/R(2010)6, Benchmark Calculations on Halden IFA-650 LOCA Test Results, Organization for Economic Co-Operation and Development (OECD) – Nuclear Energy Agency (NEA), www.oecd.org/publishing/corrigenda, November 2010.

7-206. B. C. Oberlander, M. Espeland, N. O. Solum, H. K. Jenssen, LOCA IFA650-4: Fuel Relocation Study, LOCA Workshop/HPG Meeting, Prague, September 2007.

7-207. NUREG/CR-0103, ORNL/NUREG/TM-200, Multirod Burst Test Program Progress Report for July-December 1997, US Nuclear Regulatory Commission, Washington DC.

7-208. K. Wiehr and U. Harten, Datenericht REBEKA-6, KfK 3986, March 1986.

7-209. K. Wiehr, REBEKA-Bundelversuche Untersuchungen zur Wechselwirkung zwischen aufblahenden Zircaloyhullen und einsetzender Kernnotkuhlung, Institut fur Reaktorbauelemente, Kerrnforschungszzentrum, Karlsrihe, Germany, KfK 4407, Mai 1988.

7-210. Fairbairin, F.A, and Piggott, B.D.G, " Studies on the Effects of
        Blockage Upon LWR Emergency Core Cooling Systems, "
        Proceedings of a Seminar on the Results of the European
        Communities' Indirect Action Research Programme on Safety of
        Thermal Water Reactors held in Brussels, October 1-3, 1984.

7-211. P. Dore, K.G. Pearson, "ACHILLES Ballooned Cluster Experiments,"
        AEEW-2590, July 1991.

7-212. J. Chiou, L.E. Hochreiter, et. al., Spacer Grid Heat Transfer Effects
        during Reflood, NUREG/CR-0043, U.S. NRC 1982.

7-213. C.Y. Paik, L.E. Hocjreiter, et. al., "Analysis of FLECHT-SEASET 163-
        Rod Blocked Bundle Data Using COBRA-TF," NUREG/CR-4166,
        EPRI NP-4111, WCAP-10375, October 1985.

7.10   *Heat Structure Models*

7.10.1   Heat Conduction Numerical Technique

Heat structures provided in S-RELAP5 permit calculation of the heat transferred across solid boundaries of hydrodynamic volumes. Modeling capabilities for heat structures are general and include fuel pins or plates with nuclear or electrical heating, heat transfer across steam generator tubes, and heat transfer from pipe and vessel walls. Heat structures are assumed to be represented by one-dimensional heat conduction in rectangular, cylindrical, or spherical geometry. [

] Surface multipliers are used to convert the unit surface of the one-dimensional calculation to the actual surface of the heat structure. Temperature-dependent thermal conductivities and volumetric heat capacities are provided in tabular or functional form either from built-in or user-supplied data.

Finite differences are used to advance the heat conduction solutions. Each mesh interval may contain a different mesh spacing, a different material, or both. The spatial dependence of the internal heat source may vary over each mesh interval. The time-dependence of the heat source can be obtained from reactor kinetics, one of several tables of power versus time, or a control system variable. Boundary conditions include symmetry or insulated conditions, a correlation package, tables of surface temperature versus time, heat transfer rate versus time, and heat transfer coefficient versus time or surface temperature. The heat transfer correlation package can be used for heat structure surfaces connected to hydrodynamic volumes, and contains correlations for convective, nucleate boiling, transition boiling, and film boiling heat transfer from the wall to water and reverse transfer from water to wall including condensation (see Section 4.0).

AREVA Inc.

EMF-2103NP
Revision 3

Realistic Large Break LOCA Methodology for Pressurized Water Reactors
Topical Report
Page 7-360

The following describes the numerical techniques for heat conduction. The integral form of the heat conduction equation is

$$\iiint_v \rho(T,\mathbf{x})\frac{\partial T}{\partial t}(\mathbf{x},t)\,dV = \iint_s k(T,\mathbf{x})\nabla T(\mathbf{x},t)\cdot d\mathbf{s} + \iiint_v S(\mathbf{x},t)\,dV \tag{7.752}$$

where:

k   =   the thermal conductivity;

s   =   the surface (vector);

S   =   the internal heat source;

t   =   time;

T   =   temperature;

V   =   volume;

x   =   the space coordinates (vector); and

ρ =   the volumetric heat capacity.

The boundary conditions applied to the exterior surface have the form

$$A(T)T(t)+B(T)\frac{\partial T(t)}{\partial n}=D(T,t) \tag{7.753}$$

The n denotes the unit normal vector away from the boundary surface. Thus, if the desired boundary condition is that the heat transferred out of the surface equals a heat transfer coefficient, h, times the difference between the surface temperature, T, and the sink temperature, T_{sk}; i.e.,

$$-k\frac{\partial T}{\partial n}=h(T-T_{sk}) \tag{7.754}$$

then the correspondence between the above expression and Equation (7.753) yields

$$A = h, \quad B = k, \quad \text{and} \quad D = h\,T_{sk} \tag{7.755}$$

In one-dimensional problems, boundary conditions are applied on the left and right

surfaces. In steady-state problems, a valid physical problem requires that A be nonzero

on at least one of the two boundary surfaces. If a transient or steady-state problem has

cylindrical or spherical geometry and a zero radius for the left surface (that is, a solid

cylinder or sphere), the left boundary condition is normally the symmetry condition,

$\dfrac{\partial T}{\partial n} = 0$. Under these conditions, if B is nonzero, the numerical technique forces the

symmetry boundary condition, even if it is not specified.

7.10.2   Mesh Point and Thermal Property Layout

Figure 7-43 illustrates the placement of mesh points at which temperatures are to be

calculated. The mesh point spacing for a rectangular problem is taken in the positive x

direction. For cylindrical and spherical problems, the mesh point spacing is in the

positive radial direction. Mesh points are placed on the external boundaries of the

problem, at the interfaces between different materials, and at desired intervals between

the interfaces, boundaries, or both.

Figure 7-43 Mesh Point Layout
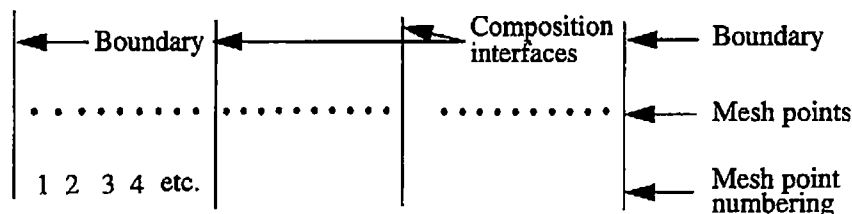
Figure 7-44 represents three typical mesh points. The subscripts are space indexes

indicating the mesh point number; and l and r (if present) designate quantities to the left

and right, respectively, of the mesh point. The δs indicate mesh point spacings that are

not necessarily equal. Between mesh points, the thermal properties, k and ρ, and the

source term, S, are assumed spatially constant; but k_{lm} is not necessarily equal to k_{rm}

and similarly for ρ and S.

To obtain the spatial-difference approximation for the m-th, interior mesh point, Equation (7.752) is applied to the volume and surfaces indicated by the dashed line shown in Figure 7-44. For the spatial difference approximation at the boundaries, Equation (7.752) is applied to the volumes and interior surfaces indicated by the dashed lines shown in Figure 7-45 and Equation (7.753) is used to define the gradient along the exterior surfaces. If the coefficient of the gradient in the boundary equation is zero, the surface temperature is given directly from Equation (7.753). Since the code is one-dimensional, the dimensions of the volume for other than the x or r coordinate are set to one. For rectangular geometry, the volume is a rectangular solid; for cylindrical geometry, the volume is a cylindrical annulus; and for spherical geometry, the volume is a spherical shell.

Figure 7-44 Typical Mesh Points
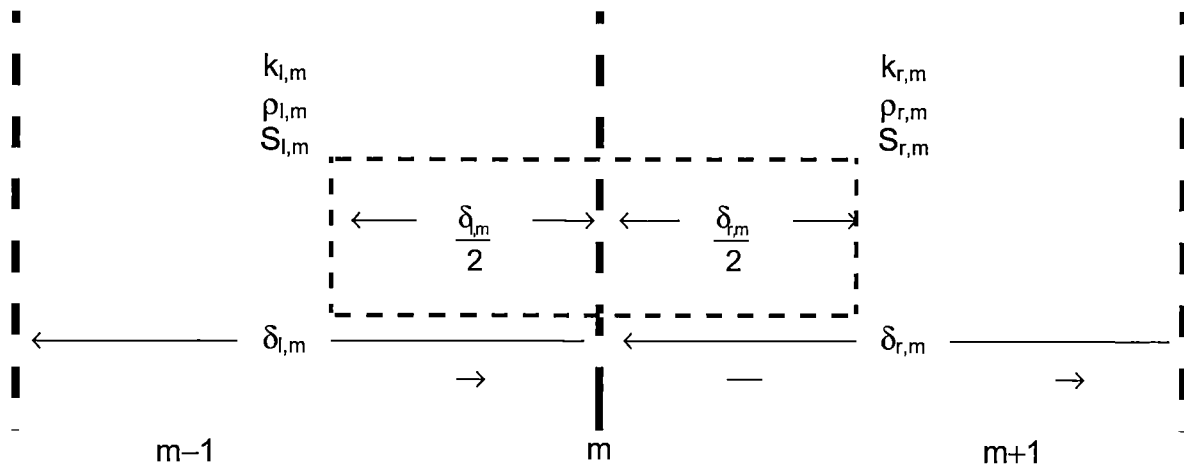
Figure 7-45 Boundary Mesh Points

AREVA Inc.

Realistic Large Break LOCA Methodology for Pressurized Water Reactors
Topical Report

EMF-2103NP
Revision 3

Page 7-363
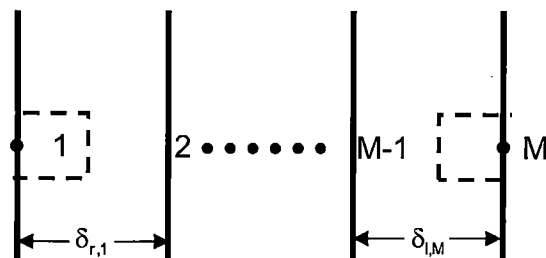
The spatial finite-difference approximations use exact expressions for the space and volume factors and simple differences of the gradient terms. To condense the expressions defining the numerical approximations and to avoid writing expressions unique to each geometry, the following quantities are defined.

For rectangular geometry,

$$\delta_{l,m}^v = \frac{\delta_{l,m}}{2}, \delta_{r,m}^v = \frac{\delta_{r,m}}{2}, \delta_{l,m}^s = \frac{1}{\delta_{l,m}}, \delta_{r,m}^s = \frac{1}{\delta_{r,m}}, \delta_m^b = 1 \tag{7.756}$$

For cylindrical geometry,

$$\delta_{l,m}^v = 2\pi \frac{\delta_{l,m}}{2}\left(x_m - \frac{\delta_{l,m}}{4}\right), \delta_{r,m}^v = 2\pi \frac{\delta_{r,m}}{2}\left(x_m + \frac{\delta_{r,m}}{4}\right),$$

$$\tag{7.757}$$

$$\delta_{l,m}^s = \frac{2\pi}{\delta_{l,m}}\left(x_m - \frac{\delta_{l,m}}{2}\right), \delta_{r,m}^s = \frac{2\pi}{\delta_{r,m}}\left(x_m + \frac{\delta_{r,m}}{2}\right), \delta_m^b = 2\pi x_m$$

For spherical geometry,

$$\delta_{l,m}^v = \frac{4\pi}{3}\left[x_m^3 - \left(x_m - \frac{\delta_{l,m}}{2}\right)^3\right], \delta_{r,m}^v = \frac{4\pi}{3}\left[\left(x_m + \frac{\delta_{r,m}}{2}\right)^3 - x_m^3\right],$$

$$\tag{7.758}$$

$$\delta_{l,m}^s = \frac{4\pi}{\delta_{l,m}}\left(x_m - \frac{\delta_{l,m}}{2}\right)^2, \delta_{r,m}^s = \frac{4\pi}{\delta_{r,m}}\left(x_m + \frac{\delta_{r,m}}{2}\right)^2, \delta_m^b = 4\pi x_m^2$$

For all geometries,

$$G_m = \rho_{l,m}\delta_{l,m}^v + \rho_{r,m}\delta_{r,m}^v \tag{7.759}$$

The superscripts, v and s, refer to volume and surface-gradient weights. The δ_m^b is a surface weight used at exterior boundaries and in heat transfer rate equations.

7.10.3 Difference Approximation at Internal Mesh Points

Using a forward difference for the time derivative, the first term of Equation (7.752) for the volume of Figure 7-43 is approximated by

$$\iiint_v \rho(T,x)\frac{\partial T}{\partial t}(x,t)dV = \left(T_m^{n+1} - T_m^n\right)\frac{G_m}{\Delta t} \tag{7.760}$$

The superscript n refers to time; thus, T_m^n indicates the temperature at mesh point m at

time t^n, and T_m^{n+1} indicates the temperature at mesh point m at time $t^{n+1} = t^n + \Delta t$.

The second term of Equation (7.752) for the surfaces of Figure 7-44 is approximated by

$$\iint_s k(T,\mathbf{x})\nabla T(\mathbf{x},t)\square d\mathbf{s} = (T_{m-1} - T_m)k_{l,m}\delta_{l,m}^s + (T_{m+1} - T_m)k_{r,m}\delta_{r,m}^s \tag{7.761}$$

Note that the above expression includes the standard interface conditions of continuity

of temperature and heat flow. The surface integral of Equation (7.752) is usually

evaluated by integrating only along the exterior surfaces of the volume indicated by the

dashed line in Figure 7-44. If, however, the volume is divided into two sub-volumes by

the interface line and the surface integrals of these sub-volumes are added, the surface

integrals along the common interface cancel because of the continuity of heat flow. The

continuity of temperature is implied by use of a single-valued temperature at the

interface.

A contact resistance interface condition cannot be specified directly since the

temperature, instead of being continuous at the interface, is given by $q = h_c\Delta T$, where q

is the heat transfer rate across the interface, h_c is the contact conductivity, and ΔT is the

temperature change across the interface. This condition can be specified by defining a

small mesh interval with thermal properties of $k = h_c\delta$ and $\rho = 0$. The size of the mesh

interval, δ, is arbitrary except in cylindrical or spherical geometry where the surface and

volume weights are dependent on the radius. This mesh interval is usually chosen to

be very small with respect to the dimensions of the problem.

The space and time dependence of the source term in Equation (7.752) is assumed to

be separable into functions of space and time,

$$S(\mathbf{x},t) = P_f P(t)Q(\mathbf{x}) \tag{7.762}$$

where P_f is the factor that relates the reactor power (or power from a table) to the heat

generation rate for a particular heat structure; P(t) is the time varying function and may

be reactor power, power from a table, or a control variable; and Q(x) is the space-

dependent function. The value of Q(x) is assumed constant over a mesh interval, but

each interval can have a different value. The third term of Equation (7.752) is then approximated as

$$\iiint_v S(x,t)dV \approx P_f P(t)\left(Q_{l,m}\delta_{l,m}^v + Q_{r,m}\delta_{r,m}^v\right) \tag{7.763}$$

Gathering the approximations of terms in Equation (7.752), the basic difference equation for the m-th mesh point is

$$\frac{\left(T_m^{n+1} - T_m\right)G_m}{\Delta t} = -\left(T_m - T_{m-1}\right)k_{l,m}\delta_{l,m}^s + \left(T_{m+1} - T_m\right)k_{r,m}\delta_{r,m}^s + P_f P(t)\left(Q_{l,m}\delta_{l,m}^v + Q_{r,m}\delta_{r,m}^v\right) \tag{7.764}$$

Using the symbol, ζ_m, to represent the right side, Equation (7.764) can be written as

$$\frac{\left(T_m^{n+1} - T_m^n\right)G_m}{\Delta t} = \zeta_m \tag{7.765}$$

Thus far, the time superscripts for G_m and ζ_m have been omitted, and the procedure for approximating the temperature dependence of the thermal properties has not been mentioned. The procedures for temperature-dependent thermal properties are discussed later. However, superscripts for thermal properties are written here even though their significance is not explained until later. For steady-state, the difference approximation becomes

$$\zeta_m = 0 \tag{7.766}$$

and no time superscripts are needed. For the time-dependent case, an equation of the type

$$\frac{\left(T_m^{n+1} - T_m^n\right)G_m}{\Delta t} = w\zeta_m^{n+1} + (1-w)\zeta_m^n \tag{7.767}$$

is an explicit formula if w is zero, and is an implicit formula when w is nonzero.

S-RELAP5 uses the implicit formulation with $w = \dfrac{1}{2}$, sometimes called the Crank-Nicolson method.

Writing Equation (7.767) in full, the difference approximation for the m-th interior mesh point for transient and steady-state cases is

$$a_m^n T_{m-1}^{n+1} + b_m^n T_m^{n+1} + c_m^n T_{m+1}^{n+1} = d_m \tag{7.768}$$

AREVA Inc.

EMF-2103NP
Revision 3

Realistic Large Break LOCA Methodology for Pressurized Water Reactors
Topical Report

Page 7-366

$$a_m^n = -\frac{k_{l,m}^n \delta_{l,m}^s \Delta t}{\sigma + 1} \tag{7.769}$$

$$b_m^n = \sigma G_m^n - a_m^n - c_m^n \tag{7.770}$$

$$c_m^n = -\frac{k_{r,m}^n \delta_{r,m}^s \Delta t}{\sigma + 1} \tag{7.771}$$

$$d_m = -\sigma a_m^n T_{m-1}^n + \sigma \left(G_m^{n} + a_m^n + c_m^n \right) T_m^n - \sigma c_m^n T_{m+1}^n + \Delta t P_f \left(\frac{P^{n+1} + \sigma P^n}{\sigma + 1} \right) \left(Q_{l,m} \delta_{l,m}^v + Q_{r,m} \delta_{r,m}^v \right) \tag{7.772}$$

σ is 1 for transient cases, and σ is 0 and Δt is 1.0 for steady-state cases. Separate subroutines are used for steady-state and transient cases, and σ and Δt do not appear in the steady-state coding.

7.10.4 Difference Approximation at Boundaries

To obtain the difference approximations for the mesh points at the boundaries, Equation (7.752) is applied to the volumes of Figure 7-45 with Equation (7.753) used to define the gradient at the surface. The second term of Equation (7.752) at $x = x_l$ is approximated by

$$\iint_s k(T,x) \nabla T(x,t) \bullet ds = -\frac{k_{r,1}}{B_1} (A_1 T_1 - D_1) \delta_1^b + k_{r,1} (T_2 - T_1) \delta_{r,1}^s \tag{7.773}$$

The complete basic expression for the left boundary mesh point becomes

$$\frac{\left(T_1^{n+1} - T_1^n \right)}{\Delta t} \rho_{r,1} \delta_{r,1}^v = -\frac{k_{r,1}}{B_1} (A_1 T_1 - D_1) \delta_1^b + k_{r,1} (T_2 - T_1) \delta_{r,1}^s + P_f P(t) Q_{r,1} \delta_{r,1}^s \tag{7.774}$$

If B in the boundary condition equation is zero, the above equation is not used, since the boundary condition alone determines the temperature. Also in that case, a divide by zero would be indicated if Equation (7.774) were used. Approximations for the boundary at $x = x_m$ are derived in a similar fashion. These equations for the boundary mesh points are converted to the implicit formulas in the same manner as for the interior mesh points, except that the boundary condition information is evaluated completely at the n + 1 time level. Thus, for the left boundary

$$b_1^{n+1} T_1^{n+1} + c_1^{n+1} T_2^{n+1} = d_1 \tag{7.775}$$

$$b_1^n = \sigma \rho_{r,1}^n \, \delta_{r,1}^v + \frac{k_{r,1}^n \, A_1^n \, \delta_1^b \, \Delta t}{B_l^n} - c_1^n \tag{7.776}$$

$$c_1^n = \frac{k_{r,1}^n \, \delta_{r,1}^s \, \Delta t}{\sigma + 1} \tag{7.777}$$

$$d_1 = -\sigma \, c_1^n \, T_2^n + \sigma \left(\rho_{r,1}^n \, \delta_{r,1}^v + c_1^n \right) T_1^n + \frac{k_{r,1}^n \, \delta_1^b \, D_1^n \, \Delta t}{B_1^n} + P_f \frac{\left(\sigma P^n + P^{n+1} \right) Q_{r,1} \delta_{r,1}^v \, \Delta t}{\sigma + 1} \tag{7.778}$$

For the right boundary,

$$a_M^{n+1} \, T_{M-1}^{n+1} + b_M^{n+1} \, T_M^{n+1} = d_M \tag{7.779}$$

$$a_M^n = \frac{-k_{l,M}^n \, \delta_{l,M}^s \, \Delta t}{\sigma + 1} \tag{7.780}$$

$$b_M^n = \sigma \rho_{l,M}^n \, \delta_{l,M}^v + \frac{k_{l,m}^n \, A_M^n \, \delta_M^b \, \Delta t}{B_M^n} - a_M^n \tag{7.781}$$

$$d_M^n = -\sigma a_M^n T_{M-1}^n + \sigma \left(\rho_{l,M}^n \, \delta_{l,M}^v + a_M^n \right) T_M^n + \frac{k_{l,M}^n \, \delta_M^b \, D_M^n \, \Delta t}{B_M^n} + P_f \frac{\left(\sigma P^n + P^{n+1} \right) Q_{l,M} \, \delta_{l,M}^v \, \Delta t}{\sigma + 1} \tag{7.782}$$

7.10.5 Thermal Properties Parameters

The thermal conductivity, k, and the volumetric heat capacity, ρ, are considered functions of temperature and space. These thermal properties are obtained for each interval by using the average of the mesh point temperatures bounding the interval

$$k_{l,m} = k \left(\frac{T_{m-1} + T_m}{2} \right) = k_{r,m-1} \tag{7.783}$$

$$k_{r,m} = k \left(\frac{T_m + T_{m+1}}{2} \right) = k_{l,m+1} \tag{7.784}$$

where $k(T)$ denotes that k is a function of T (temperature). The quantity, ρ, is treated in the same manner.

7.10.6 Boundary Conditions

The development of the difference equations uses a general form for the boundary conditions. The specific conditions implemented in RELAP5 are covered by this general form. For heat structure boundaries attached to hydrodynamic volumes, a heat transfer correlation package is typically used to define the boundary conditions. In addition,

symmetry or insulated conditions are provided, and for special situations, tabular based conditions can be specified.

7.10.6.1 Heat Transfer Correlation Conditions

The general expression of total heat flux from a heat structure to a hydrodynamic volume is shown in Equation (7.472). The parameter T_W in the equation is the surface temperature and corresponds to T_1 or T_M in the conduction equation development of Section 7.10.4. The heat transfer coefficients are evaluated based on the old time surface temperature and fluid temperatures. Equation (7.472) can be recast into the following form:

$$q'' = h_{c,total}\, T_W^{n+1} + q_0'' - h_{c,total}\, T_W^n$$

(7.785)

$$q_0'' = h_{cf}(T_W^n - T_f) + h_{csat}(T_W^n - T_{sat}) + h_{cg}(T_W^n - T_g)$$

The coefficient $h_{c,total}$ is defined in Equation (7.473). The heat transfer correlations routines compute, among other things, the parameters $h_{c,total}$ and q_0'' for use in the conduction difference equations. In terms of the general expression, Equation (7.753), one has:

$$A = h_{c,total}, \; B = k, \; \text{and} \; D = q_0'' - c_{c,total}\, T_W^n$$

(7.786)

7.10.6.2 Insulated and Tabular Boundary Conditions

The other boundary conditions implemented in RELAP5 are given below. The first two conditions are flux-specified conditions; the first condition is a symmetry or insulated condition and is just a special case of the second condition. The third condition is a convection condition similar to that used with the correlation package except that only a total heat transfer coefficient which is a tabular function of time or surface temperature is used. The last condition directly specifies the surface temperature.

$$-k\frac{\partial T}{\partial x} = 0$$

(7.787)

$$-k\frac{\partial T}{\partial x} = q_{TA}(t)$$

(7.788)

AREVA Inc.

Realistic Large Break LOCA Methodology for Pressurized Water Reactors
Topical Report

EMF-2103NP
Revision 3

Page 7-369

$$-k\frac{\partial T}{\partial x} = h_{TA}\left(T - T_{TA}\right) \tag{7.789}$$

$$T = T_{TA}\left(t\right) \tag{7.790}$$

where:

q_{TA} = the total heat flux as a function of time obtained from input tables;

h_{TA} = the total heat transfer coefficient as an input tabular function of either time or surface temperature; and

T_{TA} = either an input tabular function of time or the void fraction weighted average of the liquid and vapor temperatures of the hydrodynamic volume attached to the boundary.

For the temperature-specified boundary, the heat flux is computed from the boundary difference equation (even though it was not used to compute the temperature). The expression for the right boundary (the left is similar) is

$$q_M^{n+1}\delta_{I,M}^n = \frac{k_{I,M}^n}{\sigma+1}\left(T_{M-1}^{n+1} - T_M^{n+1}\right)\delta_{I,M}^s + \frac{\sigma k_{I,M}^n}{\sigma+1}\left(T_{M-1}^n - T_M^n\right)\delta_{I,M}^s$$

$$+ P_f\frac{\left(\sigma P^n + P^{n+1}\right)}{\sigma+1}Q_{I,M}\delta_{I,M}^v - \frac{\sigma\rho_{I,M}^n}{\Delta t}\left(T_M^{n+1} - T_M^n\right)\delta_{I,M}^v \tag{7.791}$$

7.10.7 Solution of Simultaneous Equations

The difference approximation for the mesh points (Equations (7.768), (7.775), and (7.779)) lead to a tri-diagonal set of M equations.

$$\begin{bmatrix} b_1 & c_1 & & & & \\ a_2 & b_2 & c_2 & & & \\ & \bullet & \bullet & & & \\ & & \bullet & \bullet & \bullet & \\ & & & a_{M-1} & b_{M-1} & c_{M-1} \\ & & & & a_M & b_M \end{bmatrix} \begin{bmatrix} T_1 \\ T_2 \\ \bullet \\ \bullet \\ T_{M-1} \\ T_M \end{bmatrix} = \begin{bmatrix} d_1 \\ d_2 \\ \bullet \\ \bullet \\ d_{M-1} \\ d_M \end{bmatrix} \tag{7.792}$$

AREVA Inc.

Realistic Large Break LOCA Methodology for Pressurized Water Reactors
Topical Report

EMF-2103NP
Revision 3

Page 7-370

Equations 1 and M correspond to the left and right boundary mesh points respectively, and equations 2 through M–1 correspond to the interior mesh points. The coefficient matrix is symmetric unless a boundary condition specifies the surface temperature. In that case, the corresponding off-diagonal element is zero and thus symmetry may not exist in the first and/or last rows. The solution to the above equation is obtained by

$$E_1 = \frac{c_1}{b_1} \text{ and } F_1 = \frac{d_1}{b_1} \qquad (7.793)$$

$$E_j = \frac{c_j}{b_j - a_j E_{j-1}} \text{ and } F_j = \frac{d_j - a_j F_{j-1}}{b_j - a_j E_{j-1}} \quad \text{for } j = 2, 3, ..., M-1 \qquad (7.794)$$

$$g_M = \frac{d_M - a_M F_{M-1}}{b_M - a_M E_{M-1}} \qquad (7.795)$$

$$g_j = -E_j g_{j+1} + F_j \qquad \text{for } j = M-1, M-2, ..., 3, 2, 1 \qquad (7.796)$$

$$T_j^{n+1} = g_j \quad \text{for all } j \qquad (7.797)$$

These procedures can be derived by applying the rules for Gaussian elimination. This method of solution introduces little roundoff error if the off-diagonal elements are negative and the diagonal is greater than the sum of the magnitudes of the off-diagonal elements. From the form of the difference equations, these conditions are satisfied for any values of the mesh point spacing, time step, and thermal properties.

7.10.8   Reflood Two-Dimensional Conduction Solution

A two-dimensional conduction scheme is used in the reflood model for cylindrical or rectangular heat structures. Figure 7-46 shows an elemental cell around the mesh point (i,j). For a cylindrical geometry, the volume elements are

$$V_1 = \frac{\pi \delta_t \delta_l}{2} \left(r_i - \frac{\delta_l}{4} \right) \qquad (7.798)$$

$$V_2 = \frac{\pi \delta_t \delta_r}{2} \left(r_i + \frac{\delta_r}{4} \right) \qquad (7.799)$$

$$V_3 = \frac{\pi \delta_b \delta_l}{2} \left(r_i - \frac{\delta_l}{4} \right) \qquad (7.800)$$

$$V_4 = \frac{\pi \delta_b \delta_r}{2} \left(r_i + \frac{\delta_r}{4} \right) \qquad (7.801)$$

AREVA Inc.

EMF-2103NP
Revision 3

Realistic Large Break LOCA Methodology for Pressurized Water Reactors
Topical Report

Page 7-371

and the surface elements are

$$A_1 = \pi\delta_l\left(r_i - \frac{\delta_l}{4}\right) \tag{7.802}$$

$$A_2 = \pi\delta_r\left(r_i + \frac{\delta_r}{4}\right) \tag{7.803}$$

$$A_3 = \pi\delta_t\left(r_i + \frac{\delta_r}{2}\right) \tag{7.804}$$

$$A_4 = \pi\delta_b\left(r_i + \frac{\delta_r}{2}\right) \tag{7.805}$$

$$A_5 = A_2 \tag{7.806}$$

$$A_6 = A_1 \tag{7.807}$$

$$A_7 = \pi\delta_b\left(r_i - \frac{\delta_l}{2}\right) \tag{7.808}$$

$$A_8 = \pi\delta_t\left(r_i - \frac{\delta_l}{2}\right) \tag{7.809}$$

Figure 7-46 Volume and Surface Elements Around a Mesh Point (i,j)

AREVA Inc.

EMF-2103NP
Revision 3

Realistic Large Break LOCA Methodology for Pressurized Water Reactors
Topical Report

Page 7-372
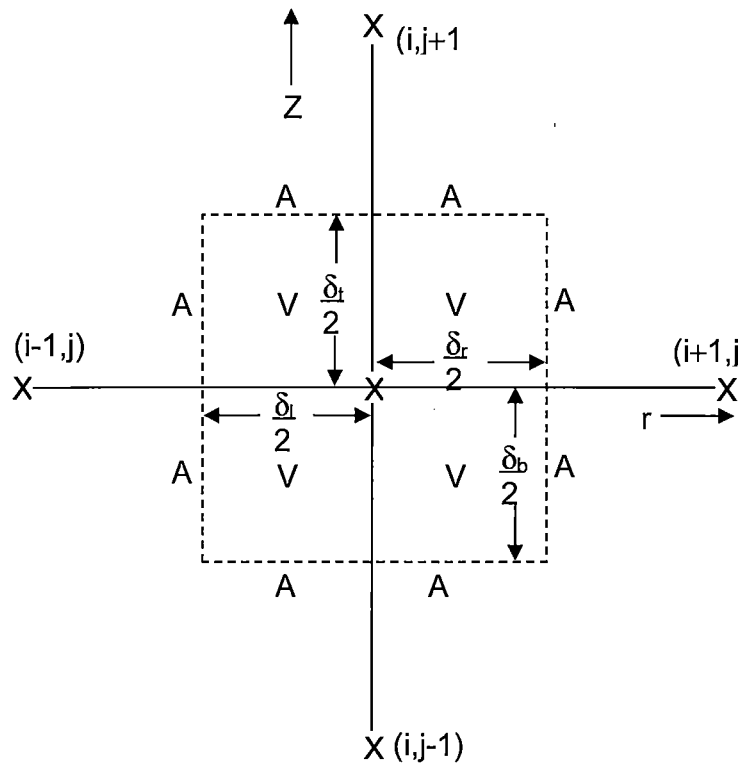
Integration of the heat conduction Equation (7.752) over the elemental cell yields the following form of finite difference equation

$$G_{i,j}\frac{\left(T_{i,j}^{n+1}-T_{i,j}^{n}\right)}{\Delta t}=a_{i,j}^{L}T_{i-1,j}+a_{i,j}^{R}T_{i+1,j}+a_{i,j}^{T}T_{i,j+1}+a_{i,j}^{B}T_{i,j-1}-\left(a_{i,j}^{L}+a_{i,j}^{R}+a_{i,j}^{B}+a_{i,j}^{T}\right)T_{i,j}+S_{i,j} \qquad (7.810)$$

By defining the material properties, $\rho_{i,j}$ and $k_{i,j}$, at the center of the r-direction interval between mesh points i,j and i+1,j, the coefficients $G_{i,j}$, $a_{i,j}^{R}$, and $a_{i,j}^{T}$ of Equation (7.810) can be written as

$$G_{i,j}=\rho_{i-1,j}\left(V_{1}+V_{3}\right)+\rho_{i,j}\left(V_{2}+V_{4}\right) \qquad (7.811)$$

$$a_{i,j}^{R}=k_{i,j}\frac{\left(A_{3}+A_{4}\right)}{\delta_{r}} \qquad (7.812)$$

$$a_{i,j}^{T}=\frac{\left[\left(k_{i,j}+k_{i,j+1}\right)\dfrac{A_{2}}{2}+\left(k_{i-1,j}+k_{i-1,j+1}\right)\dfrac{A_{1}}{2}\right]}{\delta_{t}} \qquad (7.813)$$

The other two coefficients, $a_{i,j}^{L}$ and $a_{i,j}^{B}$, are obtained by the symmetry relations

$$a_{i,j}^{L}=a_{i-1,j}^{R} \qquad (7.814)$$

$$a_{i,j}^{B}=a_{i,j-1}^{T} \qquad (7.815)$$

The space and time dependence of the source term, S, described in Equation (7.762) is extended to the two-dimensional cases as

$$S=P_{f}P(t)\,Q(r,z) \qquad (7.816)$$

with the assumption that Q is independent of z within a heat structure. Accordingly, the heat source term $S_{i,j}$ of Equation (7.810) is

$$S_{i,j}=P_{f}P\left(t\right)\left(Q_{i}^{T}V_{1}+Q_{i}^{B}V_{3}+Q_{r}^{T}V_{2}+Q_{r}^{B}V_{4}\right) \qquad (7.817)$$

Here, $Q_{i}^{T}=Q_{i}^{B}$ and $Q_{r}^{T}=Q_{r}^{B}$ if the entire cell is within the same heat structure.

AREVA Inc.

Realistic Large Break LOCA Methodology for Pressurized Water Reactors
Topical Report

EMF-2103NP
Revision 3

Page 7-373

Equation (7.810) is written for an interior point (i,j). For a point on the boundary, some of the coefficients, $a_{i,j}^L$, $a_{i,j}^B$, and $a_{i,j}^T$, should vanish. For example, at the bottom corner, $a_{i,j}^L$ and $a_{i,j}^B$ are zero. Also some of the terms in Equations (7.813) and (7.817) disappear. Furthermore, the boundary condition must be added. To be consistent with the one-dimensional heat conduction scheme, an assumption is made that no heat is fluxed across the top and bottom ends. For the right and left boundaries, the boundary condition can be represented by one of the forms described in Equation (7.785) and Equations (7.787) through (7.789). The boundary condition specifying the surface temperature as a function of time, Equation (7.790), has been dropped in the two-dimensional scheme for computational efficiency.

The difference equation, Equation (7.810), is solved using the alternating direction implicit (ADI) method. The scheme is represented by two steps as follows:

1. Column Inversion:

$$\frac{\left(T_{i,j}^{n+1/2} - T_{i,j}^n\right)G_{i,j}}{\frac{\Delta t}{2}} = a_{i,j}^L T_{i-1,j}^n + a_{i,j}^R T_{i+1,j}^n + a_{i,j}^B T_{i,j-1}^{n+1/2} + a_{i,j}^T T_{i,j+1}^{n+1/2} - \left(a_{i,j}^L + a_{i,j}^R\right)T_{i,j}^n - \left(a_{i,j}^T + a_{i,j}^B\right)T_{i,j}^{n+1/2} + S_{i,j} \quad (7.818)$$

2. Row Inversion:

$$\frac{\left(T_{i,j}^{n+1} - T_{i,j}^{n+1/2}\right)G_{i,j}}{\frac{\Delta t}{2}} = a_{i,j}^L T_{i-1,j}^{n+1} + a_{i,j}^R T_{i+1,j}^{n+1} + a_{i,j}^B T_{i,j-1}^{n+1/2} + a_{i,j}^T T_{i,j+1}^{n+1/2} - \left(a_{i,j}^L + a_{i,j}^R\right)T_{i,j}^{n+1} - \left(a_{i,j}^T + a_{i,j}^B\right)T_{i,j}^{n+1/2} + S_{i,j} \quad (7.819)$$

Here the superscripts n, n+½, and n+1 denote the values at times t, $t + \frac{Dt}{2}$, and t+Δt, respectively.

7.10.9   Reflood Fine Mesh Rezoning

A fine mesh-rezoning scheme is implemented to efficiently use the two-dimensional conduction solution for reflood calculations. The scheme is similar to the one used in COBRA-TF (Reference 7-103) and is intended to resolve the large axial variation of wall temperatures and heat fluxes. The number of axial nodes in the heat structures is varied in such a way that fine nodes exist in the nucleate boiling and transition boiling regions.

A heat-structure geometry, which is composed of from 1 to 99 heat structures as specified by the user, is selected as an elementary unit for the reflood model. Figure 7-47 shows a typical heat structure geometry with one fluid-control volume connected to each heat structure. The dots are radial mesh points. At the initiation of the reflood model, each heat structure is subdivided into two axial intervals (Figure 7-47). A two-dimensional array of mesh points is thus formed. Thereafter, the number of axial intervals may be doubled, halved, or unchanged at each time step according to a set of rules to be discussed in the next paragraph. Figure 7-48 shows an example of a heat structure going through a cycle of axial nodalization variation.

The number of axial fine nodes in a structure are changed according to the following prescriptions:

a. If the volume void fraction is less than 10^{-5} (single-phase liquid), the number of axial nodes is halved if it is greater than 2 and is unchanged if it is 2.

b. If the volume void fraction is greater than 0.9999 (single-phase vapor), the number of axial nodes is doubled up to half of the maximum number specified.

c. If the maximum wall temperature within the structure is less than saturation temperature or is less than half of the sum of the CHF and saturation temperatures, the number of axial nodes is doubled up to half of the maximum number specified.

d. Otherwise (i.e., all conditions other than those stated in (a), (b), and (c)), the number of axial nodes is doubled up to the maximum number specified.

AREVA Inc.

EMF-2103NP
Revision 3

Realistic Large Break LOCA Methodology for Pressurized Water Reactors
Topical Report

Page 7-375

Note that, for (b) and (c), the number of the axial nodes is in effect halved if at the previous time step the number of axial nodes is the maximum and is in effect unchanged if the number of axial nodes has reached half of the maximum. Also, for (d), the number of axial nodes is unchanged after the maximum number has been reached.

Figure 7-47 An Elementary Heat Structure Unit for Reflood
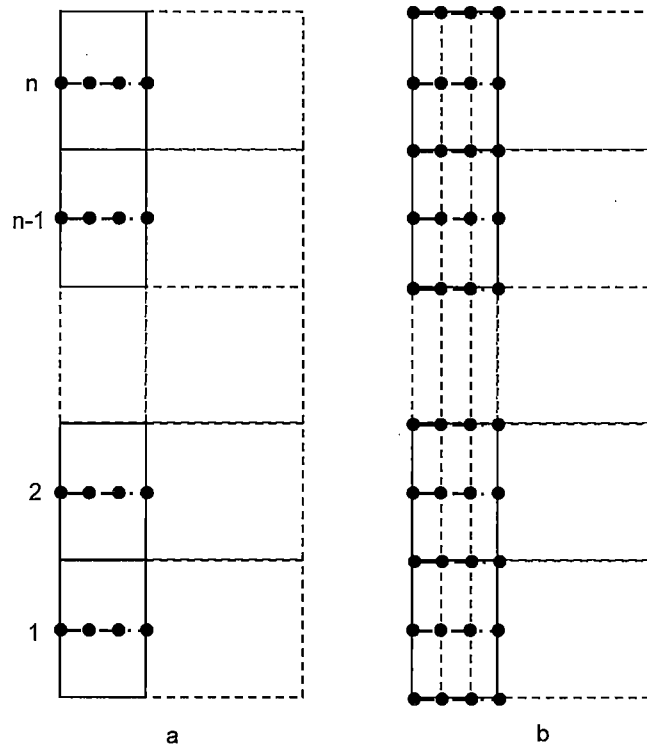
Figure 7-48 An Example of the Fine Mesh-Rezoning Process
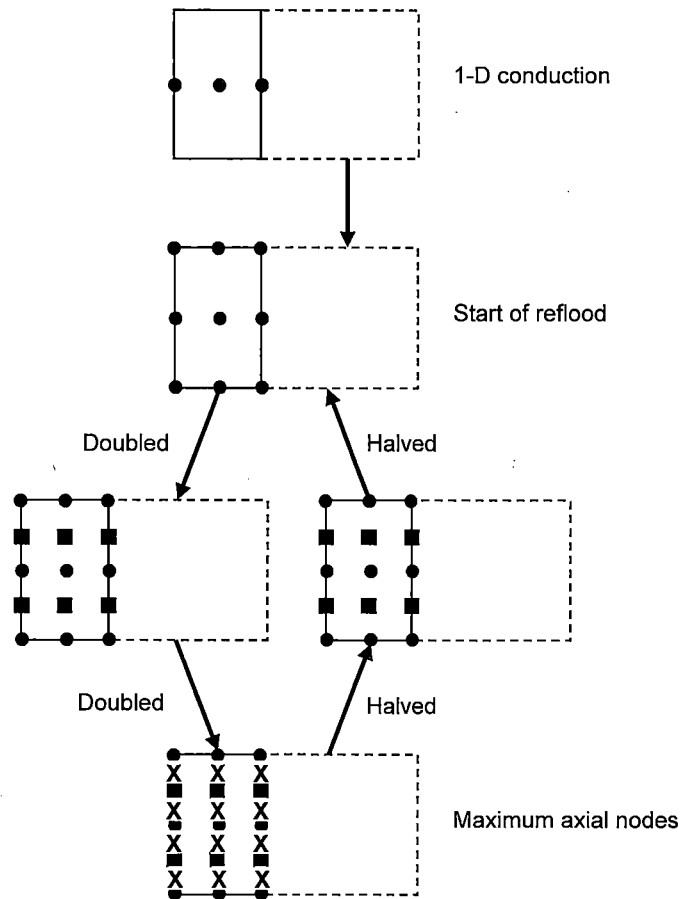
7.11   *Containment Model*

In past practice, the break pressure boundary condition for RELAP5 LOCA analysis had been supplied by use of a time-dependent volume component which simulated the reactor containment. This time-dependent volume supplied either an estimated constant containment pressure, or a time-dependent pressure obtained from a separate containment analysis code. Neither of these methods guaranteed a break pressure boundary condition that was consistent with the actual mass and energy discharge for the specific LOCA being analyzed.

In order to provide a more accurate break pressure boundary condition for S-RELAP5 best estimate LOCA analysis, a detailed containment model has been integrated into S-RELAP5. This containment model is derived from the AREVA NP Inc. licensing code

ICECON (Reference 7-111). ICECON is capable of simulating pressure-temperature transients in both dry containments and ice condenser containments. The S-RELAP5/ ICECON code integration executes the ICECON sub-code concurrently with S-RELAP5, providing a calculation of containment pressure that is consistent with the break mass flow rate and specific enthalpy currently being generated by S-RELAP5. With the concurrent execution of S-RELAP5 and ICECON sub-routines, an accurate break pressure boundary condition is always available in S-RELAP5 and the need for manual exchange of data between the two codes is eliminated.

For the S-RELAP5/ICECON sub-routine data transfer, break flow junction variables (velocities, specific enthalpies, densities, and void fractions) are transferred each time step from S-RELAP5 to the containment analysis sub-routines. These variables are then used in the containment sub-routines to generate a new containment pressure which is transferred back to S-RELAP5 and used to alter the pressure in the time-dependent volume or volumes which represent the containment in the S-RELAP5 model. At each time step, S-RELAP5 performs the necessary data transfers between the main code and the sub-code and calls for execution of the external code. After execution of the sub-code, control is returned to S-RELAP5, which continues execution.

7.11.1   Containment Physical Models

7.11.1.1 Containment Compartment Analytical Models

AREVA Inc.

EMF-2103NP
Revision 3

Realistic Large Break LOCA Methodology for Pressurized Water Reactors
Topical Report

Page 7-378

7.11.1.1.1 *Description of Generalized Compartment Model*

AREVA Inc.

Realistic Large Break LOCA Methodology for Pressurized Water Reactors
Topical Report

EMF-2103NP
Revision 3

Page 7-379

Figure 7-49 General Compartment Features

AREVA Inc.

EMF-2103NP
Revision 3

Realistic Large Break LOCA Methodology for Pressurized Water Reactors
Topical Report

Page 7-380

AREVA Inc.

EMF-2103NP
Revision 3

Realistic Large Break LOCA Methodology for Pressurized Water Reactors
Topical Report

Page 7-381

AREVA Inc.

EMF-2103NP
Revision 3

Realistic Large Break LOCA Methodology for Pressurized Water Reactors
Topical Report

Page 7-382

AREVA Inc.

Realistic Large Break LOCA Methodology for Pressurized Water Reactors
Topical Report

EMF-2103NP
Revision 3

Page 7-383

AREVA Inc.

Realistic Large Break LOCA Methodology for Pressurized Water Reactors
Topical Report

EMF-2103NP
Revision 3

Page 7-384

AREVA Inc.

Realistic Large Break LOCA Methodology for Pressurized Water Reactors
Topical Report

EMF-2103NP
Revision 3

Page 7-385

AREVA Inc.

Realistic Large Break LOCA Methodology for Pressurized Water Reactors
Topical Report

EMF-2103NP
Revision 3

Page 7-386

Figure 7-50 Pool Energy Versus System Pressure

AREVA Inc.

EMF-2103NP
Revision 3

Realistic Large Break LOCA Methodology for Pressurized Water Reactors
Topical Report

Page 7-387

AREVA Inc.

EMF-2103NP
Revision 3

Realistic Large Break LOCA Methodology for Pressurized Water Reactors
Topical Report

Page 7-388

AREVA Inc.

EMF-2103NP
Revision 3

Realistic Large Break LOCA Methodology for Pressurized Water Reactors
Topical Report

Page 7-389

Figure 7-51 Compartment Containing Liquid and Vapor Regions

AREVA Inc.

EMF-2103NP
Revision 3

Realistic Large Break LOCA Methodology for Pressurized Water Reactors
Topical Report

Page 7-391

AREVA Inc.

EMF-2103NP
Revision 3

Realistic Large Break LOCA Methodology for Pressurized Water Reactors
Topical Report

Page 7-392

AREVA Inc.

EMF-2103NP
Revision 3

Realistic Large Break LOCA Methodology for Pressurized Water Reactors
Topical Report

Page 7-393

AREVA Inc.

EMF-2103NP
Revision 3

Realistic Large Break LOCA Methodology for Pressurized Water Reactors
Topical Report

Page 7-394

AREVA Inc.

EMF-2103NP
Revision 3

Realistic Large Break LOCA Methodology for Pressurized Water Reactors
Topical Report
Page 7-395

AREVA Inc.

Realistic Large Break LOCA Methodology for Pressurized Water Reactors
Topical Report

EMF-2103NP
Revision 3

Page 7-396

AREVA Inc.

EMF-2103NP
Revision 3

Realistic Large Break LOCA Methodology for Pressurized Water Reactors
Topical Report

Page 7-397

AREVA Inc.

Realistic Large Break LOCA Methodology for Pressurized Water Reactors
Topical Report

EMF-2103NP
Revision 3

Page 7-398

7.11.1.1.2   *Dead End Compartment Model*

AREVA Inc.

Realistic Large Break LOCA Methodology for Pressurized Water Reactors
Topical Report

EMF-2103NP
Revision 3

Page 7-399

7.11.1.1.3   Drywell Compartment Model

7.11.1.1.4   Upper Compartment Model

7.11.1.1.5   Reactor Primary System Compartment Model

AREVA Inc.

EMF-2103NP
Revision 3

Realistic Large Break LOCA Methodology for Pressurized Water Reactors
Topical Report

Page 7-400

AREVA Inc.

Realistic Large Break LOCA Methodology for Pressurized Water Reactors
Topical Report

EMF-2103NP
Revision 3

Page 7-401

7.11.1.2 Compartment Mass And Energy Transfer Models

AREVA Inc.

Realistic Large Break LOCA Methodology for Pressurized Water Reactors
Topical Report

EMF-2103NP
Revision 3

Page 7-403

7.11.1.2.1   *Compartment Leakage Model*

AREVA Inc.

EMF-2103NP
Revision 3

Realistic Large Break LOCA Methodology for Pressurized Water Reactors
Topical Report

Page 7-404

AREVA Inc.

EMF-2103NP
Revision 3

Realistic Large Break LOCA Methodology for Pressurized Water Reactors
Topical Report

Page 7-405

AREVA Inc.

EMF-2103NP
Revision 3

Realistic Large Break LOCA Methodology for Pressurized Water Reactors
Topical Report

Page 7-406

AREVA Inc.

EMF-2103NP
Revision 3

Realistic Large Break LOCA Methodology for Pressurized Water Reactors
Topical Report

Page 7-407

AREVA Inc.

Realistic Large Break LOCA Methodology for Pressurized Water Reactors
Topical Report

EMF-2103NP
Revision 3

Page 7-408

7.11.1.2.2   Safety System Models

AREVA Inc.

EMF-2103NP
Revision 3

Realistic Large Break LOCA Methodology for Pressurized Water Reactors
Topical Report

Page 7-410

Figure 7-52 ECC and Cooling Spray Model

AREVA Inc.

EMF-2103NP
Revision 3

Realistic Large Break LOCA Methodology for Pressurized Water Reactors
Topical Report

Page 7-411

AREVA Inc.

Realistic Large Break LOCA Methodology for Pressurized Water Reactors
Topical Report

EMF-2103NP
Revision 3

Page 7-412

AREVA Inc.

EMF-2103NP
Revision 3

Realistic Large Break LOCA Methodology for Pressurized Water Reactors
Topical Report

Page 7-413

AREVA Inc.

EMF-2103NP
Revision 3

Realistic Large Break LOCA Methodology for Pressurized Water Reactors
Topical Report

Page 7-414

AREVA Inc.

EMF-2103NP
Revision 3

Realistic Large Break LOCA Methodology for Pressurized Water Reactors
Topical Report

Page 7-414

AREVA Inc.

EMF-2103NP
Revision 3

Realistic Large Break LOCA Methodology for Pressurized Water Reactors
Topical Report

Page 7-415

AREVA Inc.

EMF-2103NP
Revision 3

Realistic Large Break LOCA Methodology for Pressurized Water Reactors
Topical Report

Page 7-416

7.11.1.2.3 Mass And Energy Addition Tabular Models

AREVA Inc.

EMF-2103NP
Revision 3

Realistic Large Break LOCA Methodology for Pressurized Water Reactors
Topical Report

Page 7-417

AREVA Inc.

EMF-2103NP
Revision 3

Realistic Large Break LOCA Methodology for Pressurized Water Reactors
Topical Report

Page 7-418

AREVA Inc.

EMF-2103NP
Revision 3

Realistic Large Break LOCA Methodology for Pressurized Water Reactors
Topical Report

Page 7-419

7.11.1.2.4   *Heat Conducting Structure Analytical Model*

AREVA Inc.

EMF-2103NP
Revision 3

Realistic Large Break LOCA Methodology for Pressurized Water Reactors
Topical Report

Page 7-421

AREVA Inc.

Realistic Large Break LOCA Methodology for Pressurized Water Reactors
Topical Report

EMF-2103NP
Revision 3

Page 7-422

Figure 7-53 Mesh Point Layout

AREVA Inc.

Realistic Large Break LOCA Methodology for Pressurized Water Reactors
Topical Report

EMF-2103NP
Revision 3

Page 7-423

AREVA Inc.

Realistic Large Break LOCA Methodology for Pressurized Water Reactors
Topical Report

EMF-2103NP
Revision 3

Page 7-424

Table 7-13 Uchida Heat Transfer Coefficients

AREVA Inc.

EMF-2103NP
Revision 3

Realistic Large Break LOCA Methodology for Pressurized Water Reactors
Topical Report

Page 7-425

Figure 7-54 Comparison of Best Estimate Containment Heat Transfer

[   ]

AREVA Inc.

EMF-2103NP
Revision 3

Realistic Large Break LOCA Methodology for Pressurized Water Reactors
Topical Report

Page 7-427

AREVA Inc.

EMF-2103NP
Revision 3

Realistic Large Break LOCA Methodology for Pressurized Water Reactors
Topical Report

Page 7-428

7.11.1.3 Ice Condenser Models

AREVA Inc.

Realistic Large Break LOCA Methodology for Pressurized Water Reactors
Topical Report

EMF-2103NP
Revision 3

Page 7-429

7.11.1.3.1 Ice Condenser Containment Description

AREVA Inc.

Realistic Large Break LOCA Methodology for Pressurized Water Reactors
Topical Report

EMF-2103NP
Revision 3

Page 7-430

AREVA Inc.

EMF-2103NP
Revision 3

Realistic Large Break LOCA Methodology for Pressurized Water Reactors
Topical Report

Page 7-433

AREVA Inc.

EMF-2103NP
Revision 3

Realistic Large Break LOCA Methodology for Pressurized Water Reactors
Topical Report

Page 7-434

AREVA Inc.

EMF-2103NP
Revision 3

Realistic Large Break LOCA Methodology for Pressurized Water Reactors
Topical Report

Page 7-435

AREVA Inc.

Realistic Large Break LOCA Methodology for Pressurized Water Reactors
Topical Report

EMF-2103NP
Revision 3

Page 7-436

AREVA Inc.

EMF-2103NP
Revision 3

Realistic Large Break LOCA Methodology for Pressurized Water Reactors
Topical Report

Page 7-437

AREVA Inc.

EMF-2103NP
Revision 3

Realistic Large Break LOCA Methodology for Pressurized Water Reactors
Topical Report

Page 7-438

AREVA Inc.

Realistic Large Break LOCA Methodology for Pressurized Water Reactors
Topical Report

EMF-2103NP
Revision 3

Page 7-439

AREVA Inc.

EMF-2103NP
Revision 3

Realistic Large Break LOCA Methodology for Pressurized Water Reactors
Topical Report

Page 7-440

AREVA Inc.

EMF-2103NP
Revision 3

Realistic Large Break LOCA Methodology for Pressurized Water Reactors
Topical Report

Page 7-441

AREVA Inc.

Realistic Large Break LOCA Methodology for Pressurized Water Reactors
Topical Report

EMF-2103NP
Revision 3

Page 7-442

AREVA Inc.

EMF-2103NP
Revision 3

Realistic Large Break LOCA Methodology for Pressurized Water Reactors
Topical Report

Page 7-443

Figure 7-55 Typical Ice Condenser Containment

AREVA Inc.

EMF-2103NP
Revision 3

Realistic Large Break LOCA Methodology for Pressurized Water Reactors
Topical Report

Page 7-444

Figure 7-56 Ice Condenser Model

AREVA Inc.

EMF-2103NP
Revision 3

Realistic Large Break LOCA Methodology for Pressurized Water Reactors
Topical Report

Page 7-445

Figure 7-57 Lower Door Characteristic Behavior

AREVA Inc.

EMF-2103NP
Revision 3

Realistic Large Break LOCA Methodology for Pressurized Water Reactors
Topical Report

Page 7-446

Figure 7-58 Sump Model

7.11.1.3.3   *Determination of Drywell Liquid Dropout Time*

AREVA Inc.

EMF-2103NP
Revision 3

Realistic Large Break LOCA Methodology for Pressurized Water Reactors
Topical Report
Page 7-447
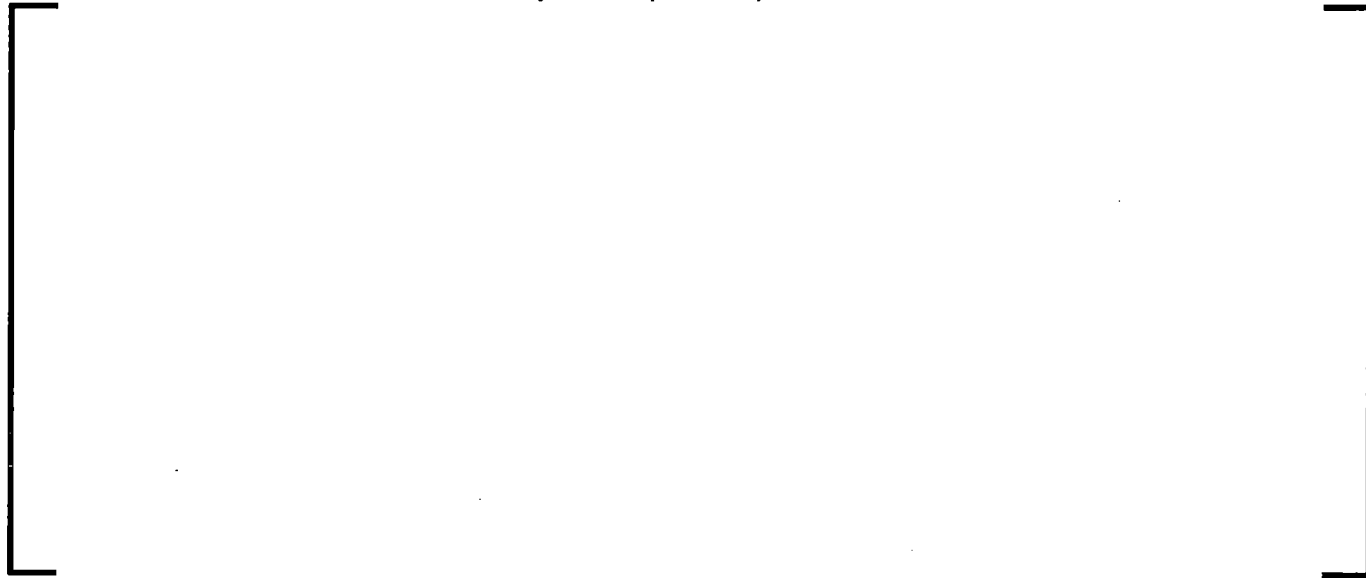
7.11.2   RELAP5-to-ICECON Data Transfer

Table 7-14 Description of Transferred Data Variables

7.11.3   ICECON-to-S-RELAP5 Data Transfer

$$\Bigg[\qquad \qquad \qquad \qquad \qquad \qquad \qquad \qquad \Bigg]$$

7.11.4   References

7-214. J. H. Keenan and F. G. Keys, Thermodynamic Properties of Steam, John Wiley and Sons, Inc., New York, NY, 1936.

7-215. T. W. Martin, WH 58, Thermodynamic Properties of Steam, SHARE Distribution 1095, 3/30/1961.

7-216. John G. Collier, Convective Boiling and Condensation, McGraw-Hill, London, 1972, Chapter 10.

7-217. R. G. Bird, E. N. Lightfoot, and W. E. Stewart, Transport Phenomena, John Wiley and Sons., Inc., New York, 1960.

7-218. M. Fishenden, and O. Saunders, An Introduction to Heat Transfer, Oxford University Press, New York, 1950.

7-219. W. H. McAdams, Heat Transmission, Third Ed., McGraw-Hill Book Company, New York, 1954.

7-220. W. W. Akers, J. E. Crawford, and S. H. Davis, Jr., "Condensation of a Vapor in the Presence of a Non-Condensing Gas," Chem. Eng. Prog. Symp. Series, 56 (30), 1960, pp. 139-144.

7-221. J. H. Keenan, J. Chao, and J. Kaye, GAS TABLES, Thermodynamic
        Properties of Air Products of Combustion and Component Gases
        Compressible Flow Functions, Second Edition (English Units), John
        Wiley and Sons, 1979.

7-222. 1967 ASME STEAM TABLES, Thermodynamic and Transport
        Properties of Steam, ASME, Second Edition, 1968.

7-223. C. R. Wilke, J. Chem. Phys., 18, 517-519 (1950).

7-224. W. M. Kays and A. L. London, Compact Heat Exchangers, Second
        Edition, McGraw-Hill Book Company, Inc., New York, 1964.

7-225. R. J. Wagner, HEAT 1 – A One-Dimensional Time Dependent or
        Steady-State Heat Conduction Code for the IBM-650, IDO-16867,
        April 1963.

7-226. H. Uchida, A. Ogama, and Y. Togo, Evaluation of Post-Incident
        Cooling Systems of Light-Water Power Reactors, in Proceedings of
        the Third International Conference on the Peaceful Uses of Atomic
        Energy held in Geneva, Switzerland August 31 to September 9, 1964,
        Vol. 13, New York: United Nations (1965), pp. 93-104
        (A/CONF.28/P.436).

7-227. T. Tagami, Interim Report on Safety Assessments and Facilities
        Establishment Project in Japan for Period Ending June, 1956 (No. 1).

7-228. T. Baumeister, ed., Standard Handbook for Mechanical Engineers,
        McGraw-Hill Book Company, New York, 1967.

7.12   *Trip System*

The trip system consists of the evaluation of logical statements. Each trip statement is a simple logical statement that has a true or false result and an associated variable, TIMEOF. The TIMEOF variable is –1.0 whenever the trip is false, and contains the time the trip was last set true whenever the trip is true. This variable allows for time delays and unit step functions based on events during the transient.

Within the structure of S-RELAP5, the trip system is considered to be only the evaluation of the logical statements. The decision of what action is needed, based on trip status, resides within other models. For example, valve models are provided that open or close the valve based on trip values; pump models test trip status to determine whether a pump electrical breaker has tripped.

Two types of trip statements are provided—variable and logical trips. Since logical trips involve variable trips and other logical trips, complex logical expressions can be constructed from simple logical statements. Both types of trips can be latched or unlatched. A latched trip, once set true, is no longer tested and remains true for the remainder of the problem or until reset at a restart. An unlatched trip is evaluated every time step.

7.12.1   Variable Trips

A variable trip evaluates the statement

$$T_{ri} = V_1 \text{ OP } (V_2 + C) \tag{7.1005}$$

The value T_{ri} is the i-th trip variable that may be true or false. Values V_1 and V_2 are quantities from the heat structures, hydrodynamics, reactor kinetics, control systems, or may be a TIMEOF quantity. C is a constant; OP is one of the arithmetic relational operations: EQ is equal; NE is not equal; GT is greater than; GE is greater than or equal; LT is less than; and LE is less than or equal.

Trips are evaluated at the beginning of the overall S-RELAP5 time advancement and are evaluated in numerical order. Except for TIMEOF variables, all other V quantities

have beginning of time step values; and the results of the trip evaluation are independent of the evaluation order. But when a variable trip statement references TIMEOF (T_{rk}), the new value of TIMEOF is used if $k < i$.

7.12.2   Logical Trips

A logical trip evaluates

$$T_{ri} = \pm T_{rj} OP \pm T_{rl} \tag{7.1006}$$

The values of T_{rj} and T_{rl} are variable or logical trips, and the minus sign, if present, denotes the complement of the trip value. The value OP is one of the logical operations AND, OR (inclusive or), or XOR (exclusive or).

Logical trips are evaluated following the evaluation of variable trips and are evaluated in numerical order. When T_{rj} (or T_{rl}) is a variable trip, new trip values are used; when T_{rj} is a logical trip used in logical trip expression i, new values are used when $j < i$ and old values are used when $j \geq i$.

7.13   *Control System*

The control system provides the capability to evaluate simultaneous algebraic and ordinary differential equations. The capability is primarily intended to simulate control systems typically used in hydrodynamic systems, but it can also model other phenomena described by algebraic and ordinary differential equations. Another use is to define auxiliary output quantities, such as differential pressures, so they can be printed in major and minor edits and be plotted.

The control system consists of several types of control components. Each component defines a control variable as a specific function of time-advanced quantities. The time-advanced quantities include hydrodynamic volume, junction, pump, valve, heat structure, reactor kinetics, trip quantities, and the control variables themselves (including the control variable being defined). This permits control variables to be developed from components that perform simple, basic operations.

In the following equations that define the control components and associated numerical techniques, Y_i is the control variable defined by the i-th control component, A_j, R, and S are real constants input by the user, i is the integer constant input by the user, V_j is a quantity advanced in time by S-RELAP5 and can include Y_i, t is time, and s is the Laplace transform variable. Superscripts involving the index n denote time levels. The name in parentheses to the right of the definition is used in input data to specify the component.

7.13.1   Arithmetic Control Components

7.13.1.1 Constant

$$Y_i = S \qquad\qquad \text{(CONSTANT)} \qquad\qquad (7.1007)$$

7.13.1.2 Addition-Subtraction

$$Y = S(A_0 + A_1 V_1 + A_2 V_2 + ...) \qquad \text{(SUM)} \qquad\qquad (7.1008)$$

7.13.1.3 Multiplication

$$Y_i = S\, V_1\, V_2\, ... \qquad\qquad \text{(MULT)} \qquad\qquad (7.1009)$$

7.13.1.4 Division

$$Y_i = \frac{S}{V_1} \text{ or } Y_i = \frac{SV_2}{V_1} \qquad \text{(DIV)} \qquad\qquad (7.1010)$$

7.13.1.5 Exponentiation

$$Y_i = SV_1^i \qquad\qquad \text{(POWERI)} \qquad\qquad (7.1011)$$

$$Y_i = SV_1^R \qquad\qquad \text{(POWERR)} \qquad\qquad (7.1012)$$

$$Y_i = SV_1^{V_2} \qquad\qquad \text{(POWERX)} \qquad\qquad (7.1013)$$

7.13.1.6 Table Lookup Functions

$$Y_i = S\ F(V_1) \qquad\qquad \text{(FUNCTION)} \qquad (7.1014)$$

where F is a function defined by table lookup and interpolation.

7.13.1.7 Standard Functions

$$Y = S\ F(V_1, V_2, V_3 \ldots) \qquad\qquad \text{(STDFNCTN)} \qquad (7.1015)$$

where F can be $|V_1|$, $\exp(V_1)$, $\ln(V_1)$, $\sin(V_1)$, $\cos(V_1)$, $\tan(V_1)$, $\tan^{-1}(V_1)$, $(V_1)^{1/2}$,

MAX(V_1, V_2, V_3,…), and MIN(V_1, V_2, V_3,…). Only MAX and MIN may have multiple arguments and must have at least two arguments.

7.13.1.8 Delay

$$Y_i = S\ V_1(t - t_d) \qquad\qquad \text{(DELAY)} \qquad (7.1016)$$

where t_d is the delay time. A user input, h, determines the number of pairs of data used to store past values of V_1. The maximum number of time-function pairs is $h + 2$. The delay table time increment is $\dfrac{t_d}{h}$. The delayed function is obtained by linear interpolation using the stored past history. As time is advanced, new time values are added to the table. Once the table fills, new values replace values that are older than the delay time.

7.13.1.9 Unit Trip

$$Y_i = SU(\pm t_r) \qquad\qquad \text{(TRIPUNIT)} \qquad (7.1017)$$

7.13.1.10 Trip Delay

$$Y_i = ST_r(t_r) \qquad\qquad \text{(TRIPDLAY)} \qquad (7.1018)$$

In the above two trip-related components, t_r is a trip number and, if negative (TRIPUNIT only), indicates that the complement of the trip is to be used; U is 0.0 or 1.0, depending on trip t_r (or its complement if t_r is negative) being false or true; and T_r is -1.0 if the trip is false, and is the time the trip was last set true if the trip is true.

No numerical approximations are involved in evaluating the algebraic components. Evaluation is done by simply performing the indicated operations. In the sequence of operations that perform a time advancement of the trip, heat conduction, hydrodynamic, reactor kinetic, and control systems of S-RELAP5, the control system is processed last. Thus, the end of time step (n+1) values for trip variables t_r and all V_j variables except control variables Y_i are available. The control components are evaluated in component number order. As the first control variable Y_1 is being evaluated, only old time values are available for all control component variables. Once Y_1 is evaluated, the new time value for Y_1 is available for the remaining control variable evaluations of Y_i. In general, while Y_i is being evaluated, new time values are available for Y_k, $k < 1$, and only old time values are available for Y_k, $k \geq i$.

In the example,

$$Y_{10}^{n+1} = A_0 + A_1 T^{n+1} + A_2 P^{n+1} + A_3 Y_8^{n+1} + A_4 Y_{10}^n + A_5 Y_{15}^n \qquad (7.1019)$$

T and P, which represent a temperature and pressure from the heat structure or hydrodynamic systems, are new time values. The value Y_8 is also a new time value because it was advanced before control component 10, and Y_{10} and Y_{15} are old time values.

Initialization of the algebraic control components is very similar to a time advancement. At the start of control component initialization, all other time-advanced qualities have been initialized. Control component input includes an initial value and a flag that indicates if initialization is to be performed. The initialization proceeds in the order of component numbers. The initial value entered becomes the initial value if no initialization is specified. If initialization is specified, it is simply the specified

computation using the available data. If component Y_i references Y_k, $k < i$, the initialized value of Y_k is used; if $k \geq i$, the entered initial value is used.

7.13.2   Integration Control Component

The integration component evaluates

$$Y_i = S \int_{t_1}^{t} V_1 dt \qquad \text{(INTEGRAL)} \qquad (7.1020)$$

where t_1 is the simulation time when the component is added to the system, and the initial value at t_1 is the input item regardless of the initialization flag.

The integral is advanced by trapezoidal approximation,

$$Y_i^{n+1} = Y_i^n + S\left[V_1^n + V_1^{n+1}\right]\frac{\Delta t}{2} \qquad (7.1021)$$

Both new time (n+1) and old time (n) values are available for V_1 except when it is a control variable, Y_k, $k > i$. For the case when $V_1 = Y_k$, $k \geq i$, the V^n and V^{n+1} are instead V^{n-1} and V^n. Use of the integral component when old time values will be used should be avoided. Consider the example

$$a = P_1 - P_2 - Bv - kd \qquad (7.1022)$$

$$v = \int a \, dt \qquad (7.1023)$$

$$d = \int v \, dt \qquad (7.1024)$$

This acceleration-velocity-distance system cannot be advanced without use of old values. As a general rule, it is considered better to use the old value in the algebraic expression and not in the integral expressions.

Thus, using $Y_1 = a$, $Y_2 = v$, and $Y_3 = d$,

$$Y_1 = P_1 - P_2 - BY_2 - kY_3 \qquad (7.1025)$$

$$Y_2 = \text{INTEGRAL}(Y_1) \qquad (7.1026)$$

$$Y_3 = \text{INTEGRAL}(Y_2) \qquad (7.1027)$$

AREVA Inc.

Realistic Large Break LOCA Methodology for Pressurized Water Reactors
Topical Report

EMF-2103NP
Revision 3

Page 7-457

7.13.3 Differentiation Control Components

Two components provide for differentiation

$$Y_i = S \frac{dV_1}{dt} \tag{7.1028}$$

One component evaluates the derivative by the inverse of the integration technique,

$$Y_i = \frac{2S}{\Delta t} \left(V_1^{n+1} - V_1^n \right) - Y_i^n \qquad \text{(DIFFERNI)} \tag{7.1029}$$

This component is not recommended, since it can be unstable, requires an accurate initial value, and does not recover from a bad initial value. The recommended derivative component uses a simple difference expression,

$$Y_i = S \frac{\left(V_1^{n+1} - V_1^n \right)}{\Delta t} \qquad \text{(DIFFERND)} \tag{7.1030}$$

Differentiation is a noisy process and should be avoided. Differentiation of control system variables can almost always be avoided. Filtering the result of differentiation of other variables should be considered. Similar to the case of the integral component, old time values are used when advancement of Y_i involves $V_1 = Y_k$, $k \geq i$.

7.13.4 Proportional-Integral Component

This component evaluates

$$Y_i = S \left[A_1 V_1 + A_2 \int_{t_1}^{t} V_1 dt \right] \qquad \text{(PROP-INT)} \tag{7.1031}$$

or, in Laplace transform notation,

$$Y_i(s) = S \left[A_1 + \frac{A_2}{s} \right] V_1(s) \tag{7.1032}$$

This component is advanced in time by

AREVA Inc.

EMF-2103NP
Revision 3

Realistic Large Break LOCA Methodology for Pressurized Water Reactors
Topical Report

Page 7-458

$$I^{n+1} = I^n + \left(V_1^n + V_1^{n+1}\right)\frac{\Delta t}{2} \tag{7.1033}$$

$$Y_i^{n+1} = S\left(A_1 V_1^{n+1} + A_2 I^{n+1}\right) \tag{7.1034}$$

The comments in the previous section concerning integration with $V_1 = Y_k$ hold for this component. If the initialization flag is off, Y° is the entered initial value and

$$I^\circ = \frac{1}{A_2}\left(\frac{Y_i^\circ}{S} - A_1 V_1^\circ\right) \tag{7.1035}$$

If the initialization flag is on,

$$I^\circ = 0 \tag{7.1036}$$

$$Y_i^\circ = SA_1 V_1^\circ \tag{7.1037}$$

7.13.5 Lag Control Component

The lag component is defined in Laplace transform notation as

$$Y_i(s) = S\left(\frac{1}{1 + A_1 s}\right)V_1(s) \qquad (LAG) \tag{7.1038}$$

Through algebraic rearrangement,

$$Y_i(s) + A_1 s Y_i(s) = SV_1(s) \tag{7.1039}$$

$$\frac{Y_i(s)}{s} + A_1 Y_1(s) = \frac{SV_1(s)}{s} \tag{7.1040}$$

$$Y_i(s) = \frac{SV_1(s) - Y_i(s)}{A_1 s} \tag{7.1041}$$

Transforming to the time domain gives

$$Y_i = \int_\circ^t \frac{[SV_1 - Y_i]dt}{A_1} \tag{7.1042}$$

The above expression is advanced numerically by

$$Y_i^{n+1} = Y_i^n + \left[S\left(V_1^n + V_1^{n+1}\right) - Y_i^n - Y_i^{n+1}\right]\frac{\Delta t}{2A_1} \tag{7.1043}$$

or

$$Y_i^{n+1} = \frac{Y_i^n \left(1 - \frac{\Delta t}{2A_1}\right) + S\left(V_1^n + V_1^{n+1}\right)\frac{\Delta t}{2A_1}}{1 + \frac{\Delta t}{2A_1}}$$ (7.1044)

If the initialization flag is not set, Y_i° is the entered initial value. If it is set,

$$Y_i^\circ = SV_1^\circ$$ (7.1045)

7.13.6 Lead-Lag Control Component

The lead-lag component is defined in Laplace transform notation as:

$$Y_i(S) = S\left(\frac{1 + A_1 s}{1 + A_2 s}\right) V_1(s) \qquad \text{(LEAD-LAG)}$$ (7.1046)

Rearranging algebraically, this yields:

$$Y_i(s) + A_2 s Y_i(s) = SV_1(s) + A_1 s SV_1(s)$$ (7.1047)

or

$$Y_i(s) = \frac{A_1 SV_1(s)}{A_2} + \frac{SV_1(s) - Y_i(s)}{A_2 s}$$ (7.1048)

Transforming to the time domain gives:

$$Y_i = \frac{A_1 SV_1}{A_2} + \int_\circ^t \left(\frac{SV_1 - Y_i}{A_2} dt\right)$$ (7.1049)

Note that the differentiation implied by the $SV_1(s)$ term has been avoided. The above expression is advanced numerically by:

$$Y_i^{n+1} = \frac{A_1}{A_2} SV_1^{n+1} + I^n + \left[S\left(V_1^n + V_1^{n+1}\right) - Y_i^n - Y_i^{n+1}\right]\frac{\Delta t}{2A_2}$$ (7.1050)

or

$$Y_i^{n+1} = \frac{\frac{A_1}{A_2} SV_1^{n+1} + I^n + \left[S\left(V_1^n + V_1^{n+1}\right) - Y_1^n\right]\frac{\Delta t}{2A_2}}{1 + \frac{\Delta t}{2A_2}}$$ (7.1051)

and finally:

$$I^{n+1} = I^n + \left[S \left(V_1^n + V_1^{n+1} \right) - Y_i^n - Y_i^{n+1} \right] \frac{\Delta t}{2A_2} \tag{7.1052}$$

If no initialization is specified, $I^\circ = 0$ and Y_i is the entered initial value. If initialization is specified, then:

$$Y_i^\circ = SV_1^\circ, \qquad I^\circ = \left(1 - \frac{A_1}{A_2} \right) SV_1^\circ \tag{7.1053}$$

For both lag and lead-lag components, if $V_1 = Y_k$: $k = i$ is an error; when $k < i$, old and new values are used as indicated; if $k > 1, V_1^n$ and V_1^{n+1} are really Y_k^{n-1}, Y_k^n.

7.13.7   Shaft Component

The shaft component is a special control component that advances the rotational velocity,

$$\sum_i I_i \frac{d\omega}{dt} = \sum_i \tau_i - \sum_i f_i \omega + \tau_c \qquad \text{(SHAFT)} \tag{7.1054}$$

where I_i is the moment of inertia from component I, τ_i is the torque from component i, f_i is the friction from component , and τ_c is an optional torque from a control component. The summations are over the pump, generator, motor, or turbine components that are connected to the shaft, and the shaft itself. The shaft and each associated component contains its own model, data, and storage for inertia, friction, and torque and has storage for its rotational velocity. Each associated component also has a disconnect trip number. If zero (no trip), the component is always connected to the shaft. If a trip is specified, the component is connected when false and disconnected when true. Any disconnected component is advanced separately and thus can have a different rotational velocity than the shaft. All connected components have the same rotational velocity.

The shaft equation is advanced explicitly by:

$$\sum_i I_i^n \frac{\left(\omega^{n+1} - \omega^n \right)}{\Delta t} = \sum_i \tau_i^n - \sum_i f_i^n \omega^n + \tau_c \tag{7.1055}$$

Inertias, torques, and friction are evaluated using old time information. The torque from the control system, τ_c, would be in terms of new time values for quantities other than control variables and would use new or old time values for control variables depending on their component numbers relative to the shaft component number. Except when a generator component is involved, the shaft component calculations consist of solving Equation (7.1055) for ω^{n+1} separately for each component disconnected from the shaft (if any) and for the shaft and the connected components as one system. For separated components, the new rotational velocity is stored with the component data, and the summations are only over terms within the component. For the shaft and the connected components, the summations are over the shaft and the connected components; and the new rotational velocity is stored as the shaft's and each connected component's rotational velocity. A tripped generator, attached or connected, is treated as described above. An untripped generator rotates at the input synchronous speed; and, if connected to the shaft, the shaft and all connected components are forced to the synchronous speed.

7.14   *Point Reactor Kinetics Model*

The point reactor kinetics model is the simplest model that can be used to compute power behavior in a nuclear reactor. The power is computed using the space-independent or point kinetic approximation which assumes that power can be separated into space and time functions. This approximation is adequate for cases in which the space distribution remains nearly constant.

The point reactor kinetics model computes both the immediate fission power and the power from decay of fission products. The immediate power is that released at the time of fission and includes power from kinetic energy of the fission products and neutron moderation. Decay power is generated as the fission products undergo radioactive decay. The user can select the decay power model based on either the American Nuclear Society Proposed Standard ANS 5.1, Decay Energy Release Rates Following Shutdown of Uranium-Fueled Thermal Reactors, revised October 1973 (Reference 7-

230), or the American National Standard for Decay Heat Power in Light Water Reactors, ANSI/ANS-5.1-1979 (Reference 7-231).

7.14.1   Point Reactor Kinetics Equations

The point kinetics equations are (References 7-232 and 7-233):

$$\frac{d}{dt}\varphi(t) = \frac{[\rho(t)-\beta]\varphi(t)}{\Lambda} + \left(\sum_{i=1}^{N_d}\lambda_i C_i(t) + S\right)v \tag{7.1056}$$

$$\frac{d}{dt}C_i(t) = \frac{\beta f_i}{\Lambda v}\varphi(t) - \lambda_i C_i(t) \qquad i = 1, 2, ..., N_d \tag{7.1057}$$

$$\psi(t) = V\Sigma_f \varphi(t) \tag{7.1058}$$

$$P_f(t) = Q_f \psi(t) \tag{7.1059}$$

where:

t =   time (s);

N_d =   Number of delay groups;

φ =   neutron flux ($\#/m^2$–s);

C_i =   number density of delayed neutron precursors of group i ($\#/m^3$);

β =   effective delayed neutron fraction;

Λ =   prompt neutron generation time (s);

ρ =   reactivity (only the time dependence has been indicated; however, the reactivity is dependent on other variables);

f_i =   fraction of delayed neutrons of group i;

λ_i =   decay constant of group i (1/s);

S =   source ($\#/m^3$–s);

AREVA Inc.

EMF-2103NP
Revision 3

Realistic Large Break LOCA Methodology for Pressurized Water Reactors
Topical Report

Page 7-463

ψ =   fission rate (#/s);

Σ_f =   macroscopic fission cross section (1/m);

P_f =   immediate fission power (MeV/s);

Q_f =   immediate fission energy per fission (MeV/fission);

v =   neutron velocity (m/s); and

V =   volume (m^3).

7.14.2   Fission Product Decay Model

The 1979 standard expresses the power $P_{s\alpha}(t)$ in MeV/s as a function of time t resulting from one fission of isotope α at t = 0 as

$$P_{s\alpha}(t) = \sum_{j=1}^{N_\alpha} a_{\alpha j} \exp(-\lambda_{\alpha j} t)$$ (7.1060)

Data are presented for three isotopes, ^{235}U, ^{238}U, and ^{239}Pu. The parameters a and λ were obtained by fitting to fission decay power data. The fitting for each isotope used 23 groups ($N_\alpha = 23$). The above expression is an impulse response to one fission and can be extended to an arbitrary fission rate, $\psi_\alpha(t)$, through the convolution integral

$$P_\alpha(t) = P_{s\alpha}(t) \psi_\alpha(t) = \sum_{j=1}^{N_\alpha} \left[a_{\alpha j} \exp(-\lambda_{\alpha j} t) \right] \psi_\alpha(t)$$ (7.1061)

where the convolution operation is defined by

$$A(t)B(t) = \int_0^t A(t-\tau)B(\tau)d\tau = \int_0^t A(\tau)B(t-\tau)d\tau$$ (7.1062)

Since numerical evaluation of convolution integrals is cumbersome, a set of differential equations equivalent to the convolution integral is derived.

Assume that the power from each group is from radioactive decay of a fission fragment i. Then

$$P_{\alpha j}(t) = \lambda_{\alpha j} \gamma_{\alpha j}(t) = a_{\alpha j} \exp(-\lambda_{\alpha j} t)$$ (7.1063)

For simplification in the following derivation, the α and j subscripts are dropped and the following expressions represent an equation for one group for one isotope. From Equation (7.1063) we have

$$\gamma(t) = \frac{a}{\lambda} \exp(-\lambda t) \tag{7.1064}$$

Laplace transforming Equation (7.1064) gives

$$\gamma(s) = \frac{a}{\lambda(s+\lambda)} \tag{7.1065}$$

Rearranging Equation (7.1065) gives

$$s\gamma(s) = \frac{a}{\lambda} - \lambda\gamma(s) \tag{7.1066}$$

Transforming to real time yields

$$\frac{d}{dt}\gamma(t) = \frac{a}{\lambda}\delta(0) - \lambda\gamma(t) \tag{7.1067}$$

where $\delta(0)$ is the impulse fraction. Applying a time-dependent fission rate, $\psi(t)$, in place of the single fission (impulse response), Equations (7.1066) and (7.1067) become

$$s\gamma(s) = \frac{a}{\lambda}\psi(s) - \lambda\gamma(s) \tag{7.1068}$$

$$\frac{d}{dt}\gamma(t) = \frac{a}{\lambda}\psi(t) - \lambda\gamma(t) \tag{7.1069}$$

Solution of Equation (7.1068) or (7.1069) (remembering that $P = \lambda\gamma$) for an impulse yields Equation (7.1060) and a similar expression in the standard. Solution of Equation (7.1068) or Equation (7.1069) for an arbitrary fission source yields Equation (7.1061). When specifying

$$\psi(t) = \begin{matrix} 1, & T \geq t \geq 0 \\ 0, & t > T \end{matrix} \tag{7.1070}$$

Equation (7.1068) or (7.1069) yields another solution given in the standard. (Note that the standard defines t as starting at zero after fissioning for T s.)

A physical model can be attached to the terms in Equation (7.1069). The first term on the right represents production of the isotope during fission; the last term is the loss of the isotope due to decay. A more mechanistic model would also provide for production of one isotope due to the decay of another (see Section 7.14.3).

The 1979 ANS standard for decay power can be implemented by advancing the differential equations, which becomes

$$\frac{d}{dt}\gamma_{\alpha j}(t) = \frac{F_\gamma a_{\alpha j}}{\lambda_{\alpha j}} F_\alpha \psi(t) - \lambda_{\alpha j}\gamma_{\alpha j}(t) \quad j = 1, 2, ...N_\alpha \quad \alpha = 1, 2, 3 \tag{7.1071}$$

$$P_\gamma'(t) = \sum_{\alpha=1}^{3} \sum_{j=1}^{N_\alpha} \lambda_{\alpha j}\gamma_{\alpha j}(t) \tag{7.1072}$$

where ψ is the fission rate from all isotopes, F_α is the fraction of fissions from isotope α, and P_γ' is the uncorrected decay power. The summation of F_α over α is 1.0. The value of F_γ is an input factor to allow easy specification of a conservative calculation. It is usually 1.0 for best-estimate calculations, and 1.2 was recommended for a conservative calculation with the 1973 data. The 1979 data should allow consistent use of 1.0 for F_γ.

The ANS standard uses a correction factor to the energy from fission product decay to account for the effects of neutron absorption. Both an equation and a table for the correction factor are provided. The table is a maximum value for the G factor. The equation is

$$G(t) = 1.0 + (3.24 \times 10^{-6} + 5.23 \times 10^{-10} t) T^{0.4} \psi_g \tag{7.1073}$$

where ψ_g is the number of fissions per initial fissile atom, T is the reactor operating time including any periods of shutdown, and t is the time since shutdown. Limits on the quantities are $3.0 \geq \psi_g T < 1.2641 \times 10^8$ seconds, and $t < 10^4$ seconds. The table is used for $t \geq 10^4$ seconds. Note that there is a discontinuity in G(t) when switching from the equation to the table. The standard allows the table to be used in place of the equation and the code through user input allows the same. The corrected decay power is given by

$$P_\gamma = G(t) P_\gamma'$$ (7.1074)

The 1973 proposed standard uses one isotope and prescribes data for 11 groups. The 1979 standard lists data for three isotopes, ^{235}U, ^{238}U, and ^{239}Pu, and uses 23 groups for each isotope. A user option also allows only the 1979 standard data for ^{235}U to be used. The data for both standards are built into the code as default data, but the user may enter different data.

7.14.3 Actinide Decay Model

The actinide model describes the production of ^{239}U, ^{239}Np, and ^{239}Pu from neutron capture by ^{238}U.

$$\frac{d}{dt}\gamma_U(t) = F_U \psi(t) - \lambda_U \gamma_U(t)$$ (7.1075)

$$\frac{d}{dt}\gamma_N(t) = \lambda_U \gamma_U(t) - \lambda_N \gamma_N(t)$$ (7.1076)

$$P_\alpha(t) = \eta_U \lambda_U \gamma_U(t) + \eta_N \lambda_N \gamma_N(t)$$ (7.1077)

The quantity F_U is user-specified and is the number of ^{239}U atoms produced by neutron capture in ^{238}U per fission from all isotopes. A conservative factor, if desired, should be factored into F_U. The λ and η values can be user-specified or default values equal to those stated in the 1979 ANS standard can be used.

The first equation describes the rate of change of ^{239}U atoms. The first term on the right represents the production of ^{239}U; the last term is the loss of ^{239}U due to beta decay. The second equation describes the rate of change of ^{239}Np. The production of ^{239}Np is from the beta decay of ^{239}U, and ^{239}Pu is formed from the decay of ^{239}Np. Solution of the actinide Equations (7.1075) and (7.1076) for the fission source given in Equation (7.1070) yields the result quoted in the 1979 standard.

AREVA Inc.

EMF-2103NP
Revision 3

Realistic Large Break LOCA Methodology for Pressurized Water Reactors
Topical Report

Page 7-467

7.14.4 Transformation of Equations for Solution

The differential equations to be advanced in time are Equations (7.1056), (7.1057), (7.1071), (7.1075), and (7.1076). Multiplying by $VX\Sigma_f$ in the first two equations and X in the other equations, where X is the conversion factor from MeV/s to watts, the equations become

$$\frac{d}{dt}\left[X\psi(t)\right] = \frac{\left[\rho(t)-\beta\right]X\psi(t)}{\Lambda} + \sum_{i=1}^{N_d}\lambda_i vVX\Sigma_f C_i(t) + vVX\Sigma_f S \qquad (7.1078)$$

$$\frac{d}{dt}\left[VX\Sigma_f C_i(t)\right] = \frac{\beta f_i X\psi(t)}{\Lambda v} - \lambda_i VX\Sigma_f C_i(t) \qquad (7.1079)$$

$$\frac{d}{dt}\left[X\gamma_{\alpha j}(t)\right] = \frac{F_\gamma a_{\alpha j} F_\alpha X\psi(t)}{\lambda_{\alpha j}} - \lambda_{\alpha j} X\gamma_{\alpha j}(t) \qquad (7.1080)$$

$$\frac{d}{dt}\left[X\gamma_U(t)\right] = F_U X\psi(t) - \lambda_U X\gamma_U(t) \qquad (7.1081)$$

$$\frac{d}{dt}\left[X\gamma_N(t)\right] = \lambda_U X\gamma_U(t) - \lambda_N X\gamma_N(t) \qquad (7.1082)$$

The total power, P_T, is the sum of immediate fission power, corrected fission product decay, and actinide decay, and now in units of watts is

$$P_T(t) = Q_f X\psi(t) + G(t)\sum_{\alpha=1}^{3}\sum_{j=1}^{N_\alpha}\lambda_{\alpha j} X\gamma_{\alpha j}(t) + \eta_U \lambda_U X\gamma_U(t) + \eta_N \lambda_N X\gamma_N(t) \qquad (7.1083)$$

For solution convenience, the following substitutions are made:

$$\rho(t) = \beta r(t) \qquad (7.1084)$$

$$X\psi(t) = \psi'(t) \qquad (7.1085)$$

$$\frac{vVX\Sigma_f \Lambda S}{\beta} = S' \qquad (7.1086)$$

$$vVX\Sigma_f C_i(t) = \frac{\beta f_i}{\Lambda \lambda_i} W_i(t) \qquad (7.1087)$$

$$X\gamma_{\alpha j}(t) = \frac{F_\gamma a_{\alpha j} F_\alpha}{\lambda_{\alpha j}^2} Z_{\alpha j}(t) \qquad (7.1088)$$

$$X\gamma_U(t) = \frac{F_U}{\lambda_U} Z_U(t) \qquad (7.1089)$$

$$X\gamma_N(t) = Z_N(t) \qquad (7.1090)$$

The equations to be advanced are now:

$$\frac{d}{dt}\psi'(t) = \frac{\beta}{\Lambda}\left[\left[r(t)-1\right]\psi'(t) + \sum_{i=1}^{N_d} f_i W_i(t) + S'\right] \quad (7.1091)$$

$$\frac{d}{dt}W_i(t) = \lambda_i\psi'(t) - \lambda_i W_i(t) \quad (7.1092)$$

$$\frac{d}{dt}Z_{\alpha j} t = \lambda_{\alpha j}\psi'(t) - \lambda_{\alpha j}Z_{\alpha j}(t) \quad (7.1093)$$

$$\frac{d}{dt}Z_U(t) = \lambda_U\psi'(t) - \lambda_U Z_U(t) \quad (7.1094)$$

$$\frac{d}{dt}Z_N(t) = F_U Z_U(t) - \lambda_N Z_N(t) \quad (7.1095)$$

$$P_T(t) = Q_f\psi'(t) + G(t)\sum_{\alpha=1}^{3}\sum_{j=1}^{N_\alpha}\frac{F_\gamma a_{\alpha j}F_\alpha Z_{\alpha j}(t)}{\lambda_{\alpha j}} + F_U\eta_U Z_U(t) + \eta_N\lambda_N Z_N(t) \quad (7.1096)$$

These equations are advanced using the modified Runge-Kutta method described in Section 7.14.7.

7.14.5   Initialization

Two initialization options are provided. In both options, the fission rate and delayed neutrons are in steady-state or equilibrium conditions, that is, their time derivatives are zero. With $r(0)$ an input quantity,

$$W_i(0) = \psi'(0) \quad i = 1, 2, ..., N_d \quad (7.1097)$$

$$S' = -r(0)\psi'(0) \quad (7.1098)$$

The first option assumes that the fission product decay and actinides are also in equilibrium. This is equivalent to assuming that the reactor has been operating at a constant total power for an infinite period of time. The initial conditions are

$$Z_{\alpha j}(0) = \psi'(0) \quad i = 1, 2, ..., N_\alpha \quad \alpha = 1, 2, 3 \quad (7.1099)$$

$$Z_U(0) = \psi'(0) \quad (7.1100)$$

$$Z_N(0) = \frac{F_U}{\lambda_N}\psi'(0) \quad (7.1101)$$

$$P_T(0) = \left[Q_f + G(0)\sum_{\alpha=1}^{3}\sum_{j=1}^{N_\alpha}\frac{F_\gamma a_{\alpha j}F_a}{\lambda_{\alpha j}} + F_U\eta_U + F_U\eta_N\right]\psi'(0) \quad (7.1102)$$

AREVA Inc.

EMF-2103NP
Revision 3

Realistic Large Break LOCA Methodology for Pressurized Water Reactors
Topical Report

Page 7-469

$$Q = Q_f + G(0)\sum_{\alpha=1}^{3} \sum_{j=1}^{N_\alpha} \frac{F_\gamma a_{\alpha j} F}{\lambda_{\alpha j}} + F_U \eta_U + F_U \eta_N \tag{7.1103}$$

The quantity Q, which is the total energy in MeV generated per fission, is either an input value or can be defaulted to 200 MeV (Reference 7-234). The quantity Q_f is defined from Equation (7.1103) and the user-specified or defaulted data, even if the second initialization option is used. The total power is an input quantity, and $\psi'(0)$ is determined from Equation (7.1102). The remaining quantities are computed from $\psi'(0)$ using Equations (7.1097) through (7.1101). Depending on a user option, the G factor is evaluated from Equation (7.1073) with the reactor operating time T set to the user input and the operating time t set to zero or from the first value in the G factor table in the standard.

The second option uses a power history to determine the initial values of the fission product and actinide quantities. The power history consists of one or more periods of constant total power. For each period, the input consists of the total power, the time duration at that power, and, in the case of three isotopes, the fraction of power from each isotope. The fission product and actinide differential Equations (7.1093), (7.1094), and (7.1095), are advanced in time starting with initial values of zero. The fission rate, ψ, is defined from Equation (7.1103). Depending on a user option, the G factor during this advancement is obtained from Equation (7.1073) with the reactor operating time T advanced in time and the time since shutdown t equal to zero or using the first value in the G factor table in the standard. The fission rate is reset to zero whenever a negative value is computed. This would occur whenever the user entered total power is less than the current fission product and actinide decay power. Thus, for shutdown periods, the user may conveniently enter zero total power even though significant decay power remains. The fission product and actinide values at the end of the power history became the initial values for the transient. The initial fission rate is computed from Equation (7.1102), using the total reactor power at the start of the transient (which may be different from the last power history value). If this fission rate is negative or zero, it is reset such that the immediate fission power is 10^{-12} times the decay power.

The differential equations for the power history calculation are advanced using the same numerical technique as for the transient advancement except for a simplified time step control. Time step control consists of starting the advancement of each history period with a time step of one second. The time step is doubled after each advancement. When the next advancement would exceed the time duration, the last advancement is with the remaining time. This scheme was selected since, with each different power value, the solution moves toward a new equilibrium condition asymptotically; and the most rapid change is at the beginning of a power change.

7.14.6   Reactivity Feedback

Either separable or tabular models can be selected for reactivity feedback in point reactor kinetics.

7.14.6.1 Separable Feedback Model

The separable model, which is similar to the RELAP4 (Reference 7-235) model, defines reactivity as

$$r(t) = r_o - r_B + \sum_{i=1}^{n_s} r_{si}(t) + \sum_{i=1}^{n_c} V_{ci} + \sum_{i=1}^{n_p} \left[W_{\rho i} R_\rho \left(\rho_i(t) \right) + a_{Wi} T_{Wi}(t) \right]$$

(7.1104)

$$+ \sum_{i=1}^{n_F} \left[W_{Fi} R_F \left(T_{Fi}(t) \right) + a_{Fi} T_{Fi}(t) \right]$$

The quantity r_o is an input quantity that represents the reactivity corresponding to assumed steady-state reactor power at $t = 0$. The quantity r_B is the bias reactivity which is calculated during input processing such that $r(0) = r_o$ and is printed in the input level printout. Should the user check the bias reactivity computation using Equation (7.1104), the temperature used in the $a_{Wi} T_{Wi}(t)$ and $a_{Fi} T_{Fi}(t)$ terms should be absolute temperature; i.e., Kelvin in SI units and Rankine in British units. The temperature used in the table lookup term $W_{Fi} R(T_{Fi}(t))$, however, should still use Kelvin in SI units and Fahrenheit in British units.

The quantities r_{si} are obtained from input tables defining n_s reactivity curves as a function of time. The quantities V_{ci} are n_c control variables that can be user-defined as reactivity contributions. R_ρ is a table defining reactivity as a function of the current density of water $\rho_i(t)$ in the hydrodynamic volume i; $W_{\rho i}$ is the density weighting factor for volume i; $T_{Wi}(t)$ is the spatial density average temperature of volume i; a_{Wi} is the temperature coefficient (not including density changes) for volume i; and n_ρ is the number of hydrodynamic volumes in the reactor core. The quantity R_F is a table defining reactivity as a function of the volume average fuel temperature $T_{Fi}(t)$ in heat structure i; W_{Fi} and a_{Fi} are the fuel temperature weighting factor and the fuel temperature coefficient, respectively; and n_F is the number of heat structures in the reactor core.

The model assumes nonlinear feedback effects from moderator density and fuel temperature changes and linear feedback from moderator temperature changes. It is called the separable model because each effect is assumed to be independent of the other effects. Boron feedback is not provided, but a user-defined boron feedback can be implemented with the control system. The separable model can be used if boron changes are quite small and the reactor is near critical about only one state point.

7.14.6.2 Tabular Feedback Model

The tabular feedback model computes reactivity from multi-dimensional table lookup and linear interpolation. The tabular model overcomes the objections of the separable model since all feedback mechanisms can be nonlinear and interactions among the mechanisms are included. The penalty for the expanded modeling capability is greatly increased input data requirements.

Two different options within the tabular feedback option are available. One option allows two different sets of independent variables. Both sets of variables use a boron related variable as one of the four variables. The second option chooses between three or four independent variables and the boron related variable is omitted when only three variables are used.

7.14.6.2.1 Standard Variables

With standard independent variables, the tabular model defines reactivity as

$$r(t) = r_o - r_B + \sum_{i=1}^{n_s} r_{si} + \sum_{i=1}^{n_c} V_{ci} + R\left(\bar{\rho}(t), \bar{T}_W(t), \bar{T}_F(t), \bar{\rho}_b(t)\right) \tag{7.1105}$$

$$\bar{\rho}(t) = \sum_{i=1}^{n_p} W_{\rho i} \rho_i(t) \tag{7.1106}$$

$$\bar{T}_W(t) = \sum_{i=1}^{n_p} W_{\rho i} \left[\frac{\alpha_{fi}\rho_{fi}T_{fi}(t) + \alpha_{gi}\rho_{gi}T_{gi}(t)}{\alpha_{fi}\rho_{fi} + \alpha_{gi}\rho_{gi}} \right] \tag{7.1107}$$

$$\bar{\rho}_b(t) = \sum_{i=1}^{n_p} W_{\rho i} \rho_{bi}(t) \tag{7.1108}$$

$$\bar{T}_f(t) = \sum_{i=1}^{n_F} W_{Fi} T_{Fi}(t) \tag{7.1109}$$

The variables r_o, r_B, r_{si}, and V_{ci} are the same as for separable feedback, ρ_i is the density in volume i (mass of liquid, vapor, and noncondensable divided by volume of volume), T_{fi} and T_{gi} are liquid and vapor temperatures of volume i; α_{fi} and α_{gi} are liquid and vapor void fractions in volume i, $\rho_{bi}(t)$ is spatial boron density (mass of boron divided by volume of volume), and T_{Fi} is the volume averaged fuel temperature for heat structure i. The average quantities are obtained with the use of one weighting factor for each hydrodynamic volume $W_{\rho i}$ contributing to reactivity feedback and one weighting factor for each heat structure W_{Fi} contributing to reactivity feedback. The reactivity function R is defined by a table input by the user. In the S-RELAP5 Input Data Requirements (Reference 7-234), the TABLE3 and TABLE4 options refer to the above set of independent variables; the TABLE4 option specifies a four-dimensional table, the TABLE3 option assumes no boron dependence and the table is then three-dimensional.

7.14.6.2.2 Alternate Variables

With alternate independent variables, the tabular model defines reactivity as

$$r(t) = r_o - r_B + \sum_{i=1}^{n_s} r_{si} + \sum_{i=1}^{n_c} V_{ci} + R\left(\bar{\alpha}_g(t), \bar{T}_f(t), \bar{T}_F(t), \bar{C}_b(t)\right) \tag{7.1110}$$

$$\bar{\alpha}_g(t) = \sum_{i=1}^{n_p} W_{\rho i} \alpha_{gi}(t) \tag{7.1111}$$

$$\overline{T}_f(t) = \sum_{i=1}^{n_p} W_{pi} T_{fi}(t) \tag{7.1112}$$

$$\overline{C}_b(t) = \sum_{i=1}^{n_p} W_{pi} \frac{\rho_{bi}}{\alpha_{fi}\rho_{fi}}(t) \tag{7.1113}$$

$$\overline{T}_f(t) = \sum_{i=1}^{n_F} W_{Fi} T_{Fi}(t) \tag{7.1114}$$

The quantity C_b, which is equal to $\frac{\rho_b}{\alpha_f \rho_f}$, is the boron concentration in mass of boron per mass of liquid water and the other quantities are the same as for the standard variables. Input options TABLE3A and TABLE4A specify the alternate set of independent variables; TABLE4A selects four independent variables and TABLE3A selects only three independent variables with the boron concentration being omitted.

7.14.6.2.3   Interpolation Procedures

The reactivity function R is evaluated by a direct extension of the one-dimensional table lookup and linear interpolation scheme to multiple dimensions. One-dimensional table lookup and interpolation of the function $V = F(W)$ uses an ordered set of N_W independent variable values W_i, with the corresponding values of the dependent variable V_i, to determine the value of V corresponding to a search argument W. The independent variable is searched such that W_i and W_{i+1} bracket W; an equation for a straight line is fitted to the points W_i, V_i, and W_{i+1}, V_{i+1}; and the straight line equation is evaluated for the given W.

Using subscripts 0 and 1 for the bracketing independent values and corresponding dependent values, and defining $w = \frac{W - W_0}{W_1 - W_0}$ so that w varies from 0 through 1 as W varies from W_0 through W_1, the interpolation equations are

$$V = \sum_{i=0}^{1} a_i w^i \tag{7.1115}$$

$$a_0 = V_0 \tag{7.1116}$$

$$a_1 = V_1 - V_0 \tag{7.1117}$$

For two-dimensional interpolation of $V = F(W,X)$, two sets of independent variables are used; N_W values of W_i and N_x values of X_j. A total of $N_W N_x$ dependent values of V_{ij} are entered, one value for each combination of variables from the two sets of independent variables. Graphically, the two sets of independent variables form a rectangular grid when the W_i and X_j variables are plotted on horizontal and vertical coordinates, respectively. The dependent variables are entered corresponding to the intersections of the mesh lines. The search for bracketing values in each independent set locates a mesh rectangle, and the dependent values at the four corners are used to form an interpolation equation which is the product of two straight line functions, one for each independent variable. Using 0 and 1 subscripts for the bracketing values,

$$V = \sum_{i=0}^{1} \sum_{j=0}^{1} a_{ij} w^i x^j \tag{7.1118}$$

$$x = \frac{X - X_0}{X_1 - X_0} \tag{7.1119}$$

$$a_{00} = V_{00} \tag{7.1120}$$

$$a_{01} = V_{01} - V_{00} \tag{7.1121}$$

$$a_{10} = V_{10} - V_{00} \tag{7.1122}$$

$$a_{11} = V_{11} - V_{01} - V_{10} + V_{00} \tag{7.1123}$$

This process is simply extended to three and four dimensions. Three sets of independent variables define a three-dimensional rectangular grid; and eight dependent quantities corresponding to the corners of a rectangular solid are used to define the interpolation equation, which is the product of three straight line functions. In four dimensions, four sets of independent variables are defined; and 16 dependent values are used to define the interpolation equation, which is the product of four straight line functions.

For three-dimensional interpolation,

$$V = F(W, X, Y) \tag{7.1124}$$

$$y = \frac{Y - Y_0}{Y_1 - Y_0} \tag{7.1125}$$

$$V = \sum_{i=0}^{1} \sum_{j=0}^{1} \sum_{k=0}^{1} a_{ijk} w^i x^j y^k \tag{7.1126}$$

$$a_{000} = V_{000} \tag{7.1127}$$

$$a_{001} = V_{001} - V_{000} \tag{7.1128}$$

$$a_{010} = V_{010} - V_{000} \tag{7.1129}$$

$$a_{100} = V_{100} - V_{000} \tag{7.1130}$$

$$a_{011} = V_{011} - V_{001} - V_{010} + V_{000} \tag{7.1131}$$

$$a_{101} = V_{101} - V_{001} - V_{100} + V_{000} \tag{7.1132}$$

$$a_{110} = V_{110} - V_{010} - V_{100} + V_{000} \tag{7.1133}$$

$$a_{111} = V_{111} - V_{011} - V_{101} - V_{110} + V_{001} + V_{010} + V_{100} - V_{000} \tag{7.1134}$$

For four-dimensional interpolation,

$$V = F(W, X, Y, Z) \tag{7.1135}$$

$$z = \frac{Z - Z_0}{Z_1 - Z_0} \tag{7.1136}$$

$$V = \sum_{i=0}^{1} \sum_{j=0}^{1} \sum_{k=0}^{1} \sum_{m=0}^{1} a_{ijkm} w^i x^j y^k z^m \tag{7.1137}$$

$$a_{0000} = V_{0000} \tag{7.1138}$$

$$a_{0001} = V_{0001} - V_{0000} \tag{7.1139}$$

$$a_{0010} = V_{0010} - V_{0000} \tag{7.1140}$$

$$a_{0100} = V_{0100} - V_{0000} \tag{7.1141}$$

$$a_{1000} = V_{1000} - V_{0000} \tag{7.1142}$$

$$a_{0011} = V_{0011} - V_{0001} - V_{0010} + V_{0000} \tag{7.1143}$$

$$a_{0101} = V_{0101} - V_{0001} - V_{0100} + V_{0000} \tag{7.1144}$$

$$a_{0110} = V_{0110} - V_{0010} - V_{0100} + V_{0000} \tag{7.1145}$$

$$a_{1001} = V_{1001} - V_{0001} - V_{1000} + V_{0000} \tag{7.1146}$$

$$a_{1010} = V_{1010} - V_{0010} - V_{1000} + V_{0000} \tag{7.1147}$$

$$a_{1100} = V_{1100} - V_{0100} - V_{1000} + V_{0000} \tag{7.1148}$$

$$a_{0111} = V_{0111} - V_{0011} - V_{0101} + V_{0110} + V_{0001} + V_{0010} + V_{1000} - V_{0000} \tag{7.1149}$$

$$a_{1011} = V_{1011} - V_{0011} - V_{1001} + V_{1010} + V_{0001} + V_{0010} + V_{1000} - V_{0000} \tag{7.1150}$$

$$a_{1101} = V_{1101} - V_{0101} - V_{1001} + V_{1100} + V_{0001} + V_{0100} + V_{1000} - V_{0000} \tag{7.1151}$$

$$a_{1110} = V_{1110} - V_{0110} - V_{1010} + V_{1100} + V_{0010} + V_{0100} + V_{1000} - V_{0000} \tag{7.1152}$$

AREVA Inc.

EMF-2103NP
Revision 3

Realistic Large Break LOCA Methodology for Pressurized Water Reactors
Topical Report

Page 7-476

$$a_{1111} = V_{1111} - V_{0111} - V_{1011} - V_{1101} - V_{1110} + V_{0011} + V_{0101} + V_{0110}$$

$$+ V_{1001} + V_{1010} + V_{1100} - V_{0001} - V_{0010} - V_{0100} - V_{1000} + V_{0000}$$

(7.1153)

The interpolating equations define a continuous function. There is no discontinuity in the dependent quantity as any one or combination of dependent variables pass to the next bracketing pair of values.

Using N_W, N_X, N_Y, and N_Z as the number of values in the four sets of independent variables, the number of data points for a three-dimensional table is $N_W N_X N_Y$ and is $N_W N_X N_Y N_Z$ for a four-dimensional table. Using only four values for each independent variable, a four-dimensional table requires 256 data points.

7.14.7 Reactor Kinetics Numerical Procedures

The reactor kinetics equations are advanced in time using the modified Runge-Kutta method of Cohen (Reference 7-236). A first order differential equation is written as

$$\dot{n}(t) = \alpha n(t) + R(n,t)$$

(7.1154)

where α is constant over the time step, and $R(n,t)$ contains the remaining terms of the differential equation, including the non constant portion of any coefficient of $n(t)$. If the coefficient $n(t)$ is $\beta(n,t)$, α would be $\beta(n(0),0)$; and $R(n,t)$ would contain a term of $\beta(n(t),t)$ $- \alpha n(t)$. Multiplying Equation (7.1154) by an integrating factor, $e^{-\alpha t}$, and integrating gives

$$n(t) = n(0)e^{\alpha t} + \int_0^t e^{\alpha(t-\lambda)}R(n,\lambda)d\lambda$$

(7.1155)

Since

$$n(0)e^{\alpha t} = n(0) + \int_0^t \alpha n(0)e^{\alpha(t-\lambda)}d\lambda$$

(7.1156)

$$n(t) = n(0) + \int_0^t \left[\alpha n(0) + R(n,\lambda)\right]e^{\alpha(t-\lambda)}d\lambda$$

(7.1157)

Letting $\lambda = ut$, then $d\lambda = tdu$, and

$$n(t) = n(0) + t\int_0^1 \left[\alpha n(0) + R(n, u)\right]e^{\alpha t(1-u)}du \qquad (7.1158)$$

the numerical technique for advancing the solution over the time step consists of making approximations to the behavior of $R(n,u)$ over the time step. For convenience in the following expressions, the following function is defined,

$$C_m(x) = \int_0^1 u^{m-1}e^{x(1-u)}du \qquad (7.1159)$$

Stage 1:

Assume $R(n, \lambda) = R(n(0),0) = R_0$ and write $n(o)$ as n_o; then compute $n\left(\dfrac{h}{2}\right)$ by

$$n_1 = n\left(\frac{h}{2}\right) = n_0 + \frac{h}{2}[\alpha n_0 + R_0]C_1\left(\alpha\frac{h}{2}\right) \qquad (7.1160)$$

Stage 2:

Assume straight line variation of $R(n, \lambda)$ between R_0 and $R_1 = R\left(n_1, \dfrac{h}{2}\right)$ and compute $n\left(\dfrac{h}{2}\right)$ by

$$R(n,\lambda) = R_0 + \frac{2(R_1 - R_0)\lambda}{h} \qquad (7.1161)$$

$$R(n,\lambda) = R_0 + (R_1 - R_0)u \qquad (7.1162)$$

$$n_2 = n\left(\frac{h}{2}\right) = n_1 + \frac{h}{s}[R_1 - R_0]C_2\left(\alpha\frac{h}{2}\right) \qquad (7.1163)$$

Stage 3:

Assume straight line variation of $R(n, \lambda)$ between R_0 and $R_2 = R\left(n_2, \dfrac{h}{2}\right)$ and compute by

$$R(n,\lambda) = R_0 + \frac{2}{h}[R_2 - R_0]\lambda \qquad (7.1164)$$

$$R(n,u) = R_0 + 2[R_2 - R_0]u \qquad (7.1165)$$

$$n_3 = n(h) = n_0 + h(\alpha n_0 + R_0)C_1(\alpha h) + 2h(R_2 - R_0)C_2(\alpha h) \qquad (7.1166)$$

Stage 4:

Assume quadratic through points R_0, R_2, $R_3 = R(n_3 h)$, then compute n(h) by

$$R(n,u) = (2R_0 + 4R_2 + 2R_3)u_2 + (-3R_0 + 4R_2 - R_3)u + R_0 \tag{7.1167}$$

$$n_4 = n(h) = n_3 + h(R_4 - R_3)\left[2C_3(\alpha h) - C_2(\alpha h)\right] \tag{7.1168}$$

Stage 5:

Assume quadratic through points R_0, R_2, $R_4 = R(n_4 h)$, then compute n(h) by

$$n_5 = n(h) = n_4 + h(R_4 - R_3)\left[2C_3(\alpha h) - C_2(\alpha h)\right] \tag{7.1169}$$

The third-, fourth-, and fifth-order approximations are obtained by terminating the process at the end of the third, fourth, and fifth stages, respectively. RELAP5 uses only the fifth order approximation.

By direct integration, the function $C_1(x)$ is given by

$$C_1(x) = \frac{e^x - 1}{x} \tag{7.1170}$$

Using integration by parts, a recursion relation for $C_m(x)$ is

$$C_{m+1}(x) = \frac{mC_m(x) - 1}{x} \tag{7.1171}$$

During machine calculations of the $C_m(x)$ functions for $x \le 1$, excessive loss of significance occurs. For this range, $C_3(x)$ is computed from its MacLaurin series expansion

$$C_3(x) = 2\left[\frac{1}{3!} + \frac{x}{4!} + \frac{x^2}{5!} + \frac{x^3}{6!} + \frac{x^4}{7!} + \frac{x^5}{8!} + \frac{x^6}{9!} + \frac{x^7}{10!}\right] \tag{7.1172}$$

C_2 and C_1 are evaluated by solving Equation (7.1171) for $C_m(x)$.

During the advancement in time of the solution, the time increment is automatically increased or decreased to maintain a specified degree of accuracy. After the calculations for a reactor kinetics time advancement, an empirical formula is used to estimate the error. If the error is excessive, the time increment is halved and the advancement calculation is redone. If the error is sufficiently small, the time interval is doubled for the next time step. If the estimated error is between limits, the same interval is used for the next time advancement. These procedures for time step control, taken from the AIREK code (Reference 7-237) are as follows:

$$\omega_1 = \frac{\dot{\psi}'(0)}{\psi'(0)} \tag{7.1173}$$

$$\omega_3 = \frac{\dot{\psi}'(h)}{\psi'(h)} \tag{7.1174}$$

$\bar{\omega}$ is defined by

$$\psi'(h) = \psi'(0) e^{\bar{\omega}h} \tag{7.1175}$$

$$Q = \frac{hC_2(\alpha h)}{1 + C_1(\alpha h)}[\omega_1 - 2\bar{\omega} + \omega_3] \tag{7.1176}$$

The α in Equation (7.1176) is that of the neutron flux, Equation (7.1091).

$$\delta = \text{MAX}\left[\frac{n_{1i} - n_{01}}{n_{1i}}\right] \tag{7.1177}$$

The Q_L and Q_H appearing below are 0.0001 and 0.001 respectively.

1. If $\delta < 2^{-15}$ and $Q \geq Q_L$, the program continues with the same time step.

2. If $\delta < 2^{-15}$ and $Q < Q_L$, the program doubles the time step for the next advancement.

3. If $\delta \geq 2^{-15}$ and

    a. $Q < Q_L$, the time step is doubled for the next advancement.

    b. $Q \leq Q_H$, the same time step is used for the next advancement.

    c. $Q > Q_H$, the time advancement is recalculated with half the time step.

4. The time advancement is also recomputed with the time step halved if

a. αh of any equation > 88.0.

b. negative or zero power is computed.

If the coefficient of the neutron flux in Equation (7.1091) is negative, a subtraction is involved in determination of the derivative and a loss of significant digits can occur. If this coefficient is negative, a check is made of the number of bits lost in the subtraction. If more than sixteen bits are lost, the value of neutron flux computed by the current stage of the advancement procedure is discarded; instead, neutron flux is determined from the expression obtained by setting the neutron flux derivative to zero

$$\psi(t) = \frac{-\sum_{i=1}^{N_d} f_i W_i(t) - \frac{S\Lambda}{\beta}}{r(t) - 1} \tag{7.1178}$$

The transfer of information between the reactor kinetics calculation and the other calculations is explicit. Hydrodynamic and heat conduction/transfer calculation precede reactor kinetics, and the control system calculation follows reactor kinetics. The reactor power used in hydrodynamics and heat conduction is the value at the beginning of the time step. The reactivity used at the end of time step in the kinetics advancement is computed from the end of time step values from hydrodynamics and heat conduction and the beginning of time step values from the control system.

The reactor kinetics equations are advanced at the same time step as the hydrodynamics, and reactivity is assumed to vary linearly between time step values. The maximum time step for the reactor kinetics advancement is the hydrodynamic time step. That time step is reduced, if necessary, as described above.

7.14.8   References

7-229. American Nuclear Society Proposed Standard, ANS 5.1, Decay Energy Release Rate Following Shutdown of Uranium-Fueled Thermal Reactors, October 1971, Revised October 1973.

7-230. American National Standard for Decay Heat Power in Light Water Reactors, ANSI/ANS-5.1-1979, August 1979.

AREVA Inc.

EMF-2103NP
Revision 3

Realistic Large Break LOCA Methodology for Pressurized Water Reactors
Topical Report

Page 7-481

7-231. S. Glasstone and A. Sesonske, Nuclear Reactor Engineering, Von Nostrand Reinbold, New York, 1981.

7-232. J. R. Lamarsh, Introduction to Nuclear Reactor Theory, Addison-Wesley, 1972.

7-233. EMF-CC-097(P) (latest version) S-RELAP5 Input Data Requirements (Users' Manual), AREVA NP Inc.

7-234. EG&G Idaho, Inc., RELAP4/MOD6; A Computer Program For Transient Thermal-Hydraulic Analysis of Nuclear Reactors and Related Systems, Users Manual, CDAP-TR-003, May 1978.

7-235. E. R. Cohen, "Some Topics In Reactor Kinetics," Proceedings, Geneva Conference Volume 11, 302, 1958.

7-236. A. Schwartz, Generalized Reactor Kinetics Code AIREK II, NAA-SR-Memo-4980, 1960.